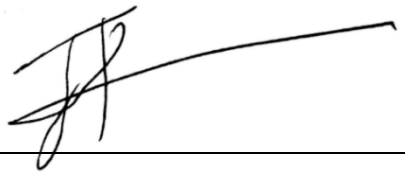
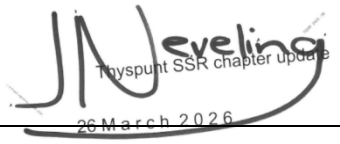
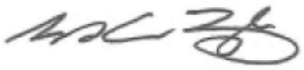
SECTION 5.14: *SEISMIC HAZARD*		
Author's declaration:	I declare that appropriate diligence and quality assurance was applied in the compilation of this report. As such I am confident in the results here described and the conclusions drawn. Name: Julian J. Bommer 	Date: 25-03-2026
Technical Writer Review:	Name: Johann Neveling 	Date: 26-03-2026
Project Manager Authorisation:	Name: Johann Neveling 	Date: 26-03-2026
Eskom NSS Technical Lead Acceptance:	Name: M van Zyl 	Date: 2026-03-27
Eskom NSS Employer's Agent Acceptance:	Name: F van Mosseveld 	Date: 2026-03-27

AMENDMENT RECORD			
Rev	**Draft**	**Date**	**Description**
0		April 2015	New section. Thyspunt Site Safety Report compiled in support of Eskom's Nuclear Installation Site Licence for the Thyspunt site.
0a		March 2026	Section updated to comply with the updated SSR template.

© Eskom 2026/Rev 0a

EXECUTIVE SUMMARY

The seismic hazard characterization of the Thyspunt site is based on a probabilistic seismic hazard analysis (PSHA) conducted as a Senior Seismic Hazard Analysis Committee (SSHAC) Level 3 process as specified in the regulatory guidelines issued by the United States Nuclear Regulatory Commission. The project assembled comprehensive databases of geological, seismological and geotechnical data, including several new datasets collected as part of the project to provide improved constraints on the input models and reduce the associated uncertainties. The objective evaluation of all data, methods and models was conducted under the observation of the Participatory Peer Review Panel (PPRP), who were present at the three formal Workshops that constitute the backbone of the SSHAC Level 3 process as well as having an observer at the formal Working Meetings of the Technical Integration Teams. The closure letter of the PPRP confirmed that the PSHA had been conducted in full compliance with the requirements for a SSHAC Level 3 process and had effectively captured the epistemic uncertainty in the final hazard estimates.

The seismic source characterization (SSC) model included five major geological faults. Only one of these, the Kango, for which paleoseismological investigations reveal clear evidence of geologically recent activity, was included as an unambiguously active seismogenic fault. Four other faults (Agulhas, Gamtoos, Pletenberg, and Worcester) were included in the PSHA with a probability of 20% of being seismogenic, based on absence of evidence for Quaternary movement on these faults established through geomorphological investigations, particularly of the marine terraces in the region, and cosmogenic dating of rock samples drilled at multiple locations.

The SSC model also included five area source zones for all potential future earthquakes not associated with the fault sources. The earthquake activity rates within these sources were determined from an earthquake catalogue for the region developed for the project and extended in time through retrieval and interpretation of historical descriptions of the felt and observed effects of earlier earthquakes. Intensities were inferred from these descriptions, and these intensities were then used to estimate earthquake magnitudes, using empirical relationships whose applicability was confirmed using data from more recent earthquakes with instrumentally determined magnitudes. The historical investigations confirmed the low seismicity rates in the region surrounding the Thyspunt site, as reflected in the recurrence model for the host Extended Continental Crust (ECC) source zone. Maximum magnitudes for earthquakes in the source zones were estimated following well-established approaches for stable tectonic regions, applying Bayesian updating, informed by the local earthquake catalogue, of analogues from global databases.

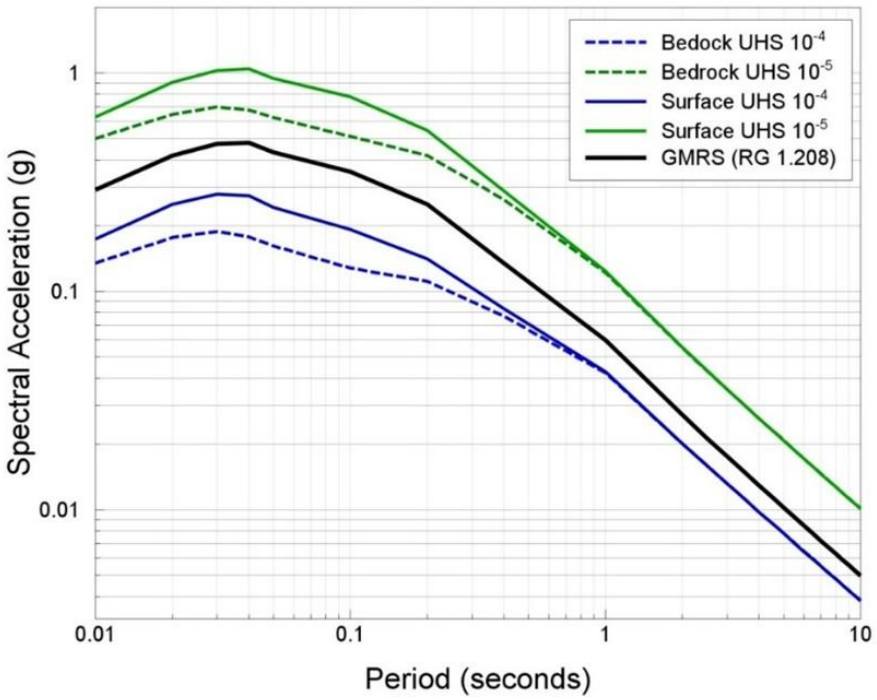
© Eskom 2026/Rev 0a

The ground motion characterization (GMC) model consisted of two components, designed to fully capture both the characteristics of seismicity in the region and the modifications of the seismic waves due to shallow geological structure below the site, which was determined through shear-wave velocity measurements in many deep boreholes drilled on the site. A reference rock horizon was established at a depth of about 60 m below the target surface rock elevation, and a logic-tree was developed for the prediction of spectral accelerations at this level. This model was developed using the backbone approach, selecting empirical ground-motion prediction equations (GMPEs) displaying attenuation characteristics consistent with those inferred from seismograph recordings and intensity data in South Africa. The predictions from these GMPEs were adjusted to the reference rock condition by applying corrections for differences in shear-wave velocity and high-frequency attenuation (kappa) between the site and the host regions of the GMPEs. Site response analyses were conducted for the upper 60 m at the site to determine frequency-dependent amplification factors (AF), which were then convolved with output of the PSHA calculations performed at the reference rock horizon, to yield hazard estimates at the target surface horizon.

The PSHA calculations were performed using the FRISK88 software, which had previously undergone extensive Quality Assurance (QA) for application to nuclear sites. To provide additional QA on the hazard results, parallel PSHA calculations were performed for a large subset of the inputs using the OpenQuake software developed by the Global Earthquake Model (GEM) project. Disaggregation of the reference baserock hazard estimates show the high-frequency hazard estimates to be dominated by moderate-magnitude earthquakes within the host ECC source zone.

The baserock hazard estimates were convolved with AFs for the overlying rock layers in order to produce the final output of seismic hazard curves and uniform hazard response spectra at the target surface rock horizon (see figure below).

© Eskom 2026/Rev 0a



Uniform hazard spectra at the bedrock (dashed) and surface (solid) elevations for annual frequencies of exceedance (AFEs) of 10-4 and 10-5, and the resulting ground motion response spectra (GMRS)

© Eskom 2026/Rev 0a

CONTENTS

EXECUTIVE SUMMARY 5.14-3

5.14 SEISMIC HAZARD.....5.14-20

5.14.1 Introduction 5.14-20

5.14.2 Purpose and Scope.....5.14-21

5.14.3 Regulatory Framework.....5.14-24

5.14.4 Approach.....5.14-30

5.14.5 The SSHAC Framework.....5.14-106

5.14.6 Monitoring Programmes.....5.14-242

5.14.7 Management of Uncertainties 5.14-259

5.14.8 Management System 5.14-276

5.14.9 Conclusions 5.14-281

5.14.10 References.....5.14-298

© Eskom 2026/Rev 0a

TABLES

Table 5.14.1 Summary of Essential Steps in a SSHAC Level 3 Study (*Reference 5.14.2*) 5.14-29

Table 5.14.2 Events in Catalogue Region with Direct Estimates of M_w.....5.14-53

Table 5.14.3 SSC Proponent Experts 5.14-111

Table 5.14.4 GMC Proponent Experts 5.14-112

Table 5.14.5 SSC TI Team Prioritisation of Data That Can Be Used to Address the Attributes of the Criteria for Identifying Seismic Sources 5.14-118

Table 5.14.6 Summary of Seismic Source Zone Characteristics Included in the SSC Model 5.14-151

Table 5.14.7 Summary of Fault Source Characteristics Included in the SSC Model.5.14-181

Table 5.14.8 Summary of Activities, Links, and Quality Requirements 5.14-279

Table 5.14.9 Seismic hazard curves for the 10 specified oscillator periods at the bedrock elevation 5.14-286

Table 5.14.10 Seismic hazard curves for the 10 specified oscillator periods at the surface elevation 5.14-287

Table 5.14.11 UHS and GMRS at the surface elevation.....5.14-293

Table 5.14.12 Disaggregated scenarios at AFE of 10^{-4} 5.14-296

Table 5.14.13 Disaggregated scenarios at AFE of 10^{-5} 5.14-296

Table 5.14.14 Disaggregated scenarios at AFE of 10^{-6} 5.14-297

© Eskom 2026/Rev 0a

FIGURES

Figure 5.14-1(a) Locality Map Showing the 320 km-radius Site Region and 40 km-radius Site Vicinity. (b) Locality Map Showing the 40 km-radius Site Vicinity, 8 km-radius Site Area and 1 km-radius Site Location (represented by the dot) 5.14-36

Figure 5.14-2 Extent of Catalogue Study Region Used in the Development of the SSC Model (*green rectangle*). The Site Region as defined by USNRC (*Reference 5.14.3*) is also shown for reference (*dashed green circle*). 5.14-37

Figure 5.14-3 Locations of Early Seismograph Stations in the South African Region. *(Yellow symbols indicate stations that were operational before 1949, red symbols those that started operating after this date. The green rectangle indicates the boundaries of the study region).* 5.14-40

Figure 5.14-4 Map of the SANSN Network (*Reference 5.14.20*).....5.14-41

Figure 5.14-5 Alternative Epicentres Provided by the Various Approaches Implemented in the MEEP2 Software and Best Estimate Epicentre Adopted in the Thyspunt PSHA Study for the 21 May 1850 Event. 5.14-46

Figure 5.14-6 Bootstrapped Epicentres for the Various Methods Implemented in the MEEP2 Software, for the 21 May 1850 Event. The Location Uncertainties Are Based on the Spatial Distributions of these Bootstrapped Epicentres, with Event-Specific Weights Applied to Each Method. 5.14-47

Figure 5.14-7 Locations of Aftershocks of the 1969 Ceres Event Determined from Recordings on a Temporary Local Network by Green & Bloch (*Reference 5.14.21*). *"A" is a map of aftershocks; "B" is a cross section along the length of the aftershock sequence; "C" is a cross section normal to the length of the aftershock sequence. The vertical scale of the cross sections is 10 km.* 5.14-48

Figure 5.14-8 Summary of Instrumental Focal Depth Determinations of South African Earthquakes, Including Uncertainties Where Available.....5.14-51

Figure 5.14-9 Summary of Earthquake Fault Plane Solutions for South Africa. Red and green "beach balls" are Focal Mechanisms for Tectonic and Mining Events, Respectively. .5.14-52

Figure 5.14-10 Calibration of Local Magnitude Scale in South Africa, Other Regions of Africa and Selected SCR Regions. 5.14-55

Figure 5.14-11 M_L-M_w Relation Adopted in the Thyspunt PSHA Study.....5.14-56

Figure 5.14-12 Intensity Magnitudes Obtained from Using the Different Methods Implemented in the MEEP2 Software Compared with Instrumentally Determined Magnitudes.

The uncertainty bars for M_l reflect the standard deviation of the bootstrap solutions obtained for each approach using the MEEP2 software, while the M_w uncertainties are those listed in the catalogue (or similarly determined). 5.14-59

Figure 5.14-13 Distribution of magnitude uncertainties in Thyspunt PSHA project catalogue. 5.14-61

Figure 5.14-14 Results of Applying the Gardner & Knopoff Declustering Algorithm (*Reference 5.14.86*) to the Thyspunt PSHA Project Catalogue. *The source zones shown correspond to the preliminary Thyspunt PSHA SSC model*. 5.14-63

Figure 5.14-15 Equivalent Periods of Completeness Considered for the Various Source Zones in the Thyspunt PSHA SSC Model. 5.14-66

Figure 5.14-16 Privileged Observation Points in the Area of Study 5.14-68

Figure 5.14-17 Intensity Data Points Collected by Albini (*Reference 5.14.27*), Covering the Period 1820-1936. *The area enclosed by the dashed rectangle is shown in more detail in the next figure.* 5.14-69

Figure 5.14-18 Detail of the Study Region of Albini (*Reference 5.14.27*). This Region Was Assessed for Negative, As Well As Positive Evidence of Earthquakes. 5.14-70

Figure 5.14-19 Seismic Histories Compiled at Selected Locations by Albini (*Reference 5.14.27*). 5.14-71

Figure 5.14-20 Magnitude-Distance Distribution of the Macroseismic Intensity Database (*Reference 5.14.98*). 5.14-72

Figure 5.14-21 Locations of Earthquakes That Are Included in the Instrumental Intensity Database (*Reference 5.14.98*). 5.14-73

Figure 5.14-22 Venn diagram showing the types of macro seismic information with the 57 earthquakes in the intensity database (*Reference 5.14.98*). *The number in brackets reflects the total number of IDPs associated with each event in each category*. 5.14-74

Figure 5.14-23 Intensity-Distance Plot of the Geologically Classified IDPs of Selected Earthquakes in the Instrumental Intensity Database (*Reference 5.14.98*). *The Bakun & Scotti French-SCR model (Reference 5.14.62) for a depth of 10 km is shown as a grey curve, dashed outside the applicability range; the identified outliers for the 1969 Ceres event. Open symbols represents IDPs that were newly assigned, whilst the closed symbols were obtained from published data.* 5.14-77

Figure 5.14-24 Magnitude-Distance distribution of the Final Instrumental Intensity Database, Grouped by Intensity Level (*Reference 5.14.98*).....5.14-78

Figure 5.14-25 Ray Coverage in the Weak Motion Database for the Two Temporal Periods Considered. *The blue triangles denote recording stations while the red dots show the epicentral positions of the events. Black lines connect the source and site locations.* 5.14-81

Figure 5.14-26 Local Magnitude-Epicentral Distance Distribution of the Dataset Over the Two Temporal Periods Considered. *The recordings of the tectonic events are shown using the red markers, while the mining-related recordings are shown using black markers.* 5.14-81

Figure 5.14-27 Equivalence Between Frequency-Independent, but Depth-Dependent, Anelastic Attenuation (*black curves*) and Frequency-Dependent Anelastic Attenuation (*red curves*) (*Reference 5.14.68*) 5.14-83

Figure 5.14-28 Variation of Stress Drop With Respect to Magnitude Obtained from Four Publications Concerning Stress Drop Estimation in Interplate Regions. *The solid black line corresponds to the variable stress drop model of Rietbrock et al. (Reference 5.14.112).* 5.14-84

Figure 5.14-29 Stacked Spectra from Earthquakes of Local Magnitude Between 2.0-2.2 Occurring Within a Distance of 100 km from Station HVD. 5.14-87

Figure 5.14-30 Frequency Response Function (Transfer Function) for Site HVD Showing the Effect of Impedance Contrasts Over the Uppermost Kilometre of the Site. The Near-Surface Profile Used to Generate this Response Function is Shown in the Inset. 5.14-87

Figure 5.14-31 Comparison of Observed Spectra at Site HVD and the Stochastic Model Predictions of Rietbrock Using the Site Transfer Function Shown in *Figure 5.14.30* and a Range of Alternative Kappa Values Ranging from 0.001 s (black) to 0.005 s (orange). .5.14-88

Figure 5.14-32 Point Representations of Hazard Curves Generated for a Site at the Centre of a Simple Circular Source Zone, Sampling the Full Ranges of Parameters in the Five GMPEs Retained After Application of Exclusion Criteria *(see text for explanation of how the mean and standard deviation values were obtained)*.....5.14-96

Figure 5.14-33 Shear-Wave Velocity Profiles for Turkish Strong-Motion Stations with V_{s30} Values in the Range from 550-670 m/s, Compared with the Generic California Rock Site Profile of Boore & Joyner (*Reference 5.14.138*) 5.14-99

Figure 5.14-34 Comparison of Shear-Wave Velocity Profiles for Turkey and for California from Compiled as Explained in the Text. 5.14-100

Figure 5.14-35 Rock Drop Source and Geophone Array for Active MASW Testing.5.14-102

Figure 5.14-36 Borehole Preparation for PS Logging and Suspension Logging Probe. 5.14-103

Figure 5.14-37 Locations of Phase 1 and Phase 2 PS Suspension Logging Sites. ..5.14-104

Figure 5.14-38 Average and Individual Shear-Wave Velocity Profiles Measured Within the Goudini and Cedarberg Formations. 5.14-105

Figure 5.14-39 Variability in the Shear-Wave Velocities (σ_{lnVs}) and Number of V_s Points Available Versus Depth. 5.14-106

Figure 5.14-40 Organisational Structure for the SSHAC Level 3 Thyspunt PSHA. (*Notes*: * Resigned for health reasons after Workshop #1; ** Resigned for personal reasons after Workshop #2; *** Joined PPRP after Workshop #2) 5.14-107

Figure 5.14-41 Illustration of the Skills and Experience Required for Different Roles in a SSHAC Level 3 PSHA. *The length of the bar in each column reflects the degree to which the attribute is required for the role: if the bar fills the width of the column, it is an indispensable requirement, whereas if the column is blank, the attribute is not needed for that specific role.* 5.14-108

Figure 5.14-42 Overview of the SSHAC Level 3 Process Applied to the Thyspunt PSHA. *Time runs vertically down from the top of the figure.* 5.14-109

Figure 5.14-43 Overview of the SSHAC Level 3 Process Applied to the Thyspunt PSHA, expanded from *Figure F-5.14.42*. *WM is Working Meeting*. 5.14-114

Figure 5.14-44 Magnitude-Frequency Models of Earthquake Recurrence for a Given Mmax = 7 and for a Constant Seismic Moment Rate. The Truncated Exponential Model is Used for Seismic Source Zones and the Characteristic Earthquake and Maximum Moment Models are used for Fault Sources. *(Modified from Reference 5.14.147)* 5.14-122

Figure 5.14-45 Seismic Source Zones and Fault Sources of the SSC Model. 5.14-125

Figure 5.14-46 Schematic Overview of the Overall Logic Tree for the Hazard Analysis Showing the Components for the SSC and GMC Parts. 5.14-129

Figure 5.14-47 Part 1 of the SSC Logic Tree Portraying Those Assessments That Relate to the Coordinates of All Seismic Sources for the Hazard Analysis. 5.14-129

Figure 5.14-48 Part 2 of the SSC Logic Tree for the Seismic Source Zones ECC, SYN, KAR, NAM, and CK. *Those weights that are source-specific are labelled "ss".* 5.14-130

Figure 5.14-49 Part 2 of the SSC Logic Tree forFault Sources PLET, GAM, AFZ, KNG and WOR. *Those weights that are source-specific are labelled "ss."* 5.14-131

Figure 5.14-50 Focal Depth Distribution for the CEUS Region Developed from High-Quality Depth Determinations and With Removal of Fixed Depths. The D_{90} for This Distribution is 17

km. 5.14-136

Figure 5.14-51 Diagrammatic Illustration of the Bayesian Mmax Approach *The various panels show (a) the prior distribution, (b) the likelihood function, and (c) the posterior distribution. The posterior distribution is represented by a discrete distribution (d) for implementation in hazard analysis. The prior shown is a normal distribution with mean M 6.4 and standard deviation 0.85.* The likelihood function is based on two observed earthquakes larger than M 4.5, with the largest being 5.3. (*Reference 5.14.69*). 5.14-145

Figure 5.14-52 Seismic Source Zones Defined in the SSC Model (*black lines*), Including Alternative Boundaries for the ECC Host Zone, and Earthquake Epicentres from the Declustered Project Catalogue. 5.14-148

Figure 5.14-53 Mmax Distributions for the Seismic Source Zones in the SSC Model....5.14-149

Figure 5.14-54 Largest Observed Earthquakes Within the Region of the Thyspunt site. 5.14-150

Figure 5.14-55 Summary of Earthquake Recurrence Relationships for the Source Zones included in the SSC Model. *The lower right panel shows the b-values determined for each of the source zones, with the prior distribution based on the regional b-value shown in grey.* 5.14-150

Figure 5.14-56 Logic Tree Summarising the Epistemic Uncertainties in the Characterisation of the ECC Source Zone. *Epistemic uncertainties that are common to multiple source zones such as seismogenic thickness are discussed in Subsection 5.14.5.4.(c).* 5.14-153

Figure 5.14-57 Map Showing the Two Structural Branches in the Cape Fold Belt, the Setting of the Syntaxis, and Alternative Source Zone Boundaries Superimposed Upon a Regional DEM. *Location names are as follows: CA = Cape Agulhas; CE = Ceres; CH = Cape Hangklip, MG = McGregor; MU = Montagu; TO = Touwsrivier (Modified from Reference 5.14.174).* 5.14-156

Figure 5.14-58 Rose Diagram of the ECC Zone Showing the Prominent West-Northwest Structural Trends. *The diagram was developed by measuring the average orientation and approximate lengths of structural trends within the ECC zone.*.....5.14-157

Figure 5.14-59 Summary of Aleatory Assessments for the ECC Source Zone. 5.14-159

Figure 5.14-60 Location of a Possible Completeness Boundary Within the ECC Source Zone (*dashed red line*). 5.14-160

Figure 5.14-61 Schematic Interpretation of the Syntaxial Core Showing the Differences in Structural Subdomains to the North and South of the Worcester Fault (*Reference 5.14.174*).

.....5.14-162

Figure 5.14-62 Logic Tree Summarising the Epistemic Uncertainties in the Characterisation of the SYN Source Zone. *Epistemic uncertainties that are common to multiple source zones such as seismogenic thickness are discussed in Subsection 5.14.5.4.(c).* 5.14-162

Figure 5.14-63 Map Showing the Two Structural Branches in the Cape Fold Belt, the Setting of the Syntaxis, Distribution of Seismicity, and Alternative Source Zone Boundaries Superimposed Upon a Regional DEM. *Location names are as follows: CH = Cape Hangklip, MG = McGregor; MU = Montagu; TO = Touwsrivier (Modified from De Beer, 1998).* 5.14-164

Figure 5.14-64 Positions of the Kaapvaal Craton and the Namaqua-Natal Mobile Belt (NNMB). The Southern Cape Conductive Belt (SCCB) and the Beattie Magnetic Anomaly (BMA) Are Also Shown. *The vertical hatches show the extent of the Karoo Basin (Reference 5.14.206).* 5.14-166

Figure 5.14-65 Logic Tree Summarising the Epistemic Uncertainties in the Characterisation of the KAR Source Zone. Epistemic uncertainties that are common to multiple source zones such as seismogenic thickness are discussed in Subsection 5.14.5.4.(c). 5.14-167

Figure 5.14-66 The Beattie Set of Magnetic anomalies in the KAR Source Zone Shown on the Magnetic Map of South Africa (*Subsection 5.13.5.1.(d) ii*). The Source Zones and Fault Sources developed in the Thyspunt PSHA SSC Model are also shown. 5.14-168

Figure 5.14-67 Rose diagram of the KAR showing the prominent east-west structural grain in the KAR zone. The diagram was developed by measuring the average orientation of structural trends within the KAR. 5.14-169

Figure 5.14-68 Doringberg-Hartbees Fault Zone, Marks the Western and Southern Margin of the Kaapvaal Craton and the Southwestern Boundary of the CK Source Zone. *Other faults on the Kaapvaal Craton such at the Brakbos (BF), Colesberg, and Trompsburg Faults are shown. The three source zones polygons; NAM (red), CK (purple), and KAR (blue) are superimposed on this gravity map* (*Reference 5.14.210*).....5.14-171

Figure 5.14-69 Logic Tree Summarising the Epistemic Uncertainties in the Characterisation of the CK Source Zone. *Epistemic uncertainties that are common to multiple source zones such as seismogenic thickness are discussed in Subsection 5.14.5.4.(c).* 5.14-172

Figure 5.14-70 Rose Diagram Showing the Orientation of Major Structures and Structural Trends Within the CK Source Zone. *The diagram was developed by measuring the average orientation of faults and structural trends within the CK source zone*.....5.14-174

Figure 5.14-71 Logic Tree Summarising the Epistemic Uncertainties in the Characterisation

of the NAM Source Zone. 5.14-176

Figure 5.14-72 Rose Diagram Showing the Orientation of Major Structures and Structural Trends within the NAM Source Zone. *The diagram was developed by measuring the average orientation of faults and structural trends within the NAM.* 5.14-178

Figure 5.14-73 Overview of the Fault Sources Included in the SSC Model, With Alternative Coordinates for KNG and AFZ Highlighted. 5.14-180

Figure 5.14-74 Summary of Earthquake Recurrence Relationships for the Fault Sources Included in the SSC Model 5.14-180

Figure 5.14-75 Logic Tree for the Kango Fault Source (KNG), Including the Source-Specific Epistemic Uncertainties. *Epistemic uncertainties that are common to multiple fault sources are the magnitude-frequency distribution model and the b-value, discussed in Subsection 5.14.5.4.(c)* 5.14-183

Figure 5.14-76 Map Showing Three Alternative Lengths for the KNG. *Dashed blue line represents a distance of 320 km from the site, which is indicated by the red star.* ...5.14-183

Figure 5.14-77 Logic Tree for the AFZ Fault Source, Including the Source-Specific Epistemic Uncertainties. *Epistemic uncertainties that are common to multiple fault sources are the magnitude-frequency distribution model and the b-value, discussed in Subsection 5.14.5.4.(c)* 5.14-187

Figure 5.14-78 Logic Tree for the GAM Fault Source, Including the Source-Specific Epistemic Uncertainties. *Epistemic uncertainties that are common to multiple fault sources are the magnitude-frequency distribution model and the b-value, discussed in Subsection 5.14.5.4.(c)* 5.14-192

Figure 5.14-79 Logic Tree for the PLET Fault Source, Including the Source-Specific Epistemic Uncertainties. *Epistemic uncertainties that are common to multiple fault sources are the magnitude-frequency distribution model and the b-value, discussed in Subsection 5.14.5.4.(c)* 5.14-194

Figure 5.14-80 Topographic Profiles Showing the Morphology of the Seafloor Across the Plettenberg Fault (*Reference 5.14.254*). *The Late Glacial Maximum (LGM) shoreline is expressed as a planed surface at a depth of ~125 m or slightly lower. East-west-trending seafloor ridges observed at depths of between ~100 m and 125 m are interpreted to be aeolian dunes formed during the LGM, or possibly much older Pleistocene/Pliocene aeolianites.* 5.14-197

Figure 5.14-81 Logic Tree for the WOR Fault Source, Including the Source-Specific Epistemic Uncertainties. *Epistemic uncertainties that are common to multiple fault sources*

are the magnitude-frequency distribution model and the b-value, discussed in Subsection 5.14.5.4.(c) 5.14-198

Figure 5.14-82 Location of 1969 Ceres Aftershocks (*red dashed line*) relative to the Groenhof and Worcester Faults *(Modified from Reference 5.14.249)*. 5.14-199

Figure 5.14-83 Map Showing Locations of Fault Corridor Study Areas (*outlined in black*) Investigated to Assess the Seismogenic Probability of the Baviaanskloof, Coega, Kouga, and Cape St Francis Faults. 5.14-201

Figure 5.14-84 Unfaulted Tg Surface at Site M2.60 (*Reference 5.14.258*). The Unconformity Between the Tg Surface and Underlying Palaeozoic Bedrock (*dashed yellow line*) is Unfaulted. 5.14-204

Figure 5.14-85 Summary Diagram Showing Correlations of Pliocene and Quaternary Marine Terraces from West of Mossel Bay to East of Port Elizabeth Based on Hanson *et al.* (*Reference 5.14.186*). *The locations of the Eastern Coega Fault and Cape St Francis Fault at the coastline are shown.* 5.14-205

Figure 5.14-86 Peak Ground Acceleration (PGA) Values (*blue triangles*) Recorded on Soil Sites During the Magnitude 6.0 Earthquake that Occurred in Parkfield, California, in September 2004, Plotted as a Function of Distance, and Compared with Predictions From a Californian GMPE. *The predicted PGA values are shown for the median values and for one and two standard deviation above and below the logarithmic mean. Figure adapted from Reference 5.14.269*. 5.14-209

Figure 5.14-87 Site Amplification Functions for Generic V_s Profiles, Anchored to the V_{s30} Values Indicated, Relative to a Very Hard Rock Condition (*Reference 5.14.124*). ...5.14-211

Figure 5.14-88 Fourier Spectra Site Effect Operators Obtained by Multiplying Site Amplification Operators for Various Sites With a Kappa Filter (*Reference 5.14.120*). 5.14-211

Figure 5.14-89 Comparison of the Target V_s profile with Selected Profiles and the Average V_s From Kgaswane *et al*. (*Reference 5.14.150*).....5.14-213

Figure 5.14-90 Data Compiled From Various Studies for Pairs of V_{s30}-κ_0, and Three Correlations Proposed Between These Two Parameters (*Reference 5.14.273*). 5.14-215

Figure 5.14-91 Final V_s-Kappa Adjustments for the Three Backbone GMPEs (*indicated by colours*) and the Three Target Site Kappa Values (*symbols*).....5.14-216

Figure 5.14-92 Factors to Be Applied to Ground-Motion Amplitudes in Order to Account for an Increase in Stress Drop from an Initial Value of 100 Bar to a New Value of 200 Bar. 5.14-218

Figure 5.14-93 Logic-Tree for Median Ground Motions 5.14-219

Figure 5.14-94 Intensity Residuals Calculated for the IDPs From the 1969 Ceres and 1976 Koffiefontein Earthquakes. 5.14-221

Figure 5.14-95 Sammon's Map of the GMC Median Models (*green, red and purple*) and the South African (*pink/salmon, orange and light blue*) and CEUS (*dark blue*) Stochastic Equations for Spectral Accelerations at Periods above 0.1s, of M_w 5-6.5, and Distances of 20 to 50 km. 5.14-223

Figure 5.14-96 Comparison of Distance Attenuation from the Vs-Kappa Adjusted Backbone GMPEs for Sa(1.0s) (*blue*), the South African Stochastic Models (*red*) and a Suite of GMPEs in Current Use in the Central and Eastern US (*grey*). *The curves are for a scenario defined by the following parameters: V_{s30}=620m/s and M_w 6.5.* 5.14-225

Figure 5.14-97 (a) Median Shear-Wave Velocity Profile (b) Associated Standard Deviation. 5.14-226

Figure 5.14-98 Examples of Simulated Shear-Wave Velocity Profiles.....5.14-227

Figure 5.14-99 Median Shear-Wave Velocity and σ_{lnVs} Profiles of Simulated Shear-Wave Velocity Profiles. 5.14-228

Figure 5.14-100 Simulated Modulus Reduction (*upper*) a and Damping (*lower*) Curves. 5.14-230

Figure 5.14-101 Scenario Spectra for AFE = 10^{-4}, 10^{-5}, and 10^{-6} Used as Input Into the Site Response Analyses 5.14-231

Figure 5.14-102 (a) Computed Amplification Factors for 100 Monte Carlo Simulations and the AFE 10^{-5} LF Scenario Spectrum (b) Standard Deviation of the Natural Logarithm of AF (σ_{lnAF}). 5.14-232

Figure 5.14-103 Ratios of Surface-to-Bedrock Spectral Accelerations at Various Mean Annual Exceedance Frequencies 5.14-233

Figure 5.14-104 Values of Single-Station phi ($\boldsymbol{\phi ss}$) and Ergodic phi ($\boldsymbol{\phi}$) for Different Regional Data Sets (*Reference 5.14.268*). 5.14-235

Figure 5.14-105 Different Components of the Epistemic Standard Deviation. $\boldsymbol{\sigma Vs\kappa}$ is the standard deviation implicit in the median logic tree branches for the Vs-kappa correction. $\boldsymbol{\sigma lnAF}$ is a preliminary estimate of the standard deviation of the site amplification function. These two standard deviations are combined in the $\boldsymbol{\sigma epi, site}$ term. The blue line represents a minimum target value for the epistemic uncertainty in the site term chosen by the GMC TI

team. The red line ($\delta\phi S2S$) is the additional component to single-station within-event standard deviation needed to reach this target 5.14-237

Figure 5.14-106 Schematic Representation of the Sigma Logic-Tree.....5.14-238

Figure 5.14-107 Active MASW Results and Inferred Dispersion Curve Corresponding to the Fundamental Mode at the HVD Seismograph Station 5.14-246

Figure 5.14-108 Shear-Wave Velocity Profile, and Associated Error Bounds, Inferred for the HVD Seismograph Station From the Dispersion Curve Shown in *Figure 5.14.107*. *Note the starting value on the x-axes. The V_{s30} value from this profile is 2 750 m/s.*.....5.14-247

Figure 5.14-109 Calculated Mean HVSR for the HVD Seismograph Station Calculated From 138 Recordings at This Location. *The thinner blue lines correspond to ±1 standard deviation. The horizontal black and red lines indicate ratios of unity and 2.0 respectively; HVSR with a pronounced peak (usually meaning that it passes the horizontal red line) to the left of the vertical red line would be typical of soil or soft rock sites.* 5.14-247

Figure 5.14-110 Phases of a SSHAC Level 3 PSHA, Indicating the Role of Technical and Process Review by the PPRP (*Reference 5.14.297*). *Items in normal fonts are processes, those in italic are products. Thick outlines indicate elements for which there are formal QA requirements.* 5.14-251

Figure 5.14-111 V_s-Kappa adjustment Factors developed by Frank Scherbaum (*blue*) for the Model of Abrahamson & Silva (*Reference 5.14.129*), and the Interpolated Values at the Thyspunt PSHA Response Periods (Peter Stafford). *The three curves, consistently from top to bottom are the factors for the target Kappa of 0.001, 0.003 and 0.005. Vertical grey lines denote the Thyspunt PSHA periods.* 5.14-253

Figure 5.14-112 Surface Response Spectra Calculated by STRATA and Shake91 for Linear Elastic (LE) and Equivalent-Linear (EQL) Analyses.....5.14-254

Figure 5.14-113 Mean Hazard Curves obtained for the Fault sources Using FRISK88® (*solid curves*) and *OpenQuake-engine* (*dashed curves*). *The sources are identified in Figure 5.14.73 (Subsection 5.14.5.4.(e)); the selected parent GMPE of the GMC logic-tree branch used in each case is indicated in parentheses: AC10 – Akkar and Çağnan (Reference 5.14.134), AS08 – Abrahamson and Silva (Reference 5.14.129), CY08 – Chiou and Youngs (Reference 5.14.132).* 5.14-257

Figure 5.14-114 Hazard Curves for Sa(0.10s) Obtained for the Various Source Zones (see *Figure 5.14.52*; *Subsection 5.14.5.4.(d)*) and GMPE Combinations Using FRISK88® (*solid curves*) and *OpenQuake-engine* (*dashed curves*). See Caption of *Figure 5.14.113* for Details. 5.14-258

Figure 5.14-115 Hazard Curves Obtained for the Host ECC Source (see *Subsection 5.14.5.4.(d) i*) Using FRISK88® (*solid curves*) and *OpenQuake-engine* (*dashed curves*) for Different Combinations of GMPE and Response Period (See Caption of *Figure 5.14.113* for Details). 5.14-258

Figure 5.14-116 Overview of Steps Involved in a PSHA. *Adapted from Reference 5.14.307.* 5.14-263

Figure 5.14-117 Example of a Simple Logic Tree for a Site-Specific PSHA (*Reference 5.14.311*). *The first three nodes from the left correspond to the SSC model, the final node is the GMC model. The numbers in the final column are the total weight, or probabilities, associated with the hazard curve obtained combining the branches leading to that end point, obtained from the product of the individual branch weights.*.....5.14-265

Figure 5.14-118 Mean Hazard Curves for Sa(0.10s) at the Bedrock Elevation and the Contributions from Individual Seismic Sources 5.14-270

Figure 5.14-119 Mean Hazard Curves at Six Different Oscillator Periods (*labelled on each plot*), Showing the Relative Contributions From All of the Area Source Zones and All of the Fault Sources Grouped Together.....5.14-271

Figure 5.14-120 The Mean Hazard for Sa(1.0s) Due to the ECC Source Using the Full SSC Logic-Tree Compared With the Results That Would Be Obtained Using Each Mmax Branch Alone.....5.14-273

Figure 5.14-121 The Mean Hazard for Sa(0.10s) Due to the ECC Source Using the Full SSC Logic-Tree Compared With the Results That Would Be Obtained Using Each of the *b*-value Branches Associated with the Mmax = 7.1 Branch Alone. 5.14-273

Figure 5.14-122 Mean Hazard Curves for Sa(0.01s) Obtained With the Full Logic-Tree and Assuming That Each of the Three Backbone GMPEs Was Used As the Sole Model. 5.14-274

Figure 5.14-123 Mean Hazard Curves for Sa(1.0s) Obtained With the Full Logic-Tree and Assuming That Each Of the Three Backbone GMPEs Was Used as the Sole Model.....5.14-274

Figure 5.14-124 Overall Mean Hazard Curve for Sa(2.0s) and the Conditional Mean Hazard Curves Obtained Using Each of the Sigma Logic-Tree Branches Alone 5.14-275

Figure 5.14-125 Disaggregation for Sa(0.10s) at an AFE of 10^{-5}.....5.14-277

Figure 5.14-126 Mean and Fractile Hazard Curves for Sa(0.20s) at the Bedrock Elevation 5.14-288

Figure 5.14-127 Mean Hazard Curves Calculated at the Bedrock Elevation 5.14-289

Figure 5.14-128 Mean Hazard Curves Calculated at the Surface Elevation 5.14-289

Figure 5.14-129 Uniform Hazard Spectra at the Deep Bedrock Level 5.14-290

Figure 5.14-130 Uniform Hazard Spectra at the Surface Elevation Level.....5.14-290

Figure 5.14-131 Predicted Values of the Control Period Defining the Start of Constant Displacement Plateau, From Seismological Theory, for Various Combinations of Magnitude and Stress Drop 5.14-291

Figure 5.14-132 Uniform Hazard Spectra at the bedrock (*dashed*) and Surface (*solid*) Elevations for AFEs of 10^{-4} and 10^{-5}, and the Resulting GMRS.....5.14-292

Figure 5.14-133 Horizontal and Vertical GMRS at the Surface Elevation 5.14-294

5.14 SEISMIC HAZARD

5.14.1 Introduction

This section of this Site Safety Report (SSR) discusses the ground motion hazards, due to natural tectonic earthquakes, for the planned nuclear installation at the Thyspunt site. The hazard associated with earthquake-induced ground shaking has been analysed through a formal multiple-expert assessment following the requirements and specifications of a Level 3 study as defined by the Senior Seismic Hazard Analysis Committee (SSHAC; ***References 15.4.1*** and ***15.4.2***). This approach involves a comprehensive database compilation supplemented by some new data collection activities, followed by the evaluation of these data by a team of experts. The process leads to a characterisation of the seismic hazard at the site including identification, quantification and integration of all sources of uncertainty. The entire process, including three formal workshops and eight structured working meetings, is reviewed by an international panel of experts for compliance with process requirements, completeness of the data and models considered in the evaluation, and rigorous technical justification for all decisions taken in developing the input to the seismic hazard calculations. The purpose and intent of the SSHAC guidelines is to ensure that the seismic characterisation captures the centre, the body and the range of technically-defensible interpretations (the CBR of the TDI) of all the available data, methods and models. A Level 3 study provides an enhanced assurance that the full distribution reflecting the centre, body and range has been captured in the earthquake hazard analysis. The centre, body and range collectively reflect both what is known about seismicity and earthquake hazard at the site and the uncertainty associated with the characterisation of the seismic hazard that cannot be eliminated with the currently available data and state-of-knowledge about the region and the site. The nature of the different types and sources of uncertainty, and how these are quantified and accounted for in the assessment of the earthquake hazard is explained in ***Subsection 5.14.7***.

The compilation and evaluation of the databases are described in ***Subsection 5.14.4*** and the integration process leading to the development of seismic source characterisation (SSC) and ground motion characterisation (GMC) models in ***Subsection 5.14.5***. Monitoring is addressed in ***Subsection 5.14.6*** and the Management System adopted for the seismic hazard assessment in ***Subsection 5.14.8***. The final results in terms of representation of the seismic hazard in terms of ground shaking due to tectonic earthquakes are presented in ***Subsection 5.14.9***.

Other earthquake-related hazards are addressed elsewhere in this SSR. An analysis of the potential for surface faulting at this site and the surrounding area,

which could affect the feasibility of construction and safe operation of the nuclear installation, is included in ***Section 5.13*** (Geology). Other phenomena of permanent ground displacement (e.g. liquefaction, slope instability, subsidence and collapse) are discussed in ***Section 5.15*** (Geotechnical Characterisation) and seismically-induced flooding that is related to foundation safety is discussed in ***Section 5.10*** (Hydrology) and ***Section 5.13*** (Geology).

5.14.2 Purpose and Scope

The geological, seismological and engineering characteristics of a nuclear installation site and its environment need to be investigated with sufficient scope and level of detail to permit evaluation of the acceptability of a proposed site (***Reference 5.14.3***). Therefore ***Section 5.13*** (Geology), this ***Section 5.14*** (Seismic Hazard) and ***Section 5.15*** (Geotechnical Characterisation) of the SSR are developed in a complementary manner to provide sufficient information to support estimates of the vibratory ground-motion hazard, as well as the hazard due to permanent deformation of the ground (*e.g.*, fault rupture) at or near the surface, and to permit adequate engineering solutions to be confirmed and potential geological and seismic threats at the proposed site.

The specific purpose of this ***Section 5.14*** is to present the characterisation of the seismic hazard at the Thyspunt site in terms of earthquake-induced ground shaking and to demonstrate the adequacy of this characterisation both in terms of the quality and completeness of the data on which it has been based and also in terms of the identification, quantification and systematic incorporation of uncertainties. In accordance with international best practice and with regulatory guidance and requirements (***Subsection 5.14.3***), the assessment of seismic hazard at a nuclear site must begin with investigations that include *inter alia*:

- extensive review of existing literature, historical reports and other datasets;
- remote sensing and geophysical interpretation;
- geological, geomorphological, palaeoseismological and geophysical investigative techniques and interpretation;
- laboratory dating of geological samples;
- compilation of instrumental and historical records of earthquake occurrences in the region under study;
- compilation of instrumental recordings of seismic motions, which can serve to characterise the strength, propagation and attenuation of seismic waves in the region;

© Eskom 2026/Rev 0a

- field measurements to characterise the dynamic properties of the near-surface geo-materials at the site.

Furthermore, the studies that are to be considered for the evaluation of the seismic hazard of a proposed site include *inter alia*:

- studies that augment and complement previous studies related to geological, geomorphic and chronostratigraphic studies of key geological surfaces, their ages and relation to faults (*e.g.*, marine terraces, alluvial terraces);

- studies that investigate rates of uplift and deformation, such that potential capable faults can be identified or precluded within the site vicinity;

- focused tectonic geomorphic, studies of Quaternary-age fault behaviour as appropriate and fault-specific studies constraining recency, maximum earthquake magnitude (Mmax), and slip rate;

- retrieval of previously undiscovered historical accounts of earthquake effects, and investigations of the completeness and reliability of such non-instrumental sources of earthquake information in different areas and historical periods;

- compilation of a catalogue of intensity data points from earthquakes for which instrumentally-determined source parameters to calibrate relationships for the estimation of historical (pre-instrumental) earthquake magnitudes and locations, as well as providing additional insight into ground-motion characteristics in the region.

As is discussed in ***Subsection 5.14.4*** (Approach to Evaluation), all of the above studies have been conducted for the Thyspunt site and the results of those studies have led to the SSC and GMC models described in ***Subsection 5.14.5*** (The SSHAC Framework). These models are combined in a probabilistic seismic hazard analysis (PSHA; ***Subsection 5.14.7.2***) leading to the final seismic hazard characterisation presented in ***Subsection 5.14.9.3***.

The scope of this section is restricted to the evaluation of the vibratory ground-motion hazard at the site resulting from tectonic earthquakes. Other earthquake-related hazards, such as surface deformation due to fault rupture, seismically-triggered slope instability and liquefaction of surface deposits are addressed in ***Section 5.13*** (Geology) and ***Section 5.15*** (Geotechnical Characterisation). Earthquake-related flooding is addressed in ***Section 5.9*** (Oceanography and Coastal Engineering) for tsunami and ***Section 5.10***

(Hydrology and Hydraulics) for dam breaks, with inputs from ***Section 5.13*** (Geology).

In terms of the scope of the seismic hazard assessment, the focus is exclusively on ground shaking resulting from natural earthquakes of tectonic origin. Earthquakes induced or triggered by anthropogenic activities, such as mining, quarrying and reservoir impoundment, are excluded from the earthquake catalogue (***Subsection 5.14.4.4***) and are not considered in the PSHA. These earthquakes do not follow the same spatial or temporal patterns as the seismic activity of tectonic origin and would require separate models to be developed to predict their future occurrence. However, the earthquakes generated by anthropogenic causes are all of small magnitude and occur only in close proximity to the location of the activity. In the case of both mineral mines in South Africa and reservoir schemes in Lesotho are both sufficiently remote from the Thyspunt site to render their contributions to the ground shaking hazard.

There is also a potential new source of anthropogenically-generated earthquakes in South Africa as a result of applications for permits by several oil and gas companies to perform hydraulic fracturing in the Karoo region in order to extract shale gas. Shale gas is believed to be present in the Permian shales of the Ecca formation and in particular the Whitehill shale formation that persists across most of the basin. Reserves of technically recoverably shale gas in South Africa have been estimated at 13.7 trillion m^3 (***Reference 5.14.4***) although others claim that the reserves are not yet proven (***Reference 5.14.5***). There are numerous examples of induced or triggered seismicity associated with fluid injection and hydrocarbon extraction, but the magnitudes of the earthquakes have generally been small. The experience database in hydraulic fracturing for shale gas is still limited since this energy technology has only become widespread in recent years, but there has been more extensive experience with hydraulic fracturing for enhanced geothermal systems. The largest earthquake associated with geothermal systems occurred in 1982 in the Geysers field in California, with a magnitude M_L 4.6 (***Reference 5.14.6***). The only two other occurrences of earthquakes of magnitude 4.0 or greater have been recorded in enhanced geothermal systems (***Reference 5.14.7***). Davies *et al.* (***Reference 5.14.7***) report that the earthquakes expected to occur in association with hydraulic fracturing for shale gas are smaller than those caused by enhanced geothermal systems, although they note that the triggering of an incipient earthquake as a result of fluids entering an existing fault plane and the resulting reduction in effective stress leading to earthquakes. The largest earthquake that has been reported to be associated with hydraulic fracturing for shale gas occurred in Canada and had a magnitude of M_L 3.8 (***Reference 5.14.7***). Davies *et al.* (***Reference 5.14.7***) report two other cases of earthquakes associated with hydraulic fracturing for shale gas, in the US and

UK, with magnitudes of 2.8 and 2.3 respectively. They also note that these are the only three documented cases of seismicity from among hundreds of hydraulic fracturing operations for shale gas.

The closest approach of any of the areas covered by permit applications for shale gas exploitation is just over 100 km north of the Thyspunt site. Excluding the possibility of a tectonic earthquake being triggered by the fluid injection intersecting a major fault, the earthquakes that could be expected on the basis of previous global experience are expected to be small and, significantly, below the minimum earthquake magnitude (M_w 5) considered in the PSHA calculation (***Subsection 5.14.7.2***). Any earthquakes that did occur would have shallow focal depths comparable to the depths at which the shale gas reservoirs are found, which are estimated at between 2 and 4.5 km (***Reference 5.14.5***). Very shallow earthquakes, even though they may cause locally high amplitudes of ground shaking, will tend to attenuate very rapidly as a result of the nature of the rocks in the uppermost part of the crust. Additional assurance is given by the fact that there is very good evidence for induced seismicity occurring in very close proximity (< 10 km) to the location of the activity causing the earthquakes (***Reference 5.14.8***). These factors all suggest that induced seismicity from hydraulic fracturing in the Karoo is very unlikely to produce ground shaking of any consequence at the Thyspunt site. At the same time, this is a source of seismic activity that can be controlled, and greater assurance could be provided by limiting the closest operations to the Thyspunt site to greater distances and requiring shale gas extraction utilities to quantify the potential for induced seismicity as part of their license to operate. An indispensable requisite would be for all shale gas operations to undertake studies, such as seismic reflection, to identify the presence of faults in the vicinity of injection wells to minimise the possibility of triggering larger earthquakes. Guidelines for mitigating the seismic risks associated with these operations have been developed in some countries (*e.g.*, ***Reference 5.14.9***) and these could be adopted or adapted in South Africa.

The assessment and control of seismic hazard due to hydraulic fracturing, however, is beyond the scope of this ***Section 5.14***, and regulation of these activities should take account of any potential for induced or triggered seismicity affecting safety-critical facilities in South Africa.

5.14.3 Regulatory Framework

This subsection presents the regulatory requirements applicable to the characterisation of the vibratory ground-motion hazard at the site, and the guidelines and regulatory documents adhered to in order to meet these requirements.

5.14.3.1 National Nuclear Regulator (NNR) Requirements

The only national regulations specifically relevant to a seismic hazard study for an SSR site are the *Regulations on Siting of New Nuclear Installations* (***Reference 5.14.10***). The regulations broadly applicable to seismic hazard are:

- Requirements for the siting of new nuclear installations, regulation 3 (2)(a): 'be supported by a Site Safety Report containing such information as listed in Regulation 5…'

- Factors to be considered when evaluating sites, regulation 4: 'Factors to be considered in the evaluating an application for nuclear installation site licence will include….'

- Regulation 5 (3): 'The characteristics of the site relevant to design assessment, risk and dose calculations, include inter alia: (a) *external events*…'

The above regulations are not specific in terms of seismic hazard and were therefore not adopted as the basis for the seismic hazard assessment other than to identify the fundamental objective of the Thyspunt PSHA as being to provide a seismic characterisation of the site as the basis for the relevant chapter of the SSR. Consistent with this objective, the study has taken cognisance of the requirements and regulations of the NNR, particularly RD-0024 (***Reference 5.14.11***). However, RD-0024 addresses generic safety criteria and general concepts of risk assessment for nuclear installations, and does not provide any detailed guidance on specific requirements for seismic characterisation of a nuclear site. For this reason, it was decided to adopt the guidelines of the USNRC (United States Nuclear Regulatory Commission) for the conduct of a site-specific PSHA for nuclear facilities, as explained in ***Subsection 5.14.3.3***. More recently, the NNR has issued a draft position paper on the requirements for external events for new nuclear installations. This position paper, PP-0014 (***Reference 5.14.12***), has a strong focus on seismic hazards and is generally consistent with ASCE 43-05 (***Reference 5.14.13***)—which is itself consistent with the adopted USNRC guidelines—and specifically permits the use of these guidelines to define the design basis ground motions. Although in draft format, the final results of the Thyspunt site-specific PSHA are entirely consistent with and satisfy the requirements of the relevant parts of PP-0014.

NNR Requirement Documents relevant to Quality Assurance and to verification of calculations were adhered to throughout the project, as discussed in ***Subsection 5.14.8***.

© Eskom 2026/Rev 0a

5.14.3.2 IAEA Requirements and Guidelines

The International Atomic Energy Agency (IAEA) issues documents referred to as the Safety Standards Series, which specify information at three different levels: (1) Safety Fundamentals, which are broad governing principles that express the safety goals for nuclear installations; (2) Requirements, which must be met to demonstrate compliance with safety goals; and (3) Safety Guides, which provide more specific detailed guidance on the studies and steps required to satisfy the safety requirements.

As established in the Safety Requirements publication, *Site Evaluation for Nuclear Installations* (***Reference 5.14.14***) establishes the following requirements, cited *ad verbatim*:

- "*The seismological and geological conditions in the region and the engineering geological aspects and geotechnical aspects of the proposed site area shall be evaluated*." (para. 3.1.)

- "*The hazards associated with earthquakes shall be determined by means of seismotectonic evaluation of the region with the use to the greatest possible extent of the information collected*." (para. 3.3.)

- "*Hazards due to earthquake induced ground motion shall be assessed for the site with account taken of the seismotectonic characteristics of the region and specific site conditions. A thorough uncertainty analysis shall be performed as part of the evaluation of seismic hazards*." (para. 3.4.)

- "*The potential for surface faulting (*i.e. *the fault capability) shall be assessed for the site . . .*" (para. 3.5.)

The guidelines of the IAEA relevant to fulfilling the above requirements in terms of seismic hazard assessment of nuclear sites are contained in Specific Safety Guide SSG-9 *Seismic Hazards in Site Evaluation for Nuclear Installations* (***Reference 5.14.15***). Chapters 8 and 9 of this Safety Guide address the hazard of surface fault rupture, which is addressed in ***Section 5.13*** of this SSR. The remainder of SSG-9 provides guidance on the conduct of seismic hazard assessment, in terms of database compilation (Chapter 3) and development of appropriate models for seismic sources (Chapter 4) and for ground-motion prediction (Chapter 5). The adherence to the USNRC guidelines for PSHA (***Subsection 5.14.3.3***) for the Thyspunt site satisfies all of the IAEA specifications for a site-specific PSHA (Chapter 6). The only element of SSG-9 that was not followed in the Thyspunt PSHA is the suggestion in paragraph 5.1 to conduct both PSHA and deterministic seismic hazard assessment (DSHA):

> "*The ground motion hazard should preferably be evaluated by using both probabilistic and deterministic methods of seismic hazard analysis. When both deterministic and probabilistic results are obtained, deterministic assessments can be used as a check against probabilistic assessments in terms of the reasonableness of the results, particularly when small annual frequencies of exceedance are considered.*"

As explained in ***Subsection 5.14.7***, DSHA does not provide an effective framework for the incorporation of all elements of aleatory variability associated with the occurrence and characteristics of future earthquakes and the ground motions that these may generate. Comparisons between the results of PSHA and DSHA are potentially confusing and highly misleading, and serve little purpose, especially at the low annual exceedance frequencies (10^{-4} to 10^{-5}) relevant to the definition of design motions for nuclear installations.

5.14.3.2 USNRC Regulatory Guidance

In order to satisfy the intentions of the NNR requirements, it was decided to adopt methodologies for the conduct of the PSHA and definition of the seismic loading that are recognised and approved by the US Nuclear Regulatory Commission. Specifically, for guidance as to how a PSHA study should be executed and an acceptable approach to defining design basis ground motions for nuclear facilities, the following two documents were adopted for the Thyspunt PSHA:

- Regulatory Guide 1.208. *A Performance-Based Approach to Define the Site-Specific Earthquake Ground Motion* (***Reference 5.14.3***)
- ASCE/SEI 43-05 *Seismic Design Criteria for Structures, Systems, and Components in Nuclear Facilities* (***Reference 5.14.13***)

These documents are widely regarded as representing international best practice and as stringent procedures for conducting analyses of the seismic loading to be considered in the design of nuclear power plants. As noted in ***Subsection 5.14.3.1***, these guidelines for the development of a ground motion response spectrum (GMRS) through site-specific PSHA are also fully consistent with the draft position paper of the NNR *Considerations of External Events for New Nuclear Installations* (***Reference 5.14.12***).

Regulatory Guide 1.208 (***Reference 5.14.3***) specifies the areas in which seismological and geological investigations are to be conducted for a site (***Subsection 5.14.4.2***), including the characterisation of the dynamic properties of the site itself (***Subsection 5.14.4.8***), and the procedures to conduct the PSHA calculations (***Subsection 5.14.7.2***), including incorporation of all

uncertainties (***Subsection 5.14.9.2***). For the incorporation of dynamic site response into the assessment of the ground shaking (***Subsection 5.14.5.5.(b)***), the approach adopted was that referred to as Approach 3, for which the basic guidance is provided in ***Reference 5.14.16***.

In terms of characterisation and inclusion of uncertainties, the PSHA study was conducted in the framework of a SSHAC Level 3 process (***Reference 5.14.1***), which is specifically recommended in RG 1.208 (***Reference 5.14.3***). The SSHAC Guidelines (***Reference 5.14.1***) provide guidance on conducting a PSHA in terms of database compilation, expert assessments of the available data, and an integration process to develop SSC and GMC models for input to the PSHA that reflect both the best estimates and the associated uncertainties. The SSHAC Guidelines specify four levels of study, with the complexity increasing from 1 through to 4. Only Level 3 and 4 studies are considered suitable for nuclear sites, but USNRC makes no distinction between Levels 3 and 4 in terms of regulatory assurance, which may be viewed as alternatives for achieving the same objectives—namely "*capturing the center, the body and the range of technically-defensible interpretations of the available data, methods and models*" (***Reference 5.14.2***)—rather than Level 4 being in any sense a superior approach to Level 3.

The essential steps in a SSHAC Level 3 study are listed in ***Table 5.14.1***, all of which must be fulfilled to qualify as being a SSHAC Level 3 study. As noted in the table, a key requirement is the conduct of both technical and process review by a Participatory Peer Review Panel (PPRP). The final letter from the PPRP must express unqualified concurrence that the project fully satisfied all of these steps in terms of both adhering to the SSHAC process and meeting all of the technical requirements, in order to demonstrate that the SSHAC Level 3 requirements were met. As discussed in ***Subsection 5.14.5.5***, the PPRP for the Thyspunt PSHA did give complete endorsement that all of these steps were fully satisfied in the project, which therefore indicated adherence to both the guidelines for conducting a SSHAC Level 3 study (***Reference 5.14.2***) and the guidelines for a site-specific PSHA (***Reference 5.14.3***).

© Eskom 2026/Rev 0a

Table 5.14.1
Summary of Essential Steps in a SSHAC Level 3 Study
(*Reference 5.14.2*)

Essential Step	Discussion
1. Select SSHAC Level	• **Document decision criteria and process**
2. Develop Project Plan	• **Includes project organization and all technical and process activities**
3. Select project participants	• **Includes all management, technical, and peer review participants**
4. Develop project database	• **Includes compilation of existing, available data** • **Can include focused new data collection** • **Data dissemination to all evaluator experts (Level 4) or TI Team members (Level 3)**
5. Hold workshops (minimum of three)	**Workshop topics:** • **Hazard-significant issues and available data** • **Alternative interpretations** • **Feedback**
6. Develop preliminary model(s) and Hazard Input Document (HID)	• **Preliminary models developed prior to Feedback workshop** • **HID provides input to hazard calculations**
7. Perform preliminary hazard calculations and sensitivity analyses	• **Intermediate calculations should display the impact of elements of the expert models** • **Hazard calculations should show the significance of all elements of the models** • **Sensitivity analyses should include the contributions to uncertainties**
8. Finalize models in light of feedback	• **Feedback provides a basis for prioritizing and focusing the finalization process**
9. Perform final hazard calculations and sensitivity analyses	• **Should be conducted to develop the required deliverables for subsequent use of the hazard results**
10. Develop draft and final project report	• **Fundamental documentation of SSHAC process, technical bases, and results**
11. Participatory peer review of entire process	• **Periodic written reviews of key products and activities** • **Review of draft report** • **Final written review of technical evaluations and process used**

© Eskom 2026/Rev 0a

5.14.4 Approach

The fundamental goal of a SSHAC Level 3 process is to carry out properly and document completely the activities of evaluation and integration (***Subsection 5.14.5.3***), which are defined as follows:

Evaluation: The consideration of the data, models, and methods proposed by the larger technical community that are relevant to the hazard analysis.

Integration: Representing the centre, body, and range of technically defensible interpretations in light of the evaluation process.

The dual aspects that define a SSHAC Level 3 process are conducted by *evaluator* and *integrator* experts, roles filled by the same individuals in SSHAC Level 3 studies who form the Technical Integration (TI) Teams (***Subsection 5.14.5.1***). The *evaluator expert* is an individual or a team that objectively examines available data, diverse models, challenging their technical bases and underlying assumptions, and, where possible, testing the models against observations. A SSHAC Level 3 study begins with an identification and compilation of available data, models, and methods. These are then evaluated by the evaluator experts in an objective manner for their quality and consistency with all available information within the larger technical community, as well as for their potential applicability to the region and site under study.

Informed by their consideration of the data, models, and methods during the evaluation phase, the *integrator experts* then build models that capture the centre, body, and range of technically defensible interpretations. The models are typically logic trees that capture the knowledge and uncertainties in key seismic source characterisation (SSC) and ground motion characterisation (GMC) conceptual models and parameter values.

This subsection describes the development of the project databases, for both the SSC and GMC components of the PSHA model, and their evaluation.

5.14.4.1 Database Compilation and Evaluation

The first stage of a site-specific PSHA must be the compilation of databases of all available information and studies that could be relevant to the characterisation of the seismic hazard at the site. This information may include digital databases of seismological and geophysical information, published papers and reports, unpublished reports, geological maps, geotechnical information from site investigations, among others. One of the roles of the PPRP is to ensure that the databases compiled are complete, and that no key dataset or reference has been omitted from consideration by the TI Teams. All

© Eskom 2026/Rev 0a

of the databases compiled for the project are owned by Eskom but responsibility for their storage and maintenance also resides with the Council for Geoscience.

The SSHAC Level 3 process provides a framework for assessing the distribution of epistemic uncertainty that is associated with the best estimate models (***Subsection 5.14.7.3***). The best estimate models are informed by the evaluation of the databases and the epistemic uncertainty by the assessment of the limitations and incompleteness of the databases. Epistemic uncertainty is generally reduced by gathering and evaluating additional data, for which reason it is desirable to not only compile existing data but also to undertake activities specifically focused on collecting new data. A number of such activities were initiated for the Thyspunt PSHA, all of which are summarised in this Section:

- Geological investigations, including fault corridor and marine terrace studies, and dating of geological samples from boreholes, trenches and outcrops (***Subsection 5.14.4.3, Section 5.13***).

- Retrieval of instrument earthquake information from global and national agencies, and archive-based studies to retrieve historical accounts of earthquake effects in South Africa (***Subsection 5.14.4.4***).

- Collection of descriptions of felt earthquake effects and their interpretation to develop a database of macroseismic intensities (***Subsection 5.14.4.4***).

- Collection and processing of weak-motion recordings from seismographs to generate Fourier amplitude spectra and then perform stochastic inversions to estimate parameters representing the characteristics of earthquake sources, wave propagation paths and near-surface wave transmission in South Africa (***Subsection 5.14.4.6***).

- In situ measurements of shear-wave velocity in the uppermost layers at the Thyspunt site to characterise the dynamic properties of the rock horizon to which the ground shaking hazard is referenced (***Subsection 5.14.4.4***).

The evaluation of the databases of new and existing data is undertaken through focused study of the TI Teams, informed additionally by presentations made by Resource and Proponent Experts (***Subsection 5.14.5.1***) at the project Workshops. Each TI Team conducts four Working Meetings during the course of the project, and the evaluation work is a major focus of these meetings (***Subsection 5.14.5.2***). At the first Working Meeting, data sources are identified and criteria for their evaluation in the specific context of the project established. At the second Working Meeting the focus is entirely on evaluation, and at the third Working Meeting the process transitions from evaluation to integration.

© Eskom 2026/Rev 0a

The TI Teams must document their evaluations to the satisfaction of the PPRP. This means that they needed to provide adequate technical justification for excluding certain data, models and methods, on the basis of being of unreliable quality, irrelevance to the site, or redundant in terms of adding no additional information or constraint. Similarly, the TI Teams are obliged to document choices for data, models and methods that are employed in the development of the SSC and GMC models and the relative weight that each of these is given in the final PSHA calculations. The final letter of the PPRP expressed concurrence that both of these objectives were met (***Subsection 5.14.5.5***).

The approaches to evaluation adopted by the SSC and GMC TI Teams as a result of dealing with very different databases. There is a very large database relevant to the development of the SSC model including geological studies, geophysical datasets, geological maps, and an extensive range of publications on tectonics, crustal structure and seismicity. In order to efficiently organise this very large database, the SSC TI Team produced Data Summary Tables, listing the following information:

- Author
- Title
- Year
- Description and relevance to SSC
- Indication of whether the data are relied upon in the SSC model or not
- Discussion of potential data use
- GIS (Geographic Information System) code
- Originator

The description of the potential relevance to SSC is important because it provides the reader with an indication of exactly what aspects of the paper might relate to SSC technical issues. The very nature of the seismic source characterisation activity and the models and parameters that comprise an SSC model are multidisciplinary and involve a wide range of potential data sources. Thus, it is not unusual for a particular journal article on, say, the regional geologic setting to not contain much information that is pertinent to SSC. Likewise, some papers are based on data that are of poor quality or that have been superseded by subsequent studies. In these cases, the potential relevance to SSC would be included in the table to document the fact that the

data were considered, but the answer to whether the data were relied upon for the SSC model would be “no.” In those cases where the data were relied upon, a data evaluation table was developed, as described below. A “discussion of potential data use” in the data summary table provides the data evaluator a location to provide his/her perceptions of the aspects of the data that might be useful to developing the SSC model, as well as other observations that may be relevant (*e.g.*, quality and vintage of the data, limitations and uncertainties in the data).

The development and interval review by the TI Team of the Data Summary Tables served to identify those data sources that were retained for use in development of the SSC model, and simultaneously to document the reasons for excluding other sources. Data Evaluation Tables were then developed for only those data that were actually relied upon in the development of the SSC model. Therefore, the tables are designed to document the aspects of the SSC model that were informed by the particular data set and the judgments by the TI Team expert evaluators of the degree of reliance placed on the data and the quality of the data. The Data Evaluation Tables include the following information:

- Naming of the table according to whether it applies to a seismic source zone, fault source, the entire SSC model, or a particular methodology used in the development of the SSC model
- Author
- Title
- Year
- Relevant Information, judged according to give different attributes that are ranked in terms of their usefulness in constraining a feature of the SSC model (earthquake recurrence; maximum earthquake magnitude; fault characteristics such as style of rupture, orientation; seismogenic probability of faults).
- Use for SSC: Quality and Reliance ratings for each of the following:
    - Fault or Seismic Source Characteristics
        - Seismogenic Probability
        - Seismic Source or Fault Geometry
        - Recurrence/Recency & Slip Rate/Recurrence Intervals
        - Mmax
    - Future Earthquake Characteristics

© Eskom 2026/Rev 0a

- Rupture Geometry (strike, dip)
- Style of Faulting
- Seismogenic Thickness

The full set of Data Summary Tables and Data Evaluation Tables are included in Appendix 5 of the PSHA report (***Reference 5.14.17***).

The evaluation approach used by the GMC TI Team was different since the region- and site-specific databases available for the ground motion characterisation were limited. Data summary reports were developed for the three key GMC databases: intensity database (***Subsection 5.14.4.4***), weak-motion database (***Subsection 5.14.4.4(l)***), and geotechnical site data (***Subsection 5.14.4.4(n)***), each referenced in the relevant subsections below. The TI Team evaluated these datasets and made decisions regarding the degree to which they could be depended upon in developing the final GMC model. These decisions were justified to the satisfaction of the PPRP in the final PSHA report (***Reference 5.14.17***).

As a consequence of the relatively sparse local and regional datasets available to characterise the GMC model, greater emphasis was placed on evaluation of approaches in terms of methods and existing models. In particular, the GMC TI Team needed to make a careful evaluation of the most appropriate approaches to developing ground-motion prediction equations (GMPEs) for South Africa, and also how to incorporate the influence of the dynamic response of the site itself (***Subsection 5.14.4.5***). For these aspects of the GMC evaluation process, white papers and technical notes were produced by TI Team members and circulated for comment and discussion, followed up in all cases by presentation and discussion in Working Meetings and Workshops. These interim documents were also all transmitted, for information, to the PPRP as they were prepared. These documents were not included as appendices to the main PSHA report but rather were distilled into the main body of the report. The main example of this approach was the evaluation of published GMPEs and the selection of equations for use in the GMC model for the Thyspunt PSHA (***Subsection 5.14.4.5***).

5.14.4.2 Geographical Areas of Investigation and Data Compilation

As discussed in ***Subsection 5.14.4.3***, the geoscientific investigations and compiled databases considered in the Thyspunt PSHA aims to provide increasingly detailed information as they proceed from the regional level down to the site. To this effect, the radii recommended by the USNRC in ***Reference 5.14.3*** were adopted, as defined below and summarised in ***Figure 5.14.1***:

- **Site Region**: area within 320 km of the site;
- **Site Vicinity**: area within 40 km of the site;
- **Site Area**: area within 8 km of the site;
- **Site Location**: area within 1 km of the site.

However, based on experience from PSHA projects in other Stable Continental Regions (SCRs), the SSC model described in ***Subsection 5.14.5.4*** was developed over a region considerably wider than the 320 km radius, in order to include all potentially hazard-significant sources.

Consequently, the region considered for the compilation of the geological database (***Subsection 5.14.4.3***), earthquake catalogue (***Subsection 5.14.4.4***), and intensity database (***Subsection 5.14.4.4***) covers most of South Africa south of 28° latitude south, as illustrated in ***Figure 5.14.2***.

Additionally, in order to characterise the dynamic properties of the rock horizon to which the ground shaking hazard is referenced, geotechnical investigations were performed at the site location (1 km radius, as described in ***Subsection 5.14.4.2***).

5.14.4.3 Geological Investigations and Database

The results of the geological investigations described in ***Section 5.13***, as well as published geological information relevant to the area of investigation described in ***Subsection 5.14.4.2***, were evaluated as described in ***Subsection 5.14.4.1*** using Data Summary Tables and Data Evaluation Tables. These tables are included in Appendix 5 of ***Reference 5.14.17***. Implications of these results for the identification and characterisation of the seismic sources included in the SSC model developed as part of the Thyspunt PSHA are discussed in ***Subsection 5.14.5.4***.

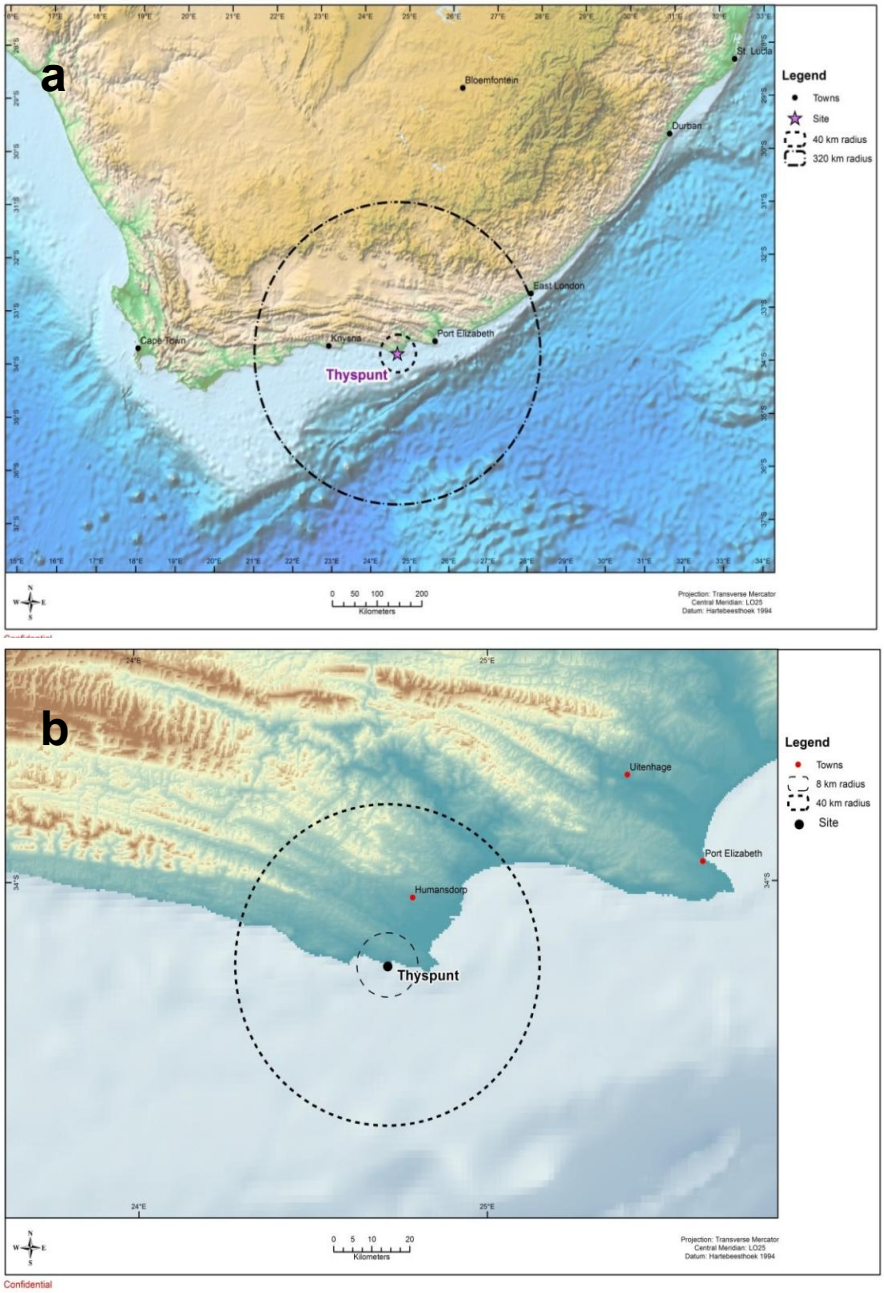


Figure 5.14-1(a) Locality Map Showing the 320 km-radius Site Region and 40 km-radius Site Vicinity. (b) Locality Map Showing the 40 km-radius Site Vicinity, 8 km-radius Site Area and 1 km-radius Site Location (represented by the dot)

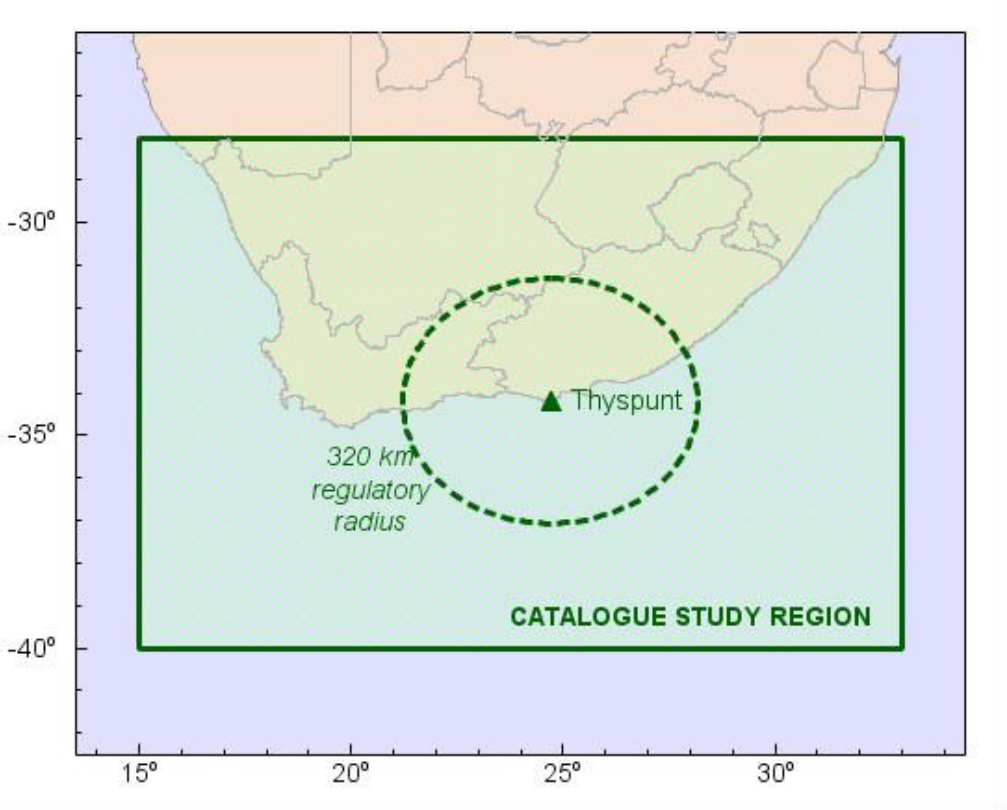


Figure 5.14-2
Extent of Catalogue Study Region Used in the Development of the SSC Model (*green rectangle*). The Site Region as defined by USNRC (*Reference 5.14.3*) is also shown for reference (*dashed green circle*).

5.14.4.4 Seismological Database and Earthquake Catalogue

This subsection presents the seismological database, focusing in particular on the earthquake catalogue developed for the Thyspunt PSHA project (***Reference 5.14.18***). Following a section defining the scope of the catalogue compilation study (***Subsection 5.14.4.4.(a)***), the data sources for this compilation are summarised in ***Subsection 5.14.4.4.(b)***. Subsequent sections go on to discuss the determination of source parameters and associated uncertainties, focusing on origin time and epicentral locations (***Subsection 5.14.4.4.(c)***), hypocentral depth (***Subsection 5.14.4.4.(d)***), and focal mechanisms (***Subsection 5.14.4.4.(e)***). This is followed by an overview of the catalogue analysis steps undertaken, comprising the homogenisation of

© Eskom 2026/Rev 0a

magnitudes (***Subsection 5.14.4.4.(f)***), catalogue declustering (***Subsection 5.14.4.4.(g)***) and the assessment of catalogue completeness (***Subsection 5.14.4.4.(h)***). The full technical details can be found in Chapter 6 of ***Reference 5.14.17***, as well as in ***Reference 5.14.18***.

a) Catalogue Region and Parameter Limits

As noted in ***Subsection 5.14.4.2***, the boundaries of the region for which the seismicity catalogue is compiled have to be selected in such a way as to cover the geographic extent of the source zones that have been identified as potential contributors to the seismic hazard at the site. The seismicity catalogue documented therefore covers the region stretching from latitude 40° to 28° south, and longitude 15° to 33° east (***Figure 5.14.2***).

A lower limit of $M_L \geq 3.0$ is chosen for the catalogue development because of the greater abundance of data at lower magnitudes that provides constraint both on spatial distribution of seismicity in South Africa and on recurrence relations. A prior assessment of completeness suggests that the record becomes very incomplete below the M_L 3.0 threshold except for the most recent time period, thus limiting the usefulness of data below this threshold. Additionally, below this limit the uncertainties associated with source parameters become very large, counteracting the benefits of increasing the sample size. Finally, small-magnitude earthquakes have also been shown to exhibit different behaviour in terms of magnitude conversions than those in the magnitude range of interest to the Thyspunt PSHA project. Selected sets of data from events with $M_L < 3.0$ have nevertheless been used for specific exploratory analyses where the aforementioned issues did not arise and an increased sample size was desirable.

As discussed in ***Subsection 5.14.2***, the Thyspunt PSHA project is concerned exclusively with seismic hazard from tectonic sources, hence any seismic events related to human activity, such as explosions, quarry blasts, rockbursts and mining-related events, as well as events related to reservoir impoundment, are excluded from the present study. The catalogue developed in the present report covers all known events in the region of study up to and including December 2011.

b) Earthquake Data Sources

Seismicity catalogues are generally compiled from multiple primary data sources, often updating and cross-checking previous compilations. The following paragraphs discuss the sources of information available for the extraction of earthquake parameters for the region of interest, since these were used in the reappraisal of the source parameters of the events in the catalogue.

© Eskom 2026/Rev 0a

Instrumental seismic recording in southern Africa started with the installation of a Milne instrument at Cape Town in 1899, followed by a Weichert instrument in Johannesburg in 1910 (***References 5.14.19 and 5.14.20)***. REDACTED [redacted] Instruments in neighbouring countries, such as the instrument at Windhoek (Namibia) and the network of instruments run and maintained by the Goetz Observatory in Bulawayo (Zimbabwe), also contributed to early source parameter determinations for South African earthquakes. A map of early seismograph stations is shown in ***Figure 5.14.3***.

Following the occurrence of the M_w 6.2 Ceres earthquake on 29 September 1969, a temporary network of five mobile stations was deployed in the epicentral region (***Reference 5.14.21***). The network recorded more than 2,000 events during its first five weeks of operation. The number of stations was later reduced to three for operational reasons. This deployment enabled the accurate location of 125 events. Unfortunately, with the exception of the largest aftershocks, the location parameters of these events are only provided in graphical form by Green & Bloch (***Reference 5.14.21***), and therefore they are most useful in terms of delimiting the causative source of this event. The non-inclusion of these events in the Thyspunt PSHA project catalogue ultimately has little impact on the final hazard, since they are dependent events that would have been removed at the declustering stage (see ***Subsection 5.14.4.4.(g)***).

In addition to the SANSN permanent network, a temporary array of fifty-five broad-band instruments was deployed at 81 sites between April 1997 and July 1999 as part of the South African Seismic Experiment (SASE; ***Reference 5.14.23***). The average inter-station distance is of the order of 100 km, which significantly increases station density compared to the permanent network. All tectonic events with M_L 3.0 recorded by the SASE are already included in the CGS catalogue, and therefore, these data contribute no additional events to the catalogue compilation. However, the waveforms recorded as part of this experiment have been used in the determination of additional source parameters such as focal depth (***Subsection 5.14.4.4.(d)***) and focal mechanisms (***Subsection 5.14.4.4.(e)***), as well as direct M_w estimates from regional moment tensor solutions (***Reference 5.14.24***; ***Subsection 5.14.4.4.(f)***).

© Eskom 2026/Rev 0a



As a consequence of its location at the southern tip of Africa, South Africa has few neighbour states that are in a position to contribute readings that will help constrain locations of regional events. A number of networks from neighbouring countries nevertheless contributed data to the Thyspunt PSHA project catalogue. However, from the establishment of the SANSN onwards, the importance of these stations becomes increasingly marginal due to the densification of the local network, and their contributions are essentially through inclusion in the listings of global agencies.

© Eskom 2026/Rev 0a

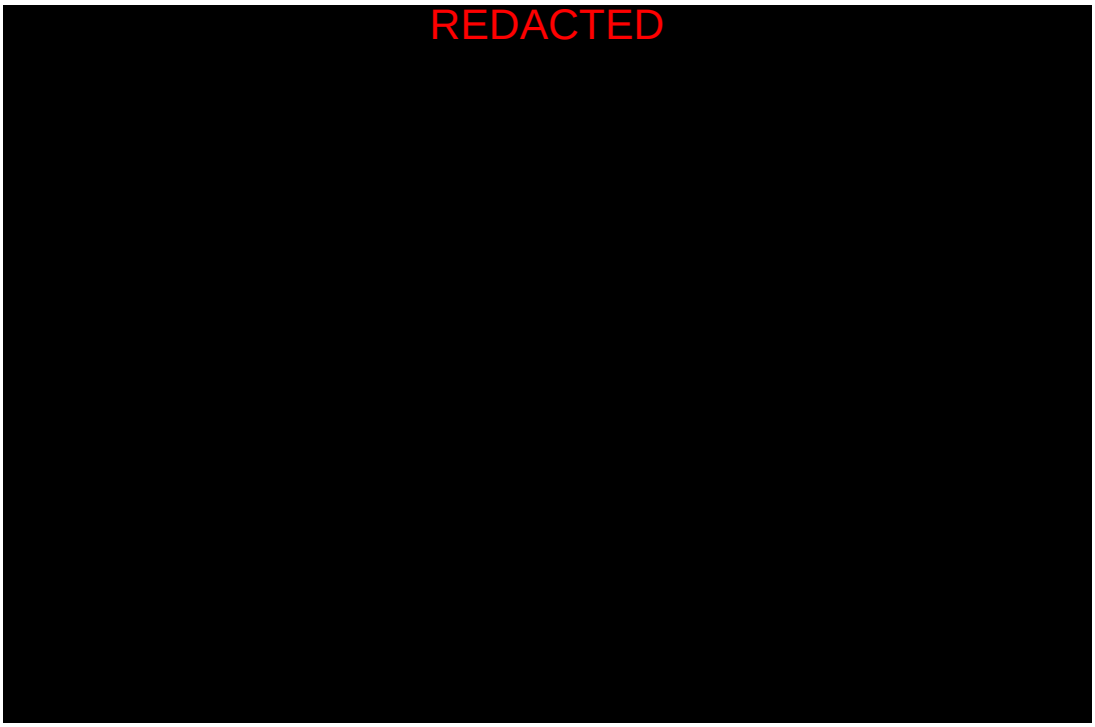


Figure 5.14-4 Map of the SANSN Network (*Reference 5.14.20*).

The South African stations regularly contributed to the International Seismological Summary (ISS), which constitutes one of the main sources of information for instrumentally recorded earthquakes in the time span between its inception (1918) and its transformation into the International Seismological Centre (ISC) in 1964. The phase readings listed in the ISS bulletins scanned and made available as part of the EUROSISMOS project were retrieved and used in the checking of the few events contained in this compilation that fall within the catalogue study region. The ISS bulletins also provide the data for the re-analyses of events by Gutenberg & Richter (***Reference 5.14.25***) and Engdahl *et al.* (***Reference 5.14.26***).

The ISC was founded in 1964 as a continuation of the ISS, independently from but concurrently with the establishment of the World-Wide Standard Seismograph Network (WWSSN). Its mission was to continue the gathering of instrumental recordings worldwide, previously undertaken by the ISS, in order to calculate source parameters that are well constrained. The ISC Bulletin typically presents the source parameters calculated by the individual agencies contributing the data, followed by a reappraised solution considering all available data calculated by ISC staff. For the southern Africa region, the ISC Bulletin lists source parameters from 1964 onwards, contributed mainly by the CGS (or its predecessor, the Geological Survey) and the Goetz Observatory at

© Eskom 2026/Rev 0a

Bulawayo (BUL). The National Earthquake Information Center (NEIC) of the US Geological Survey also contributes solutions for larger events, but these have been found to be less well-constrained and hence less reliable than the ISC solutions as far as the southern Africa region is concerned.

Other organisations, including the Geological Survey Department of Zambia, and the Geophysical Survey of the Russian Academy of Sciences, also occasionally contribute sets of source parameters, but their solutions are generally unreliable due to the limited number of recordings used, as well as the large distance from the source at which these recordings were obtained. In consequence, only solutions contributed by BUL or reappraisals by the ISC are considered in the present study as alternatives to those determined by the CGS. As noted above, most of the solutions published by the NEIC are included in the ISC bulletin. Exceptions include the most recent data (2009-2011), for which the ISC solutions had not yet been reviewed, but solutions were published by NEIC. Also, the determinations circulated by the US Coast and Geodetic Survey (USCGS) contributed international teleseismic solutions in particular for the period prior to 1964.

In addition to the systematic compilations of instrumentally recorded data released by the operating networks described above, a number of regional earthquake catalogues based on instrumental recordings, but also on reports of felt effects, have been compiled. These cover in particular the historical (pre-1900) and early instrumental (1900-1969) periods. A number of local contemporary reports of historical earthquakes have been collected by South African researchers over time, which appear in interpreted form in subsequent studies. For the region of interest, additional material of this nature has been collected by Albini (***Reference 5.14.27***) within the Thyspunt PSHA project. The Albini study (***Reference 5.14.27***) is the main source of information in terms of intensity data points (IDPs) for the historical part of the catalogue. Data for events with instrumental source parameters were similarly compiled by Midzi *et al.* (***Reference 5.14.28***), who also reviewed published isoseismal maps, as discussed in more detail in ***Subsection 5.14.4.4***.

Seismological compilations (***References 5.14.29 to 5.14.39***), whether contemporaneous with the events compiled, or collated at a later date, are the principal contributors of data up to the 1960s-1970s. An important aspect to acknowledge is the overlap and interdependencies that exist between these different compilations, as noted in ***Reference 5.14.27***, in order to avoid treating related assessments as if they were independent. Additionally, a number of monographs about more notable events were published by the staff of the South African Geological Survey. These monographs focus predominantly on macroseismic information, but also present instrumental phase readings when

available. They include the monograph about the 31 December 1932 off Cape St Lucia event by Krige & Venter (***Reference 5.14.40***), the monographs about the 12 and 16 January 1936 Swaziland and Fauresmith events by Krige (***Reference 5.14.41***), as well as the Krige & Maree compilation (***Reference 5.14.42***) of individual studies of 11 events having occurred in South Africa between 1938 and 1944.

In addition to the source parameters determined as part of routine seismological monitoring, seismological studies investigating specific events in more detail are sometimes carried out. For the Thyspunt PSHA project catalogue region, such studies are limited to monographs of the 1969 Ceres event and its aftershock sequence (*e.g.*, ***Reference 5.14.21***). Most of these studies are summarised in a special publication of the Geological Survey (***Reference 5.14.43***). A recent re-analysis of the teleseismic data available for the 1969 Ceres event (***Reference 5.14.44***) supplements these studies. ***Reference 5.14.45*** contains monographs on three African events that have occurred in the stable part of the continent, including the 1 July 1976 Koffiefontein event. Similarly, a number of studies focussing predominantly on larger sub-Saharan African events (***References 5.14.46 to 5.14.51***) or investigating the characteristics of Stable Continental Region (SCR) earthquakes (***References 5.14.52 and 5.14.53***) provide source parameters for the 1969 Ceres and 1976 Koffiefontein events. A number of studies investigate the source parameters of a few moderate South African events (***References 5.14.54 to 5.14.56 and Reference 5.14.24***), but often have a strong focus on mining-related events.

c) Epicentral Locations

Using the data sources described in the previous section, a catalogue was compiled using the following rules. In the case of multiple determinations of the source parameters (date, location and magnitude), all possible options were reviewed and the solution considered the best constrained and/or the best documented was retained as the preferred solution, with the remaining data informing parameter uncertainty. This methodology was adopted in preference to a more algorithmic approach, since the number of events with multiple solutions is relatively small, which renders an event-by-event analysis less impractical than in the case of large datasets. Furthermore, choice of the "best-quality" solution among different available options relies on criteria that have been found to vary strongly from one event to another, thus hampering the development of general rules, particularly with a limited number of events. Note that in terms of location, this section focuses on epicentral coordinates, and hypocentral depth is addressed separately in ***Subsection 5.14.4.4.(d)***. Given the relatively sparse nature of the recording network, depths of earthquakes in

South Africa are not well resolved, and are in most cases fixed in the calculations in order to obtain a more robust estimate of the epicentral coordinates.

The catalogue was divided into the following four subsets to reflect the varying nature of the information on which the estimation of source parameters and magnitude values is based:

- **Historical period**: This subset includes all events reported that occurred prior to the installation of the first seismograph in South Africa at the Royal Observatory of the Cape of Good Hope in Cape Town in August 1899. The assessment of source parameters for this subset is based exclusively on macroseismic data. Existing macroseismic information was supplemented by the detailed investigation of Albini (***Reference 5.14.27***).

- **Early instrumental period**: This subset includes all events reported in the study region starting with the first instrumentally recorded South African earthquake, which occurred in Cape Town on 15 September 1899 until the earthquake that occurred near Heidelberg on 11 September 1969. For the time period covering the years 1899 to 1949, the approach adopted is very similar to that of the historical period, with the Albini study (***Reference 5.14.27***) contributing a further 15 events to this subset of the catalogue. For larger events, macroseismic information is in some cases supplemented by instrumental information from the two South African seismographs and early global networks.

- **Ceres sequence**: The Ceres sequence, defined for the purposes of this study as the 29 September 1969 main shock and its aftershocks until and including the 28 September 1971 event, which is the last event listed in the compilation by Theron (***Reference 5.14.33***).

- **Modern instrumental data**: This subset includes all events other than the Ceres sequence (as defined above) recorded since the establishment of the SANSN in 1970.

For the Eastern and Southern Cape region, the authoritative primary data source is the Albini study (***Reference 5.14.27)***, which was undertaken specifically for the Thyspunt PSHA project. This study contributes individual studies of 15 events for the time period up to 1899, including seven newly identified events. As well as adding these new events, the Albini study (***Reference 5.14.27)*** also highlighted a number of doubtful events, and identified a few occurrences of fake events. A further 15 events in the time period 1900-1949 were also studied. For events whose occurrence was confirmed, the information is provided in the form of a field of intensity data

points (IDPs) which were analysed using third-generation techniques to determine source parameters (location and magnitude) along with their associated uncertainties.

The MEEP2 software (***Reference 5.14.57***) is used for this purpose. This software includes implementations of four different methods for source parameter determination:

- The Bakun & Wentworth approach (***Reference 5.14.58***), which relies on the specification of an intensity prediction equation (IPE) giving macroseismic intensity as a function of magnitude and distance.

- The Macroseismic Estimation of Earthquake Parameters (MEEP) approach (***Reference 5.14.57***), which combines the Kövesligethy equation (***Reference 5.14.59***) with the Frankel model (***Reference 5.14.60***). The former relates the average spacing of isoseismal contours with regional attenuation properties, and the latter provides a physically based model allowing the estimation of magnitude from the felt area.

- A centroid method based on the BOXER algorithm of Gasperini *et al.* (***Reference 5.14.61***), which determines the optimal epicentral location based on the spatial distribution of the IDPs with the highest intensity levels.

- Finally, a method based on pairwise comparisons of IDPs, which favours epicentral locations closer to the IDP with higher intensity.

Following the assessment that the South African macroseismic intensity database (***Reference 5.14.28; Subsection 5.14.4.4.(e)***) was too sparse to allow the derivation of a robust local calibration through regression, the French-SCR IPE of Bakun & Scotti (***Reference 5.14.62***) was adopted for the calibration of the Bakun method in the MEEP2 software, following a review of published IPEs. This IPE was also found to be consistent with South African isoseismal areas inferred from IDPs and isoseismal maps. The MEEP method was then calibrated such as to be compatible with the Bakun & Scotti IPE (***Reference 5.14.62***). The centroid and pair-wise approaches do not require additional calibration parameters for the determination of locations, and rely on the same parameters as the MEEP approach to determine magnitudes using the Frankel formulation (***Reference 5.14.60***).

For the events analysed using the MEEP2 software, uncertainties in location were assessed by considering the spatial distributions of bootstrapped epicentres generated by the software for each of the different methods, combined with weights reflecting the performance of each of the methods, as illustrated in ***Figures F-5.14.5*** and ***F-5.14.6***.

© Eskom 2026/Rev 0a

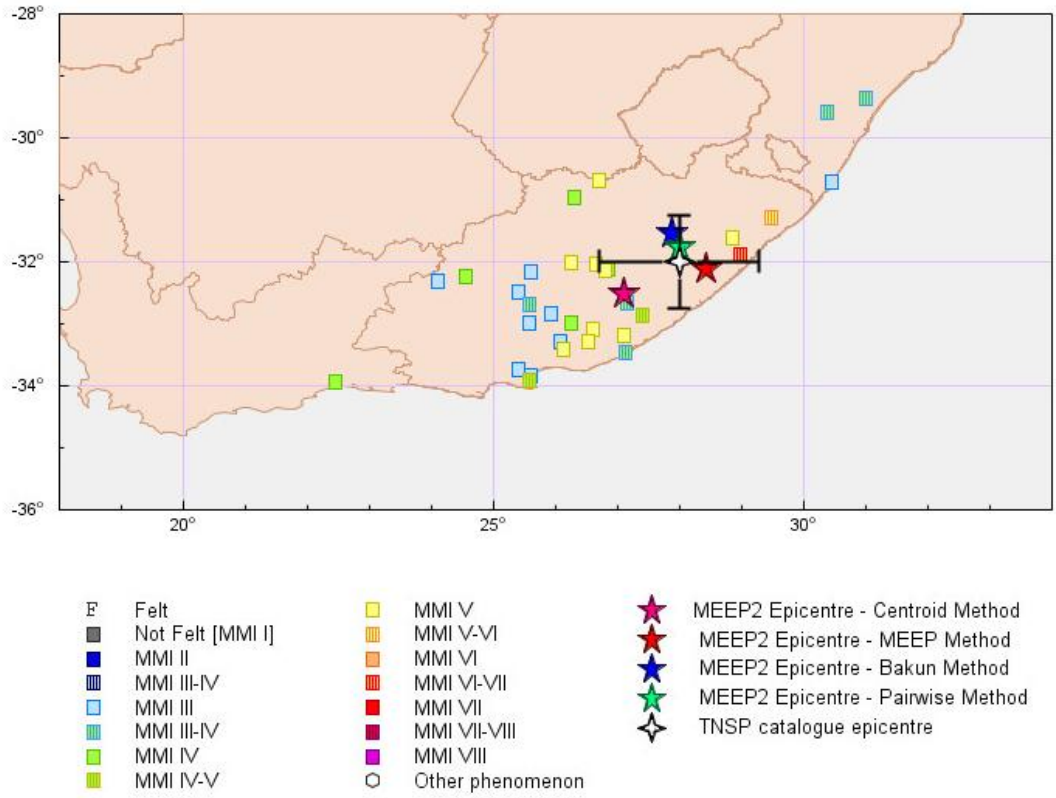


Figure 5.14-5 Alternative Epicentres Provided by the Various Approaches Implemented in the MEEP2 Software and Best Estimate Epicentre Adopted in the Thyspunt PSHA Study for the 21 May 1850 Event.

For all other events in the time period up to 1949, the epicentral locations listed in ***Reference 5.14.39*** were retained. These were based predominantly on the compilation by Finsen (***Reference 5.14.31***), supplemented by macroseismic locations from the studies by Krige & Maree (***Reference 5.14.42***), Theron (***Reference 5.14.33***) and De Klerk & Read (***Reference 5.14.35***).

For events occurring between 1949 and 1968, the locations determined by Oliver and his co-workers at the Bernard Price Institute (BPI) using the five-station Geological Survey network represent the preferred solutions for South African events when they are available. For some events, these solutions also considered the recordings on the Wiechert seismograph at the Union Observatory in Johannesburg. The quality of the solutions depends mainly on

the number of stations available, and thus increases with the magnitude of the event. It is noteworthy that the epicentral locations published in ***References 5.14.63 and 5.14.64*** and the BPI Seismological Bulletins include confirmatory macroseismic evidence where available, and that the authors include information regarding the quality of the solution.

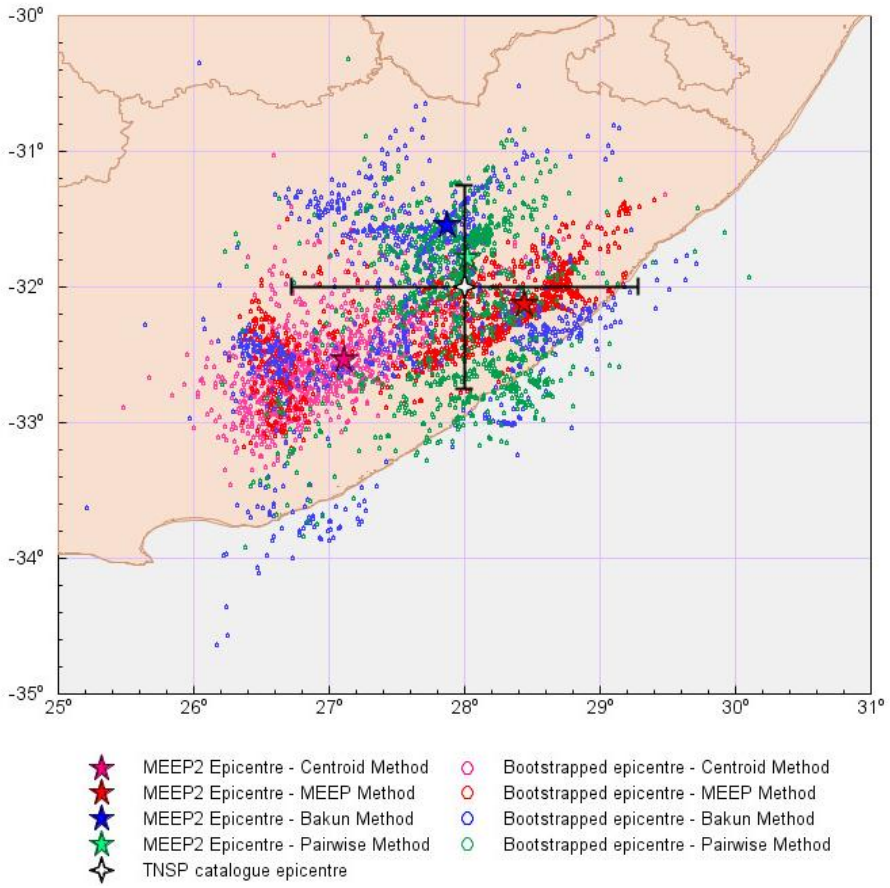


Figure 5.14-6 Bootstrapped Epicentres for the Various Methods Implemented in the MEEP2 Software, for the 21 May 1850 Event. The Location Uncertainties Are Based on the Spatial Distributions of these Bootstrapped Epicentres, with Event-Specific Weights Applied to Each Method.

Where additional macroseismic data was available from the compilation of De Klerk & Read (***Reference 5.14.35***) or other sources investigated as part of the compilation of the intensity database (***Subsection 5.14.4.4***), these data were

used as an additional check on the BPI instrumental location and uncertainty estimate.

The events of the 1969-1971 Ceres seismic sequence are treated separately as they are better documented, in terms of both instrumental and macroseismic information, than other similar-sized events from the same period (***References 5.14.21, 5.14.43 and 5.14.65***). Locations and magnitudes are primarily determined from instrumental data, but macroseismic observations are used to inform the selection of source parameters among available options.

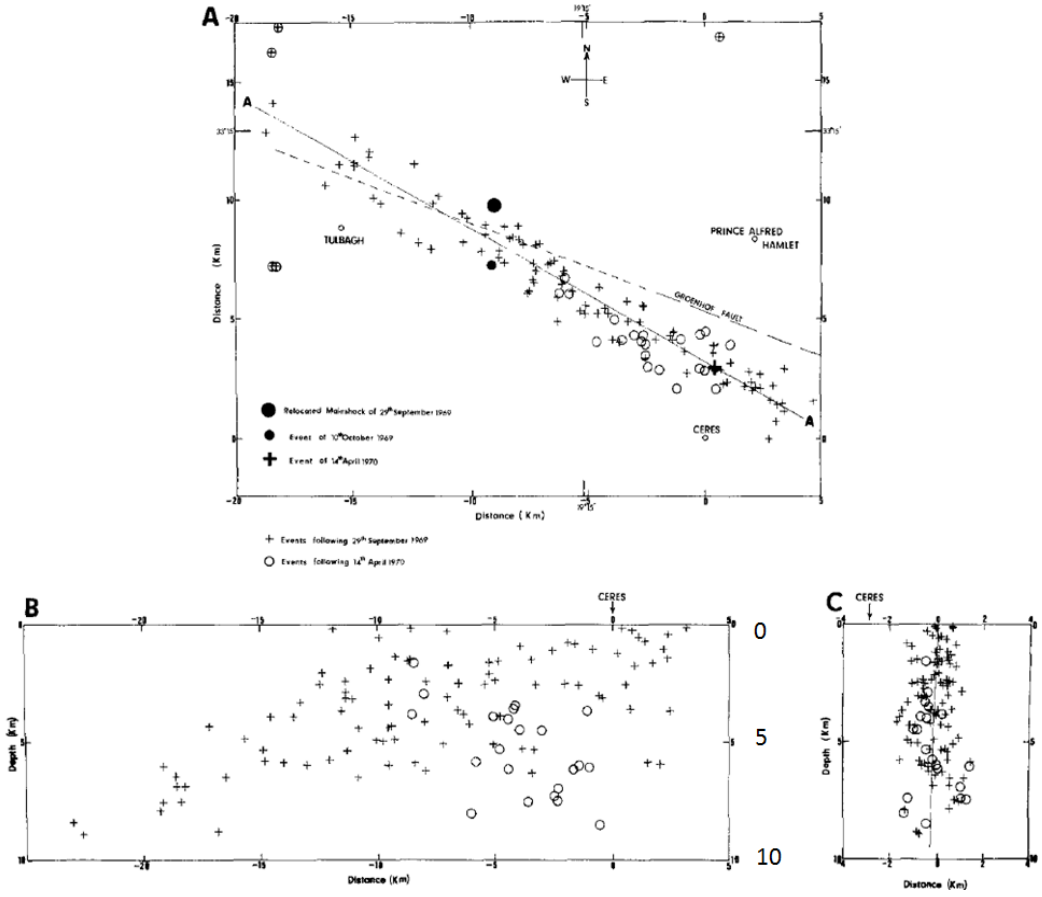


Figure 5.14-7 Locations of Aftershocks of the 1969 Ceres Event Determined from Recordings on a Temporary Local Network by Green & Bloch (*Reference 5.14.21*).

"A" is a map of aftershocks; "B" is a cross section along the length of the aftershock sequence; "C" is a cross section normal to the length of the aftershock sequence.

The vertical scale of the cross sections is 10 km.

Reference 5.14.21 presents the results of an aftershock study carried out by the BPI following the deployment of a temporary local seismograph network. As shown in ***Figure 5.14.7***, the aftershocks delineate a near-vertical structure with an orientation close to the strike of the mapped Groenhof Fault (see ***Subsection 5.14.5.4.(d) ii*** and ***Subsection 5.14.5.4.(e) v***).

Green & Bloch (***Reference 5.14.21***) use these results to determine the location of the main shock, which is constrained within 1-2 km and hence adopted in the present study. A report by the Goetz Observatory in Bulawayo (***Reference 5.14.65***) presents magnitude estimates ranging from 3.4 to 6.0 for 79 events of the Ceres sequence, from the 29 September mainshock until 6 December 1969. Epicentral locations are given for a subset of 34 of these events, which have been recorded by 4 or more stations. ISC locations have not been considered for the Ceres data as they have been found to be in contradiction with macroseismic evidence, which indicates that all larger aftershocks were felt most strongly in the Ceres-Tulbagh area. The poor location accuracy of the ISC solutions is thought to be linked to azimuthal biases resulting from a very uneven station distribution.

Locations and magnitudes for the period 1970-2011 are determined from instrumental data, but macroseismic observations are used in some instances to qualify the results. The primary source of information is the CGS database described above. Alternative solutions determined by the Goetz Observatory in Bulawayo (BUL) and by the International Seismological Centre (ISC) are available for most larger events (until 1993 for BUL, until 2008 for ISC). BUL also provides a number of additional events for the period from 1970 to 1983, for which no determinations are available from other agencies.

In the case of multiple solutions, the preferred solution would normally be the ISC solution, since it is calculated using additional data compared to the solutions provided by the individual networks, and thus better constrained. ISC solutions also have the advantage of systematically providing an estimate of the uncertainty associated with the location. However, many of the ISC solutions are significantly at odds with the macroseismic epicentre, in particular for events in the Ceres-Tulbagh region that occurred in the 1970s and early 1980s, for which the quality of the location is affected by the poor azimuthal distribution of the data, which is strongly biased to the northeast. Therefore, the following approach was adopted:

- If the ISC and CGS epicentral locations were significantly different, macroseismic information was used to determine the more credible solution;
- If no macroseismic information was available, or if the difference in location is small, the ISC solution was retained as it is of better quality (smaller

location uncertainty and azimuthal gap as a result of using a larger number of stations);

- In the case of inconsistent solutions, the phase data for the individual stations were checked to determine the solution most consistent with locally applicable travel-time curves (both in terms of P-waves and in terms of S-P intervals).

While location uncertainties are not directly incorporated into the PSHA, they nevertheless influence the SSC model development, in particular regarding the definition of source boundaries. For determinations based on instrumental data, the quality of the location depends critically on the number of stations, their distance to the source, as well as their azimuthal distribution. The best-constrained solutions are obtained from dense, close-in networks surrounding the source. With the exception of the local network deployed by Green & Bloch (***Reference 5.14.21***) to record aftershocks of the 1969 Ceres sequence, such recording conditions are generally not available for South African earthquakes of tectonic origin, for which determinations are generally based on determinations from fairly distant stations, with only 1 or 2 close-in stations.

Location uncertainties are routinely determined as part of the location process. CGS provides estimates in terms of latitude and longitude error, whereas ISC provides the dimensions of the major and minor axes of an error ellipse, S_{max} and S_{min}. The error ellipses for the events in the current dataset are mostly oriented NS or EW, hence the CGS and ISC location error parameters can be considered equivalent. For ease of comparison with the uncertainties determined from macroseismic data, which are expressed as radii, equivalent error radii are defined by taking the geometric mean of the two location error parameters. These equivalent error radii are then used as estimates of the location uncertainty. It should, however, be noted that due to lack of stations offshore the western and southern coasts, the error driving the uncertainty assignment is the longitude error for locations along the western coast, and latitude error along the southern coast.

Location uncertainties determined from macroseismic data were determined as discussed above for events analysed using the MEEP2 software, and assessed on the basis of the number, quality and spatial distribution of macroseismic information otherwise.

d) Hypocentral Depth

South African data on hypocentral depth are very limited, given that the sparse nature of the recording network requires the depth value to be fixed in routine determinations in order to obtain a stable estimate of the epicentral location.

The very few depth values available from larger South African events were reviewed, and supplemented within the Thyspunt PSHA project by additional depth determinations for 9 events using data from the temporary SASE array. These additional depth determinations were assessed by considering additional, depth-sensitive regional phases, using the synthetic-seismogram-based method of Ma & Atkinson (***Reference 5.14.66***). Additional depth determinations from reanalysis of the data recorded during the recent (2008-2010) seismic swarm at Augrabies were also included in the compilation.

The instrumental focal depth determinations of South African earthquakes reviewed as part of the development of the seismicity database are summarised in ***Figure 5.14.8***. Despite being limited in number, these data cover a number of locations across South Africa. Overall, they indicate shallow crustal depths in the range of 4–20 km. Determinations of depth using macroseismic data are hampered by the limited number of intensity observations close to the epicentre; however, exploratory analyses found that the ranges of depths compatible with the observations confirm the shallow focal depths found instrumentally.

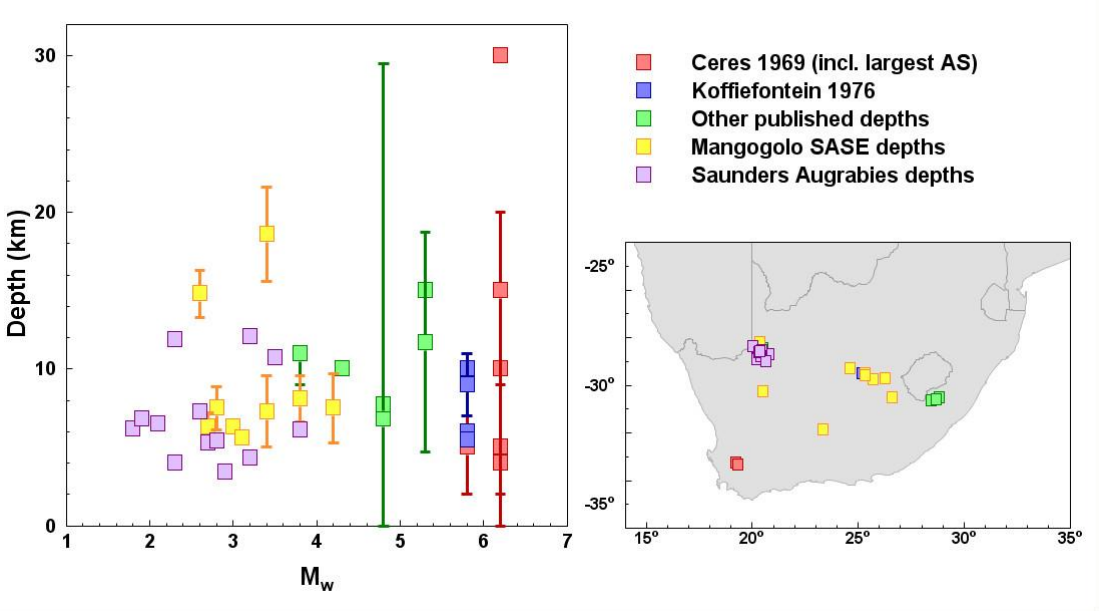


Figure 5.14-8 Summary of Instrumental Focal Depth Determinations of South African Earthquakes, Including Uncertainties Where Available.

e) Focal Mechanism Solutions

Another source parameter of interest for future earthquake characteristics (***Subsection 5.14.5.4.(a) iii***) is the focal mechanism, from which style-of-faulting and fault geometries of future earthquakes can be derived. The focal mechanism solutions including published focal mechanisms, as well as unpublished solutions recently developed at CGS using SANSN and SASE data were gathered. This compilation (***Figure 5.14.9***, see also ***Subsection 5.13.5.1.(d) i***; ***Table T-5.13.4***) includes 17 tectonic earthquakes with magnitudes M_w ranging from 3. to 6.2, as well as four moderate-magnitude (M_w > 4.0) mining events. The latter are included since they are related to slippage on pre-existing geological faults, and hence contain some information regarding the orientation of regional tectonic stresses, despite being anthropogenic in origin. Overall, events in the southwest (Ceres, events 1a-1g and 2) and the northwest (Augrabies, events 8 and 16-21b) of South Africa exhibit predominantly strike-slip faulting. Lesotho and neighbouring areas are characterised by normal faulting (events 4 and 10). In the Koffiefontein region (events 3a-3c, 13a-13b and 14), as well as the Free State (events 5-6) and Witwatersrand (events 7 and 12) gold mining areas, there is a mixture of normal and normal-oblique faulting.

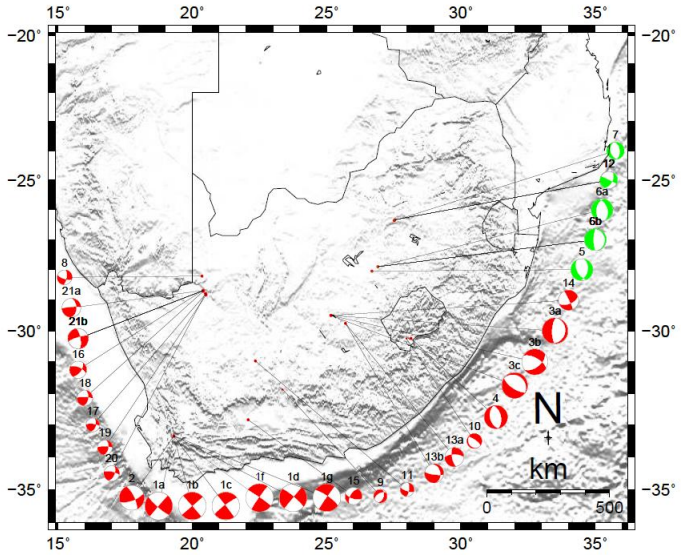


Figure 5.14-9 Summary of Earthquake Fault Plane Solutions for South Africa. Red and green "beach balls" are Focal Mechanisms for Tectonic and Mining Events, Respectively.

f) Homogenisation of Magnitudes

For a meaningful downstream utilisation of the catalogue, it is essential that the relative sizes of the earthquakes listed are derived in a consistent manner. The Thyspunt PSHA catalogue has been developed in terms of moment magnitude (M_w, ***Reference 5.14.67***) for compatibility with future calculations as part of the seismic hazard analysis, in particular to avoid conversion issues when using modern GMPEs formulated in terms of M_w. The use of a magnitude scale that does not saturate is also important in the selection and testing of source scaling relations.

There are, however, only a handful of earthquakes in the catalogue for which a value of M_w has been directly determined from the long-period part of the spectrum of available recordings through moment tensor inversion or wave-form modelling. These are summarised in ***Table T-5.14.2***. The limited number of such determinations is due to the rare occurrence of events large enough to allow a teleseismic determination, combined with the sparse nature of the local recording network, which usually yields insufficient data for a moment tensor inversion of local events. For the 4 February 1999 Koffiefontein event, Brandt & Saunders (***Reference 5.14.24***) determined a moment tensor solution using waveforms recorded by the temporary SASE array, which provided a much denser coverage than the permanent South African network.

Table 5.14.2
Events in Catalogue Region with Direct Estimates of M_w

Event	M_w	Study Type
1969-09-29 Ceres Mainshock	6.2	Moment Tensor from teleseismic data (*Reference 5.14.44*)
1970-04-14 Ceres Aftershock	5.8	Body-wave inversion (*Reference 5.14.49*)
1976-07-01 Koffiefontein	5.8	Body-wave inversion (*Reference 5.14.45*)
1986-10-05 Matatiele region	5.3	Global Centroid Moment Tensor (Harvard)
1999-02-04 Koffiefontein	3.8	Regional Centroid Moment Tensor *Reference 5.14.24*)
2011-12-18 Augrabies	4.3	Global Rapid Moment Tensor (USGS NEIC)

© Eskom 2026/Rev 0a

Additionally, estimates of M_w have been obtained for a set of events that occurred between 2006 and 2011, for which good-quality digital recordings were selected by A. Rietbrock and S. Drouet (***Reference 5.14.68***) to perform inversions using two different inversion methods in order to derive suites of parameters for the calibration of stochastic models considered as part of the GMC component of the project (see ***Subsection 5.14.4.5***). This dataset consisted essentially of weak-motion data, and extended beyond the study region considered for the catalogue compilation, also including mining-related events. The inversion process provided estimates of seismic moment M_0 obtained through fitting of the Fourier spectra of the selected records; these were converted to M_w using the Hanks & Kanamori relation (***Reference 5.14.67***), with the resulting values adopted as estimates of M_w for tectonic events falling within the catalogue compilation region. An excellent agreement was observed for the values obtained by the two methods for common events; where M_w estimates from both methods were available, the arithmetic mean of these values was used as the best estimate of M_w.

For those events for which no direct estimate of M_w is available, the primary references used in the compilation of the catalogue provide magnitudes in the following scales:

- Local magnitude, M_L
- Body-wave magnitude, m_b
- Surface-wave magnitude, M_S
- Magnitude determined by the Goetz Observatory in Bulawayo, m_{BUL}

Additionally, for historical events as well as a number of events from the early instrumental period, M_w values have been estimated from macroseismic intensity observations.

By far the greatest fractions of magnitudes requiring conversion are expressed in terms of local magnitude, M_L, which is the magnitude routinely reported by CGS and its predecessor organisations. This magnitude scale required an additional homogenisation step to be carried out prior to conversion, in order to avoid inconsistencies related to change in magnitude determination practice over time. Such changes have been found to affect conversions in other projects (*e.g.*, ***Reference 5.14.69***) even when the magnitude under consideration was nominally determined by the same agency using the same conventions. Therefore, all available local magnitude values were uniformly recalibrated using a preliminary version of the calibration for the local magnitude scale determined by Saunders *et al.* (***Reference 5.14.70***), based on

a selection of recent (2006-2009) digital high-quality recordings from tectonic events recorded at a minimum of 5 stations. As shown in ***Figure 5.14.10***, the rate of attenuation predicted by this calibration is very similar to that of other SCRs, such as Norway (***Reference 5.14.71***) or Western Australia (***Reference 5.14.72***).

The uniformly recalibrated local magnitude values M_L* for events with an estimate of M_w (either from direct calculation or from an estimate of M_0) are plotted in ***Figure 5.14.11***, along with a number of published conversion relations (***References 5.14.73*** and ***5.14.74***). These data are then used to develop an M_L-M_w relation for South Africa. At small magnitudes, the conversion is based on regression analyses of the small-magnitude data with M_w based on M_0 estimates obtained from fitting weak-motion data (see ***Subsection 5.14.4.4***). The slopes obtained from these regressions are in good agreement with the slopes of 0.6 to 0.8 found in other relations derived from data in a comparable magnitude range (***References 5.14.74*** to ***5.14.77***). At larger magnitudes, the limited data available supports the 1:1 scaling between M_L and M_w that would be expected theoretically (***Reference 5.14.78***).

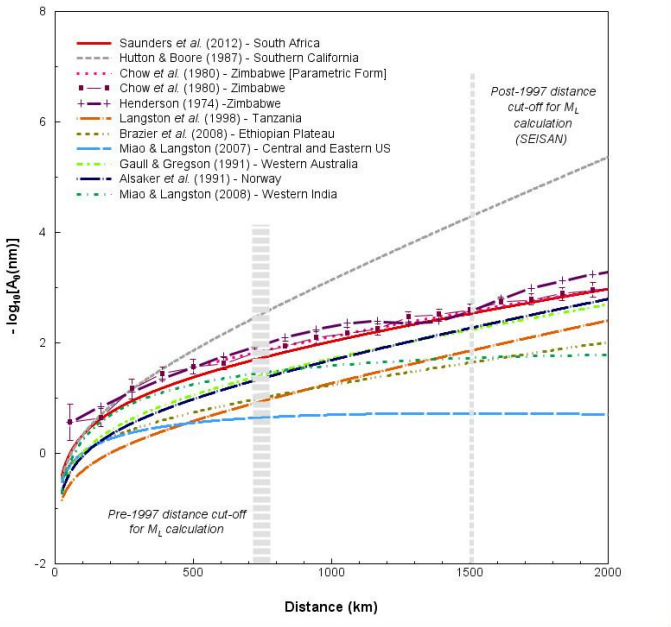


Figure 5.14-10 Calibration of Local Magnitude Scale in South Africa, Other Regions of Africa and Selected SCR Regions.

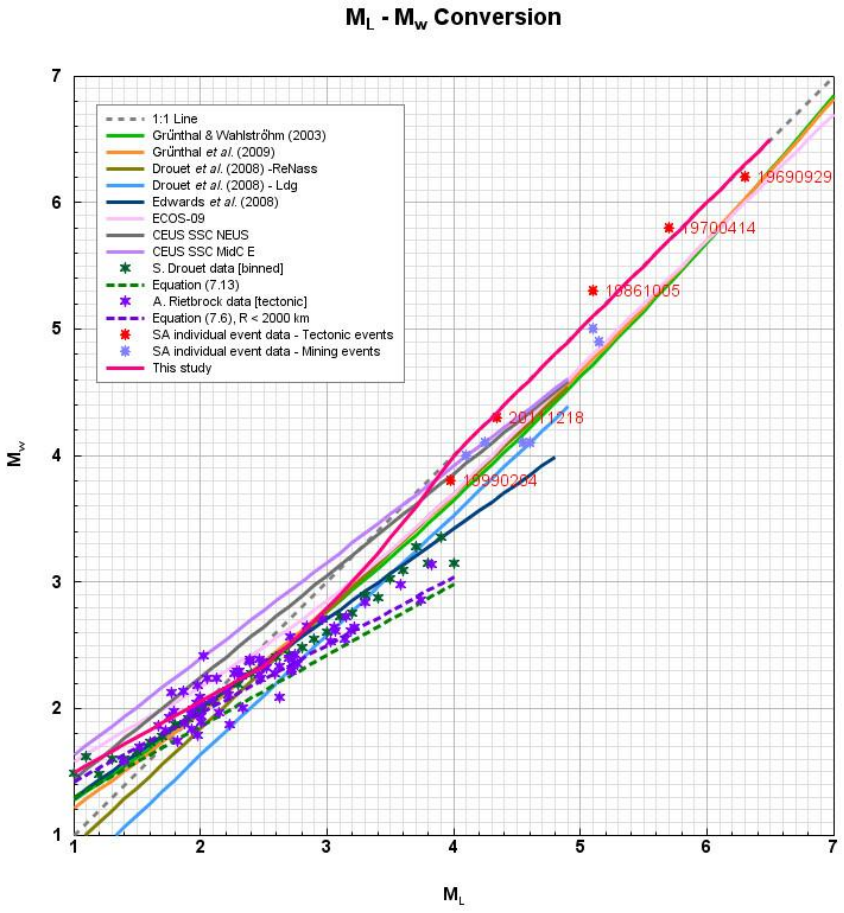


Figure 5.14-11 M_L-M_w Relation Adopted in the Thyspunt PSHA Study.

Differences in scaling in the M_L-M_w relationship between small and moderate magnitudes have been observed in other regions, and are generally addressed by using a nonlinear functional form for the conversion relations. Following Goertz-Allmann *et al.* (***Reference 5.14.74***), linear relations at small and moderate magnitudes were linked with a quadratic functional form to bridge intermediate magnitudes. Various physical explanations have been suggested for the non-linear behaviour at a smaller magnitudes ($M_w \leq 4.0$), including the breakdown of self-similar scaling and an interpretation as a scaling artefact due to the difficulty of reliably determining the corner frequency f_c of the spectrum at small magnitudes, notably because of the kappa filter. Whatever the cause of the non-linearity, it is likely to bias the estimation of recurrence parameters, which is undesirable (*e.g.*, ***Reference 5.14.69***). Therefore, events with moment magnitudes M_w smaller than 4.0 were not used in the recurrence calculations.

For a small number of events in the catalogue, teleseismic body-wave magnitudes have been calculated by ISC and/or NEIC (or its predecessors). Most of these are comparatively poor determinations from a very limited number of stations, and dating back to the early to mid-1970s, when m_b determinations across agencies did not follow uniform conventions. The ISC determinations are generally preferred as being based on a larger number of stations, but these are also not without problems, appearing in some cases to be affected by saturation. The Johnston m_b-M_w relation (***Reference 5.14.79***), developed based on data from global SCRs, was adopted to convert m_b values, based on a comparison of published conversion relations with the scarce South African m_b-M_w data available.

The issue of conversion from M_S is limited to those values determined from early instrumental recordings on intermediate-period instruments by Ambraseys & Adams (***Reference 5.14.36***) for the 20 February 1912 Koffiefontein (M_S = 6.2) and 4 December 1920 offshore (M_S 6.4) earthquakes. The M_S determinations by Ambraseys & Adams (***Reference 5.14.36***) are obtained using the Prague formula, but without applying the band-limitation to a period of around 20s used in modern instrumental M_S determinations. However, differences between the band-limited and broadband determinations are only pronounced for station magnitudes obtained at short distances, therefore the values included here should be directly comparable to modern instrumental M_S determinations. The commonly used equivalence $M_w = M_S$ (*e.g.*, ***Reference 5.14.80***) was adopted for these events.

The exact calculation method of the Gutenberg-Richter magnitude (M_{GR}) remains unknown, however it is generally considered to be close to the surface-wave magnitude M_S, with some authors finding that the M_{GR} values need to be reduced by 0.2 magnitude units in order to reconcile early instrumental and modern seismicity rates. A comparison between the M_{GR} values and re-evaluated M_S values of the sub-Saharan African events studied by Ambraseys & Adams (***Reference 5.14.36***) supports the observation that M_{GR} values for this region sometimes deviate significantly from re-evaluated values. In the current catalogue, this conversion is solely required for one event in the intensity database, namely the 31 December 1932 event off Cape St Lucia. While there is close to no data available to constrain the conversion relation, the event itself is well-documented, with a reasonably well-constrained epicentral location. The plentiful macroseismic data supports a smaller magnitude than the value of 6¾ listed by Gutenberg & Richter (***Reference 5.14.25***). The M_w value for this event is therefore determined as a composite estimate of 6.3 ± 0.3 by considering the range of magnitude values that would be consistent with the epicentral location and observed macroseismic intensity field, as well as the instrumental amplitude recorded on the Union Observatory seismograph in Johannesburg.

© Eskom 2026/Rev 0a

The final instrumental magnitude scale for which a conversion is required is the magnitude calculated by the Goetz Observatory in Bulawayo based on the data registered by the network of stations located in present-day Zimbabwe, Zambia and Malawi. This conversion concerns events that occurred in the late 1960s and early 1970s, in particular the foreshock-aftershock sequence of the 1969 Ceres earthquake, for which no other reliable estimate of magnitude is available. The Bulawayo magnitude is close to an m_{bLg} magnitude (***Reference 5.14.81***) since it is nominally calculated based on the A/T ratio. However, for events in South Africa, Chow *et al.* (***Reference 5.14.82***) note that T is difficult to determine and therefore a value T = 1.0s is assumed, which effectively makes the magnitudes determined by this institution comparable to local magnitudes. As shown in ***Figure 5.14.10***, the distance correction term implemented at the time is found to be very similar to that of Saunders *et al*. (***Reference 5.14.70***), therefore these magnitudes are considered to be equivalent to M_L* as described previously. Note that the M_L values given by Fernández (***Reference 5.14.83***) for a number of events of the Ceres sequence also use the Bulawayo distance corrections, and are therefore also considered directly equivalent to M_L*.

In the late 1970s and early 1980s, the calibration of the Bulawayo magnitudes was revised to match the m_b estimates provided by NEIC. This was not necessarily an improvement, given that early NEIC m_b values for southern Africa have been found to be frequently unreliable (*e.g.*, ***Reference 5.14.53***). However, this update does not affect the present study given that by that time, local magnitudes from the SANSN represent the preferred magnitude option for events in the study region.

For events for which a set of IDPs is available, magnitudes are estimated using the third-generation algorithms implemented in the MEEP2 software (***Reference 5.14.57***). While there are four algorithms for location, the magnitude determinations use one of two methods:

- The implementation of the Bakun & Wentworth method (***Reference 5.14.58***) in the MEEP2 software uses a predefined IPE (in this case, the French-SCR relation of Bakun & Scotti, ***Reference 5.14.62***) to determine the best-estimate magnitude;

- The three other methods use the calibration of the Frankel formula (***Reference 5.14.60***) to determine magnitude.

The performance of the methods is illustrated ***Figure 5.14.12*** using the events analysed by Midzi *et al.* (***Reference 5.14.28***) that also have an instrumental determination of magnitude, with M_w estimated as described above. These plots show, in general, a good agreement between the intensity magnitude M_I

© Eskom 2026/Rev 0a

and the instrumental M_w estimate, with the exception of cases where the Bakun algorithm does not converge. As a result, the intensity magnitude values M_I determined from calculations using the MEEP2 software are taken as directly equivalent to M_w. This is also consistent with the fact that both the Frankel formula (***Reference 5.14.60***) and the Bakun & Scotti IPE (***Reference 5.14.62***) are formulated in terms of M_w.

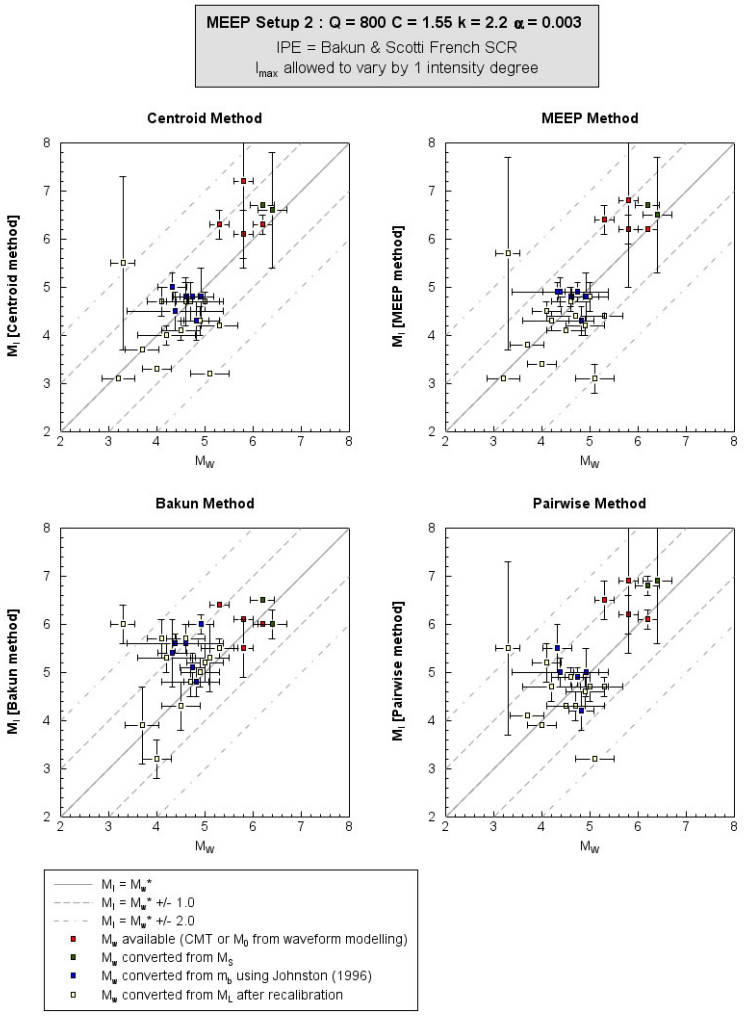


Figure 5.14-12 Intensity Magnitudes Obtained from Using the Different Methods Implemented in the MEEP2 Software Compared with Instrumentally Determined Magnitudes.

The uncertainty bars for M_I reflect the standard deviation of the bootstrap solutions obtained for each approach using the MEEP2 software, while the M_w uncertainties are those listed in the catalogue (or similarly determined).

In the case of events without an instrumental magnitude or IDP field but for which an isoseismal map is available, the intensity magnitude is determined based on the equivalent areas calculated from the isoseismal contours, in combination with the relevant equations from Johnston (***Reference 5.14.84***). These are compatible both with the calibration used in the MEEP software, and with the Johnston I_0-M_w equation (***Reference 5.14.84***) used when only a single point of intensity is available

Given the limited amount of data available for the vast majority of the magnitude determination, as well as the significant uncertainties associated with the conversions to moment magnitude, the specification of the uncertainties associated with the magnitude values is an essential component of the catalogue. The hierarchical approach of Johnston *et al.* (***Reference 5.14.53***) was used as a guide for the determination of uncertainties. For most conversions, the uncertainty values determined for the global SCR dataset by Johnston *et al.* (***Reference 5.14.53***) can be treated as lower bound estimates for the uncertainties encountered in the Thyspunt PSHA catalogue. There are, however, the following two exceptions to this rule: firstly, the conversion uncertainty for the regional set of uniformly recalibrated M_L* values considered in this study is expected to be lower than the uncertainty determined by Johnston *et al.* (***Reference 5.14.53***) for an inhomogeneous global set of M_L values, and comparable to the conversion uncertainty for the m_{bLg} magnitude. Secondly, the magnitude uncertainties determined from the Albini IDP sets (***Reference 5.14.27***) analysed using MEEP2 are expected to be lower than the values quoted for isoseismal contours by Johnston *et al.* (***Reference 5.14.53***) for well-behaved datasets, since the IDPs have been uniformly reappraised and a more objective estimation technique is used.

Figure 5.14.13 shows a summary of the magnitude uncertainties for events with $M_w \geq 2.0$ in the Thyspunt PSHA project catalogue. These uncertainties are large in comparison to those encountered in catalogues with more plentiful instrumental data (*e.g.*, ***Reference 5.14.69***).

g) Declustering of Earthquake Catalogue

The Thyspunt PSHA catalogue is used primarily for the estimation of seismicity recurrence parameters to characterise the various seismic sources comprising the SSC model. In view of the limited number of earthquakes available, the analysis is limited to time-independent models and therefore the usual assumption of a Poissonian distribution is made to characterise earthquake occurrences in time. Under this assumption, the rate parameter of the Poissonian distribution characterises the long-term rate of seismicity.

© Eskom 2026/Rev 0a

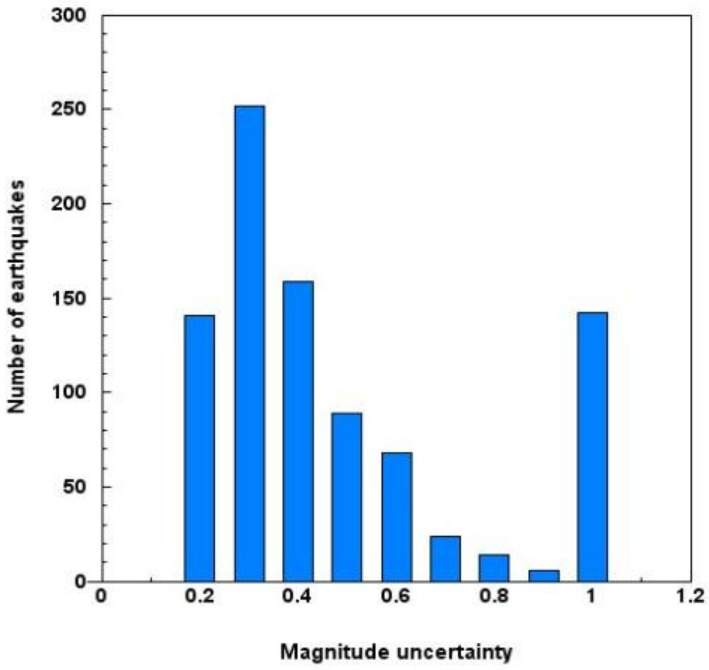


Figure 5.14-13 Distribution of magnitude uncertainties in Thyspunt PSHA project catalogue.

This assumption requires events to occur independently from one another; therefore events whose occurrence is causally linked to that of other events, such as foreshocks and aftershocks, which effectively represent short-term perturbations of seismicity rate, need to be removed from the catalogue prior to undertaking the rate calculations. This is done through the use of algorithms identifying dependent events, often called declustering algorithms, for which available options are reviewed in the next section. The ZMAP catalogue analysis package (***Reference 5.14.85***) is used for practical implementation of these routines.

Algorithms for identifying dependent events fall into three main categories:

- window-based approaches, which as their name indicates, identify dependent events based on spatio-temporal windows (*e.g.,* the Gardner & Knopoff algorithm, ***Reference 5.14.86***);

- cluster-link approaches, such as the frequently-used Reasenberg algorithm (***Reference 5.14.87***), which link sequences of events into clusters considering multiple levels of dependencies;

- rate-based and stochastic approaches (***References 5.14.88*** to ***5.14.90***), which essentially consider deviations from the long-term background rate and/or the Poissonian distribution assumption.

Most of the methods described above require the specification of parameters that have typically been derived empirically for a specific catalogue and a given geographic region. This raises the issue of whether this calibration can be considered universal and applied to other regions, or whether locally derived parameters may be required. In the context of seismic hazard analysis, this may need to be considered, since the improvement in methodology may be counter-acted by increased epistemic uncertainty regarding the parameters. This is particularly an issue in cases where empirical data available for calibration are very sparse, as is the case here.

Cluster-link models such as Reasenberg (***Reference 5.14.87***) and more sophisticated models such as rate-thinning and stochastic models were not considered as it would be problematic to calibrate such models with confidence with the limited data available. Also, for the cluster-link models, the deviation from the Poissonian model and related overestimation of the proportion of main shocks may adversely affect the recurrence calculation by reducing even further the influence of the already very sparse moderate-to-large events.

Based on the discussion in preceding sections, the Gardner & Knopoff algorithm (***Reference 5.14.86***) is applied to the full Thyspunt PSHA project catalogue. The results are shown in ***Figure 5.14.14***. The declustering results using the Gardner & Knopff algorithm (***Reference 5.14.86***) were examined in more detail for events in the Ceres and Koffiefontein regions. These results confirm that this algorithm is efficient at detecting the immediate aftershocks of larger events, but otherwise considers events to be independent unless they occur very closely in space and time.

h) Catalogue Completeness

In addition to the removal of dependent events through declustering, the catalogue used for the calculation of seismicity rates also needs to be assessed in terms of its completeness. An earthquake catalogue can be said to be complete above a given magnitude M_c (magnitude of completeness) over a period T_c (period of completeness) if all earthquakes with magnitudes equal or greater to M_c that have occurred during the period T_c in the region covered by the catalogue are listed in the catalogue. If any of these events are missing, the catalogue is said to be incomplete. Catalogue incompleteness needs to be taken into account in the recurrence calculations, since failure to do so may result in biased estimation of seismicity rates and *b*-values, and thus may affect the final hazard results.

© Eskom 2026/Rev 0a

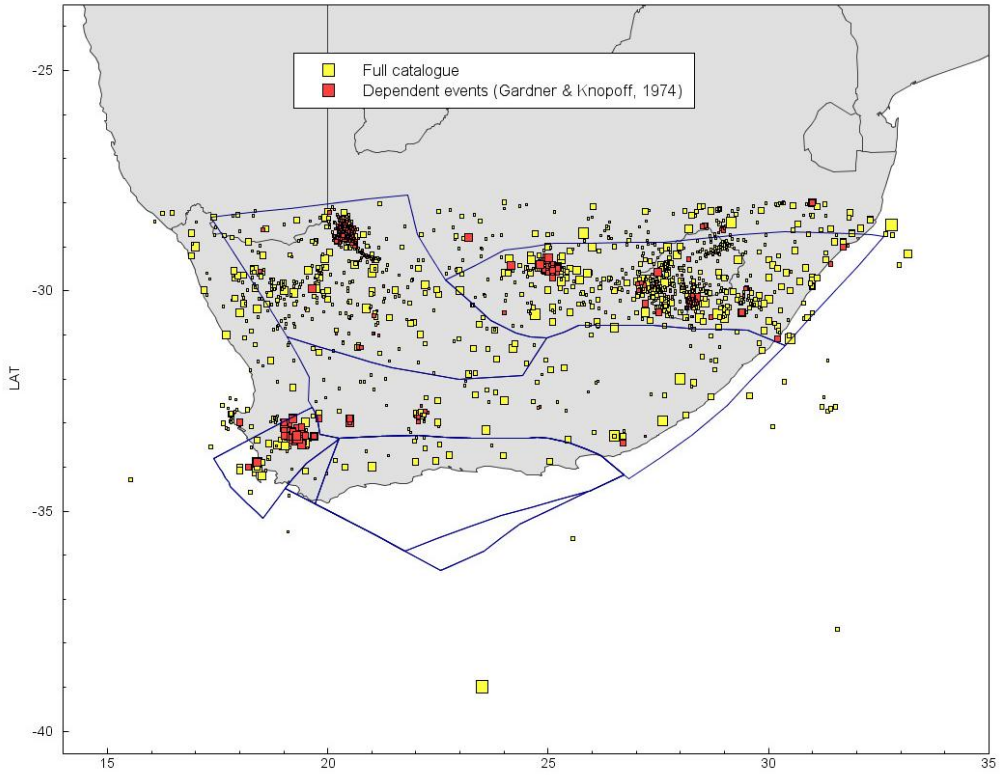


Figure 5.14-14 Results of Applying the Gardner & Knopoff Declustering Algorithm (*Reference 5.14.86*) to the Thyspunt PSHA Project Catalogue.

***The source zones shown correspond to the preliminary Thyspunt PSHA SSC model*.**

A variety of approaches are available to address the issue of catalogue completeness. For a given magnitude level, completeness can vary significantly in both time and space, due to factors related to earthquake detection capabilities for the instrumental part of the data, as well as factors related to reporting practices and record survival for the historical part of the data.

Most commonly, catalogue completeness is determined through statistical analysis of the (declustered) earthquake catalogue, typically by considering the evolution of the cumulative number of events against time (*e.g.* ***References 5.14.91 and 5.14.92***) or magnitude (***Reference 5.14.93***). Under the assumption of a Poisson distribution, the cumulative rate of events should remain constant in time, hence variations in this rate can be interpreted as

pointing to incompleteness. Alternatively, historical approaches (***Reference 5.14.94***) consider historical factors influencing completeness, insisting in particular on the importance of the assessment of the quality of available documentation, as well as the importance of negative evidence of earthquakes. Finally, probability of detection approaches (*e.g.* ***Reference 5.14.95***) make use of network properties to obtain station-specific properties of detection which are then combined to obtained regional estimates. An alternative probability of detection approach was considered in the CEUS SSC study (***Reference 5.14.69***), where the probabilities of detection were determined through a maximum-likelihood fit to spatially gridded data.

A probability of detection approach leading to equivalent periods of completeness, similar to that used in the CEUS SSC project (***Reference 5.14.69***), was adopted in the Thyspunt PSHA study, for the following reasons:

- Rather than eliminating data below the threshold of completeness, this type of approach preserves all available data, correcting for missing data by adjusting the period of completeness accordingly. This is a desirable feature in view of the very limited number of data available.

- A probability of detection approach can incorporate, within a uniform, quantitative framework, different types of information, both qualitative and quantitative, from a variety of sources pertaining to both the historical and instrumental parts of the catalogue.

- Unlike purely statistical approaches, this type of approach can incorporate the negative evidence gathered in the historical study by Albini (***Reference 5.14.27***), as well as information regarding the historical evolution of the recording network.

In view of the significant contribution of historical, qualitative information to the overall knowledge available for assessing catalogue completeness, the values for the probability of detection were developed deterministically for the historical part of the catalogue. Values based on statistical analysis of the data were used for the modern instrumental part of the catalogue. This approach differs somewhat from that adopted in the CEUS SSC study (***Reference 5.14.69***), which relies more heavily on the data by determining spatially varying maximum-likelihood values for the probabilities of detection by fitting the catalogue data. While the data-fitting aspect of this method was not deemed appropriate for the present study in view of the data limitations, the underlying principle of probabilities of detection increasing in a monotonic manner with time and with magnitude was maintained, in particular to constrain the transition between the historical and modern instrumental parts of the catalogue.

© Eskom 2026/Rev 0a

For the historical part of the catalogue, the assessment of the catalogue completeness essentially boils down to answering the following questions:

- Would an earthquake of magnitude M be noticed?
- If so, how likely is it that a record of this event was made?
- Assuming that such a record was made, how likely is it to have survived to the present day and to have been considered in the catalogue compilation?

Taken in the negative, this series of questions also addresses the interpretation of negative evidence, *i.e.* the likelihood that the absence of records of earthquakes genuinely reflects an absence of seismicity. Answers to the question above will be strongly dependent on location, being influenced by factors such as population density and historical developments in terms of recording. These topics were explicitly addressed in the Albini study (***Reference 5.14.27***) undertaken specifically for the Thyspunt PSHA, and therefore the conclusions of this study were incorporated in the completeness assessment.

Instrumental considerations for completeness revolve primarily around the development of a local seismographic network, as well as the evolution of the relative quality of coverage by global seismograph networks. Available information on these topics was therefore reviewed. Analysis of the subset of 1997-2011 data (for which the lower magnitude cut-off is controlled by the detection capability of the network) in terms of the evolution of M_c versus time provides the following results: M_c~2.0 from 1997, M_c~1.9 from 2003, M_c~1.8 from 2007. These results are consistent with the analysis of the full SANSN catalogue (***Reference 5.14.96***). Similarly, review of the information available in terms of detection by global networks, in particular the threshold values reported by agencies such as ISC and NEIC, as well as studies of the regional variations (*e.g.*, ***Reference 5.14.97***), lead to the conclusion that it is reasonable to assume the Thyspunt PSHA catalogue to be complete at least down to M_w 4.5 from 1964 onwards.

Based on the considerations above, time intervals corresponding to dates delimiting periods for which the probability of detection is expected to remain uniform were determined. These were used for the assessment of magnitude-dependent probabilities of detection for each of the source zones, using the information regarding the completeness of the instrumental and historical parts of the catalogue. These probabilities of detection were subsequently used to estimate equivalent periods of completeness used in the recurrence calculations (see ***Subsections 5.14.5.4.(a) iv*** and ***5.14.5.4.(c) vii***), and are summarised in ***Figure 5.14.15***.

© Eskom 2026/Rev 0a

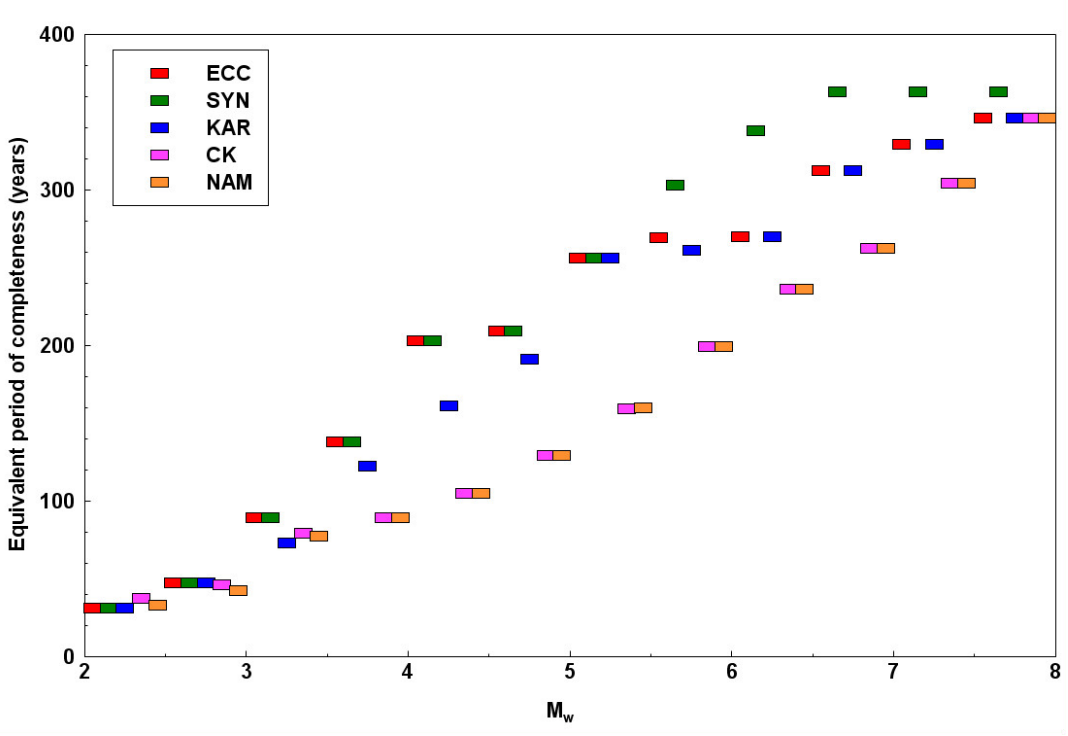


Figure 5.14-15 Equivalent Periods of Completeness Considered for the Various Source Zones in the Thyspunt PSHA SSC Model.

i) Macroseismic Intensity Database

Macroseismic intensity values are measures of ground shaking defined according to standardised scales that relate observations of the effect of ground motion on people, objects and buildings to discrete intervals or degrees. The macroseismic intensity database consists of two parts: a historical database, comprising events which are documented exclusively in terms of macroseismic intensity (***Subsection 5.14.4.4.(a)***), and an instrumental database, comprising those events for which independent, instrumentally determined source parameters are available (***Subsection 5.14.4.4.(b)***). Intensity values at specific locations for earthquakes with instrumentally-determined epicentral locations and magnitudes are potentially the most useful data in the analysis of historical earthquakes (see ***Subsection 5.14.4.4***) and also in testing of ground-motion prediction equations (GMPEs), especially where strong-motion data are not available (see ***Subsection 5.14.4.5***). Full details of the development of the

macroseismic intensity database can be found in the reports by Albini (***Reference 5.14.27***) and Midzi *et al.* (***Reference 5.14.28***).

j) Historical Intensity database

A detailed study of the historical seismicity of the Southern and Eastern Cape regions was undertaken by Albini (***Reference 5.14.27***) as part of the additional data gathering activities for the Thyspunt PSHA project. This study focused in particular on the seismic history of the region, collecting negative as well as positive evidence in order to establish historical catalogue completeness. This study also incorporates individual studies of 30 events in the time span 1850-1936, including seven newly identified events. As well as adding these new events, the Albini study (***Reference 5.14.27***) also highlighted a number of doubtful events, as well as identifying a few occurrences of fake events (*i.e.*, observations of effects that were ascribed to earthquakes, but on inspection revealed to be caused by another phenomenon, such as the meteorite blaze observed in the Bloemfontein region in June 1862).

The Albini study (***Reference 5.14.27***) investigated in particular the background historical context, with special attention given to the settlement distribution and related administrative issues. This material was indispensable:

- to reconstruct the network of the places at which macroseismic observations might have been made,
- to find out who might have documented the earthquakes in a written form, and the repositories where these documents are stored today.

Based on these materials, the locations identified in ***Figure 5.14.16*** were identified as privileged observation places for the following reasons:

- they were the earliest established settlements in the area
- they had a steady, continuous production of documentary sources
- they have repositories storing documents of relevance for the investigation.

The investigation was undertaken in the main European repositories storing documentation on the area and period in study, located in London (UK), in particular the British Library (St Pancras and Colindale locations), and the National Archives (Kew Gardens), as well as the main South African repositories, visited many times during the research.

The repositories visited in South Africa, in four different visits, included the following:

- Cape Town:
  (i) South African Public Library;
  (ii) National Archives of South Africa;
  (iii) University of Cape Town-UCT Library.

- Grahamstown:
  (i) Cory Library for Historical Research, Rhodes University;
  (ii) Bowker Library,1820 Settlers Memorial Museum, Albany Museum.

- Graaff-Reinet:
  Urquhart Museum Archive

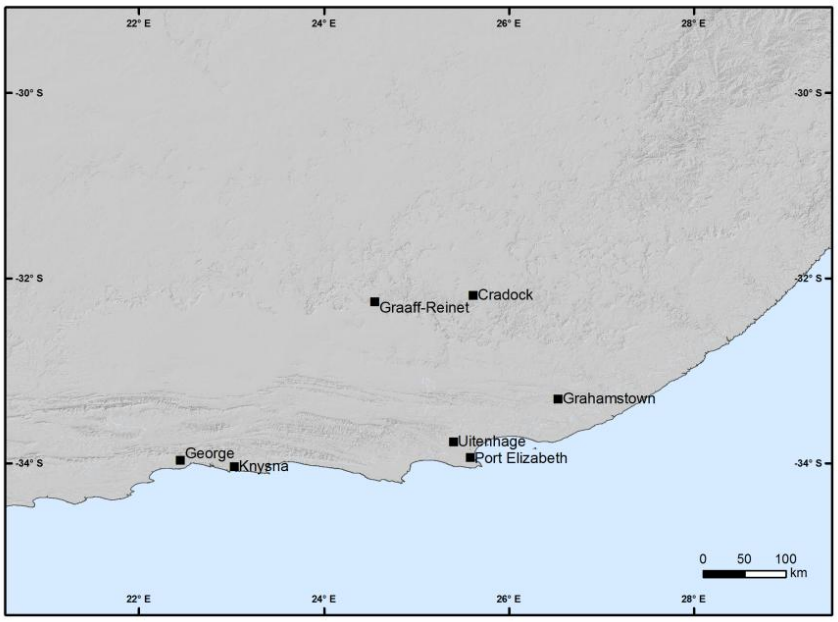


Figure 5.14-16 Privileged Observation Points in the Area of Study

Each individual event study included a table of macroseismic observations in MMI-1956 scale, a map, and a documentary appendix including full-text records. For each earthquake studied, a comprehensive commentary was supplied, especially in the case of records that could not fully confirm the earthquake occurrence and/or location. In a few cases, a schematic overview

of the relationships among sources was drawn, with the aim of documenting how the earthquake records have been analysed and interpreted in terms of reliability and independence of the information they supply. The final historical database, shown in ***Figure 5.14.17*** and also in ***F-5.14.18***, includes 435 intensity values and 277 identified locations.

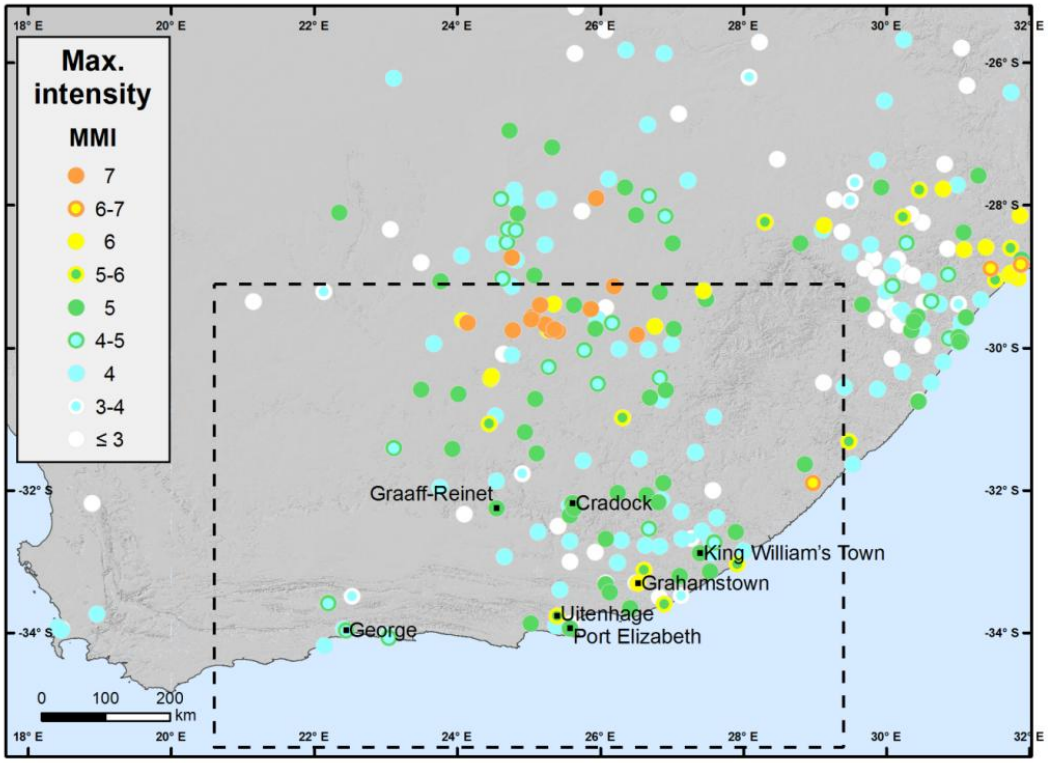


Figure 5.14-17 Intensity Data Points Collected by Albini (*Reference 5.14.27*), Covering the Period 1820-1936.

The area enclosed by the dashed rectangle is shown in more detail in the next figure.

© Eskom 2026/Rev 0a

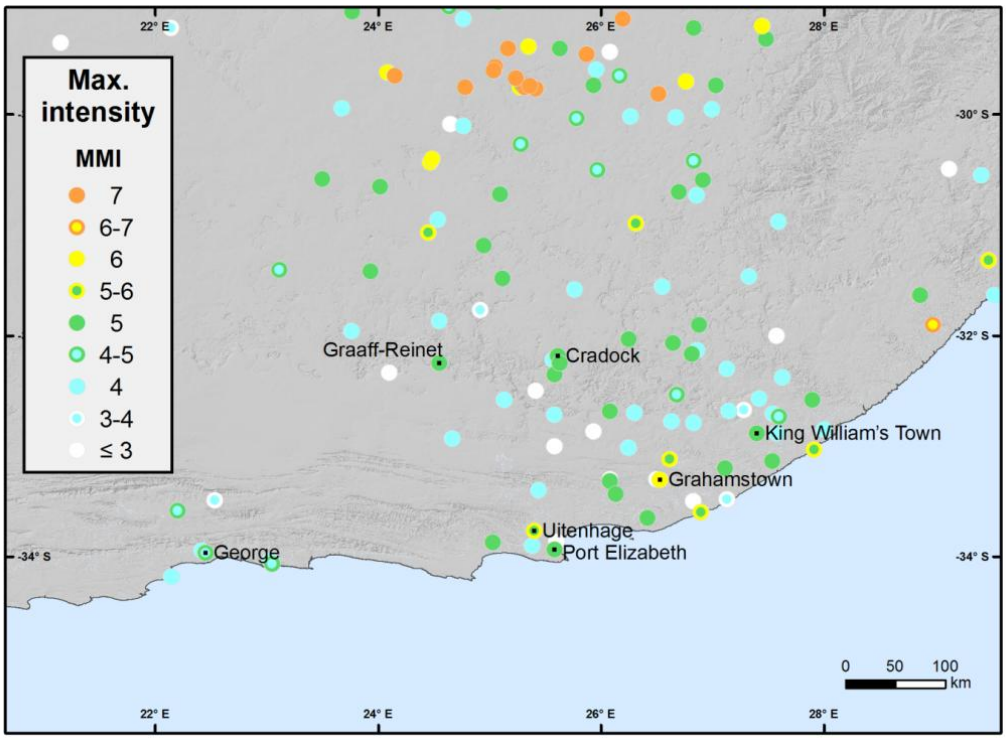


Figure 5.14-18 Detail of the Study Region of Albini (*Reference 5.14.27*). This Region Was Assessed for Negative, As Well As Positive Evidence of Earthquakes.

As a result of these investigations, Albini (***Reference 5.14.27***) was able to develop seismic histories at a number of localities shown in ***Figure 5.14.19***. Based on the analysis of the data in its historical context, Albini (***Reference 5.14.27***) concluded that these histories are complete to at least the intensity VI-VII level for the time period 1820-1936. This information was incorporated in the completeness assessment of the historical part of the catalogue (see ***Subsection 5.14.4.4.(h)***)

© Eskom 2026/Rev 0a

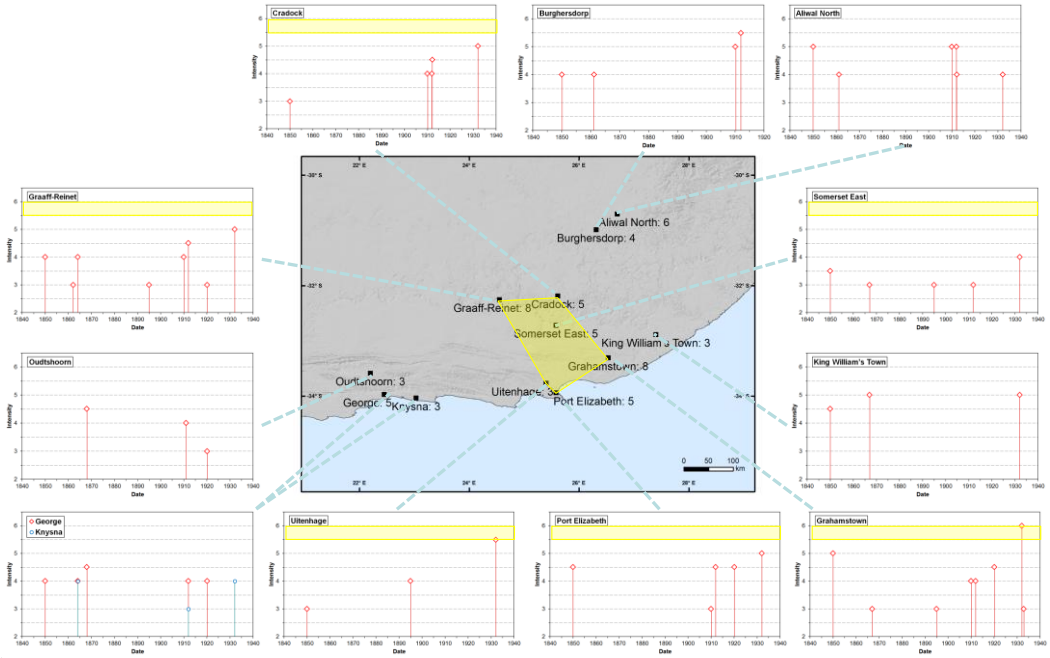


Figure 5.14-19 Seismic Histories Compiled at Selected Locations by Albini (*Reference 5.14.27*).

k) Instrumental Intensity Database

A database of intensity observations from instrumentally-recorded earthquakes in South Africa has been compiled as a contribution to the characterisation of seismic hazard at Thyspunt. The database contains 1,059 intensity data points (IDPs) from 57 earthquakes with magnitudes in the range of M_w 2.2 to 6.4, at epicentral distances up to 1 000 km (***Figure 5.14.20***). Sixteen events have 20 or more IDPs, with half of these events having more than 80 IDPs. The database is dominated by relatively low intensity values, mostly determined from human perception of shaking rather than structural damage. However, 19 IDPs correspond to intensity values greater than VI MMI-56. The locations of the contributing events, shown in ***Figure 5.14.21*** are distributed across South Africa. Except for the larger, instrumentally-recorded events, such as the 1969 Ceres, 1976 Koffiefontein and 1986 Matatiele events, the moment magnitudes are generally obtained by conversion from other scales using empirical relationships (see ***Subsection 5.14.4.4.(f)***).

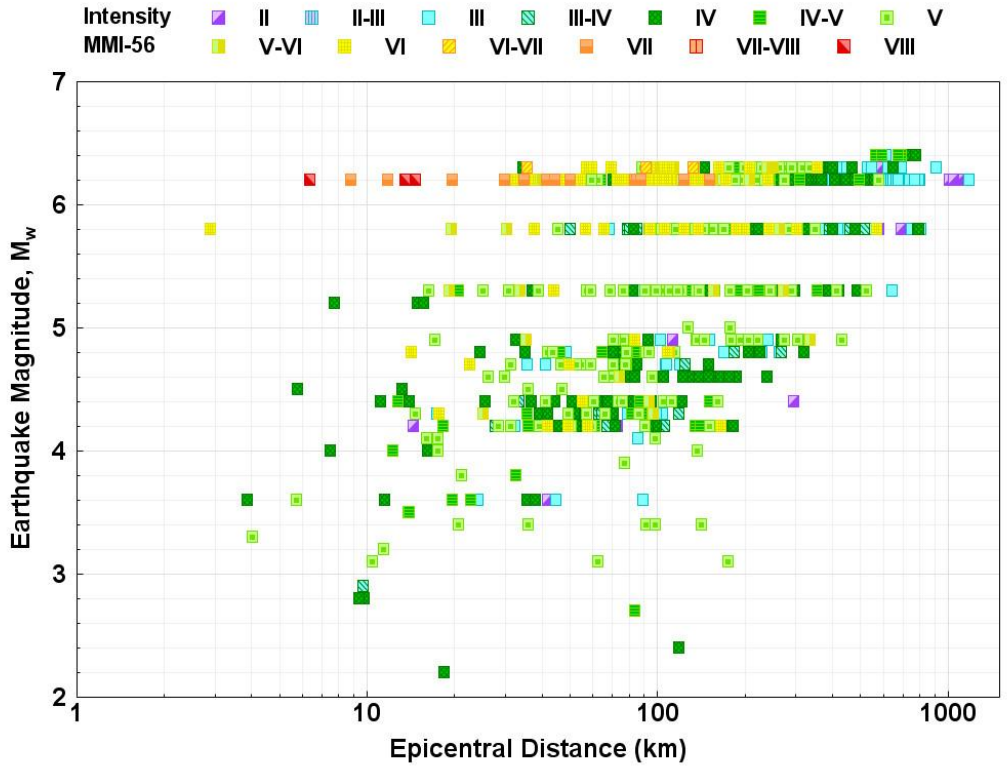


Figure 5.14-20 Magnitude-Distance Distribution of the Macroseismic Intensity Database (*Reference 5.14.98*).

The IDPs have been assigned from macroseismic observations retrieved from newspaper reports and questionnaires, and also digitised from previously published isoseismal maps. The methodology followed to translate this information into IDPs is essentially that recommended by Musson & Cecić (***Reference 5.14.99***). These IDPs were created from 1,450 observations, broken down into 990 questionnaires and 460 descriptions of earthquake effects within newspaper reports. In a number of cases macroseismic data from both newspaper reports and questionnaires were used in creating IDPs for individual earthquakes. However, newspaper reports were the main source of data for earthquakes that occurred before 1977.

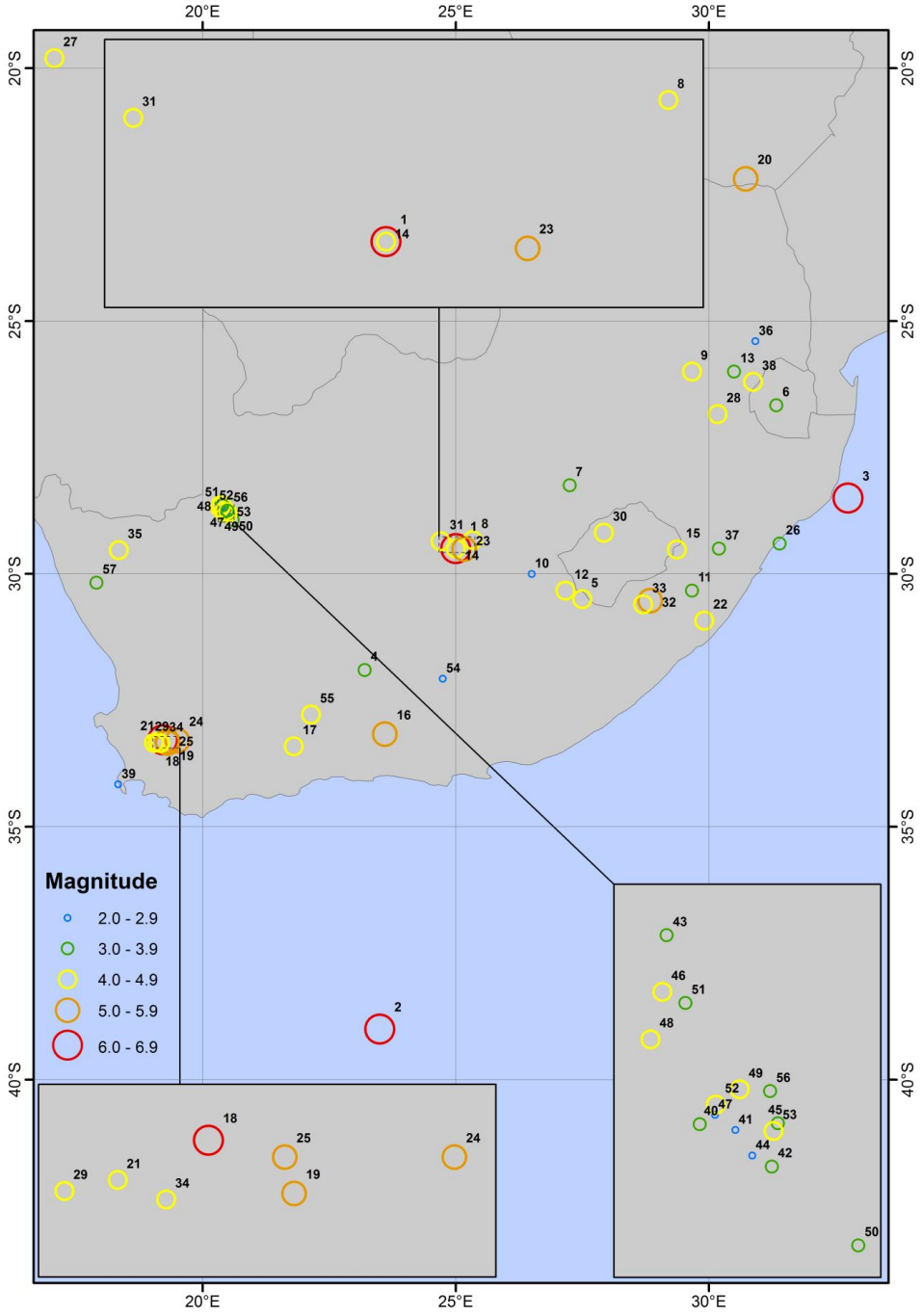


Figure 5.14-21 Locations of Earthquakes That Are Included in the Instrumental Intensity Database (*Reference 5.14.98*).

Figure 5.14.22 illustrates the overall composition of the intensity database in terms of numbers of earthquakes and the types of macroseismic information sources available for each of these. The most valuable information, in terms of providing the best opportunities for assigning reliable intensity values, are the questionnaires, which are available for 32 of the earthquakes. However, all sources of macroseismic information that were available have been incorporated into the database with a view to providing the most extensive set of IDPs possible. Thus six of the earthquakes also contributed IDPs that were on published isoseismal maps. These digitised IDPs are ranked lower than those that were assigned from questionnaires or newspaper reports. Similar ranking of IDPs was observed in the report by Allen *et al.* (***Reference 5.14.100***) where author-assigned IDPs were considered more reliable than values obtained from digitised published maps. Thus where there was duplication between the assigned IDPs and digitised IDPs, only those assigned in this study were included in the database.

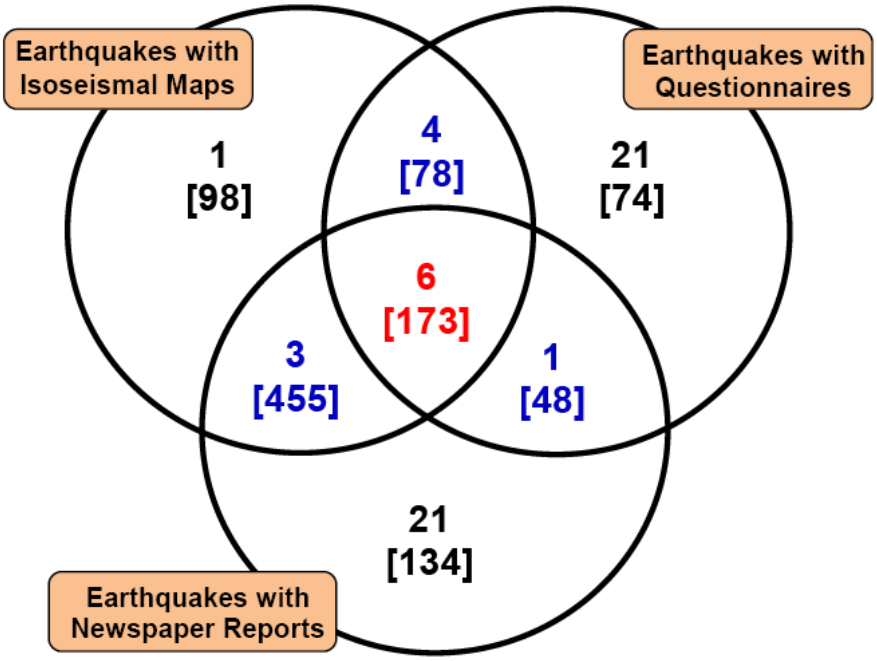


Figure 5.14-22 Venn diagram showing the types of macro seismic information with the 57 earthquakes in the intensity database (*Reference 5.14.98*).

The number in brackets reflects the total number of IDPs associated with each event in each category.

All intensity values were assigned using values to be uniformly expressed in terms of the 1956 version of the Modified Mercalli Intensity (MMI) scale (MMI-56; ***Reference 5.14.101***). Most of the existing isoseismal maps for South Africa are expressed in terms of the MMI scale. However, it is not always distinguished whether these correspond to MMI-31 (***Reference 5.14.102***) or MMI-56 (***Reference 5.14.101***), but it is generally thought to be the latter. It is also noted that when IDPs assigned previously by others have been adopted for South African earthquakes, these have also generally been MMI values. When reviewing the published isoseismal maps and IDPs for which there was no clear indication as to whether the MMI-31 or MMI-56 scale was used, an implicit assumption was made that intensities assigned on these two scales may be treated as being entirely equivalent. This assumption was based on the similarities noted in making comparisons of the two scales, in particular at the lower degrees of intensity (MMI < VI) making up the bulk of the database, and on the general equivalence of most 12-degree intensity Cancani scales (***Reference 5.14.103***).

The influence of soft deposits on the nature and strength of earthquake ground-motion has been recognised for a long time (*e.g.*, ***Reference 5.14.104***). The quantification of this influence is thus a core component of specifying seismic loading, from general building codes to site-specific studies for critical facilities. Guidelines for the assessment of intensities often indicate that observations from locations on substantially different surface geology, and states of geological weathering, should not be grouped together. Using geological maps of South Africa, the sites of 60% the IDPs were geologically classified as either ‘rock’ or ‘soil’, the uncertainty in locations precluding such a classification for the remaining data points.

In some cases, observations previously grouped under one place were found to be located on different geology in terms of rock or soil. These were then separated, regrouped according to the geological classification, and the intensity values reassigned. This occurred, however, for only 25 of the IDPs from all events. All IDPs obtained from observations with exact locations as well as IDPs obtained from previously published reports were classified following the process described above.

Out of 1102 IDPs, 677 were geologically classified, with most of them (535) located on rock and 142 IDPs located on soil. A large proportion of the IDPs (425) were not classified mainly because the exact location of the observations (*i.e.*, newspaper reports) used in creating the IDPs was not available. Most of the IDPs that were not classified were from the earlier earthquakes where observations were in the form of newspaper reports only. Others corresponded to more recent cases with ambiguous or now obsolete place names. IDPs

© Eskom 2026/Rev 0a

digitised from published isoseismal maps, such as that for the 29 September 1969 Ceres main shock (***Reference 5.14.105***), were geologically classified using their geographical location as extracted from the maps. Such cases can be a source of inaccuracy because it is not known if the surface geology at the IDP location is equivalent to that at the locations of the contributing observations.

The influence of the site classification is usually illustrated in the intensity-distance plots for the IDPs (*e.g.*, ***Figure 5.14.23***). In assessing the effect of local soil conditions, such plots were prepared for all the earthquakes that had more than one IDP and had been geologically classified. Some of the plots show a clear influence of the geology on the IDP values, such as for the 29 September 1969 and 1 July 1976 earthquakes (upper panels of ***Figure 5.14.23***). However, for some events absolutely no correlation was observed between site classification and position with respect to the general trend in the data (*e.g.*, 5 October 1986 earthquake, lower panel of ***Figure 5.14.23***). As a result of these analyses for all earthquakes in the database, a number of IDPs, such as the Durban and Uitenhage IDPs highlighted in ***Figure 5.14.23***, were identified for which there was a clear possibility of locally enhanced shaking levels as a result of site amplification effects. These IDPs were flagged for subsequent consideration in applications of the database.

In assessing the quality of the IDPs created in this current study, it is useful to consider the number of observations used to create the IDPs. For higher intensity values, IDPs based on few observations may be unrepresentative of the overall level of shaking, picking up higher levels of damage to isolated cases of more vulnerable structures. For lower levels of intensity, the determination of the intensity value relies on the proportion of people (few, many, all) who report given effects, so single observations can be equally misleading. Many (434) of the IDPs in this study were created using information from single observations. Only about a third of the IDPs (312) were created with more than two observations, with 11 IDPs created using information from 10 or more observations.

Only unambiguous data and non-trivial IDPs with intensities of at least MMI=II, which are not determined from single macroseismic observations (which are considered to be poorly constrained, as discussed above), can usually be utilized in further studies such as comparisons with predicted motions from GMPEs. In order to make unbiased comparisons between observations and predictions, IDPs that reflect strong local influences should be removed from the dataset if the interest is in the general trends. These are defined as those IDPs with intensity values that do not seem to fit the general trend displayed by

the set of IDPs for the earthquake, many of which had already been removed after being identified as likely to have been affected by local site amplification. Other 'outlier' points were removed simply on the basis of lying far out from the general trend of the data from each earthquake. Only those earthquakes found to have at least five 'useful' IDPs after this process were selected for the 'useful' intensity database. A total of 436 useful IDPs were obtained after removing 248 trivial IDPs (MMI=I), 207 IDPs each created using information from a single observation, four outlier IDPs with low intensity values and 12 outliers with high intensity values. Seven other IDPs that were digitised from isoseismal maps published by ***Reference 5.14.64*** for the 20 May 1955 and 30 July 1955 earthquakes, were also removed since they corresponded to arithmetically averaged intensities and had been superseded by the IDPs reappraised from the original questionnaires

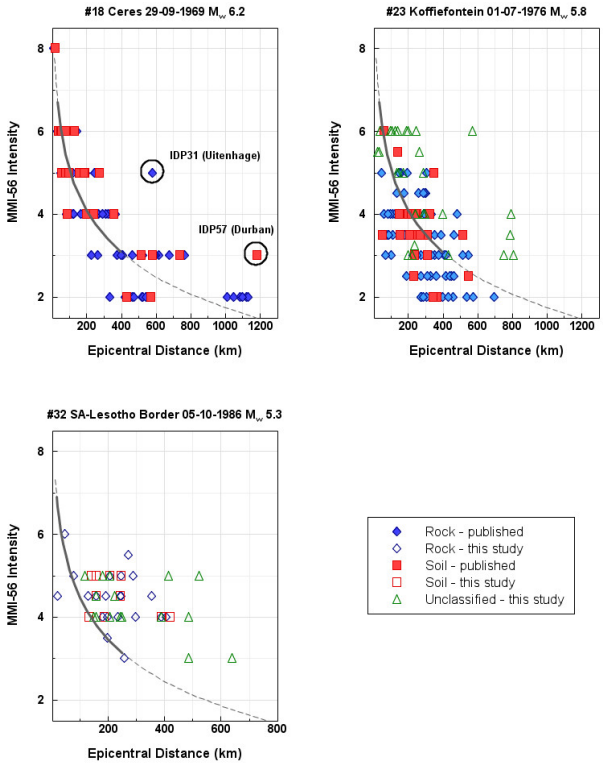


Figure 5.14-23 Intensity-Distance Plot of the Geologically Classified IDPs of Selected Earthquakes in the Instrumental Intensity Database (*Reference 5.14.98*).

The Bakun & Scotti French-SCR model (Reference 5.14.62) for a depth of 10 km is shown as a grey curve, dashed outside the applicability range; the identified outliers for the 1969 Ceres event. Open symbols represents IDPs that were newly assigned, whilst the closed symbols were obtained from

published data.

The final database has IDPs at epicentral distance between 6 km and 1000 km, for earthquakes of magnitude values between 4 and 6.5 (***Figure 5.14.24***). The bulk of the database is contributed by IDPs with intensities between III and V which are well distributed across the full range of magnitudes and distances. As would be expected, larger intensities (VI and above) are only observed at shorter distances for the smaller events (M_w < 6). Intensities VII and VIII come exclusively from the M_w 6.2 1969 Ceres and 1912 Koffiefontein events, the other two M_w > 6.0 events being located offshore and therefore not contributing intensities close to the epicentre. The final database is also well distributed with respect to site classification.

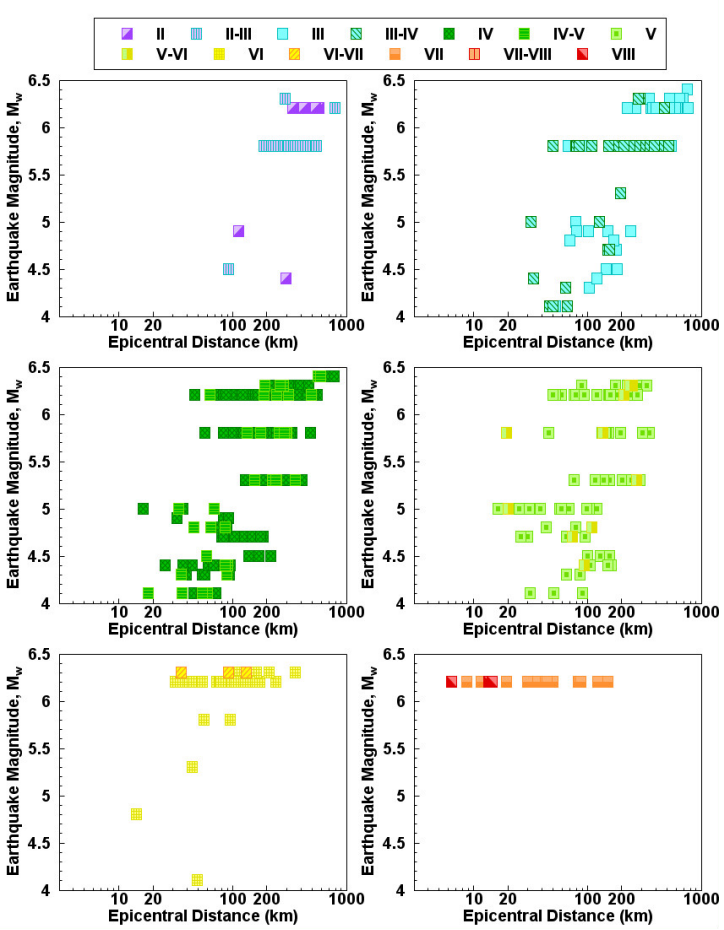


Figure 5.14-24 Magnitude-Distance distribution of the Final Instrumental Intensity Database, Grouped by Intensity Level (*Reference 5.14.98*).

l) Weak-Motion Recordings Database

There are no strong-motion recordings of tectonic earthquakes available in South Africa, and this probably holds for the whole of sub-Saharan Africa. This fact precludes from the outset the possibility of deriving empirical GMPEs for response spectral accelerations in South Africa directly, and requires other approaches to be used.

While there are no native strong-motion recordings of South African earthquakes, there is a considerable database of weak-motion recordings that have been made on the national seismograph network. In order to make use of these data for obtaining information of relevance to the present project, two specialty contractors, Professor Andreas Rietbrock and Dr Stephane Drouet, were invited to apply their individual inversion strategies on the South Africa weak-motion data. The original choice of the GMC TI Team was to contract Prof. Rietbrock, on the basis that he has a long track-record working in this area and his inversion technique has matured through several years of ongoing research as well as multiple applications. However, it was also considered highly beneficial to have a second and parallel analysis of the data both to provide a check on the data itself and also to obtain insight into the degree of uncertainty associated with the inversions in general. It was decided that the data would be processed by Prof. Rietbrock and that both analysts would then make use of the same set of Fourier spectra from the processed data (even if they each chose to then select different subsets for their analyses) so that differences could be interpreted as being primarily due to differences in modelling approaches.

The database of weak-motion recordings that were used by both contractors were selected from an initial database that consisted of around 50,000 waveforms from 3780 events. These recordings included a large portion of mining-related recordings (~2800 events) with the remainder being of tectonic origin. The events were all recorded over two short time periods spanning the years 2006-2008 and also the period from 2009 to January 2011. This original dataset was then processed by Rietbrock (***Reference 5.14.68***) using standard techniques. Specifically, the following criteria were imposed to refine the initial database:

- An on-scale signal window of 20 seconds around the manually estimated S-wave train had to be available. Noise estimates were computed through windowing of an interval prior to the P-wave arrival with a length of 5 seconds. Fourier amplitude spectra were also calculated for a fixed (20 seconds) and a variable window length based on encapsulating the time between 5 and 75% accumulation of the energy in the S-wave train.

© Eskom 2026/Rev 0a

- Both signal and noise windows were then tapered using multi-taper algorithms (***References 5.14.106 and 5.14.107***) with 5-3π prolate tapers. The maximum bandwidth of each record was limited to 1.0-30.0Hz. The maximum usable bandwidth for the spectral inversion was subsequently estimated based on the signal-to-noise ratio. Only amplitude spectra for which all spectral ordinates are at least three times greater than the noise at that frequency and for which the usable frequency band contains at least the frequency band between 5.0-10.0Hz were included in the usable data set.

- Finally, at least three waveforms from each event have to fulfil the spectral characteristics outlined above before these waveforms are included.

The overall database compiled in this manner consisted of around 1700 events (225 of which were of tectonic origin). The database was then made available to both contractors who could then include or omit records or events as they deemed appropriate.

The ray coverage of the dataset can be seen in ***Figure 5.14.25*** for the two temporal periods considered and the local magnitude-epicentral distance distribution is shown in ***Figure 5.14.26***, in which the mining-related and tectonic events are distinguished. It is important to note from ***Figure 5.14.26*** that no events of local magnitude above 5 have been recorded at distances of less than 200 km. ***Figure 5.14.26*** emphasises the important point that while the weak-motion database is quite large, the coverage in magnitude-distance space has effectively no overlap with the magnitude-distance combinations that typically contribute most to the results from probabilistic seismic hazard analyses.

Both analysts perform inversions to estimate parameters related to a Brune single-corner source spectrum (***References 5.14.108 to 5.14.110***) as an idealised representation of the Fourier amplitude spectrum of far-field seismic radiation. The parameters of relevance to the GMC model development are the following:

- stress drop ($\Delta\sigma$), which is a measure of the strength of the high-frequency radiation from the earthquake;

- the geometric spreading model, describing how the wave front expands (and hence energy density of the seismic radiation decays) with distance;

- the quality factor, Q, which indicates the efficiency with which the seismic waves are transmitted through the crust, with lower Q values implying greater anelastic attenuation.

© Eskom 2026/Rev 0a

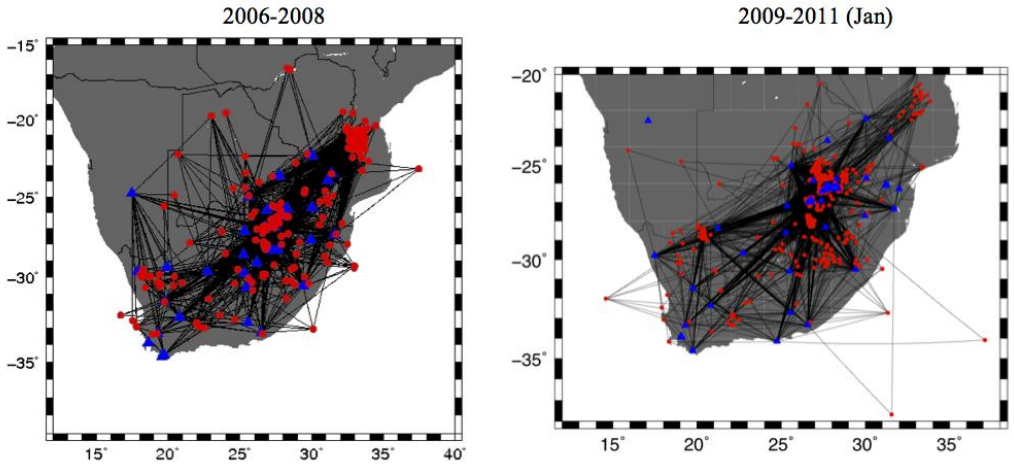


Figure 5.14-25 Ray Coverage in the Weak Motion Database for the Two Temporal Periods Considered.

The blue triangles denote recording stations while the red dots show the epicentral positions of the events. Black lines connect the source and site locations.

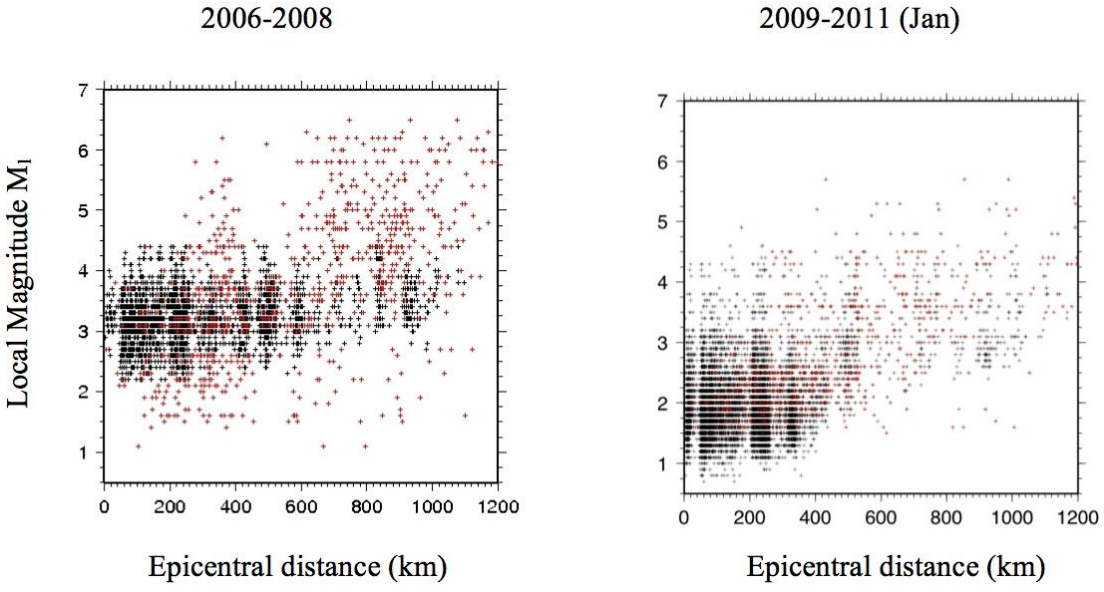


Figure 5.14-26 Local Magnitude-Epicentral Distance Distribution of the Dataset Over the Two Temporal Periods Considered.

The recordings of the tectonic events are shown using the red markers, while the mining-related recordings are shown using black markers.

The different formulations of the inversions by the two analysts resulted in rather different stochastic parameter sets, with the Rietbrock model including a depth-dependent, frequency-independent Q model whereas the Drouet inversion yielded a frequency-dependent Q that was a constant through the crust. However, comparisons of individual parameters from stochastic inversions is misleading since there are trade-offs between the influences of the parameters on the predicted spectra. Comparisons of predicted Fourier spectra at different distances (***Figure 5.14.27***) show that the two different Q models produce very similar results in the frequency range for which the weak-motion recordings are reliable (which is determined by the instrument characteristics). Such comparisons provided confidence that the two sets of stochastic conversions were mutually consistent, which provided confidence in terms of their application.

The plots in ***Figure 5.14.27*** are normalised to match the two predictions in terms of amplitude, which in stochastic simulations for an earthquake of specified seismic moment is mainly dependent on the stress drop. The stress drops estimated from the inversions are small, with Drouet obtaining estimates in the range 2-10 bar and Rietbrock mean values of 17.6 bar (with formal error bounds of 7.3-31.9). Restricting the data to recordings obtained at distances of less than 500 km, Rietbrock obtained a higher mean estimate of 63 bar (with error range of 16.9-114.0). As can be appreciated from ***Figure 5.14.26***, however, this restriction on distance implies an even greater limitation on the magnitudes of the earthquakes from which the recordings have been obtained. Bearing in mind that the hazard calculations consider earthquakes from magnitude 5 and greater, up to values on the order of magnitude 8 (***Subsection 5.14.5.4***), this is an issue that warrants careful consideration with regards to selecting stress drop values for South African earthquakes of larger magnitude. The issue of magnitude-scaling of stress drop is much debated in the technical literature, with some studies making the case for apparent magnitude scaling being an artefact of the data analysed rather than a physical phenomenon (***Reference 5.14.111***). Other studies have inferred magnitude-dependent stress drop models, such as that proposed by Rietbrock *et al*. for the United Kingdom (***Reference 5.14.112***). using data from intraplate regions extracted from the studies of Edwards *et al.* for the United Kingdom (***Reference 5.14.75***), Atkinson for Southeast Canada and Northeast United States (***Reference 5.14.113***), and Allen *et al.* (***References 5.14.77 and 5.14.114***) for both south-eastern and south-western Australia.

© Eskom 2026/Rev 0a

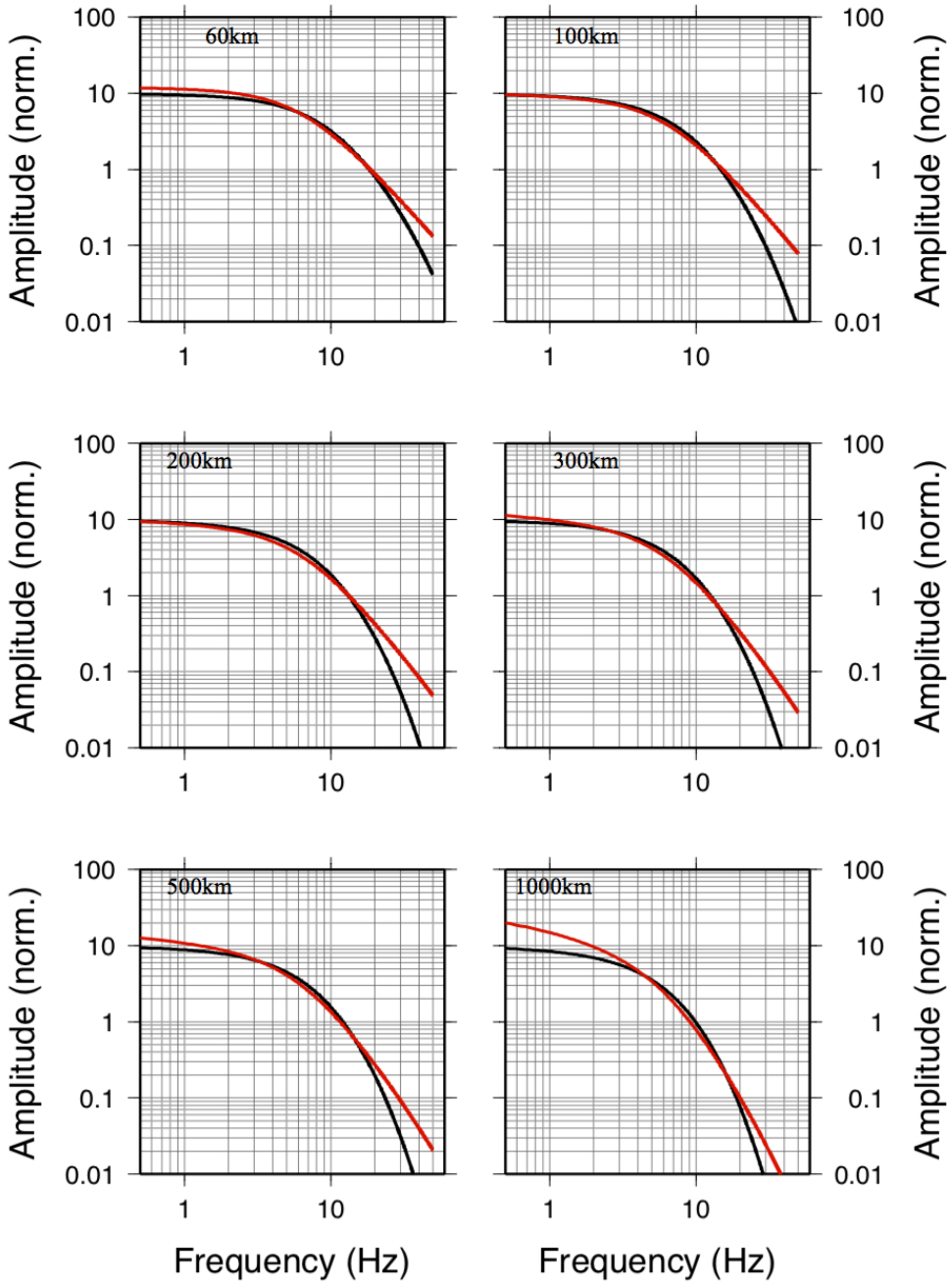


Figure 5.14-27 Equivalence Between Frequency-Independent, but Depth-Dependent, Anelastic Attenuation (*black curves*) and Frequency-Dependent Anelastic Attenuation (*red curves*) (*Reference 5.14.68*)

Figure 5.14.28 presents a collation of data from four different studies that together have determined Brune stress drop estimates for magnitudes spanning a very large range, using interplate region data. The study of Archuleta *et al*. (***Reference 5.14.115***) considers earthquakes in California, from the Mammoth Lakes sequence; García García *et al.* (***Reference 5.14.116***) compute stress drops for events in Southern Spain; while Bressan *et al*. (***Reference 5.14.117***) focus on events in Northeastern Italy. The study of Moghaddam *et al*. (***Reference 5.14.118***) relates to the events California, Taiwan and other active regions. All studies use comparable approaches in order to estimate their stress drops. Superimposed upon this figure is the variable stress drop model of Rietbrock *et al*. (***Reference 5.14.112***) and it is clear that there is very good agreement over the majority of the considered magnitude range.

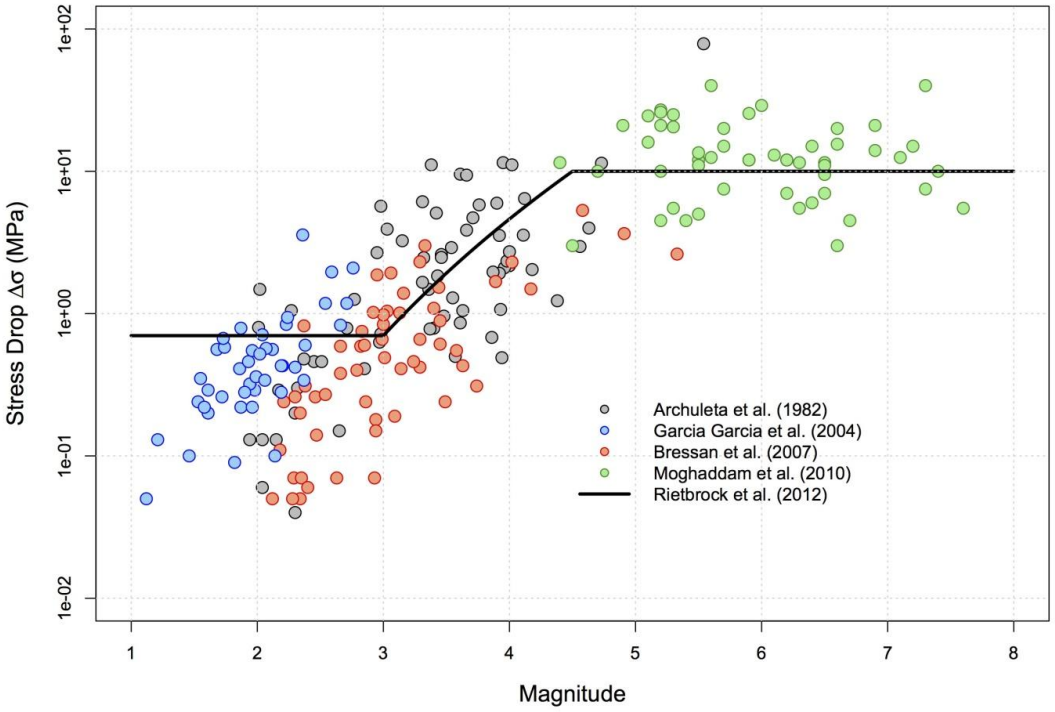


Figure 5.14-28 Variation of Stress Drop With Respect to Magnitude Obtained from Four Publications Concerning Stress Drop Estimation in Interplate Regions.

The solid black line corresponds to the variable stress drop model of Rietbrock et al. (Reference 5.14.112).

The GMC TI Team concluded that while the assumption of constant stress drop over the moderate-to-large magnitude range is not obviously wrong from consideration of the literature, there are valid reasons why apparent breaks in stress drop scaling would occur at magnitudes of around M_w 3. This magnitude is precisely where the stress drop estimates from the weak motion inversions originate and hence it was difficult to confidently state how the stress drop estimates from these inversions can be used as constraints upon motions from larger earthquakes. The analysts responsible for the stochastic inversions, Prof. Rietbrock and Dr Drouet, clearly did not support the use of the average stress drops found from the weak-motion inversions for modelling ground motions from earthquakes of magnitude relevant to the PSHA calculations. Therefore, other sources of information need to be explored in order to obtain insight into possible ranges of the stress drop parameter for larger earthquakes in South Africa.

The starting point for this exercise was the premise that South Africa is a Stable Continental Region (SCR), and while that concept was originally developed purely for the purpose of constraining maximum magnitude values in Central and Eastern North America (CENA), it has been observed that average stress drops in SCRs are consistently higher than those in active regions of crustal seismicity. An extensive literature review was undertaken to identify studies that had estimated stress drops for various regions (primarily but not exclusively SCRs), which were grouped into three categories: (1) those presenting stochastic parameters for a given region, and in some cases for a single event, without a specific application; (2) those developing stochastic parameters for the purpose of producing hybrid-empirical ground-motion prediction models; and (3) those developing stochastic parameters for forward modelling to generate stochastic GMPEs for the target region. Greater credence was given to the values from the latter two categories of study, since these values were actually used to develop GMPEs and therefore the authors will have seen the consequences of the chosen values. Focusing particularly on Central and Eastern North America as a potential analogue SCR to South Africa, the TI Team concluded that a range of stress parameter values from 100 to 200 bar was well supported by these studies, with the possibility that values could also extend somewhat higher. These values were used to inform the scaling of the ground-motion predictions, as discussed in ***Subsection 5.14.5.5.(a)***.

Another stochastic parameter required to develop the GMC model for the Thyspunt site was kappa, which is a high-frequency filter on the seismic spectrum (***Reference 5.14.119***), generally considered to be due to attenuation in the uppermost few hundred metres of the crust. Kappa values were not included in the stochastic inversion parameters as a result of different approaches for modelling the influence of site response on the weak-motion

© Eskom 2026/Rev 0a

recordings. In order to obtain constraint on suitable kappa values for the target GMC horizon level within the Goudini bedrock at the Thyspunt site (***Subsection 5.14.4.5***) recordings from individual seismograph stations were studied. The stations were selected on the basis of being classified as being on very hard rock that was comparable to the deeper Goudini rock. This exercise was performed by identifying recordings that had been made at particular stations from similar-sized events and then stacking their spectra (accounting for any differences in distances from the site) so that an average spectral shape could be inferred. An example of this process is shown in ***Figure 5.14.29*** in which a set of spectra recorded at station HVD (identified as being a very hard rock site and therefore compatible with the reference target horizon for the GMC model) are shown. From consideration of such spectra it is possible to infer values of kappa by considering the extent to which spectral amplitudes fall away from a horizontal level at high frequencies. In the particular example shown for HVD in ***Figure 5.14.29***, one can see that there is an extremely sharp fall-off at a frequency of around 40Hz. However, this is not a kappa-related effect but rather corresponds to the anti-aliasing filter of the instrument. The judgement of Rietbrock when considering such spectra is that in light of the inherent noise one cannot say that there is a clear fall-off from the horizontal level even out to frequencies as high as 40Hz, and certainly not below 30Hz. This observation imposes a limit upon the value of kappa that should exist at this particular site. Although no such observations have been made at the Thyspunt site itself, analyses such as described below were used to help gain insight regarding the level of kappa that might be relevant at the Thyspunt site.

Notwithstanding the issues associated with the instrument response, an exercise was designed to conduct simple site response analyses at considered site in order to obtain estimates of the frequency response functions for the sites. An example of the frequency response function for site HVD is shown in ***Figure 5.14.30***. It is clear that in this case we have quite significant amplification at high frequencies and that we would clearly need some kappa effects in order to remove the peak that is expected in this region. Note that this additional kappa would cause appreciable filtering at very high frequencies that are above the peak, but that this would not be observed due to the instrument response.

The process to estimate values of kappa that are potentially consistent with the earlier observations of the flat spectral shapes to high frequencies as well as the presence of the site response shown in ***Figure 5.14.30***, was then to ask what additional kappa would be required to negate the effects of the site response. One approach to solving this problem would be to consider the amplitude of the peak in the site response and then to determine the amount of additional kappa that would be required.

© Eskom 2026/Rev 0a

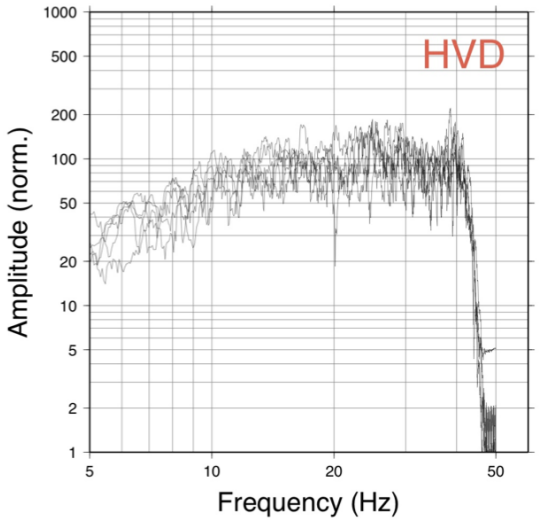


Figure 5.14-29 Stacked Spectra from Earthquakes of Local Magnitude Between 2.0-2.2 Occurring Within a Distance of 100 km from Station HVD.

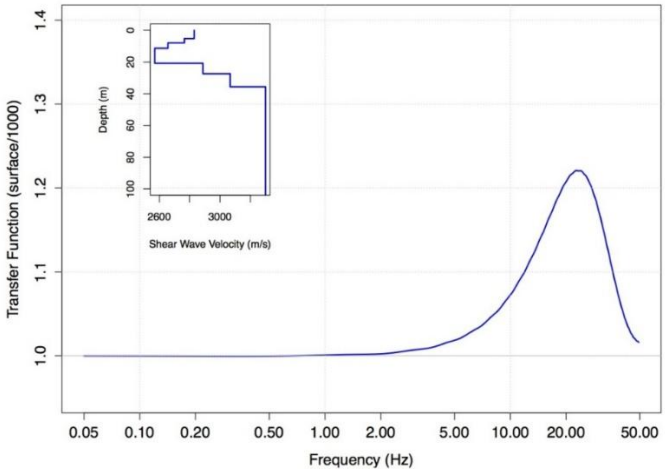


**Figure 5.14-30 Frequency Response Function (Transfer Function)
for Site HVD Showing the Effect of Impedance Contrasts Over the Uppermost Kilometre of the Site.
The Near-Surface Profile Used to Generate this Response Function is Shown in the Inset.**

The approach was to consider the observed spectral shapes and then overlay model predictions that accounted for the background Q-model for South Africa (as developed by Andreas Rietbrock) and then also include the effects of both site amplification (from impedance) and alternative values of kappa. ***Figure 5.14.31*** presents the example for site HVD. In this figure the coloured smooth curves correspond to kappa values in steps of 0.001 and starting from 0.001 (the upper black curve) and ending at 0.005 (the lower orange curve). Even when considering the largest of these kappa values it is not immediately obvious that these smooth curves do not model the observations relatively well over the frequency range for which there is reasonable constraint. For reference, in this figure the solid vertical black line corresponds to the 40 Hz limit considered initially, while the dashed vertical line is at around 35 Hz (still above where Rietbrock suggested that one could be really confident about the effects of the instrument response not influencing the spectra).

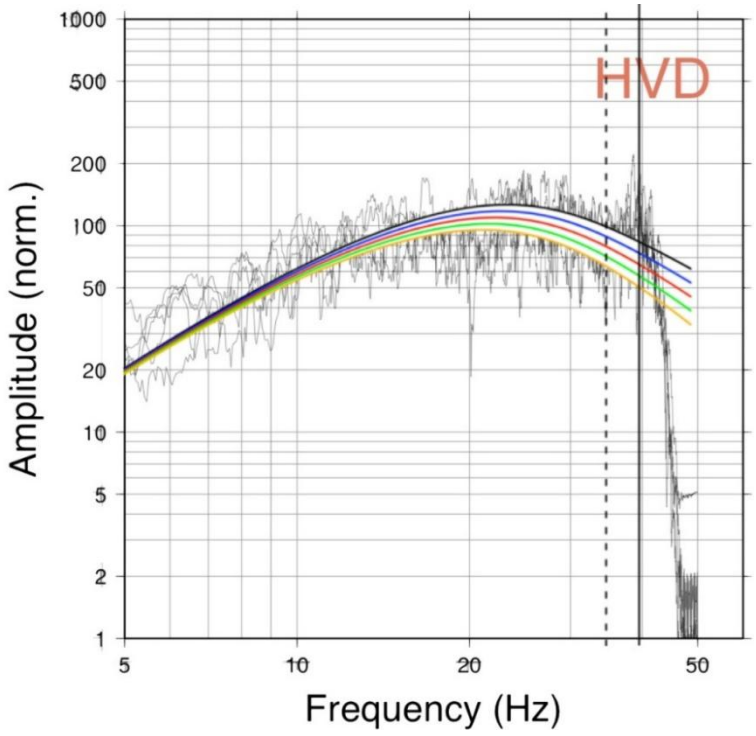


Figure 5.14-31 Comparison of Observed Spectra at Site HVD and the Stochastic Model Predictions of Rietbrock Using the Site Transfer Function Shown in *Figure 5.14.30* and a Range of Alternative Kappa Values Ranging from 0.001 s (black) to 0.005 s (orange).

On the basis of analyses such as those shown in ***Figure 5.14.31***, the GMC TI Team concluded that an appropriate upper value for kappa would be 0.005s. It was also decided that to cover the full range of uncertainty, a lower value of 0.0011s should be adopted, which means effectively no high-frequency filter in the frequency range of interest. The limits defined the range of target values of kappa were used to adjust the ground-motion models to the Thyspunt bedrock condition (***Subsection 5.14.5.5***).

m) Ground-Motion Prediction Equations

The core element of a GMC model for PSHA is a ground-motion prediction equation (GMPE), or more usually a suite of GMPEs in order to capture epistemic uncertainty in ground-motion predictions. There are essentially two different types of GMPE, the first being those derived from regression on strong-motion databases of recordings from a large number of earthquakes. Many such equations have been derived in seismically active regions such as California, Taiwan, Japan, New Zealand, the Middle East, and countries surrounding the Mediterranean (southern Europe and North Africa). In seismically less active regions, where earthquakes are less frequent and large-magnitude earthquake very rare, it is generally the case that the available databases of ground-motion recordings are not sufficiently large and do not cover a sufficiently wide range of magnitude-distance combinations to permit the derivation of GMPEs through regression analyses. In such cases, the more common approach is to develop stochastic GMPEs (***Reference 5.14.120***), using suites of parameters such as those determined from the South African weak-motion recordings (***Subsection 5.14.4.4 (l)***).

As noted previously, there are no strong-motion accelerograph recordings of shaking caused by tectonic earthquakes available for southern Africa, and there are also no locally-derived GMPEs for response spectral ordinates in this region. This prompted initial consideration of stochastic GMPEs. The first option considered was to build a GMC logic-tree based on new stochastic models for South Africa, generated using the stochastic parameter sets obtained from the weak-motion inversions (***Subsection 5.14.4.4 (l)***). This approach would potentially enable a well-constrained best estimate model to be developed, since the model would in essence be based on local and regional data. However, the data are from small-magnitude earthquakes (and the small proportion of recordings from larger events were obtained at large source-to-site distances) and hence the development of stochastic GMPEs applicable to the PSHA calculations would involve large extrapolations. As was noted in ***Subsection 5.14.4.4 (l)***, even for the fundamental stress drop parameter, the analysts performing the stochastic inversions had no confidence in the values obtained from the weak-motion data being applicable to earthquakes in the

magnitude range applicable to the PSHA calculations. Another key reason for not adopting the approach of developing region-specific stochastic GMPEs was that experience in other regions has shown that it is not straightforward to obtain equations that extrapolate in a stable and physically-consistent manner both to larger magnitudes and to short source-to-site distances.

Many stochastic GMPEs have been developed for other SCRs, especially CENA, but also for peninsular India, Australia and parts of north-western Europe, amongst others. Since the region around the Thyspunt site is considered an SCR, it might seem an obvious choice to adopt GMPEs from another SCR such as CENA, and indeed this is not an uncommon practice in PSHA. However, this would implicitly involve making the assumption that ground motions in the host (CENA) and target (South Africa) regions are very similar, which may not be the case. In order to ensure that the best estimate model was as well constrained to the region and site as possible, adjustments might need to be made using information obtained from the weak-motion inversions. To use stochastic parameters (from the inversions of South African data) to adjust a stochastic model rather than generate a new stochastic model would seem to be a strange option, unless it happened to be the case that the GMPE being adjusted brought benefits of being well constrained in terms of magnitude scaling and other features. Actually most existing stochastic GMPEs are based on extrapolations of mainly small-magnitude recordings and moreover tend to have poor constraint in the near-source region (especially when based on point-source simulations).

In light of these deliberations, the GMC TI Team adopted for an approach called the hybrid-empirical approach. The hybrid empirical approach to develop GMPEs was first proposed by Campbell (***Reference 5.14.121***) as a way to develop prediction equations for CEUS. The method is designed to develop GMPEs for regions without the benefits of extensive indigenous strong-motion databases—which is typically the case for SCRs—while taking advantage of the physical constraint on near-source behaviour and magnitude scaling provided by empirical GMPEs. The application of the method requires stochastic parameters from both the host and target regions, which would generally be expected to be determined from weak-motion inversions although an alternative for the host region is to obtain stochastic parameters directly from the inversion of the empirical GMPE (***Reference 5.14.122***). Ratios of response spectral ordinates predicted from the stochastic parameters of the host and target regions are then applied as adjustments to the host region predictions to obtain estimates of spectral ordinates in the target region.

Hybrid-empirical GMPEs have the capacity to capture the best estimate for the motions in the target region, since they are based precisely on making

© Eskom 2026/Rev 0a

adjustments to match the host region. An important caveat to note in this regard was that in choosing this approach, the TI Team did not automatically commit to the application of a full host-to-target adjustment to the selected empirical GMPEs, but only to the concept of using empirical GMPEs and applying adjustments to render them more applicable to the region and site under consideration.

The first stage of developing a hybrid-empirical model is to select an empirical GMPE. Before considering suitable selection criteria for empirical GMPEs, a decision was required as to how to incorporate site response effects—involving the dynamic behaviour of the uppermost tens of metres at the site—into the GMC model. The Thyspunt site is overlain by thick layers of sand (***Subsection 5.14.4.4 (n)***), but the target reference horizon at which the GMRS was to be defined is at the top of the underlying bedrock of the Goudini formation. One option available to the TI Team therefore was simply to target the bedrock surface elevation directly. The shortcoming with this approach is that it would essentially have ignored any impedance contrasts in the uppermost tens of metres in the bedrock and any potential resonance effects at the site. In essence, the GMC model would have predicted the average response characteristics from a larger number of sites (recording stations) with comparable shear-wave velocities, as embodied in the predictions from GMPEs. Modern GMPEs generally include a term based on the time-average shear-wave velocity over the top 30 m at the site, V_{s30}, to characterise the dynamic response. However, it has been clearly demonstrated that two sites with the same V_{s30} may have distinctly different site response characteristics as a result of different layering within the uppermost 30 m and also because of differences in the deeper stratigraphic profiles (*e.g.*, ***Reference 5.14.123***). In view of the potentially large uncertainties arising from the absence of ground-motion recordings from larger earthquakes in South Africa, it was considered important to bear in mind that the one element of the GMC model for which there was potential for good constraint is the dynamic site characteristics, provided through measurements of shear-wave velocity profiles at the site. Such measurements were made (***Subsection 5.14.4.4 (n)***) and these constituted a critical element of the GMC database.

For this reason the GMC TI Team favoured the option of anchoring the bedrock GMC model to a deeper elevation within the Goudini bedrock, and then performing site response analyses—using the V_s measurements from the site—to model the influence of the uppermost portion of the site material. This may appear as a slightly unusual choice to some given that site response analyses are most often performed to model the dynamic effect of soil layers overlying rock. However, the detailed velocity structure near the ground surface will influence ground shaking, and it was considered important to accurately

model any amplification effects at the site given that this was one of the few elements of the GMC model that could be constrained by data.

A consequence of anchoring the GMC model to the deeper Goudini bedrock would be that it would result in the model being referenced to a very high V_{s30} value for which few GMPEs (other than stochastic models developed for very hard rock conditions) are applicable. However, even at the top of the Goudini, shear-wave velocities were found to be much higher than the proposed upper limit of applicability of most GMPEs (***Subsection 5.14.4.4 (n)***). At the same time, in recent years a great deal of progress has been made with regard to the application of V_s-kappa adjustments to transform GMPEs to alternative site profiles. This gave the TI Team confidence to develop a model referenced to a deeper elevation within the Goudini formation, and thereby enable the accurate modelling of any site amplification effects. In order to be able to apply a V_s-kappa adjustment without unnecessarily compounding additional uncertainty, however, it becomes a requirement that the selected GMPE includes V_{s30} as an explicit parameter rather than using broad site classes based on ranges of this parameter, since the latter would require assumptions about the host V_{s30} value to enter into the host-to-target V_{s30} adjustment.

Compiling a database of empirical GMPEs for possible inclusion in the GMC model necessarily involved evaluating published equations both in terms of their general inherent quality (in terms of stability and ability to be extrapolated) and their potential applicability to this project (in terms of the characteristics of both the region and the site). Following the proposal of Cotton *et al*. (***Reference 5.14.124***), it was decided from the outset to adopt the approach of using pre-established objective criteria to exclude GMPEs from a comprehensive global set rather than to select equations that might be suitable. The latter approach leaves the process susceptible to various biases including the preference of the TI Team members for equations with which they are familiar or those produced by colleagues that they happen to hold in high esteem. Such biases can obviously also work in the other direction, with perfectly viable equations being ignored because the Team is unaware of them or because of the Team's perceptions regarding the model developers. The SSHAC process requires, and indeed facilitates, vigilance against all such cognitive biases.

The establishment of a database of empirical GMPEs therefore has two components: the compilation of a global listing of all available equations, and the application of a suite of objective criteria to remove those considered unsuitable by virtue of technical shortcomings. For the former, the TI Team was able to take advantage of the comprehensive global listing of GMPEs published between 1964 and 2010 compiled by Douglas (***Reference 5.14.125***). The TI

Team identified, through a thorough literature review, a handful of models published after the period covered by this compendium. However, since the field of ground-motion modelling is very active and new equations appear frequently, it was also decided that a cut-off date needed to be fixed whereby any equations appearing thereafter, even if used is comparisons, would not be considered as candidates for the population of the logic-tree. The Team felt it preferable to focus on the most careful and extensive examination of existing models rather than continuously extending the process of evaluation to include new models as they appear.

With the list of models available, the next step was to establish criteria for exclusion of those models that the TI Team would judge to be unsuitable. Consideration was given to the exclusion criteria originally proposed by Cotton *et al.* (***Reference 5.14.124***), and to the stricter criteria subsequently proposed by Bommer *et al*. (***Reference 5.14.126***). The latter had been noted as being particularly restrictive and very few current GMPEs survive application of all the requirements proposed in that publication. For this reason, the TI Team decided on a set of criteria essentially extracted from those suggested by Bommer *et al*. (***Reference 5.14.126***) but designed to be slightly more relaxed so that a larger group of candidate GMPEs could be obtained, at least in the first instance. The final criteria selected for this purpose are listed below, with brief explanations for their inclusion:

- No equations derived for application to subduction zones or volcanic areas, since neither of these are relevant to South Africa.

- No equations published prior to 1996. This is to some extent a tool of convenience, reducing the equations to be evaluated to more manageable numbers; it was found by Bommer *et al*. (***Reference 5.14.126***)—who proposed this date based on the intention of excluding equations more than 15 years old—that nearly all equations of such vintage would be eliminated by several of the other criteria anyhow.

- No equations that had been superseded by more recent models published by the same authors, provided that the new equations had been developed for application to hazard assessment rather than for the purposes of exploring a particular phenomenon or feature of the models. The rationale here is that model developers would not propose a new model if the previous were considered superior.

- No equations for which the largest earthquake in the dataset is not larger than M_w 6.5, for the simple reason that such models would require excessive extrapolation to the largest magnitudes covered by the Mmax distributions

in the SSC model.

- The minimum magnitude covered by the equation should be less than or equal to the minimum magnitude, M_{min}, considered in the PSHA calculations (M 5).

- The minimum distance range covered by the GMPE should be 100 km, since extrapolating from shorter distances to the maximum extent of the SSC sources from the Thyspunt site (>500 km) would potentially be unreliable.

- No equation in which the logarithm of spectral accelerations is only a linear function of magnitude, again because such models are not considered to extrapolate realistically to larger magnitudes.

- No equation derived from a dataset that includes a minimum, in average, of 10 earthquakes for each unit of magnitude range covered and 100 recordings for every 100 km of distance range covered. Equations failing these criteria are considered to be inadequately constrained given the current size of the global strong-motion database. One of the main consequences of applying these criteria is to exclude GMPEs derived exclusively using data from small geographical regions (in which the bias of the small data sample is interpreted, without justification, as representing a clear and systematic regional difference in ground-motion behaviour).

- GMPE must include V_{s30} as an explicit explanatory variable, to facilitate the application of site-specific adjustments, as discussed above.

Application of these exclusion criteria left just six equations in contention, one of these being the model of Hong & Goda (***Reference 5.14.127***), which only just satisfied the criterion of extending to a distance of 100 km. The Hong & Goda GMPEs (***Reference 5.14.127***) were actually developed for a study to explore the influence of different definitions of the horizontal component of motion rather than specifically to provide equations for general use in seismic hazard assessment. The study does not provide coefficients for the prediction of spectral accelerations at any short oscillator periods in the interval from 0.01 to 0.10s. For the very hard rock target site condition, this is a serious deficiency and the gap in oscillator periods is sufficiently large to render interpolation very unreliable. Another shortcoming of the Hong & Goda GMPE (***Reference 5.14.127***) is that it does not include terms for the influence of style-of-faulting. Although approximate methods can be applied to adjust such an equation to include the influence of different rupture mechanisms (***Reference 5.14.128***), such an approach would introduce an element of non-trivial uncertainty. In light of these considerations, the GMC TI Team eliminated

this equation from further consideration, leaving only five equations. These were four of the models (***References 5.14.129 to 5.14.132***) produced in the Next Generation of Attenuation (NGA) project (***Reference 5.14.133***) using a database dominated by records from California and Taiwan, and the Turkish model of Akkar & Çağnan (***Reference 5.14.134***). Codes are assigned to these five GMPEs for easier reference hereafter, noting that Atkinson & Boore (***Reference 5.14.135***) present a modified update of Boore & Atkinson (***Reference 5.14.130***):

- Abrahamson & Silva (***References 5.14.129 and 5.14.136***) AS08
- Boore & Atkinson (***References 5.14.30 and 5.14.135***) BA08
- Campbell & Bozorgnia (***Reference 5.14.131***) CB08
- Chiou & Youngs (***Reference 5.14.132***) CY08
- Akkar & Çağnan (***Reference 5.14.134***) AC10

The approach that the GMC TI Team adopted to develop the GMC logic-tree was to select a number of empirical GMPEs, adjust them to the target site conditions, and then create additional versions of each of the adjusted models, through scaling, in order to capture the full range of epistemic uncertainty in median predictions of spectral accelerations from possible future earthquakes in South Africa. A question that arose was whether all five of the pre-selected GMPEs needed to be applied in this approach, since similar final distributions could be obtained by applying one or two scaling factors to each of the five models or a greater number of scaling factors to fewer equations. Various factors were considered by the GMC TI Team in this regard, starting with exploring any redundancy in terms of GMPEs producing very similar results. Using a simple circular source of 100 km radius with a site located at the centre, hazard calculations were performed using a *b*-value of 1 and magnitudes in the range from M_w 5 to 8. Hazard curves were generated using each of the five GMPEs and sampling the following ranges of their parameter settings: 15 logarithmic bins of V_{s30} ranging from 180 to 1,300 m/s, two dip angles (30°, 90°), Z_{TOR} values of 0 and 3 km, hanging wall terms on and off, and all styles of faulting (the aftershock flag in AS08 and CY08 was not included) and for a single oscillator period (0.625s). A total of 250,000 ground-motion values were generated and used to develop hazard curves. Each hazard curve was transformed to a CDF on ground motion by subtracting the curve from 1.0, and the CDFs were then differentiated to obtain the PDFs, from which a median and standard deviation could be obtained. These two values then allowed each hazard curve to be plotted as a single point; values for spectral acceleration at 0.625s (0.125 Hz) are shown in ***Figure 5.14.32***.

© Eskom 2026/Rev 0a

The first observation that can be made from ***Figure 5.14.32*** is that the spread of points for each model to some extent reflects the complexity of the equation in terms of the number of parameters included; the simplest model is that of AC10. The most important feature revealed by this plot is that the AC10 model occupies a distinct space and the four NGA models cluster into two pairs. The fact that the provisionally selected models of AS08 and CY08 are in separate clusters indicates that their use as backbones will not introduce redundancy. Had AS08 and CB08 been chosen as the two NGA models, or equally CY08 and BA08, the two NGA models would to an appreciable extent be replicating the predicted motions and not contributing effectively to the capture of the centre, body and range of technically-defensible interpretations (or CBR of the TDI).

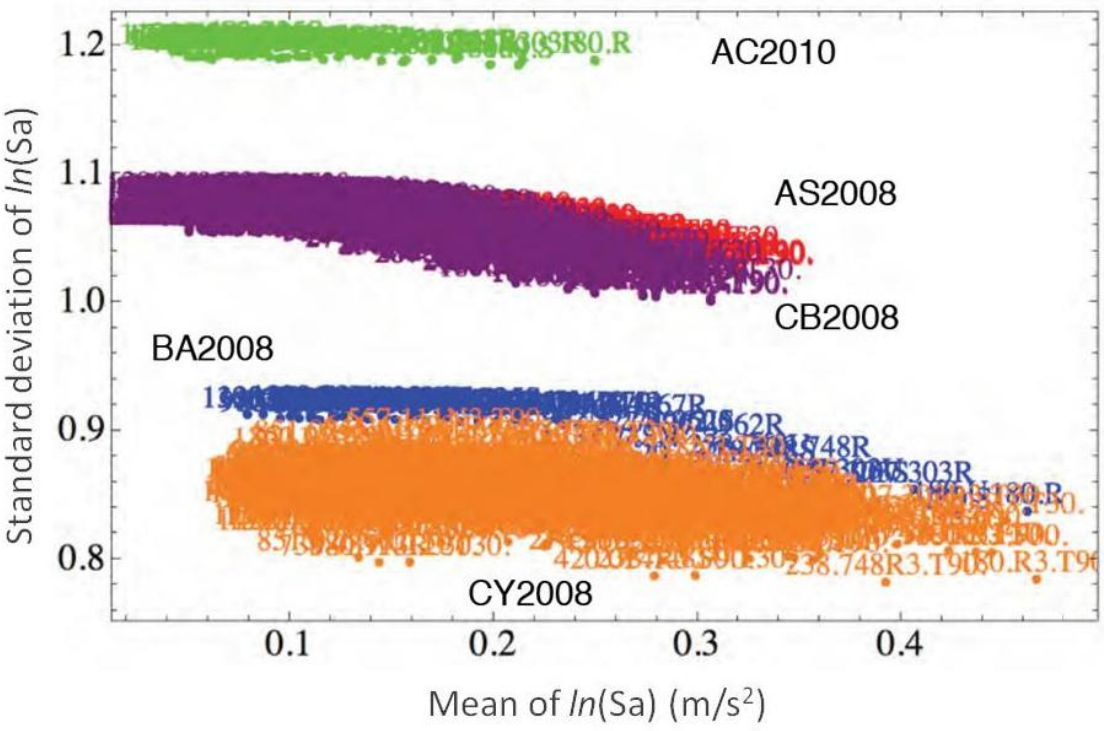


Figure 5.14-32 Point Representations of Hazard Curves Generated for a Site at the Centre of a Simple Circular Source Zone, Sampling the Full Ranges of Parameters in the Five GMPEs Retained After Application of Exclusion Criteria

(see text for explanation of how the mean and standard deviation values were obtained)

The decision was taken to then select only one of the each of the pairs of NGA models that are clustered in this figure. The criterion for making these choices was that the models chosen should have the best possible representation of the physics of ground-motion scaling with magnitude, to allow stable extrapolation to the largest Mmax values in the SSC models. In this regards, the CY08 model was shown to have a functional form for the dependence of ground-motion amplitudes on earthquake magnitude that is entirely consistent with seismological theory, which favoured the inclusion of this model over BA08. Similarly, the AS08 model was judged to have a magnitude-scaling function more consistent with seismological scaling than CB08, favouring the choice of the former model. The inclusion of AC10 as the third model is not inconsistent with this selection since this GMPE essentially adopted the same functional form as that of AS08. The inclusion of the AC10 model was also viewed very positively for another reason, namely that it is derived from a database that is rich in recordings from normal-faulting earthquakes, whereas the NGA database is lacking in accelerograms from such earthquakes. This is an important consideration because normal rupture is the predominant style-of-faulting in South Africa, particularly in the region immediately surrounding the Thyspunt site.

One final consideration in the evaluation of the chosen GMPEs was the selection of appropriate shear-wave velocity, V_s, profiles to represent the deep velocity profile in the 'host' region from where the models are derived. These profiles were needed in order to apply the V_s-kappa adjustments to transform them to be applicable to the target V_s profile of the Goudini bedrock at the Thyspunt site (***Subsection 5.14.4.5***).

Two of the three final equations are NGA models (***References 5.14.129 and 5.14.132***), derived primarily using strong-motion data from California, supplemented by records from Taiwan and small numbers of accelerograms from other countries including Turkey, Iran, Italy, Greece and New Zealand. Although Taiwanese data from the 1999 Chi-Chi earthquakes constituted a major proportion of the datasets used in the derivation of the NGA equations, they were derived primarily for application in California even if they have been found to be applicable to other regions of shallow crustal seismicity as well (***Reference 5.14.137***). For this reason, the TI Team decided that a suitable V_s profile for these four models would be the generic Californian rock profile of Boore & Joyner (***Reference 5.14.138***), which is anchored to a V_{s30} value of 618 m/s. Since none of the NGA model developers proposed making adjustments for different profiles in other contributing regions such as Taiwan (although the parameters $Z_{1.0}$ and $Z_{2.5}$, which are the depths to material with V_s values of 1.0 and 2.5km/s respectively, would partly capture gross differences), this choice was considered both reasonable and defensible.

This only leaves the question of what would be a suitable V_s profile for the Turkish equation of Akkar & Çağnan (***Reference 5.14.134***), and an investigation was undertaken to address this issue. The starting point for this exercise is the paper by Sandıkkaya *et al*. (***Reference 5.14.139***) that presents a uniform site classification for Turkish strong-motion stations using a combination of MASW and correlations with SPT N-values. Additional data came from the paper of Rathje *et al*. (***Reference 5.14.140***) who made SASW measurements at several strong-motion stations in Turkey following the 1999 earthquakes. In all, 29 V_s profiles were compiled and transformed to a common set of reference depths; this was done assuming layer models in which depth is constant over the intervals between reported values; arguably it would have been more realistic to assume a gradient (mostly simply by linear interpolation between reported values) but the assumption of simple layers was assumed adequate for this purpose. Most of the profiles do not extend to the full depth shown although most do go beyond 50 m and many deeper; in all cases the velocity at the lowest depth is assumed to remain constant thereafter. ***Figure 5.14.33*** shows the profiles for a range of V_{s30} values around the standard Californian rock value adopted as the host value for the NGA models. The profiles are grouped by ranges of V_{s30} values, together with the geometric mean V_s values at each depth and the plus-and-minus one standard deviation profiles. Also superimposed on the same figure is the generic rock profile for California from Boore & Joyner (***Reference 5.14.138***), which anchors, as noted previously, at V_{s30} = 618 m/s. The mean V_{s30} of the Turkish station profiles is 620 m/s, which is very close to the anchoring value of the generic Californian rock profile. Since many of the profiles do not extend to depths of more than 50-60m, not too much attention should be given to the velocities at depths greater than 50 m, but down to this level there is rather good agreement between the average Turkish profile and the generic Californian profile. On the basis of this comparison, it was concluded that using the same host V_{s30} value of 620 m/s for the Akkar & Çağnan equations (***Reference 5.14.134***) as for the Abrahamson & Silva (***Reference 5.14.129***) and Chiou & Youngs (***Reference 5.14.132***) models was a defensible choice. The remaining question, however, is whether the deeper Californian profile is an acceptable representation of the deeper velocity profile in Turkey.

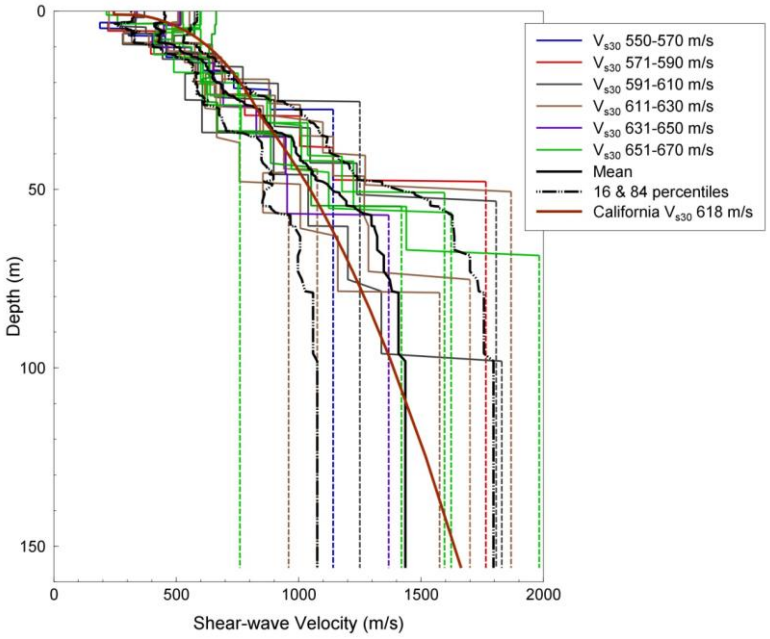


Figure 5.14-33 Shear-Wave Velocity Profiles for Turkish Strong-Motion Stations with V_{s30} Values in the Range from 550-670 m/s, Compared with the Generic California Rock Site Profile of Boore & Joyner (*Reference 5.14.138*)

A search of the literature retrieved a number of studies presenting crustal velocity models for Turkey, but most of them are rather poorly resolved, particularly at shallow depths of most interest to this project. The most useful data were found in ***Reference 5.14.141*** which presents average shear-wave velocity profiles for eastern and western Anatolia determined from analysis of surface wave dispersion. These profiles show a gradual increase with depth from velocities of about 2 km/s in the west and 2.5-2.8 km/s in the east, reaching velocities of 3 km/s at depths of 3-4 km. Tezel *et al.* (***Reference 5.14.142***) explore the variation in crustal structure, and the depth of the Moho, in western Turkey using receiver function analysis. Tezel *et al*. (***Reference 5.14.142***) also give (in their Table 3) a simplified velocity model of the crust in Turkey, reporting V_s values at 1 km interval to a depth of 5 km and at 2 km intervals thereafter. Assuming linear variation of shear-wave velocity between these points, ***Figure 5.14.34*** compares the V_s profile with that developed for California by Boore & Joyner to a depth a few kilometres. Since the Turkish model is very crudely resolved at shallow depths and in effect anchors to a very high V_{s30} of 1,920 m/s at the surface, in order to produce a more realistic Turkish model,

the mean profile is adopted for the top 47 m (where it is well constrained by several profiles), and linearly extrapolated (using the average gradient over the deepest 6.5 m) to a depth where the V_s value reaches 1,920 m/s, which is 136.7 m.

The final study considered is that of Akkar & Yenier (***Reference 5.14.143***), in which generic slowness (reciprocal of velocity) profiles were developed using a combination of shear-wave profiles from Turkey and California, the former only extending to 30 m and being extrapolated using the deeper information from the latter. This in itself suggests the assumption of equivalence between the crustal shear-wave velocity profiles in Turkey and California. ***Figure 5.14.34*** shows the rock profile of Akkar & Yenier (***Reference 5.14.143***) superimposed (with depths truncated at 6 km), compared with the other profiles discussed above. This profile corresponds to a V_{s30} of about 840 m/s, which should be taken into account in making comparisons. On the basis of these simple comparisons, it is concluded that use of the same generic rock profile for California proposed by Boore & Joyner (***Reference 5.14.138***), anchored to a V_{s30} of 620 m/s, could be used as the 'host' profile for all three GMPEs selected for the GMC model.

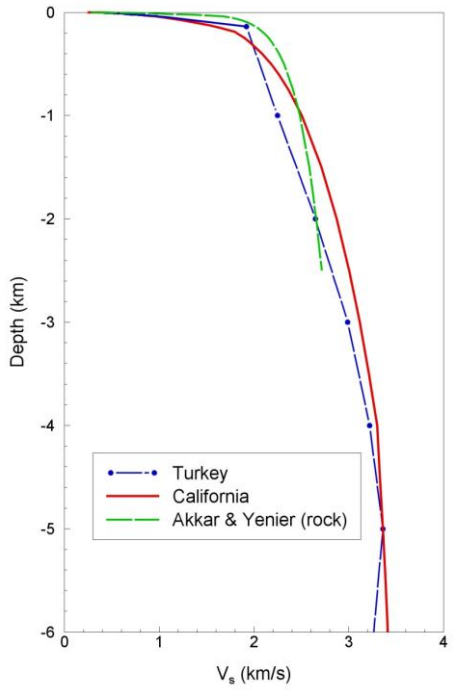


Figure 5.14-34 Comparison of Shear-Wave Velocity Profiles for Turkey and for California from Compiled as Explained in the Text.

n) Geotechnical Investigations for Thyspunt Site

The key parameter for characterising the dynamic response of a site under seismic actions, in order to determine how the upper part of the site influences the surface motions by modifying the upward propagating seismic waves, is the shear-wave velocity, V_s, which is directly related to the stiffness of the materials. Two different approaches were used to measure the V_s profile at the Thyspunt site: the multi-channel analysis of surface waves (MASW) and PS suspension logging. MASW testing was performed at six locations across the Thyspunt site. PS suspension logging took place in two phases. Phase 1 consisted of testing at six locations, while Phase 2 consisted of testing at an additional 23 locations. The second phase of testing was initiated to better constrain the shear-wave velocity model for the site, which is critical to the development of the site-specific ground motions. Detailed information about the shear-wave velocity measurements can be found in ***Reference 5.14.144***. The majority of the testing was performed within the Goudini Formation, the geologic unit underlying the location of the footprint of the Thyspunt facilities. The other testing sites were located on the adjacent formations of Skurweberg, Cedarberg, or Peninsula. A significant layer of sand overlies much of the site. This layer is absent along the southern coastline, but inland ranges from a few metres to more than 20 m thick.

Active (using a rock drop as the energy source) and passive (using ambient vibrations, particular wave action on the coastline at this site) MASW measurements were performed. Although good matches were obtained between the inferred velocity profiles and the measured dispersion curves from the MASW measurement (***Reference 5.14.145***), there was considerable uncertainty in the detailed velocity structure because of the width of the dispersion data at low frequencies. The main limitation on the MASW was that environmental and archaeological restrictions did not permit the use of higher energy sources than a large boulder dropped from a bulldozer (***Figure 5.14.35***) which severely limited the degree of resolution of the bedrock structure because of the thick overlying sand layer. The V_s values obtained were interpreted as average values over several layers, which is not useful for accurately modelling the site response. Consequently, the MASW results were not used in developing the final V_s profiles for use in site response analyses, which were instead based entirely on the results obtained from PS logging.

PS suspension logging is a borehole technique that measures the shear and compression wave velocity of the material adjacent to the borehole wall (***Figure 5.14.36***). The PS suspension logging method directly measures the shear-wave velocity at different depths within a borehole using travel time measurements between locations a known distance apart. Shear (and

compression) waves are generated by a probe (***Figure 5.14.36***) that is inserted in a fluid-filled borehole; these waves travel vertically through the soil or rock immediately adjacent the borehole, and the passage of these waves is recorded on geophones located within the borehole. By identifying the arrival of the waves at each of two receivers and knowing the distance between receivers (generally 1 m), a velocity is computed. Velocity measurements are made approximately every 0.5 m.

PS suspension logging was performed in a total of 29 boreholes. For each borehole, continuous rock cores were obtained and a geologic description and RQD were assigned. Some unconfined compressions tests and point load tests were performed in the laboratory. Twenty-one boreholes were located on the Goudini Formation (the main formation upon which the Thyspunt facilities are located), four boreholes were located on the Cedarberg Formation (adjacent to the Goudini), three boreholes were located on the Skurweberg Formation, and one borehole was located on the Peninsula Formation.



Figure 5.14-35 Rock Drop Source and Geophone Array for Active MASW Testing.



Figure 5.14-36 Borehole Preparation for PS Logging and Suspension Logging Probe.

Based on the geologic descriptions of the cores, four boreholes (NewF, NewN, NewQ, and NewU) transitioned from one geologic formation to another because of the proximity to the geologic contact and the south-dipping nature of the contact. The Skurweberg and Peninsula Formations are not representative of the Goudini Formation, and thus these results are not presented. The remaining profiles from the Goudini and Cedarberg are presented and discussed below. The shear-wave velocity profiles are plotted in groups of 5 or 6 to facilitate viewing individual profiles, and each point in these velocity profiles represents the spatial average of 5 vertically adjacent velocity measurements. ***Figure 5.14.37*** indicates these groups along with the locations of the geologic units across the site.

© Eskom 2026/Rev 0a

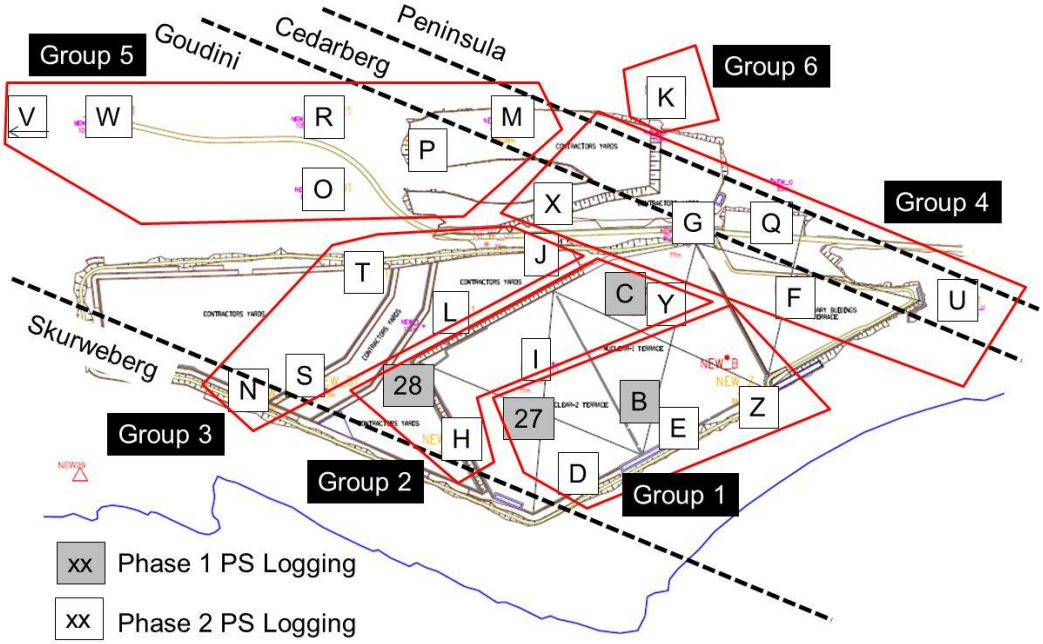


Figure 5.14-37 Locations of Phase 1 and Phase 2 PS Suspension Logging Sites.

The group-to-group variations in the V_s profiles obtained from the PS logging did were not significant compared to the within group variability, and there was no strong correlation between the velocity profiles and the geologic formation. For this reason all of the 26 profiles from within the Goudini and Cedarberg formations (on which the proposed nuclear islands are located) were grouped and are plotted together in ***Figure 5.14.38***. The average velocity profile starts at about 1,200 m/s at the top of rock and linearly increases to 3,000 m/s at about 60 m depth. There is considerable variability between the individual velocity profiles. This variability could not have been accurately quantified without the additional shear-wave velocity information obtained from the Phase 2 PS suspension logging. Plotted in ***Figure 5.14.39*** is the standard deviation of the natural log of the V_s data (σ_{lnVs}) as a function of depth, as well as the number of shear-wave velocity points available at each depth. The standard deviation is only shown over depths where there are three or more measurements of shear-wave velocity. Generally, σ_{lnVs} decreases with depth, with values of 0.2 to 0.3 near the surface and values close to 0.1 at depth. The variability increases at depths greater than about 70 m but this increase is caused by the reduction in the number of velocity profiles at these depths.

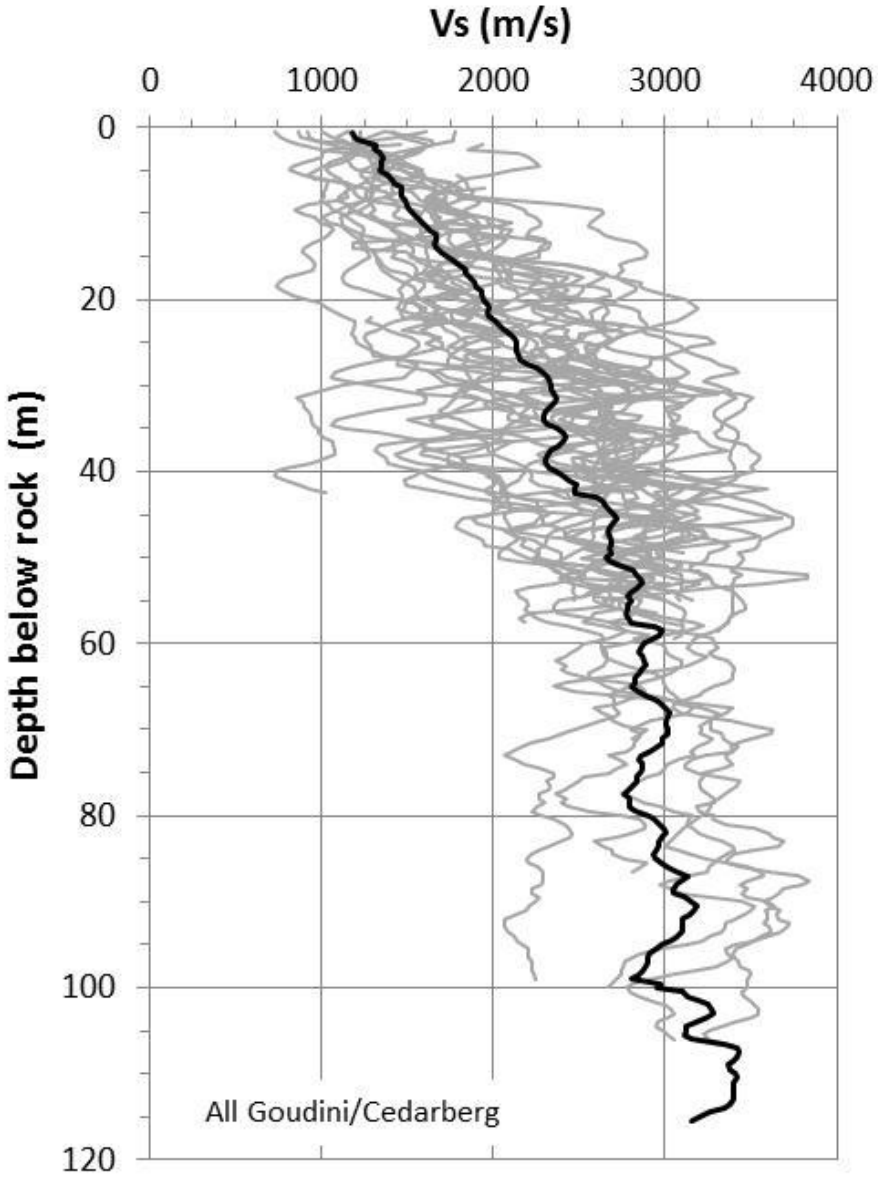


Figure 5.14-38 Average and Individual Shear-Wave Velocity Profiles Measured Within the Goudini and Cedarberg Formations.

© Eskom 2026/Rev 0a

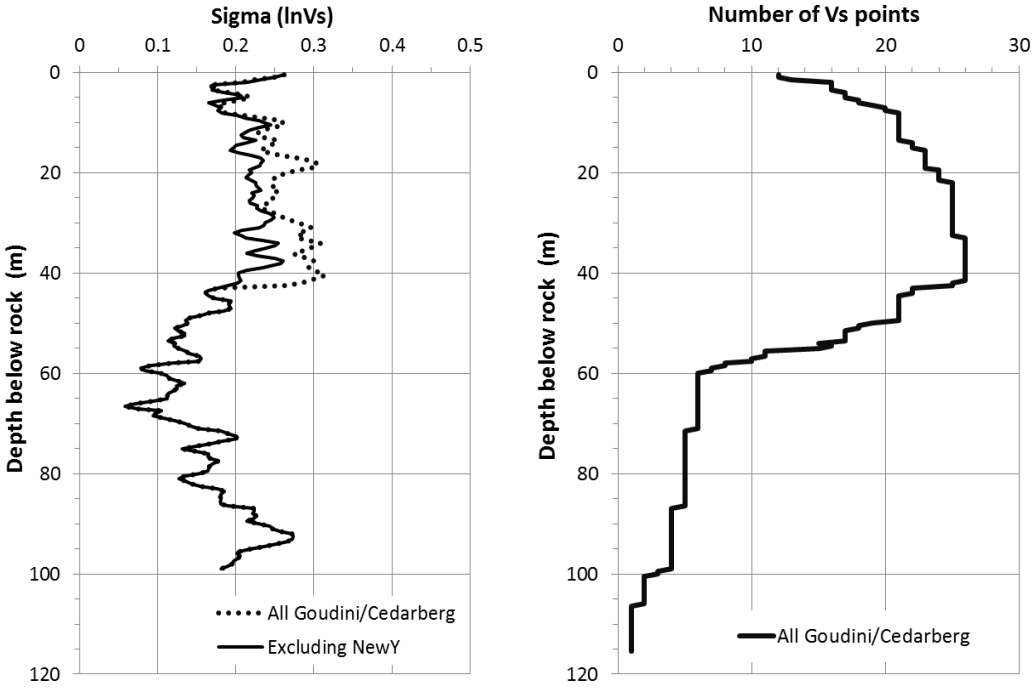


Figure 5.14-39 Variability in the Shear-Wave Velocities (σ_{lnVs}) and Number of V_s Points Available Versus Depth.

5.14.5 The SSHAC Framework

This subsection describes the development of the SSC and GMC models that together characterise the tectonic, geological, seismic and geophysical setting of the Thyspunt site and the surrounding regions. The models are based on interpretation and evaluation of the databases developed in the early stages of the PSHA project (***Subsection 5.14.4***). An important distinguishing feature of the development of these models is that the work was conducted as a SSHAC Level 3 process, in strict adherence with the guidelines specified in NUREG-2117 (***Reference 5.14.2***).

5.14.5.1 Roles and Organisational Structure of the Project

A defining feature of a SSHAC Level 3 process is the clear definition of each participant's role in the project, as well as definition of the responsibilities associated with that role, which are clearly specified in NUREG-2117

(***Reference 5.14.2***). The organisational structure of the Thyspunt PSHA project is illustrated in ***Figure 5.14.40***.

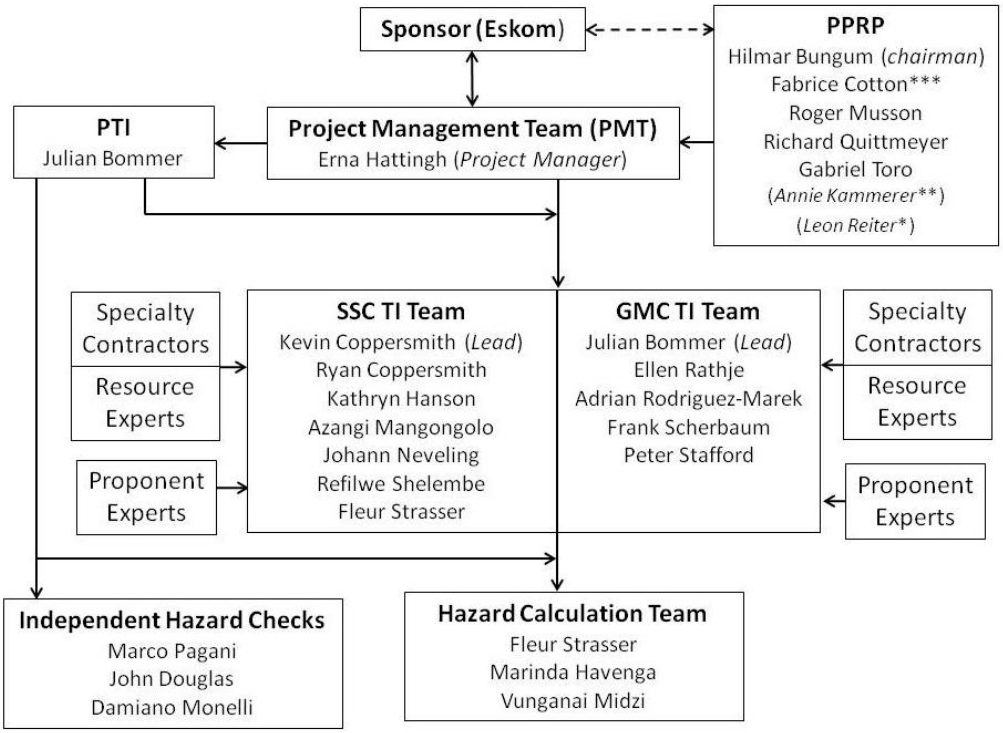


Figure 5.14-40 Organisational Structure for the SSHAC Level 3 Thyspunt PSHA.

(*Notes*: * Resigned for health reasons after Workshop #1; ** Resigned for personal reasons after Workshop #2; * Joined PPRP after Workshop #2)**

Individuals were selected for the various roles following the selection criteria specified in NUREG-2117 (***Reference 5.14.2***), which are illustrated graphically in ***Figure 5.14.41***. The TI Teams are those responsible for making the evaluations of the available data, method and models, and on the basis of this evaluation to develop models that capture the CBR of the TDI. The TI Teams must collectively assume intellectual ownership of the final SSC and GMC models, which means being prepared and able to defend the models and their technical bases. The work of the TI Teams is supported, informed and facilitated by Specialty Contractors, who are engaged to collect, process or analyse particular data sets, and Resource Experts, who impart knowledge of a particular dataset, method or model to the TI Teams. Whereas Speciality Contractors are engaged for extended periods, particularly during the early

stages of the project, Resource Experts mainly contribute through participation in the first two of three Workshops that form key elements of the SSHAC Level 3 process (***Subsection 5.14.5.2***). Proponent Experts are individuals invited to advocate the use of a particular method or model in the PSHA, and they are generally engaged at the second Workshop (***Subsection 5.14.5.2***). The overall sequence of tasks in the SSHAC Level 3 process, including the Workshops mentioned above, is shown in ***Figure 5.14.42***. The punctual engagement of Resource and Proponent Experts at the first and second Workshops is illustrated in this figure, which also indicates how most Specialty Contractors are engaged during the database development stage that continues approximately half-way through the project.

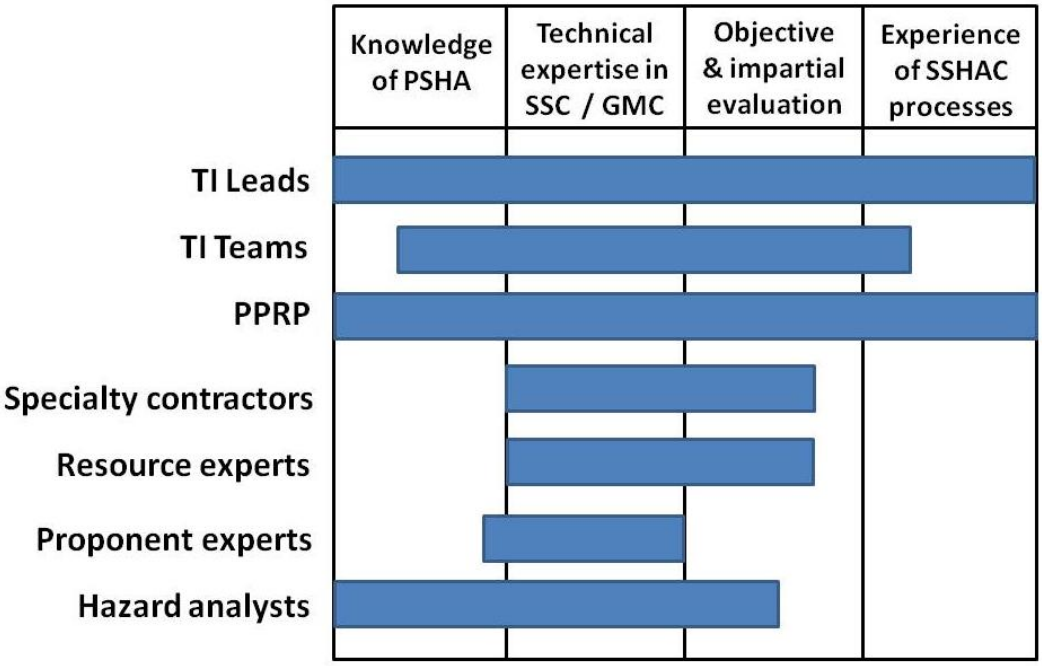


Figure 5.14-41 Illustration of the Skills and Experience Required for Different Roles in a SSHAC Level 3 PSHA.

The length of the bar in each column reflects the degree to which the attribute is required for the role: if the bar fills the width of the column, it is an indispensable requirement, whereas if the column is blank, the attribute is not needed for that specific role.

As can be appreciated from ***Figure 5.14.42***, apart from the sponsor (Eskom) providing oversight throughout the project, three other groups are engaged for the entire duration. The first of these is the Project Management (PM) Team, which was composed of several staff members at the Council for Geoscience (CGS) in Pretoria. The management system applied to the project is described in detail in ***Subsection 5.14.8***. The TI Teams participate throughout the project, being engaged in evaluation during the early phases and then integration subsequently (***Subsection 5.14.5.3***). The third group engaged throughout the project are the PPRP, who perform continuous process and technical review of the work undertaken (***Section 5.14.5.5***).

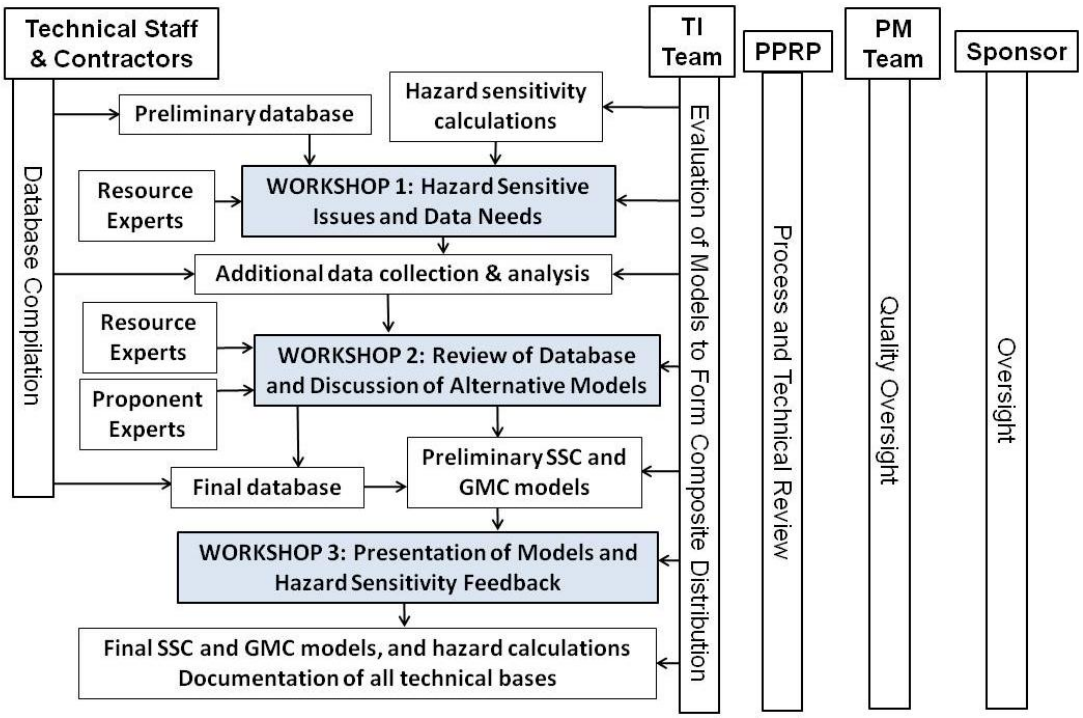


Figure 5.14-42 Overview of the SSHAC Level 3 Process Applied to the Thyspunt PSHA.

Time runs vertically down from the top of the figure.

One other role indicated in ***Figure 5.14.40*** is that of Project Technical Integrator (PTI). The PTI effectively works together with the Project Manager on the overall direction and coordination of the project, but with specific responsibility for technical issues rather than the contractual and administrative issues that fall within the remit of the Project Management Team (PMT). As illustrated in ***Figure 5.14.40***, two specific responsibilities attached to the PTI role are coordination of the two TI Teams (in order to ensure that all interface issues are addressed, primarily through communication between the SSC and GMC TI Leads) and coordination of the hazard calculations, which includes facilitating and arbitrating the independent checks on these calculations.

5.14.5.2 Workshops and Meetings

As illustrated in ***Figure 5.14.42***, the SSHAC Level 3 process is built around three formal workshops, focused on three clearly defined themes:

- Workshop #1: Hazard Sensitive Issues and Data Needs
- Workshop #2: Review of Database and Discussion of Alternative Models
- Workshop #3: Presentation of Models and Hazard Sensitivity Feedback

At the first Workshop (held in Cape Town, 11-15 April 2011), simplified hazard calculations were presented, using very preliminary SSC and GMC models, in order to identify the elements exerting the greatest influence on the hazard estimates at the site. This assisted the TI Teams in identifying the key issues on which to focus efforts in order to reduce uncertainties. The Workshop also included presentations by several Resource Experts and Specialty Contractors, as well as members of the TI Teams, on available databases relevant to the seismic characterisation of the region and the site. The outcome of the Workshop was a series of clearly defined activities regarding the compilation of the databases and additional data collection activities.

The second Workshop (held in Stellenbosch, 15-21 January 2012) reviewed the almost completed databases, and also included several presentations by Proponent Experts (***Tables T-5.14.3*** and ***T-5.14.4***). The Proponent Experts were selected on the basis of being respected scientists who have developed models directly relevant to the Thyspunt PSHA, either by virtue of being specifically for South Africa or by being applicable to approaches being adopted to define the SSC and GMC models. The invitations to Proponent Experts to present their models at Workshop #2 is an important aspect of ensuring that the evaluation by the TI Teams has given due consideration to the full range of technical views within the broader scientific communities.

© Eskom 2026/Rev 0a

At the final Workshop (held in Stellenbosch, 27-31 August 2012), the preliminary SSC and GMC models were presented by the TI Teams, who explained the technical bases of the models. The PPRP, in accordance with the specifications of NUREG-2117 (***Reference 5.14.2***), was able to question the Teams on the data they had used, their evaluations and the justification of their decisions. The Workshop also provided an opportunity to present multiple sensitivity analyses showing the impact of different elements of the preliminary SSC and GMC models on the seismic hazard estimates.

Table 5.14.3
SSC Proponent Experts

Name and Affiliation	Presentation at Workshop #2
Marco Andreoli **Necsa, South Africa**	**Implications of Neotectonic Evidence in the Eastern Cape Region**
Paul Bierman **University of Vermont. USA**	**Cosmogenic geochronology investigations for uplift rates and ages of surfaces: Implications for the tectonic stability and geomorphic evolution of Southern Africa**
Hayley Cawthra **GCS, Bellville, South Africa**	**Depositional and erosional processes occurring on the continental shelf and slope: Implications to causative mechanisms and origins of seafloor features**
Coenie de Beer **GCS, Bellville, South Africa**	**Tectonic interpretation of the Ceres earthquake area and implications to the locations of future seismicity**
Ray Durrheim **Wits University, Johannesburg / CSIR**	**Regional crustal studies and implications for seismotectonic models**
Marc Goedhart **Kainos South Africa, South Africa**	**Palaeoseismic characteristics of the Kango fault and associated uncertainties, Coega fault style and potential CFB SSZs**
Chris Hartnady **Umvoto, South Africa**	**Seismotectonic model for southern Africa and implications of tectonic features to seismic hazard**
Andrzej Kijko **Aon Benfield Natural Hazard Centre, University of Pretoria, South Africa**	**Mmax and its estimation**
Bob Youngs **AMEC, Oakland, USA**	**Bayesian approach to assessing maximum magnitude for PSHA**
	Recurrence model options and incorporation of catalogue-related uncertainties
Martin Brandt **(Presenting an overview of several Proponent Experts' positions)** **CGS, Pretoria, South Africa**	**Constraints on the processes giving rise to the African Superswell**

Table 5.14.4
GMC Proponent Experts

Name and Affiliation	Presentation at Workshop #2
Linda Al Atik **Independent consultant, CA, USA**	**Evaluation of Vs-kappa scaling using RVT and empirical ground-motion data**
Kenneth W. Campbell **EQECAT, Inc., Beaverton, Oregon, U.S.A**	**The hybrid-empirical method**
Andrzej Kijko **Aon Benfield Natural Hazard Centre, Univ of Pretoria, South Africa**	**GMPEs for PSHA in South Africa**
Oona Scotti **IRSN Institut de Radiopretection de Surete Nucleaire, France**	**Inferring geometrical spreading from the attenuation of macroseismic Intensity with distance**
Trevor Allen **Geoscience Australia, Canberra, Australia**	**Similarities and differences in SCR ground motions inferred from instrumental recordings.**

The three formal Workshops of a SSHAC Level 3 study, as noted previously, provide a unique opportunity for the TI Teams to interact with external experts and also for the PPRP and the sponsor to observe the processes. The work of developing the SSC and GMC models, however, is mainly done outside the Workshops and involves interactions among the members of the TI Teams in a number of ways, including emails, telephone calls and conference calls. A number of more formal Working Meetings are also held (***Figure 5.14.43***), in which all members of each TI Team participate, and these serve to present and discuss work carried out by individual team members prior to the meeting. Although conducted following an agenda, the Working Meetings provide a more informal setting than the Workshops and the opportunity for Team members to engage in the process of technical challenge and defence, which is vital to building a composite model for which the entire Team is able to finally assume ownership.

Each TI Team held four Working Meetings (***Figure 5.14.43***), the first between Workshops #1 and #2, the second and third in the interval prior to Workshop #3, and the final meeting after Workshop #3. The purpose of the first Working Meeting (WM1) is mainly to plan for Workshop #2, whereas the second and third Working Meetings (WM2, WM3) mark the transition from the evaluation phase to the integration phase, and it is at the second of these meetings that the preliminary SSC and GMC models are developed. The purpose of the final Working Meeting (WM4) is to modify the preliminary model in light of the feedback from Workshop #3, and to develop the final models.

© Eskom 2026/Rev 0a

5.14.5.3 Evaluation and Integration Stages

As noted in ***Subsection 5.14.4.1***, the SSHAC Level 3 process involves two main stages, evaluation and integration. The evaluation stage begins from the very outset of the project, with an assessment of previous seismic hazard studies for the region or site, and the buildings of the project databases. The evaluation continues through both of the first two Workshops, with a key milestone being the interactions of the TI Teams with Proponent Experts at Workshop #2. Following this second Workshop, the SSC and GMC databases were completed and then the TI Teams held their second Working Meetings. For both TI Teams, the second Working Meeting focused on completing the evaluation of available data, methods and models. The outcome of the evaluation stage was each TI Team coming to final decisions about which models and data would be used to construct the SSC and GMC logic-trees, as well as indications of the more favoured interpretations and the ranges of associated uncertainty.

As indicated in ***Figure 5.14.43***, at this point the TI Teams move into the integration stage, in which the objective is to construct logic-trees that capture the CBR of the TDI (***Subsection 5.14.7.3***). The development of the preliminary models was the focus on the third Working Meeting for each TI Team, which was also held during the period between Workshop #2 and Workshop #3. The preliminary models were summarised in the preliminary Hazard Input Document (HID), which is a summary of the SSC and GMC logic-trees providing all the information required to execute the PSHA but without any explanation or justification of the derivation of the models. The HID was passed to the Hazard Calculation Team at CGS, who ran extensive hazard calculations, presenting the results in a variety of ways that showed the contributions of individual branches to the total hazard.

At Workshop #3, the TI Teams presented the preliminary SSC and GMC models, explaining the technical bases for all of the decisions taken to construct these preliminary logic-trees. The PPRP questioned the TI Teams on all aspects of the model, pointing out elements that they felt were not adequately justified or where it was not clear if the CBR of the TDI was being fully captured. The TI Teams were also informed about elements of their models requiring additional attention and possible re-examination in the light of the hazard sensitivity feedback. This feedback also served to identify those parts of the logic-trees exerting only minor influence on the hazard estimates and the total uncertainty in the hazard, which helped the TI Teams to focus only on revising the more important elements of the models.

© Eskom 2026/Rev 0a

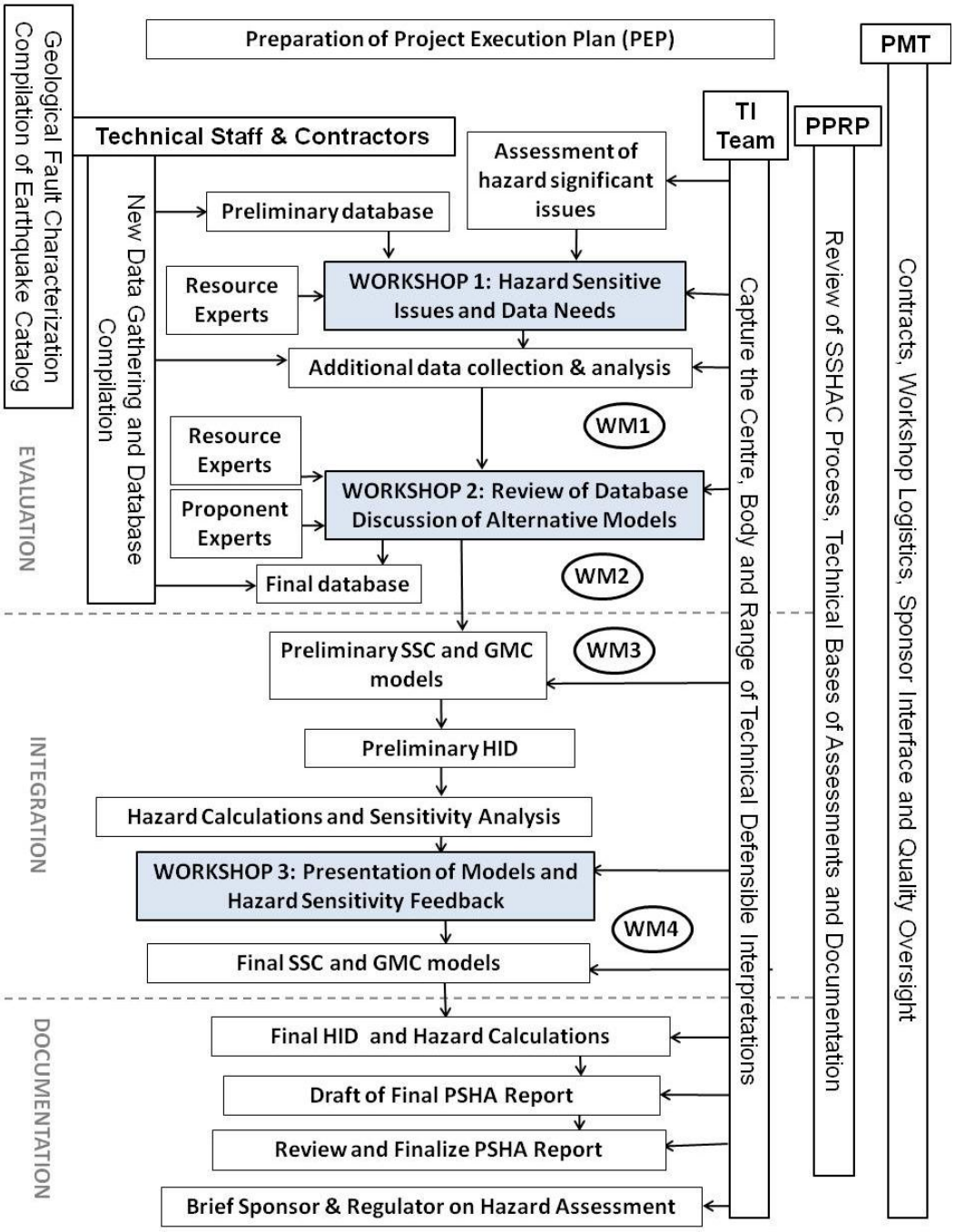


Figure 5.14-43 Overview of the SSHAC Level 3 Process Applied to the Thyspunt PSHA, expanded from *Figure F-5.14.42*.

***WM is Working Meeting*.**

Following Workshop #3, the TI Teams worked on revising their preliminary models, meeting for a fourth and final Working Meeting to finalise the SSC and GMC models. The final models were then summarised in the final HID, which was passed to the Hazard Calculation Team to perform the definitive PSHA calculations. The HID was also passed by the PTI to those conducting the independent hazard checks (***Figure 5.14.40***), to perform spot checks on the implementation of the SSC and GMC logic-trees (***Subsection 5.14.6.4***). At that point, the project moved from the integration stage to documentation of the full PSHA study, resulting in a comprehensive report with extensive appendices (***Reference 5.14.17***).

5.14.5.4 Seismic Source Characterisation (SSC) Model

An SSC model in a PSHA defines the seismogenic potential, locations, sizes, and rates of future earthquakes. This section summarises the general approaches and criteria used in the development of the SSC model (***Subsection 5.14.5.4.(a)***), as well as providing an overview of its general structure (***Subsection 5.14.5.4.(b)***), and then goes on to discuss the technical bases for the global assessments (*i.e.*, those affecting several sources) made during the development of the SSC model (***Subsection 5.14.5.4.(c)***). This is followed by an overview of the source-specific assessments for the individual seismic source zones (***Subsection 5.14.5.4.(d)***) and fault sources (***Subsection 5.14.5.4.(e)***) included in the SSC model. Finally, the technical justifications for assessing a number of faults studied during the geological investigations (***Section 5.13***) as non-seismogenic, and thus not including them in the SSC model, are discussed in ***Subsection 5.14.5.4.(f)***. The full detail of these technical justifications is given in Chapter 8 of ***Reference 5.14.17***.

a) General Approach and Criteria

The development of an SSC model comprises the identification and characterisation of seismic sources. To be useful, the SSC model should include elements that are appropriate to the tectonic environment for which it is developed. As discussed in more detail in ***Subsection 5.14.5.4.(c) i*** the Thyspunt site lies within an SCR away from any major plate boundaries and major faults. As a result, there is generally a lack of a clear definition of the causative faults giving rise to the observed seismicity, which needs to be considered in the selection of the methodologies adopted in the development of the SSC model.

Mindful of the tectonic setting and precedents for methods available to identify and characterise seismic sources within SCRs, an approach was taken that included the following steps:

© Eskom 2026/Rev 0a

- Consideration of hazard-significant technical issues and prioritisation of the data according to their importance to addressing important SSC issues;
- Compilation of available data and gathering of new data to address these issues;
- Evaluation of applicable data, models, and methods;
- Identification of seismic sources according to defined criteria;
- Characterisation of each seismic source, including the associated uncertainties using a logic tree approach.

The first two steps, pertaining to data compilation, are discussed above in ***Subsection 5.14.4***. Generic aspects of the evaluation step are also addressed therein, as well as in ***Subsection 5.14.5.3***, with specific aspects relevant to the development of the SSC model summarised in ***Subsection 5.14.5.4.(a) v*** below. The present section deals more specifically with the general approach and criteria adopted for the identification of seismic sources.

i Criteria for defining seismic sources

The criteria used by the SSC TI Team to define seismic sources in the Thyspunt PSHA were identified based on due consideration of the SCR tectonic regime, the types of seismic sources that might be present (*e.g.*, fault sources and source zones), and precedent from recent SSC models developed for similar tectonic environments and for nuclear facilities (***References 5.14.69 and 5.14.146***). Based on these considerations, unique seismic sources are defined to account for distinct *differences* in the following criteria:

- Probability that a fault is seismogenic, p[S]
- Expected future earthquake characteristics
- Earthquake recurrence rate
- Maximum earthquake magnitude (Mmax)

By “differences,” it is meant that a given potential seismic source would differ significantly in one or more of these criteria from its neighbour such that identifying a unique seismic source is justified. The first criterion, which is applicable exclusively to fault sources, determines whether a fault is explicitly included in the SSC model (p[S]>0) or not (p[S] = 0), and is discussed in more detail in ***Subsection 5.14.5.4.(a) ii***. An overview of the parameters defining future earthquake characteristics is given ***Subsection 5.14.5.4.(a) iii***, followed

© Eskom 2026/Rev 0a

by a general definition of recurrence parameters, including recurrence rate and Mmax, in Section ***Subsection 5.14.5.4.(a) iv***.

The criteria for identifying seismic sources provide a basis not only for the SSC modelling effort discussed in this section and documented in more detail in Chapter 8 of the PSHA report (***References 5.14.17***), but also for focusing and prioritising the data evaluation process (***Subsection 5.14.4***). That is, each data set evaluated was considered relative to whether the criteria were applicable and, if so, the degree of reliance on that data set was evaluated and documented, as summarised in ***Table T-5.15.5***.

ii Seismocgenic probability p[S]

In the Thyspunt PSHA, a seismogenic fault is defined by all of the following:

- Involved in the contemporary tectonic environment
- Capable of generating moderate-to-large (M > 5) earthquakes
- Worthy of being represented as a fault source in the PSHA

These attributes give rise to the types of criteria that are useful in identifying seismogenic faults as well as the manner in which seismogenic faults are included in the hazard analysis. Faults that are not identified as being seismogenic are represented by virtual faults within source zones, which are defined by random locations with given rupture orientation, style of faulting, dip, depth, and magnitude-dependent rupture dimensions (see ***Subsections 5.14.5.4.(a) iv*** and ***5.14.5.4.(c) ii*** to ***5.14.5.4.(c) vi***). In this sense, all seismic source zones are assumed to be seismogenic. However, any individual mapped fault is either seismogenic or not seismogenic from the standpoint of the PSHA; the uncertainty in this assessment is expressed as the "seismogenic probability," or p[S]. A fault assessed to have a p[S] > 0 is modelled in the PSHA as a localiser of future seismicity and the fault source is characterised by fault-specific attributes that define the style of faulting, three-dimensional geometry, M_{char}, and earthquake recurrence.

The assessment of p[S] for any particular fault is a judgment made by the SSC TI Team in light of the available data. A number of criteria were used to make the assessment, depending on the types and quality of the data available. Criteria for assessing p[S] that were considered by the SSC TI Team are listed below, in order of decreasing diagnostic power:

- *causal* association with a M > 5 historical earthquake;

Table 5.14.5
SSC TI Team Prioritisation of Data That Can Be Used to Address the Attributes of the Criteria for Identifying Seismic Sources

Criteria for Identifying Seismic Source	Attributes of the Criterion	Relative Usefulness of the Attribute[1]	Data that Address the Attributes	Relative Usefulness of the Data[2]	Comments
Earthquake Recurrence	Palaeoseismic evidence of geologically recent earthquakes	5	Geologic evidence of recent (Quaternary) fault displacement	4	Recency of slip by itself is not very diagnostic of recurrence rate
			Quaternary fault slip rate	5	
			Palaeoliquefaction data, including age, distribution, characteristics	3-4	Uncertainties in source and magnitudes
	Historical evidence for M > 5 earthquakes	5	Catalogue of historical and instrumental earthquakes: uniform moment magnitude, declustered, corrected for completeness	5	
	Historical evidence for M < 5 earthquakes	4-5	Catalogue of historical and instrumental earthquakes: uniform moment magnitude, declustered, corrected for completeness	4-5	Uncertainties in relationship between smaller- and larger-magnitude earthquakes
	Evidence of crustal strain	2	Geologic indicators of recent strain (*e.g.*, Quaternary)	5	Indicators may be clear, but relation to recurrence unknown
			Tectonic geodetic strain data	3	Same as above plus short-term observations
Maximum Earthquake Magnitude	Fault rupture dimensions (length, displacement per event, area)	5	Fault behavioural data on palaeo-displacements, rupture lengths, segmentation	5	
			Empirical relations between rupture dimensions and magnitude	4	
	Parameters for Bayesian approach for stable continental regions	3	Tectonic evidence for Mesozoic and younger extension, or not	3	Unknown physical constraints on Mmax; weak statistics
Future Earthquake Characteristics (style of faulting, orientation of ruptures, seismogenic thickness/depth)	Historical evidence of earthquake characteristics	4-5	Earthquake focal mechanisms	5	
			Focal depth distributions; seismogenic crustal thickness	3	Interpretations needed to use focal depth for seismogenic thickness
	Prehistoric evidence of earthquake characteristics	4	Fault behaviour of Quaternary faults	5	
	Contemporary seismotectonic setting	3	Contemporary stress indicators, including earthquake focal mechanisms, in-situ stress measurements	4	
			Plate tectonic setting	2	
			Comparisons with other settings wrt rates of deformation	2	
			Strain indicators and rates: geologic, geodetic, uplift	4	
			Structural evidence for orientation	2	
			Indirect Indicators of seismogenic crustal thickness, such as heat flow	1	
Seismogenic Probability p[S]	Evidence for geologically recent displacement	5	Fault behaviour of Quaternary faults	5	
			Geologic evidence for Quaternary deformation, folding, uplift, subsidence	4	
	Clear spatial association with small-earthquake seismicity	4	Historical and instrumental seismicity, uncertainties in location, mapped faults	3	
			Earthquake focal mechanisms and interpretations of fault geometry	2	

© Eskom 2026/Rev 0a

- geologic evidence for co-seismic displacement(s) during Late Quaternary to Holocene;
- geologic evidence for Quaternary displacement;
- geologic evidence for displacements that are consistent with contemporary tectonic environment, but inconsistent with previous environments;
- *spatial* association with M > 5 earthquake;
- *spatial* association with M < 5 earthquakes;
- favourable orientation relative to contemporary stress regime;
- significant extent, downdip dimension, cumulative slip.

A highly diagnostic criterion for assessing p[S] is a *causal* association with large-magnitude earthquakes (*e.g.*, faults associated with coseismic displacements associated with recorded earthquakes). In general, such an association does not exist with any of the faults evaluated for the Thyspunt PSHA (see ***Subsections 5.14.5.4.(e)*** and ***5.14.5.4.(f)***). However, the presence of co-seismic displacements during the Holocene and Late Quaternary has been established for the Kango Fault (***Subsection 5.14.5.4.(e) i***). The presence or absence of Quaternary displacement was a strong focus of the geological investigations to assess the p[S] of all of the faults evaluated. Less diagnostic criteria include the spatial association with observed seismicity. To confirm the seismogenic potential of a mapped fault, a clear alignment of a significant number of well-located earthquakes along the fault is required. No such alignments were encountered in the Thyspunt SHA study, in view of the sparse nature of the earthquake catalogue (***Subsection 5.14.4.4***), which only contains very few large-to-moderate events, and generally includes large location uncertainties for smaller earthquakes. The least diagnostic criteria are those that are related to the orientation of a fault relative to the tectonic stress regime, or to the dimensions of a fault within the crust. These latter criteria are judged to be “necessary but not sufficient” to identify a seismogenic fault.

iii Future earthquake characteristics

The earthquakes that occur within the seismic sources or along the fault sources of the Thyspunt SSC model are defined by a number of characteristics. In most cases the characteristics are those that are needed by the GMC model (***Subsection 5.14.5.5***) because the ground-motion prediction equations (GMPE) require them as input. For example, the source-to-site distance in recent GMPEs is typically characterised by the closest distance to a rupture of

finite, magnitude-dependent dimensions. This means that the finite ruptures need to be represented in a realistic manner in the SSC model, including the three-dimensional geometry of the ruptures. As a result, the SSC model includes rupture geometry information not only for the fault sources, but also for virtual faults (faults that occur at random locations) within the seismic source zones.

The term “future” in the section heading is important. *All* of the elements of an SSC model are intended to describe the expected *future* locations, sizes, and rates of earthquakes, but it is added here as a reminder to the reader. This is because there is a tendency to assume that all seismic source characteristics are simply a function of what has been observed. However, in SCRs such as the Thyspunt study region, there have been very few moderate-to-large earthquakes and, for some source zones such as the ECC source that hosts the Thyspunt site, there have been *no* $M > 5$ earthquakes in the historical record. Thus, the assessment of characteristics of, say, the rupture strike, dip, and length of ruptures associated with a M_w 7 earthquake must be based on information other than that derived strictly from within the seismic source of interest. So, although the past history of earthquakes in a region of interest as represented by the geologic and seismologic record is important, it is the *future* earthquake characteristics that we are defining for an SSC model.

The future earthquake characteristics that were defined in the SSC model are the following:

- seismogenic crustal thickness;
- depth distribution of hypocentres;
- size of ruptures, as function of magnitude;
- length-to-width aspect ratio of ruptures;
- style of faulting;
- strike and dip of ruptures;
- nature of source boundaries relative to ruptures.

The technical bases for these assessments are summarised below in ***Subsections 5.14.5.4.(c) ii*** to ***5.14.5.4.(c) vi***.

© Eskom 2026/Rev 0a

iv Characterisation of earthquake recurrence

Earthquake recurrence relationships are a key part of the SSC model for a PSHA. They characterise the temporal behaviour of future earthquakes by defining the annual frequency of earthquake of various magnitudes up to the maximum magnitude for each seismic source, Mmax.

Several models exist to characterise earthquake recurrence, as illustrated in ***Figure 5.14.44***, which shows the magnitude-frequency distributions associated with three commonly used recurrence models (***References 5.14.25, 5.14.147 and 5.14.148***). The truncated exponential model (***Reference 5.14.25***) is parameterised in terms of the maximum magnitude, Mmax, the seismic activity rate (annual number of earthquakes greater than or equal to a given minimum magnitude, also referred to as *a*-value) and the *b*-value, which characterises the slope of the exponential decay and thus the relative frequency of earthquakes of different magnitudes. The characteristic model (***Reference 5.14.147***) combines an exponential portion with the concept of a large-magnitude characteristic earthquake of magnitude M_{char} occurring at regular intervals. The maximum moment model (***Reference 5.14.148***) is a variant on the characteristic model where the source only produces characteristic events. The last two models are parameterised using the magnitude of the characteristic event (M_{char}) and the rate at which this event occurs, which can be inferred from a slip rate, or deduced from the mean recurrence interval assessed for the characteristic event.

The parameterisation of the recurrence models is undertaken on the basis of the catalogue of historical and instrumental earthquakes (***Subsection 5.14.4.4***) and/or results from palaeoseismic investigations (***Section 5.13*** and ***Subsection 5.14.4.3***), which provide information regarding the repeated pattern of larger earthquakes through time. Typically, in the context of assessing recurrence models in an SCR environment, the former approach is applied in the context of source zones in conjunction with a truncated exponential model, and the latter when characterising the recurrence of fault sources using characteristic models.

The recurrence models presented above can be further refined by removing the usual assumptions of stationarity in time and space. For such models to be technically defensible, the availability of reliable data-based constraints needs to be considered, and therefore the options available for modelling recurrence in SCRs, where observational data are sparse, are fundamentally different from those that can be considered in a plate-boundary context.

© Eskom 2026/Rev 0a

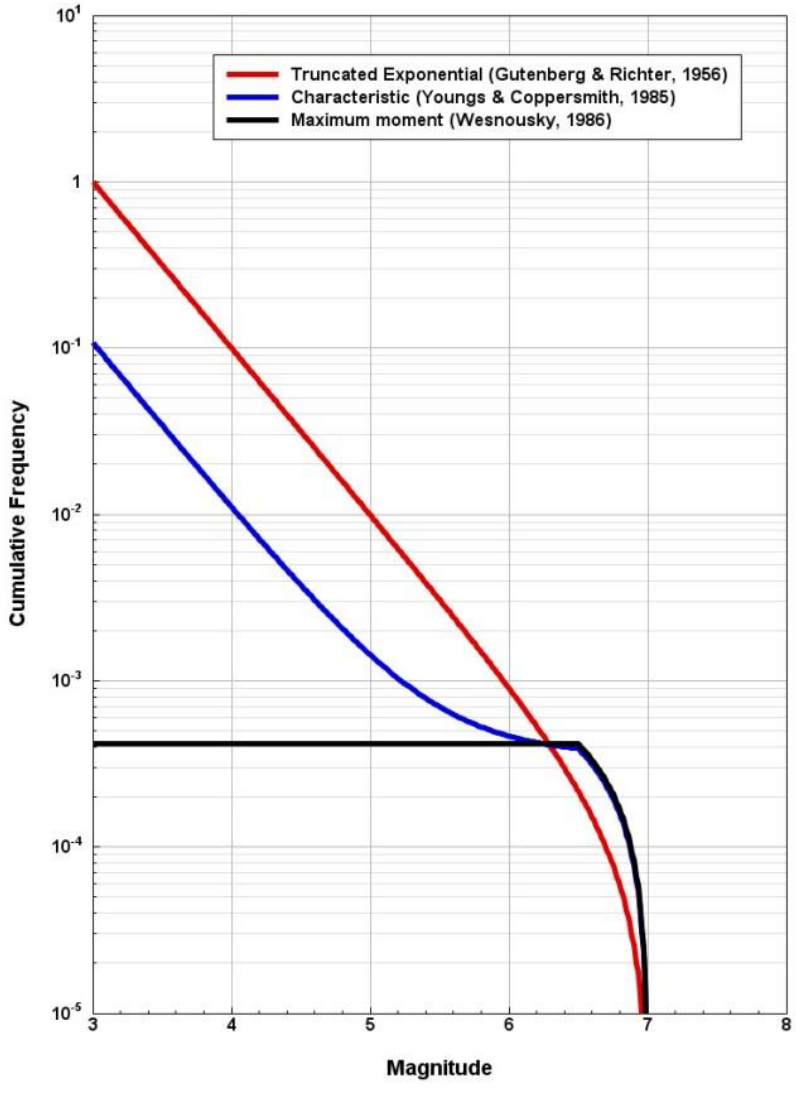


Figure 5.14-44 Magnitude-Frequency Models of Earthquake Recurrence for a Given Mmax = 7 and for a Constant Seismic Moment Rate.
The Truncated Exponential Model is Used for Seismic Source Zones and the Characteristic Earthquake and Maximum Moment Models are used for Fault Sources.

(Modified from Reference 5.14.147)

Various options to modelling recurrence as well as approaches to obtain estimates of the recurrence parameters were discussed at Workshop #2 (***Subsection 5.14.5.2***), which were then evaluated by the SSC TI team (***Subsection 5.14.5.3***), considering in particular the approaches adopted in recent projects of a similar nature (*e.g.*, ***Reference 5.14.69***), as well as the nature and quality of the data available. This resulted in the recurrence modelling approaches documented in ***Subsections 5.14.5.4.(c) vii*** to ***Subsection 5.14.5.4.(c) x***).

v Evaluation of data, models and methods.

As discussed in ***Subsection 5.14.5.3***, the evaluation process includes consideration of the models and methods that are currently proposed by members of the larger technical community, in addition to the evaluation of the data included in the seismological and geological databases (***Subsection 5.14.4.3*** and ***5.14.4.4***).

The following topics more specifically relevant to the development of the SSC model were addressed at Workshop #2 (see ***Subsection 5.14.5.3***):

- Recurrence model options and methods for incorporating uncertainty in magnitude estimates into earthquake recurrence calculations;
- Alternative methods for assessing Mmax: Bayesian approach using global SCR analogues, and approaches using observed seismicity;
- Incorporating uncertainties in Mmax;
- Upper mantle seismic structure beneath southern Africa: Constraints on the processes giving rise to the African Superswell and implications to seismic sources in South Africa;
- Regional crustal studies and implications to seismotectonic models for South Africa;
- Alternative seismotectonic models for southern Africa and implications of tectonic features to seismic hazard;
- Tectonic interpretation of the 1969 Ceres earthquake area and implications to the locations of future seismicity;
- Implications of neotectonic evidence in the Eastern Cape to identifying seismic sources;

- Depositional and erosional processes occurring on the continental shelf and slope: Implications to causative mechanisms and origins of seafloor features relative to potential fault sources;
- Marine terrace geological Investigations for the Thyspunt PSHA project and implications for regional uplift rates and local fault deformation;
- Fault corridor fault geological investigations for the Thyspunt PSHA project and implications to identifying fault sources and their characteristics;
- Preliminary cosmogenic geochronology investigations for uplift rates and ages of surfaces: Implications for the tectonic stability and geomorphic evolution of Southern Africa;
- Palaeoseismic characteristics of the Kango Fault and associated uncertainties; update on recent Coega Fault investigations;
- Implications of recent data collection efforts to the understanding of the Kango Fault: Defining seismic source characteristics and their uncertainties.

b) Overview of the SSC Model

The SSC model was developed by the SSC TI Team using the approach and criteria outlined in ***Subsection 5.14.5.4.(a)***. This section provides a general summary of the SSC model, starting with an overview of the suite of seismic sources included in the SSC model (***Section 5.14.5.4.(b) i***), followed by an outline of the SSC model logic-tree (***Section 5.14.5.4.(b) ii***).

I Seismic sources identified and characterised in the SSC Model

The seismic sources included in the SSC model comprise five source zones and five fault sources, which are shown in ***Figure 5.14.45*** and listed below:

- Seismic Source Zones
    - Extended Continental Crust (ECC)
    - Syntaxis (SYN)
    - Karoo (KAR)
    - Namaqua (NAM)
    - Cedarville-Koffiefontein (CK)

- Fault Sources
    - Kango (KNG)
    - Agulhas (AFZ)
    - Gamtoos (GAM)
    - Plettenberg (PLET)
    - Worcester (WOR)

The conceptual bases for identifying these seismic source zones and fault sources are summarised subsequently in ***Subsections 5.14.5.4.(d) and Subsection 5.14.5.4.(e),*** respectively, with the full technical details given in Sections 8.3 and 8.4 of ***Reference 5.14.17***.

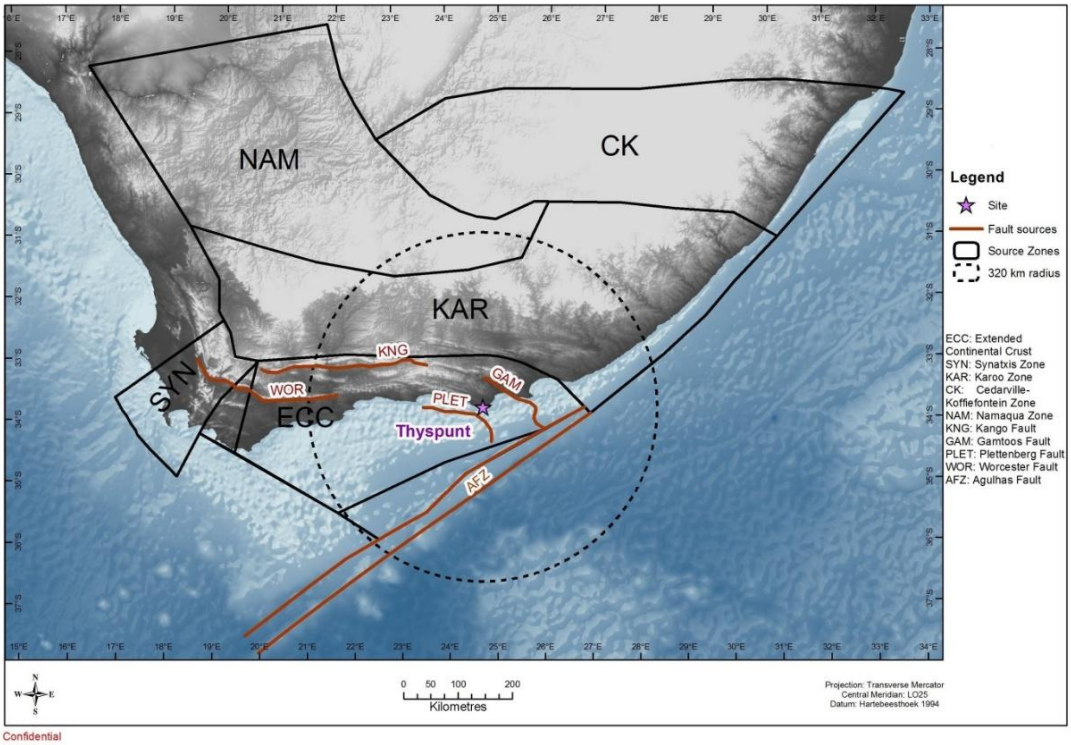


Figure 5.14-45 Seismic Source Zones and Fault Sources of the SSC Model.

The process of identifying and characterising seismic sources for the SSC model was hazard-informed such that highest priority would be given to those aspects of the model having the highest potential hazard significance. Likewise, the level of complexity of the SSC model was consistent with current knowledge and importance to hazard. As a result, the region over which the SSC model is developed was designed to extend somewhat beyond the distances that would be expected to contribute significantly to the site hazard, based on experience in other PSHAs within SCRs.

Consistent with the definition of seismic sources used in other projects, the seismic sources identified in the Thyspunt PSHA SSC model are judged to have relatively uniform seismic source characteristics within their boundaries relative to adjacent regions. That is, the recurrence rate, Mmax, p[S], and future earthquake characteristics, which are the criteria used to define each source in the first place, are judged to be relatively uniform within each source.

As discussed in ***Subsection 5.14.5.4.(a)***, one of the criteria for defining seismic sources is differences in earthquake recurrence, expressed as differences in the spatial density of earthquake occurrence defined by the pattern of observed earthquakes. Accordingly, the SSC model is based to a large extent on an assessment that spatial stationarity of seismicity will persist for time periods of interest for the Thyspunt PSHA (approximately the next 50 years). Stationarity in this sense does not mean that future locations and magnitudes of earthquakes will occur *exactly* where they have occurred in the historical and instrumental record. Rather, the degree of spatial stationarity varies as a function of the type of data available to define the seismic source. Fault sources are based on palaeoseismic evidence for localised deformation from repeated large-magnitude earthquakes that occur in approximately the same location (*i.e.,* the same fault) over periods of a few thousand years. Uncertainties in the locations and sizes of these events are a function of the types of data available. Because the record that defines the fault sources spans a relatively long time period and records large-magnitude events, repeated events for these sources are expected to occur within a restricted location defined by the fault source.

On the other hand, patterns of seismicity within seismic source zones are defined from generally small- to moderate-magnitude earthquakes that have occurred during a relatively short (*i.e.,* relative to the repeat times of large events) historical and instrumental record. Thus the locations of future events are not as tightly constrained by the locations of past events as for fault sources. Some recent studies within SCRs, such as the CEUS SSC study (***Reference 5.14.69***), have identified very large seismic source zones and have used “spatial smoothing” to express the spatial variation of recurrence rates. In that study, *b*-values vary little across the study region and *a*-values vary at

© Eskom 2026/Rev 0a

scales judged by the TI Team to reflect the belief that the observed record provides a spatial constraint on rate density variation. Likewise, in that smoothing approach, the recurrence calculation considers weighting of magnitudes in the recurrence rate calculations such that moderate events are assigned more weight than smaller events.

As discussed in Section 8.1.1 of ***Reference 5.14.17***, the adoption of a smoothing algorithm is based on the same conceptual model as defining the boundaries to seismic sources relative to differences in the expected future spatial density of earthquakes. Unlike the CEUS, the Thyspunt region is characterised by a very low level of earthquake activity and the number of moderate-to-large magnitude earthquakes is much lower. Further, the host seismic source zone (ECC, ***Subsection 5.14.5.4.(d) i***), which is the only source zone for which variations in spatial density might be hazard-significant, has very few observed earthquakes and no earthquakes larger than the M_w 4.8 1969 Heidelberg earthquake. Ultimately, any smoothing operation or source subdivision based on observed seismicity is founded on expert judgment related to the expected future distribution of moderate-to-large-magnitude events. The sparse distribution of small-magnitude earthquakes within ECC led the TI Team to conclude that spatial smoothing within the ECC source zone, or further subdivisions of the zone based on the diffuse pattern of small-magnitude events, was not technically defensible. Some more distant seismic source zones display higher rates of seismicity, but their distance to the site precludes any hazard significance to further subdivisions or spatial smoothing of recurrence within those source zones.

Furthermore, the SSC model is based on the notion that an appropriate SSC model should be one that is no more complex or detailed than required by the pertinent data. Therefore, the SCR tectonic environment, coupled with the diffuse pattern and very low rate of observed seismicity in the region, suggests that there is no compelling reason to further subdivide the region into additional source zones simply to conform with geologic or geophysical boundaries. In contrast, very specific and detailed information exists regarding the palaeoseismic history along the Kango Fault and, as a consequence, the SSC model includes detailed characterisation for that fault source (***Subsection 5.14.5.4.(e) i***). Other faults are either assessed to have an uncertain seismogenic probability, and they are included in the SSC model with appropriate levels of characterisation detail (***Subsections 5.14.5.4.(e) ii to 5.14.5.4.(e) v***), or have been assessed to have a p[S] = 0 such that they are not included in the model as fault sources (***Subsection 5.14.5.4.(f)***).

ii Structure of the SSC Model Logic Tree

This section describes the structure of the logic tree that comprises the SSC model.

As discussed in more detail in ***Subsection 5.14.7.3***, a logic tree is a tool for displaying the epistemic uncertainties that are part of the inputs to the PSHA. Each node of the tree represents an element of the model and the alternative branches at each node represent the alternative models or parameter values for that given element. Each branch is assigned a relative weight, treated as a probability in the calculations, which expresses degree of belief of the SSC TI Team that it is a more appropriate model or parameter value. Ideally, epistemic uncertainties can be reduced or even eliminated with additional data and information. The technical assessments that underlie the identification of the nodes of the tree, the alternative branches, and the weights assigned to each branch of the SSC model logic tree are documented below in ***Subsections 5.14.5.4.(c)*** to ***5.14.5.4.(e)***).

Distinct from epistemic uncertainty is aleatory variability, discussed in more detail in ***Subsection 5.14.7.2***, which expresses those aspects of a model that we consider to be random and, at least at the level of our current knowledge, not amenable to reduction with the consideration of additional data and information, for example, the time and size of the *next* earthquake that will occur on a given seismic source. Aleatory distributions are used to model parameter distributions where different parameter values can coexist, each with their relative frequency.

For the sake of clarity, aleatory assessments are clearly indicated as such in the discussion below, and the relative frequencies of aleatory alternatives will be indicated as percentages (35%), to distinguish them from the relative weights as used for epistemic alternatives [0.35], following the convention adopted in the Final HID (Appendix 3 of ***Reference 5.14.17***).

The overall structure of the SSC and GMC models in the context of the inputs to the hazard calculations is given in ***Figure 5.14.46***. The elements of the SSC logic tree that are included in “Part 1” are given in more detail in ***Figure 5.14.47***. The remaining parts of the logic tree in ***Figure 5.14.47*** involve source-specific (denoted as “ss”) weights, leading to uniquely defined coordinate options for each of the sources.

The remaining elements of the SSC logic tree are different for the seismic source zones and for the fault sources. The logic tree structure for the seismic source zones is given in ***Figure 5.14.48***. The justifications for the selection of the approaches to assess Mmax and other recurrence parameters are

discussed in ***Subsections 5.14.5.4.(c) vii*** and ***5.14.5.4.3.9***. In addition to the epistemic uncertainties captured in the logic trees for the seismic source zones, a number of aleatory assessments were made that characterise the virtual faults that are modelled within the source zones. The approaches taken to assess these future earthquake characteristics are described in ***Subsections 5.14.5.4.(c) ii*** to ***5.14.5.4.(c) vi*** and the characteristics assessed for each seismic source zone are described in detail in ***Subsections 5.14.5.4.(d) i*** through ***5.14.5.4.(d) v***.

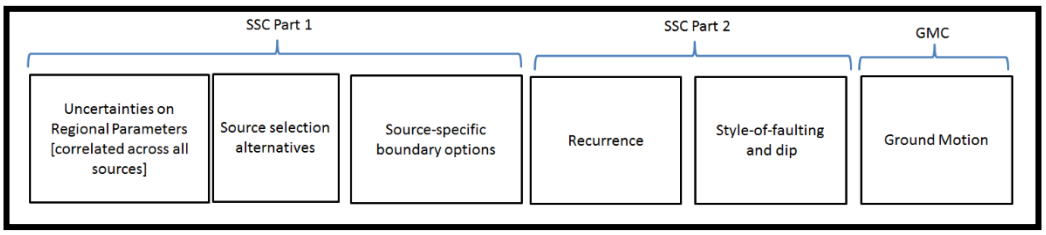


Figure 5.14-46 Schematic Overview of the Overall Logic Tree for the Hazard Analysis Showing the Components for the SSC and GMC Parts.

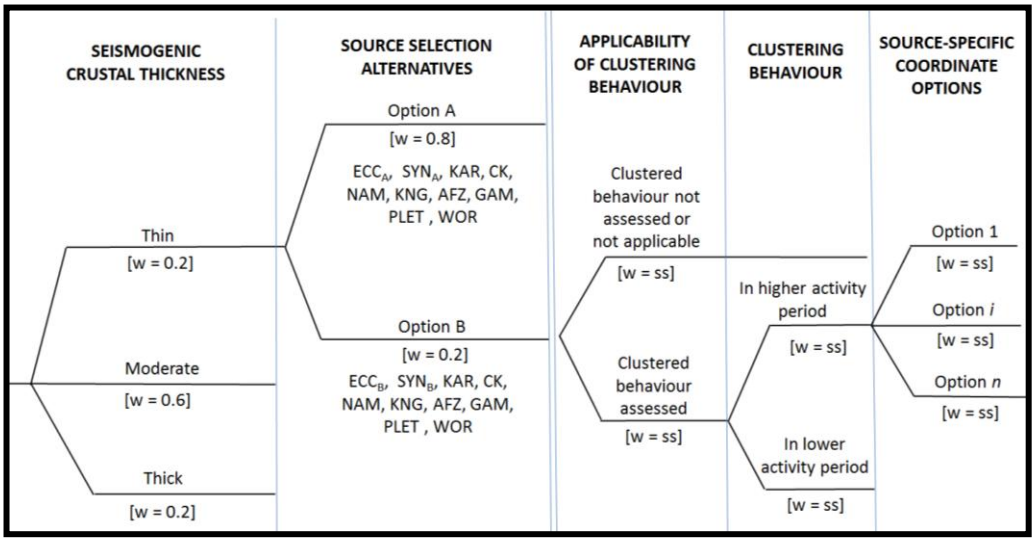


Figure 5.14-47 Part 1 of the SSC Logic Tree Portraying Those Assessments That Relate to the Coordinates of All Seismic Sources for the Hazard Analysis.

Those weights that are source-specific are labelled "ss."

The first assessment for fault sources is the seismogenic probability p[S], which is assessed based on the criteria discussed in ***Subsection 5.14.5.4.(a) ii***. Given that the seismogenic probability is greater than zero, the fault is characterised by several parameters, as shown in ***Figure 5.14.49***. The assessments include the magnitude-frequency distribution model, the magnitude of the characteristic earthquake, M_{char}, the *b*-value, the approach to assessing recurrence rates, the parameters for each recurrence approach, the style of faulting, the direction of fault dip, and the dip angle. The approaches and methodologies used to characterise the fault sources are described in ***Subsection 5.14.5.4.(c)***, and the specific assessments for each fault source are summarised in ***Subsection 5.14.5.4.(e)***.

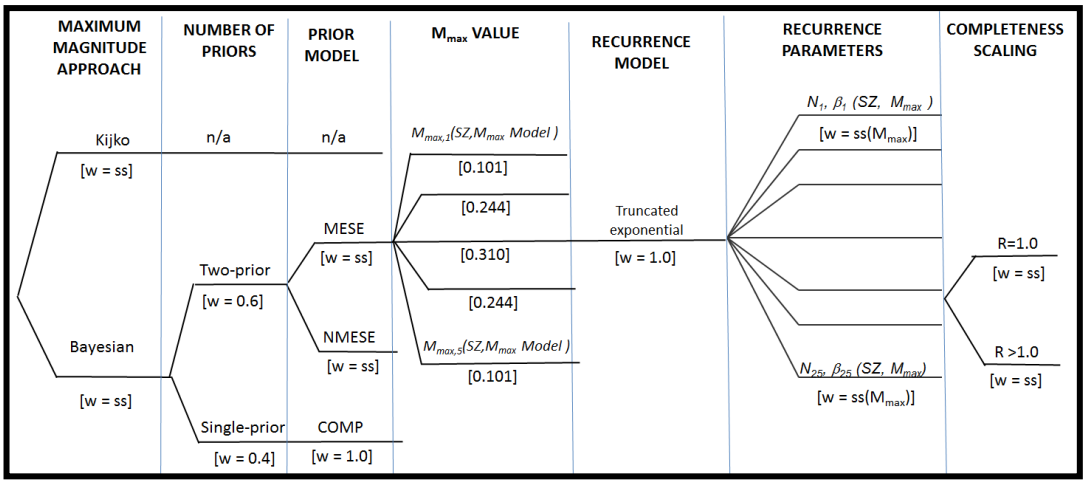


Figure 5.14-48 Part 2 of the SSC Logic Tree for the Seismic Source Zones ECC, SYN, KAR, NAM, and CK.

Those weights that are source-specific are labelled "ss".

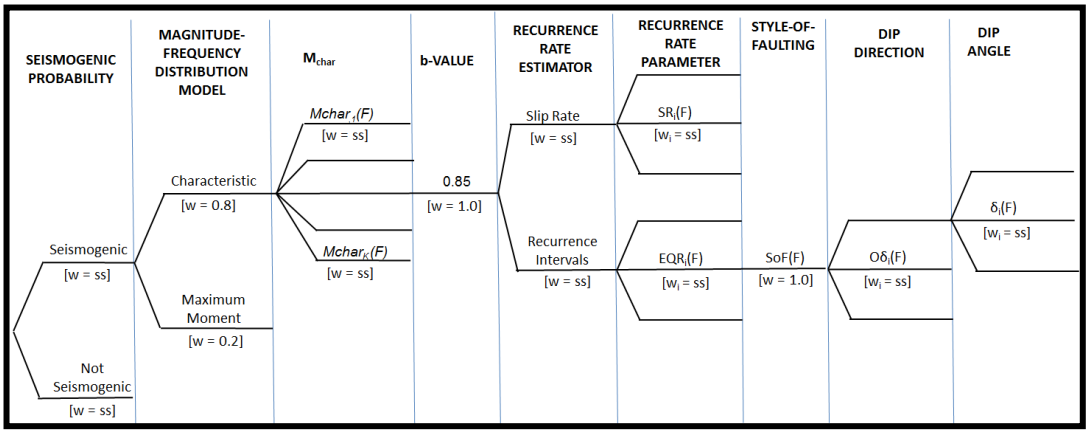


Figure 5.14-49 Part 2 of the SSC Logic Tree forFault Sources PLET, GAM, AFZ, KNG and WOR.

Those weights that are source-specific are labelled "ss."

The remainder of ***Subsection 5.14.5.4*** provides summary descriptions of the various elements of the SSC model. ***Subsection 5.14.5.4.(c)*** provides descriptions of the "global" assessments made for multiple seismic sources, as well as the approaches and methodologies that were used by the SSC TI Team to characterise seismic sources. ***Subsection 5.14.5.4.(d)*** includes the description of the seismic source zones. ***Subsection 5.14.5.4.(e)*** provides the characterisation of fault sources in the SSC model. ***Subsection 5.14.5.4.(f)*** describes those faults that were assessed to not be seismogenic and, as a result, are not included as fault sources.

c) Global Assessments and Methods

This section describes the elements of the SSC model that are "global", meaning that they are not source-specific but apply to all or more than one seismic source. This section also provides a discussion of the approaches and methodologies that have been used in the SSC model for multiple seismic sources. The assessments and approaches made by the TI Team are based on a careful consideration of available pertinent South African data combined with data from analogous tectonic regions.

The global assessments presented here include parameters whose assessment is done on a regional scale, such as the assessment of tectonic regime (***Subsection 5.14.5.4.(c) i***) and the assessment of crustal thickness and hypocentral depth distribution (***Subsection 5.14.5.4.(c) ii***). Additionally, the models used in the assessment of future earthquake characteristics are presented in their generic form (***Subsection 5.14.5.4.(c) iii*** to ***5.14.5.4.(c) vi***). Source-specific adjustments and weight assignments will be discussed for the

individual sources in ***Subsections 5.14.5.4.(d)*** and ***5.14.5.4.(e)***. Finally, the general approaches to recurrence for seismic source zones and fault sources are presented in ***Subsections 5.14.5.4.(c) vii*** and ***5.14.5.4.(c) viii***, respectively. The approaches to obtaining Mmax for source zones and M_{char} for fault sources are then discussed in ***Subsections 5.14.5.4.(c) ix*** and ***5.14.5.4.(c) x***, respectively.

i Assessment of tectonic regime

A potentially important assessment for the SSC model is whether or not the region that includes the seismic sources is a "stable continental region" (SCR) as defined by Kantor *et al.* (***Reference 5.14.149***) as part of the Johnston *et al.* study (***Reference 5.14.53***). This assessment has consequences for the selection of the approach for assessing Mmax (***Subsection 5.14.5.4.(c) ix***), as well as the selection of rupture-length-versus-magnitude scaling relationships (***Subsection 5.14.5.4.(c) iii***).

The tectonic criteria that were identified by Kantor *et al.* (***Reference 5.14.149***) deal largely with the age of various types of major tectonic or deformation-related events, including crustal rifting, major deformation, orogenic activity, and major anorogenic intrusions. Using these criteria, Johnston *et al.* (***Reference 5.14.53***) identified all of the regions worldwide that would fall into SCRs, as defined, based on a careful review of the available geologic and tectonic information.

An important characteristic of SCRs is the lack of significant tectonism and major deformation during Neogene time (past 23 Ma), which is a function of not only large distances to plate boundaries, but also tectonic stability and lack of crustal processes that may indicate incipient plate deformation. For example, the East African Rift region is excluded from the SCR categorisation of Johnston *et al.* (***Reference 5.14.53***) due to the evidence for recent major deformation and uplift due to contemporary crustal-scale rifting processes. In contrast, as discussed in ***Subsection 5.13.5.1.(d) i***, the majority of South Africa, including the whole of the Thyspunt PSHA model region (***Subsection 5.14.4.2***), displays evidence for tectonic stability and very low rates of tectonic uplift, which were further confirmed by the results of the geological investigations carried out specifically for the project (***Subsection 5.13.4.2.(c)***).

Based on consideration of the proximity of the study region to plate boundaries, confirmation of the categorisation by Johnston *et al.* (***Reference 5.14.53***), and affirmation of low, uniform regional rates of continental uplift, the TI Team concluded that the study region for the SSC model lies within an SCR. Furthermore, bearing in mind that the set of criteria given in ***Reference 5.14.53***

were originally developed with the specific intention of finding tectonic analogues to the CEUS, the issue of whether the CEUS could be considered an analogue to the study region was also considered. The assessment by the SSC TI Team concluded that there was a very close analogy between the CEUS and the study region in terms of style, timing and extent of tectonism, as well as other indicators of tectonic stability, such as rates of uplift. This enabled the use of well-documented data and models developed for the CEUS (*e.g.* ***Reference 5.14.69***) to supplement local data for assessments where the local database was very limited, for instance the assessment of the depth distribution (***Subsection 5.14.5.4.(c) ii***) or the calculation of Mmax (***Section 5.14.5.4.(c) vii***).

ii Seismogenic crustal thickness and focal depth distribution

Both the virtual faults within a seismic source zone as well as fault sources are assumed to rupture energetically within the seismogenic part of the crust. The seismogenic crust is assumed to extend from the surface down to the base of the seismogenic crustal layer and is defined for the hazard analysis as the zone within which moderate-to-large earthquakes will occur. For seismic source zones, a distribution of future earthquake focal depths is required in order to provide a basis for the location of virtual ruptures at depth in the hazard calculations. That is, each earthquake is assumed to initiate at a particular focal depth and to be associated with a rupture that has a magnitude-dependent size.

Typically, direct evidence for the seismogenic crustal thickness and the focal depth distribution in a region comes from a consideration of the depths of well-determined instrumental earthquake hypocentres. In the Thyspunt region, there are relatively few earthquakes with well-determined hypocentres, due both to the low levels of seismicity as well as the rather broadly spaced instrument locations in the national seismic network. As a result, the assessment of both the thickness of the seismogenic crust as well as the focal depth distribution in the Thyspunt region was made by both a consideration of all available South African data as well as focal depth data developed in tectonically analogous regions.

Crustal studies in the South African region (***References 5.14.23 and 5.14.150***) using seismic data recorded during the South African Seismic Experiment have found Moho depths in the range of 35–45 km. Whilst this provides an upper bound on the value of the *seismogenic* crustal thickness, little else can be deduced from these values, given that no obvious correlation exists between Moho depth and seismogenic crustal thickness.

Given the relative paucity of data for South African earthquakes regarding focal depth and seismogenic thickness (see ***Subsection 5.14.4.4.(d)***), the SSC TI

Team considered the data developed for other SCR areas (***References 5.14.151 and 5.14.152***), which generally support shallow depths (5-10 km), but also indicate a mode in the depth distribution below 30 km. Klose & Seeber (2007) found that depth distributions of earthquakes in Stable Continental Regions (SCRs) essentially follow one of two patterns: (i) well-developed bimodal distributions, with concentrations of earthquakes in the upper (0-10 km) and lower (20-35 km) thirds of the crust; or (ii) shallow unimodal distribution, with data concentrated in the upper half of the crust. The second case is similar to the depth distributions observed in active continental regions (ACRs), which have been found to be predominantly unimodal. The depth distribution developed from high-quality data for the Central and Eastern US (CEUS) Seismic Source Characterization (SSC) project (***Reference 5.14.69***) provides a good example of unimodal depth distribution of SCR earthquakes.

The limited focal depth data in the study region (***Figure F-5.14.8***) define a mode at about 5 to 10 km and maximum depths of about 20 km. If the focal depth distributions given in ***Reference 5.14.153*** are to be considered as appropriate analogues for the Thyspunt region, the question then becomes whether or not the available South African data show any indication of a deeper mode in the 20–30 km depth range. As discussed above, the available focal depth data for South Africa, including the analyses conducted for this project, suggest that the maximum focal depths are shallower than about 20 km. As a result, the SSC TI Team concluded that the SCR regions displaying evidence for a “bimodal” depth range were not appropriate analogues for the site region, but that those SCR regions having unimodal focal depths less than about 20 km were likely appropriate analogues.

Given these constraints and acknowledging the CEUS case studies included in ***Reference 5.14.153*** as being representative of unimodal depth distributions, due consideration was given to the recently developed earthquake catalogue for the CEUS SSC project as presented in ***Reference 5.14.69***. The catalogue includes a uniform estimate of M_w for all earthquakes and a study was conducted with the particular purpose of assessing the seismogenic thickness and focal depth distributions for purposes of building an SSC model (***Reference 5.14.69***), resulting in the identification of ~ 13,000 earthquakes having high-quality focal depth determinations, in particular excluding fixed depths. Given that insufficient South African data exist to draw an analogy to any particular sub-region of the CEUS, it was concluded that the distribution for the entire CEUS (***Figure F-5.14.50***)) would be most appropriate for use in the Thyspunt region. This distribution was found to be consistent with all available focal depth information in the Thyspunt region.

© Eskom 2026/Rev 0a

The assessment of seismogenic crustal thickness takes into consideration the focal depth distribution. As summarised in ***Reference 5.14.69***, given a focal depth distribution, physical considerations given by various researchers suggest that the base of the seismogenic zone is identified as lying near the base of the observed focal depths. Available studies from various regions worldwide (***Reference 5.14.154 to 5.14.156***) indicate that the 90th fractile of the depth distribution, D_{90}, is a key indicator of the thickness of the seismogenic crust in a region can be reasonably inferred from the depths of observed seismicity.

Based on the information cited above, the TI Team concluded that D_{90} is a reasonable indicator of the thickness of the seismogenic crust. As summarised in ***Figure 5.14.8***, the number of high-quality focal depths is too limited to provide a well-determined D_{90}, but the available data would suggest a D_{90} in the range of 15 to 20 km. The D_{90} for the CEUS focal depth distribution is 17 km (***Figure 5.14.50***) and, based on the assessment by the Team that the CEUS distribution is a reasonable analogue for the expected distribution in the site region, the value of 17 km is assessed to have the highest weight as the seismogenic thickness in the region. The range of uncertainty in seismogenic thickness is assessed by the Team to be 15 km to 22 km, which spans a range that exceeds the 85th to 95th percentiles for the CEUS depth distribution.

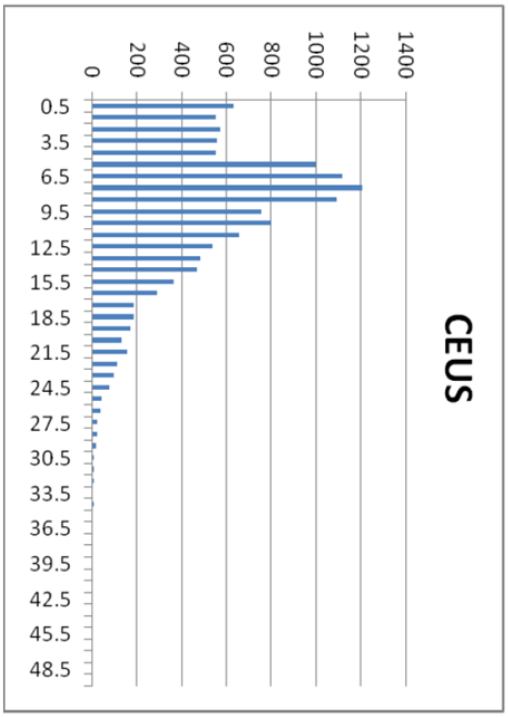
The following assessment is made of seismogenic crustal thickness for all sources except the Agulhas fracture zone:

- Thin, 15 km [0.2]
- Moderate, 17 km [0.6]
- Thick, 22 km [0.2]

Because the Agulhas fault lies within a region where the continental crust has been attenuated due to continental separation (see ***Subsection 5.14.5.4.(e) ii***), the seismogenic crust is assessed to be somewhat thinner for that source:

- Thin, 10 km [0.2]
- Moderate, 12 km [0.6]
- Thick, 15 km [0.2]

© Eskom 2026/Rev 0a



N eqs	12964
mean	9.45
5%	9.31
95%	9.59
stdev	7.98
Mode	1
Frequency	293
5th	1.1
15th	3.5
50th	8.3
85th	15.1
90th	17
95th	21

Figure 5.14-50 Focal Depth Distribution for the CEUS Region Developed from High-Quality Depth Determinations and With Removal of Fixed Depths. The D_{90} for This Distribution is 17 km.

The assessments are deemed to be completely correlated across sources, such that the assessment of “thin” seismogenic thickness for one seismic source implies “thin” thickness for all other sources. The basis for correlating seismogenic thickness between sources is that there are no apparent systematic differences in the depths of earthquakes at the known locations of seismicity (***Figure 5.14.8***) and studies of the spatial variation of focal depth distributions do not show rapid changes in D_{90} over the spatial dimensions of the seismic sources of the SSC model.

As discussed above, the focal depth distribution for the entire CEUS region is assessed to be appropriate for the Thyspunt region. However, that distribution is developed primarily based on small-to-moderate magnitude earthquakes. In order to use that distribution for moderate-to-large earthquakes, an assessment needs to be made of the magnitude dependence of focal depths. The TI Team endorses and adopts that weighting scheme that was developed for the

PEGASOS project in Switzerland (***Reference 5.14.146***), and that was subsequently embedded in the FRISK88 software. The weighting scheme begins with the assessment by the TI Team that the focal depth distribution applies to the hypocenters of earthquakes with small magnitudes (with negligible source dimensions) and is modified for the effect of magnitude-dependent rupture dimensions, based on the along-dip fraction T of the rupture plane on which hypocenters are allowed to occur. The SSC TI Team assessed that the hypocentres for moderate-to-large earthquakes will occur in the lower half of the rupture width, such that T = 0.5 in the magnitude weighting scheme. This assessment is consistent with a wide range of studies (see summary in ***Reference 5.14.157***) that conclude that moderate-to-large earthquakes tend to nucleate near the base of the seismogenic crust.

iii Rupture size and aspect ratio

The size of ruptures on the virtual faults within seismic source zones is magnitude-dependent and care has been taken to select source scaling relations that are believed to be appropriate for SCRs, since such relations are generally dependent on the tectonic regime considered. ***Reference 5.14.158*** provides rupture length and rupture area scaling relationships that are recommended for use within SCR. Both the length and width (and hence area) of ruptures are included in the hazard analyses. However, the software used in the hazard calculations (FRISK88) specifically uses a length-based scaling relation coupled with an assessment of the length-to-width aspect ratio. Hence, as explained in Section 8.2 of ***Reference 5.14.17***, the length-based scaling relation of Leonard (***Reference 5.14.158***) was adopted for the Thyspunt PSHA. The associated standard deviation was set to 0.25 (in $\log_{10}$ units) based on examination of other empirical scaling relations based on more substantial databases (*e.g.*, ***Reference 5.14.159***).

The aspect ratio (length: width) of ruptures for small magnitudes is assumed to be 1:1. With increasing magnitude and rupture length/area, the rupture width will eventually entail the bottom or the top of the seismogenic crust. Once the entire seismogenic width has ruptured, the aspect ratio increases with increasing magnitude to conserve the proper rupture length predicted by the Leonard (***Reference 5.14.158***) relation described above.

iv Style of faulting

Each seismic source is assessed according to its style-of-faulting (normal, reverse, or strike-slip), which can be important to the selection of appropriate ground motion models. The assessment of style-of-faulting for seismic source zones is based on a consideration of the tectonic regime, stress indicators, and earthquake focal mechanisms (summarised in ***Subsection 5.13.5.1.(d) i***).

© Eskom 2026/Rev 0a

Style-of-faulting for fault sources (***Subsection 5.14.5.4.(e)***) is based on kinematic indicators along the fault (*e.g.*, slip components of piercing points, slickenlines), stratigraphic separations, as well as the orientation of the fault relative to tectonic stresses.

In general, the available evidence indicates that both strike-slip and normal faulting are present within the seismic source zones (***Subsection 5.14.5.4.(d)***). Therefore, the source-specific assessment is one of the relative frequency (expressed as an aleatory percentage) of strike-slip and normal faulting.

v Rupture strike and dip

The strike, dip, and dip direction of ruptures within seismic source zones and fault sources are source-specific assessments. The strike and dip of fault sources (***Subsection 5.14.5.4.(e)***) is based on mapping in the onshore region and interpretations of subsurface geometry from geophysics in the offshore region (see ***Section 5.13***). For seismic source zones (***Subsection 5.14.5.4.(d)***), the assessment of the strike of ruptures on virtual faults is based primarily on a consideration of the orientations of major geologic structures, the geologic history, the tectonic regime, and the orientations of ruptures based on earthquake focal mechanisms. In general, the assessment of the orientation of future rupture strike is an aleatory assessment in which multiple orientations are assessed to be possible and the relative frequency of those orientations is given as a percentage. For example, the azimuthal distribution and length of mapped faults was summarised based on structural geologic data for the seismic source zones (usually given as a rose diagram). These assessments are then considered in the development of aleatory distributions of the relative frequency of the strikes of future ruptures.

In the absence of source-specific data regarding rupture geometries (*e.g.*, no historical ruptures and few focal mechanisms), the assessment of fault dip for virtual faults is based on a consideration of the dips observed for normal and strike-slip earthquakes in the global data set. For example, compilations by Jackson & White (***Reference 5.14.160***) and Collettini & Sibson (***Reference 5.14.161***) of normal-faulting earthquakes provided a reasonable basis for the SSC TI Team to make an assessment of the generic distribution of fault dips to capture the epistemic uncertainty regarding the expected dip of a normal faulting earthquake: 45° [0.2], 60° [0.6], 70º [0.2]. Similarly, generic strike-slip earthquake ruptures are assessed to be vertical (90°) to steeply dipping (70°), with equal weights of [0.5] assigned to each of these options.

Sensitivity analyses conducted with the preliminary SSC model indicated that the dip of ruptures for source zones other than ECC is not significant to the hazard due to their distance to the site. Therefore, for simplicity, the dips of

ruptures within these sources are assumed to be vertical (90°) in the final SSC model used in the hazard calculations (***Subsection 5.14.5.4.(d)***). For the fault sources, either the generic distributions given above are used, for those faults having little subsurface data, or fault-specific data are used to modify the distributions (see ***Subsection 5.14.5.4.(e)*** for details).

vi Strict and Leaky Source Zone Boundaries

The boundaries of seismic source zones are drawn based on the criteria described in ***Subsection 5.14.5.4.(a)*** and, for the host source (ECC), uncertainties in the boundary locations are included as epistemic alternatives (see ***Subsection 5.14.5.4.(d) i***). In the hazard analyses, all simulated epicentres fall within the seismic source of interest, but boundaries can either allow ruptures within a source zone to proceed into adjacent sources or not. Strict boundaries to a source mean that ruptures cannot extend into adjacent sources, and the modelled rupture is truncated at the strict boundary. Leaky boundaries allow ruptures to extend into adjacent sources but, because the epicentre occurs within the source and is located at the mid-point of the rupture, no more than one-half of the total rupture length can extend into an adjacent source.

The assessment of strict or leaky boundaries is a source-specific assessment and is based on a consideration of the orientation, geologic history, and continuity of major geologic structures relative to a source boundary. Given that the assessment of leaky versus strict boundaries is specific to the whole source zone, rather than to individual boundaries, care has been taken to define the boundary characteristics for a source according to those boundaries that are most likely to have an influence on the hazard at the Thyspunt site.

vii Recurrence models adopted for source zones

Consistent with common practice in the assessment of seismicity within seismic sources, the observed seismicity is assessed to follow a truncated exponential magnitude distribution (see ***Subsection 5.14.5.4.(a) iv***) and Poissonian behaviour. The latter assessment means that the assumption is made that the occurrence of earthquakes is “memory-less” such that the average rate of occurrence is the same at any point in time.

The parameters of the truncated exponential model are assessed using the earthquake catalogue (***Subsection 5.14.4.4***) developed for the earthquake region, more specifically the binned earthquake counts (number of earthquakes of a given magnitude) falling within the source zone, typically using a maximum-likelihood approach such as that developed by ***Reference 5.14.162***.

© Eskom 2026/Rev 0a

For this purpose, as discussed in ***Subsection 5.14.4.4***, the earthquake catalogue needs to be rendered uniform in magnitude, and declustered to remove dependent events such as foreshocks and aftershocks, in order to satisfy the assumption of Poissonian behaviour. Furthermore, the completeness as a function of magnitude, time, and location needs to be taken into account. This was done by determining equivalent periods of completeness for each source zone and magnitude bin, using a probability of detection approach (***Reference 5.14.69***) which included consideration of historical factors in the assessment of completeness (***Reference 5.14.94***).

The approach described in ***Reference 5.14.53***, based on ***References 5.14.162*** and ***5.14.163***, was followed to calculate penalised maximum likelihood estimates of the *a*-value and *b*-value parameters that were conditional on Mmax, this latter parameter having been determined as discussed below in ***Subsection 5.14.5.4(c) ix***. The penalised maximum likelihood approach includes the use of a prior estimate for the *b*-value distribution that acts as a penalty function in order to stabilise the assessment of this parameter for seismic source with limited seismicity. A distribution centred on the regional *b*-value of 0.85 assessed using the modern instrumental subset of the catalogue for the whole region was used as the prior *b*-value in this assessment. Maximising the likelihood function then yielded joint maximum likelihood estimates of the *a*-value and *b*-value parameters for each value of Mmax, resulting in source-specific distributions of recurrence parameters that captured the epistemic uncertainties in the recurrence parameters, as well as the correlations between them.

Further details of the approach to recurrence for seismic source zones are given in Section 8.2.4 of ***Reference 5.14.17***.

viii Recurrence models adopted for fault sources

The approach to assessing earthquake recurrence for the fault sources does not rely on observed seismicity, since there are essentially no earthquakes that can be readily assessed to be uniquely associated with the faults. Instead, palaeoseismic geologic data related to either earthquake recurrence intervals or fault slip rate are used to constrain recurrence. In this way, the Quaternary geologic record, which spans at least the past million years, can be used in the assessment.

The assessment of appropriate magnitude-frequency models for the fault sources in the Thyspunt model included an evaluation of the data that have been developed within the technical community on the issue, mostly within active tectonic regions, as well as data that are specific to the Thyspunt region. In addition to the characteristic earthquake and maximum moment models, the

© Eskom 2026/Rev 0a

SSC TI Team considered the possibility that an exponential model might be appropriate to define fault-specific recurrence. Review of available data and models resulted in the conclusion that, for fault sources, the characteristic earthquake model provides a better match to available geologic, seismicity, and geodetic data than the exponential model, (*e.g.*, ***Reference 5.14.164***), which tends to systematically over predict observed seismicity rates for smaller-magnitude events, for individual faults in active regions (***Reference 5.14.165***).

In the case of the faults considered for the Thyspunt PSHA, there is clear evidence for geologically recent and repeated earthquakes from the palaeoseismic record on the Kango Fault, but virtually no smaller-magnitude earthquakes in the observed seismicity record can be associated with faults. Therefore, the SSC TI Team concluded that an exponential recurrence model is not appropriate for the faults in the Thyspunt region. Hence, only the characteristic earthquake and the maximum moment models are afforded any weight in the SSC model. Between those two models, most of the weight is given to the characteristic earthquake model [0.8] versus the maximum moment model [0.2]. The maximum moment model does not provide for the occurrence of any earthquakes on the fault that are smaller than M_{char}. Hence, the characteristic earthquake model was assessed by the SSC TI Team to be the most appropriate and accorded a weight of [0.8]. Some weight [0.2] was given to the maximum moment model because of the very low levels of observed seismicity that appear to be associated with the Thyspunt region faults, which may be due to a short observed record and low fault slip rates. These weights were used for all fault sources in the Thyspunt SSC model.

For all fault sources, estimates of fault slip rate were used to assess earthquake recurrence. This involved estimates of the amount of displacement of particular geologic units or horizons that has occurred and whose ages have been estimated using various geochronologic approaches. Uncertainties in both the amount of displacement and the age of the geologic units were taken into consideration in developing the uncertainty distribution of slip rate in the logic tree.

The selection of either recurrence interval data or slip rate data to define recurrence rates was a fault-specific assessment and a function of the types of data available. In the case of the Kango Fault, data related to both approaches were available and the assessment of relative weights is a function of the quality of the data and the uncertainties that exist (see ***Subsection 5.14.5.5.(a) i***). In that case, both the recurrence interval approach and the slip rate approach are assessed to have equal weights of [0.5]. The other faults have only information related to slip rate and therefore the slip rate approach is afforded a weight of [1.0].

© Eskom 2026/Rev 0a

As discussed below in ***Subsection 5.14.5.4.(e) i***, the Kango Fault displays possible evidence of temporally clustered earthquake behaviour. This type of behaviour has been recognised for a number of SCR faults (***References 5.14.166 and 5.14.69***). Temporally clustered behaviour is characterised by a period of "in-cluster" activity during which recurrence intervals are relatively short, and "out-of-cluster" activity with relatively long recurrence intervals. Given this type of behaviour, for purposes of seismic source characterisation for PSHA, an assessment must be made of whether a given fault source currently lies within a period of higher activity or is currently out of a higher activity period. In the former case, the recurrence intervals that are applicable to the SSC model are the shorter intervals; in the latter case, the long intervals between clusters would be more appropriate to use in the SSC model.

For the Kango Fault, the assessment of whether the fault is currently within a cluster or between clusters is an epistemic uncertainty included in the source logic tree. Likewise, given that it is in a cluster, the uncertainty in the recurrence intervals is included; and given it is out of a cluster, the uncertainty in recurrence intervals is included (***Subsection 5.14.5.4.(e) i***). In either case, the recurrence behaviour is treated as a Poisson process because sufficient data are not available to define a non-Poisson recurrence model. For example, a renewal model requires good information on the time of the most recent event (elapsed time), mean recurrence times, and coefficient of variation of recurrence intervals. The application of these types of "real-time" models is typically reserved for active or plate-boundary tectonic environments, where not only are more abundant palaeoseismic data available, but the tectonic driving mechanisms for fault displacement are believed to be more constant and are better understood (***Reference 5.14.69***).

Therefore, the TI Team evaluated the available data to assess whether the application of a renewal model would be appropriate for the Kango Fault or other fault sources. The physical underpinning of a renewal model is a quasi-steady-state loading process applied to a fault. These models have been given relatively high weight in characterising earthquake occurrences on plate boundary faults, even though there may not be a well-developed palaeoseismic history (*e.g.*, ***Reference 5.14.167***). However, the physical process of steady state loading being applied to faults within SCRs, including the Thyspunt region, is more problematic. Giving due consideration to the larger technical community's views regarding recurrence models for fault sources, the TI team concluded that the available data were not sufficient to allow for the application of renewal models with any confidence. Therefore, temporal behaviour is modelled as a Poisson process defined only by the average rate of earthquake occurrence and without "memory" of the timing or size of the most recent event.

An area of ongoing research with potential implications for recurrence behaviour relates to geodetic strain rate measurements. The technical community agrees that the systematic gathering of geodetic data for purposes of identifying and analysing tectonic strain is crucial for the understanding of contemporary deformation processes. However, at the current time, the understanding by the technical community of the meaning of a short-term (few decades) strain signal relative to seismic source characteristics is embryonic. The spatial distribution and temporal stability of such strains is not known, and there is no clear method for translating these strain signals into spatial and temporal SSC models for purposes of PSHA. As discussed in ***Subsection 5.13.5.1.(d) i***, analyses of geodetic data in the Thyspunt region show no evidence of strain at statistically significant levels, but the errors are large due to the relatively short period of observation. For these reasons, the TI Team concluded that the use of geodetic data for purposes of assessing earthquake recurrence was not warranted or technically defensible, given the state of current knowledge.

Further details of the approach to recurrence for fault sources are given in Section 8.2.4 of ***Reference 5.14.17***.

ix Assessment of source zone Mmax

The selection of the methodology for assessing Mmax for the seismic source zones was significantly influenced by the recent consideration of Mmax approaches conducted as part of the CEUS SSC project (***Reference 5.14.69***). That project devoted considerable effort to the evaluation of alternative approaches to assessing Mmax and to ensuring that the associated uncertainties were properly represented (***Reference 5.14.168***). These investigations concluded that all approaches based on the observed record suffer from the long recurrence intervals for Mmax and those based on palaeoseismic evidence suffer from a general lack of data. Approaches that use tectonic analogues were assessed to be most applicable in the case of SCRs, provided that a definition of appropriate analogues can be agreed upon. For purposes of assessing Mmax, the Thyspunt PSHA SSC TI Team concluded that the tectonic criteria given in ***Reference 5.14.53*** to define tectonic analogues to the CEUS region and, by definition, to SCRs globally are appropriate. The Team also concluded that the Thyspunt region is tectonically very analogous to the CEUS (see ***Subsection 5.14.5.4.(c) i***).

After a careful consideration of the approaches that are currently available for assessing Mmax for seismic source zones within SCR and the precedents from analogous PSHAs such as the PEGASOS project (***Reference 5.14.146***), the SSC TI Team decided to use two alternative approaches as a basis for estimating the Mmax distributions for seismic source zones:

- the Bayesian procedure (***Reference 5.14.53***), which uses the prior distributions from an update and evaluation of the global SCR data conducted for the CEUS SSC project (***Reference 5.14.69***);

- the Kijko procedure (***Reference 5.14.169***), which uses the observed seismicity within a region to provide a direct (or posterior) assessment of Mmax.

The Bayesian approach, illustrated in ***Figure 5.14.51***, is representative of a category of approaches that rely on drawing analogies to tectonically comparable regions in order to estimate the Mmax for the source of interest (***Reference 5.14.168***). These approaches are based on the ergodic assumption that one can substitute time (the short period of observation) for space (other SCRs worldwide). As a result, the Bayesian approach consists in the updating of a prior distribution representative of global SCRs via a likelihood function determined from locally available data, leading to a posterior distribution that can be used in the recurrence calculations (***Subsection 5.14.5.4.(c) vii***) following discretisation.

The Kijko approach is representative of an alternative category of models that rely on the observations of seismicity entirely within the zone of interest. Because the occurrence of Mmax is rare relative to the period of observation, this category of approaches assumes—and is highly sensitive to—a given frequency distribution of earthquake sizes. To be able to apply the approaches with confidence to larger or very active regions, significant numbers of observed earthquakes are required to provide stable estimates.

The weighting scheme for the use of the Bayesian approach versus the Kijko approach is source-specific to account for the numbers and magnitudes of observed earthquakes with each seismic source zone. It was judged that in no case should the Kijko approach be given higher weight than the Bayesian approach, considering the higher reliance on the Bayesian approach (and similar analogy-based approaches) by the larger technical community. The weighting scheme for the Bayesian and Kijko approaches, developed for the CEUS SSC project (***Reference 5.14.69***) was adopted for use in the Thyspunt PSHA. This weighting scheme is based on theoretical considerations regarding the statistical stability of the Kijko approach. The resulting source-specific weights are given in the relevant sections of the individual source descriptions in ***Subsections 5.14.5.4.(d) i*** to ***5.14.5.4.(d) v***.

© Eskom 2026/Rev 0a

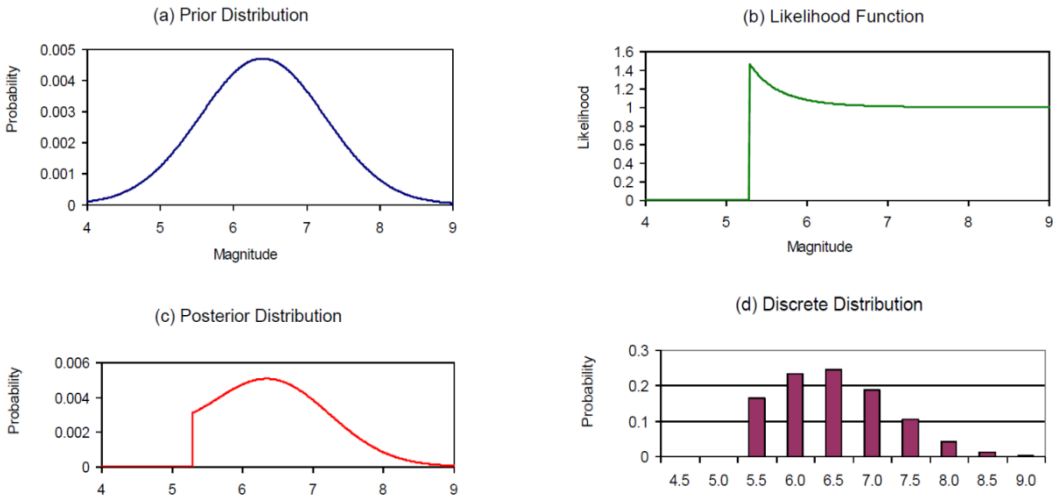


Figure 5.14-51 Diagrammatic Illustration of the Bayesian Mmax Approach

The various panels show (a) the prior distribution, (b) the likelihood function, and (c) the posterior distribution. The posterior distribution is represented by a discrete distribution (d) for implementation in hazard analysis. The prior shown is a normal distribution with mean M 6.4 and standard deviation 0.85.

The likelihood function is based on two observed earthquakes larger than M 4.5, with the largest being 5.3. (*Reference 5.14.69*).

The assessment of Mmax for seismic source zones has been designed to incorporate the uncertainties in both the conceptual models and the parameter values associated with each model. Therefore, in addition to the inclusion of the Kijko approach as an alternative method, it was decided that alternative prior distributions should be considered for the Bayesian approach, consistent with the assessment done in the CEUS SSC study (***Reference 5.14.69***). The alternative prior distribution models are based on the results of an updated statistical analysis (***Reference 5.14.69***) showing that the most significant separation of the SCR database is between superdomains that show Mesozoic-and-younger extension and those that do not. The data used are based on the domains in the SCR database, defined by their most recent age of extension. The Mmax prior distributions for the "two-prior" model are as follows:

	Mean Mmax	Sigma
• Mesozoic and younger extension (MESE):	7.35	0.75
• Non-Mesozoic and younger extension (NMESE):	6.70	0.61

The alternative to this “two-priors” model is the single or “composite-prior” model, which assumes that a single, composite-prior distribution is appropriate throughout the region covered by the Thyspunt SSC model. The composite prior represents the concept that the characteristics within SCRs that control Mmax cannot be identified with confidence. Therefore, the only distinction made is that the applicable global database must be from SCRs, but no subdivisions are imposed beyond that. This alternative conceptual model is consistent with the relatively weak statistical significance of any subdivision of the SCR as indicators of Mmax. The single-prior distribution for the composite data set is as follows:

	Mean Mmax	Sigma
• Single-Prior Composite (COMP):	7.20	0.64

The relative weights for the two-priors and single-prior composite models are assessed for all of the seismic sources. The two-priors model is assessed to have slightly higher weight [0.6] than the single-prior composite model [0.4]. Higher weight of [0.6] reflects the fact that there is some statistical significance to the separation of the data into the two Mmax zones, as well as an expectation that the locations of geologically recent crustal extension should have ample faults of sufficient dimensions for larger earthquakes. However, a higher weight than [0.6] is judged to not be appropriate because the statistical significance of the separation is not strong and could only be evaluated after multiple domains were combined into superdomains to increase sample size for statistical evaluation. For the two-prior model, source-specific weights were assigned to the MESE and NMESE options depending on the geologic characteristics of the particular source zone, as discussed in the relevant sections of ***Subsections 5.14.5.4.(d) i*** to ***5.14.5.4.(d) v***.

The Mmax prior distributions described above are represented by unbounded normal distributions. However, there is an upper limit to the size of earthquakes that can occur in the Thyspunt region, as well as a bound on the minimum size of the maximum magnitude. The upper tail of the maximum magnitude distributions for all seismic source zones was truncated at M_w 8, based on a consideration of empirical data regarding the largest observed earthquakes within SCRs worldwide. The prior distributions are also truncated at the minimum magnitude that is assessed to be technically defensible, given a consideration of the observed magnitudes of earthquakes that have occurred with SCRs worldwide, which was assessed to be 5.5 in the CEUS SSC project (***Reference 5.14.69***). The Thyspunt PSHA SSC TI Team reviewed the technical bases for these assessments and concluded that for any given seismic source zone in the Thyspunt PSHA a minimum truncation of the prior

distribution is equal to the maximum observed magnitude within that source or M_w 5.5, whichever is greater.

Further details of the approach to calculating Mmax for source zones are given in Section 8.2.4 of ***Reference 5.14.17***.

x Assessment of fault source Mchar

Unlike seismic source zones for which the dimensions of ruptures for causative faults are not known, the rupture dimensions for fault sources can often be estimated based on palaeoseismic data and information related to fault length. The assessment of the characteristic magnitude, M_{char}, is the principal assessment that is made for each fault. The various approaches to using fault-specific data to assess M_{char} are described below.

The primary approach to assess M_{char} for the fault sources is to estimate the dimensions of rupture that have occurred in the palaeoseismic record for the fault of interest. The estimated rupture dimensions, in turn, are then related to expected earthquake magnitude using appropriate empirical and theoretical relationships available from the published literature. If applicable, multiple rupture-versus-magnitude relationships are used to assist in estimating the range of epistemic uncertainty. The relationships used in the development of the Thyspunt SSC model were the subsurface rupture length, average displacement and rupture area relations of Wells & Coppersmith (***Reference 5.14.159***), and the SCR surface rupture length and rupture area relations of Leonard (***Reference 5.14.158***).

Given the range of palaeoseismic data available and the calculated magnitudes from the relationships above, the SSC TI Team developed an epistemic distribution of the M_{char} for each fault source. In some cases, limited data were available to assess fault-specific rupture dimensions other than possible rupture lengths. In other cases, data related to possible analogues were used to make an assessment of possible values of M_{char} and the associated uncertainties. The technical bases for all assessments are given in the applicable parts of ***Subsections 5.14.5.4.(e) i*** through ***5.14.5.4.(e) v***.

d) Seismic Source Zones

This section summarises the characteristics of seismic source zones identified for the SSC model. Using the criteria discussed in ***Subsection 5.14.5.4.(a)*** for defining seismic sources, five seismic source zones are identified, as shown on ***Figure 5.14.52***, where they are superimposed on the declustered seismicity catalogue developed for the project ***(Subsection 5.14.4.4***).

© Eskom 2026/Rev 0a

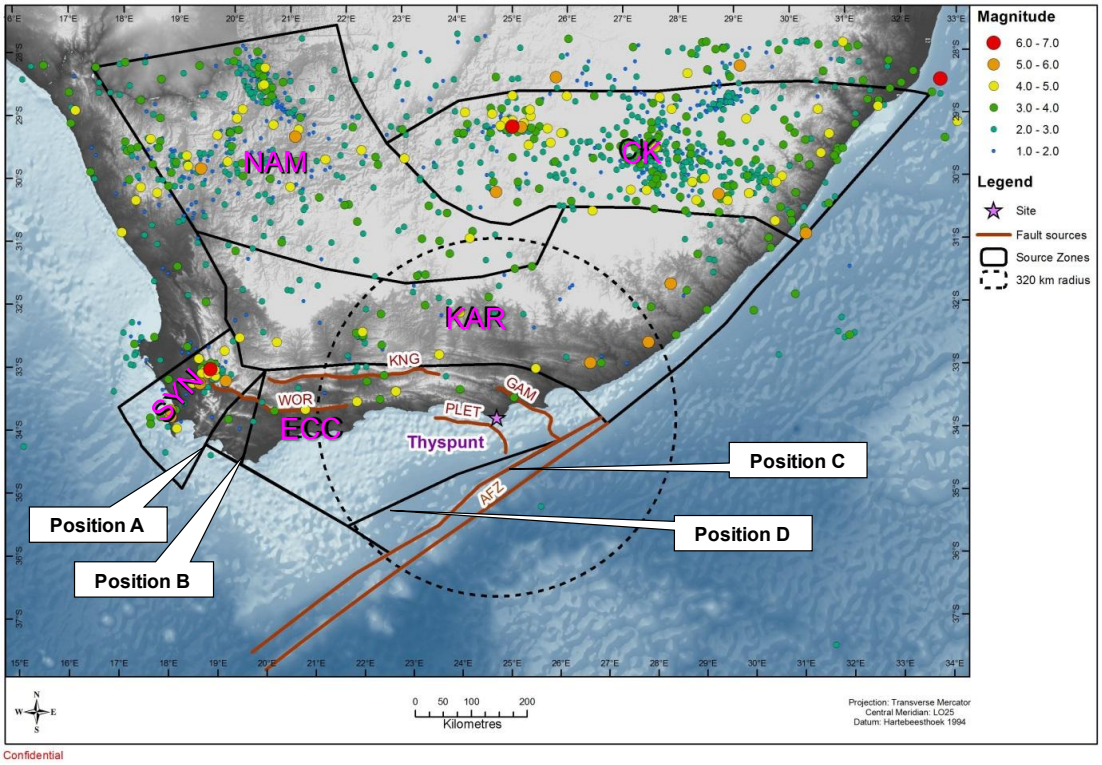


Figure 5.14-52 Seismic Source Zones Defined in the SSC Model (*black lines*), Including Alternative Boundaries for the ECC Host Zone, and Earthquake Epicentres from the Declustered Project Catalogue.

Global assessments that relate to multiple seismic sources (*e.g.*, seismogenic crustal thickness) are discussed above in ***Subsection 5.14.5.4.(c)***. In ***Sections 5.14.5.4(d) i*** through ***5.14.5.4.(d) v***, each of the seismic source zones is described and the characteristics of each zone that are part of the SSC model are summarised. The discussion includes the technical bases that support the assessments included in the model as well as the uncertainties given in the source logic trees. ***Table T-5.14.6*** summarises the source zone–specific assessments that make up the SSC model. Full details of the technical justifications are given in Section 8.3 of ***Reference 5.14.17***).

Figure 5.14.53 summarises the Mmax distributions developed for these seismic source zones using the approach described in ***Subsection 5.14.5.4.(c) ix***. The observed largest magnitude values for each source are shown in ***Figure 5.14.54***. The recurrence curve distributions

developed for the various seismic source zones using the approach described in ***Subsection 5.14.5.4.(c) vii*** are shown in ***Figure 5.14.55***.

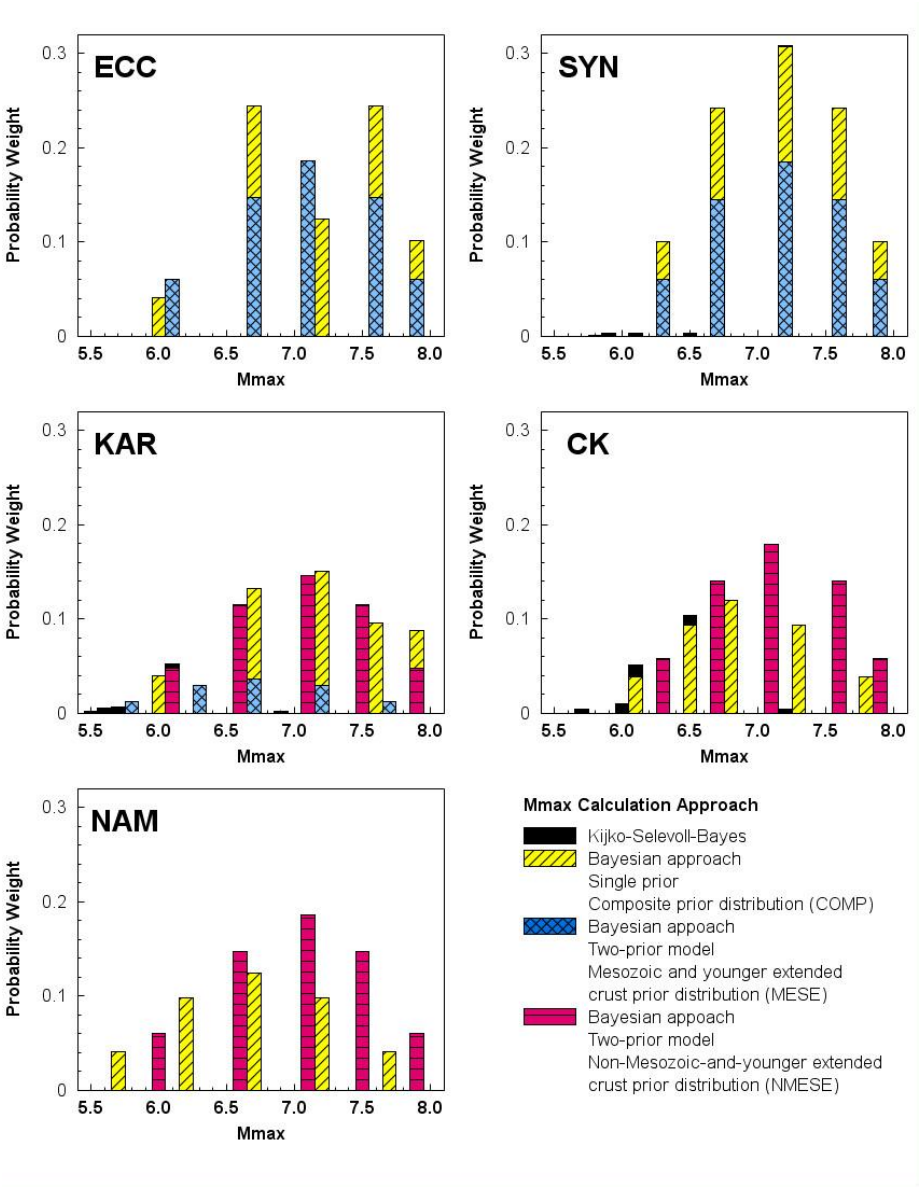


Figure 5.14-53 Mmax Distributions for the Seismic Source Zones in the SSC Model.

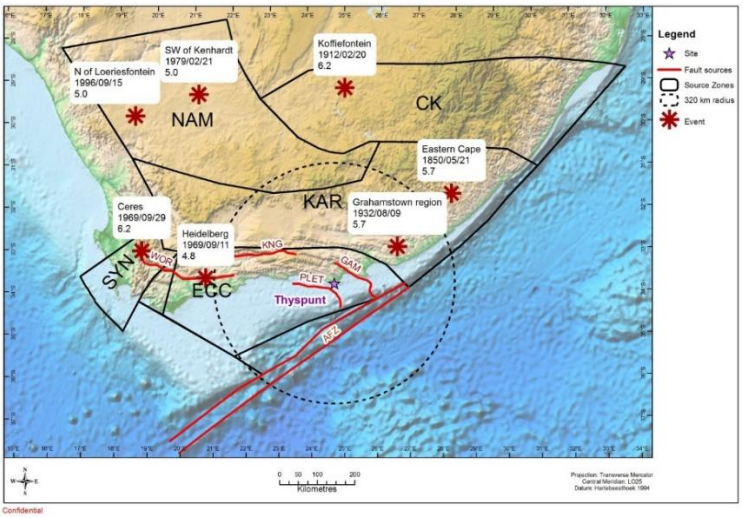


Figure 5.14-54 Largest Observed Earthquakes Within the Region of the Thyspunt site.

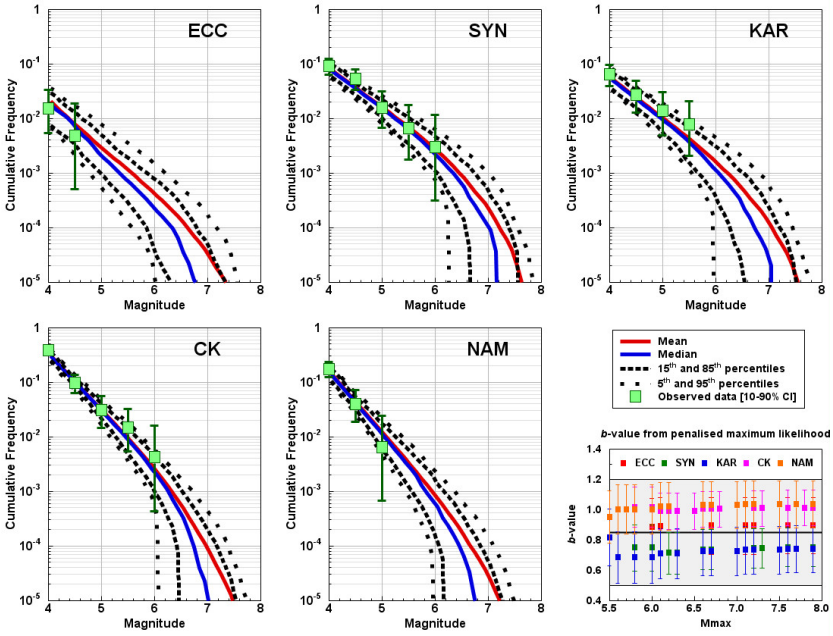


Figure 5.14-55 Summary of Earthquake Recurrence Relationships for the Source Zones included in the SSC Model.

The lower right panel shows the b-values determined for each of the source zones, with the prior distribution based on the regional b-value shown in grey.

Table 5.14.6
Summary of Seismic Source Zone Characteristics Included in the SSC Model

	ECC	SYN	KAR	NAM	CK
Boundary Alternatives	**Western Boundary** • **Position A [0.8]** • **Position B [0.2]** **Eastern Boundary** • **Position C [0.3]** • **Position D [0.7]**	**Position A [0.8]** **Position B [0.2]**	**No alternatives**	**No alternatives**	**No alternatives**
Nature of Source Boundaries	**Leaky**	**Leaky**	**Strict**	**Strict**	**Leaky**
Style of Faulting	**Normal (60%)** **Strike-slip (40%)**	**Strike-slip (100%)**	**Normal (50%)** **Strike-slip (50%)**	**Normal (50%)** **Strike-slip (50%)**	**Normal (50%)** **Strike-slip (50%)**
Strike of Ruptures	**45° (15%)** **80° (25%)** **95° (25%)** **110° (35%)**	**0-360° uniform (100%)**	**30° (15%)** **70° (20%)** **90° (30%)** **110° (20%)** **160° (15%)**	**35° (10%)** **85° (25%)** **135° (55%)** **175° (10%)**	**45° (30%)** **65° (35%)** **85° (25%)** **155° (10%)**
Dip of Ruptures	**Normal (dips to the south)** • **45º (20%)** • **60º (60%)** • **70º (20%)** **Strike-slip (dips either to the North (50%) or South (50%)** • **75º (30%)** • **90º (70%)**	**Not modelled[2]**	**Not modelled**	**Not modelled**	**Not modelled**
Mmax Bayesian Prior	**MESE [1.0]**	**MESE [1.0]**	**MESE [0.2]** **NMESE [0.8]**	**NMESE [1.0]**	**NMESE [1.0]**
Max Observed[3]	**4.8 ± 0.5** **11-09-1969 Heidelberg**	**6.2 ± 0.2** **29-09-1969 Ceres-Tulbagh earthquake**	**5.7 ± 0.4** **21-05-1850 N of Butterworth,** **5.7 ± 0.35** **09-08-1932 Grahamstown**	**5.0 ± 0.4** **21-02-1979 SW of Kenhardt,** **5.0 ± 0.4** **15-09-1996 N of Loeriesfontein**	**6.2 ± 0.25** **20-02-1912 Koffiefontein**

[1] Epistemic weights are given as probabilities in [brackets] and aleatory relative frequencies are given as percentages in (parentheses).
[2] Because of the large distance to the site, the dip of ruptures is not modelled but is assumed to be vertical.
[3] Convention for date of earthquakes is day-month-year.

i Extended Continental Crust Source Zone (ECC)

The Extended Continental Crust source zone (ECC; ***Figure 5.14.52***) is the host zone for the Thyspunt Site and encompasses the Cape Fold Belt, present coastline and extends offshore to the edge of the continental margin. It is bounded to the north by the Karoo seismic source zone (KAR; ***Subsection 5.14.5.4.(d) iii***) and to the west by the Syntaxis seismic source zone (SYN; ***Subsection 5.14.5.4.(d) ii***).

It contains (fully or partiallly) the majority of tectonic structures assessed for seismogenic probability in the Thyspunt PSHA study due to their proximity to the Thyspunt site (***Section 5.13***; ***Subsections 5.14.5.4.(e) and 5.14.5.4.(e) vi***), but is generally characterised by low levels of observed seismicity (***Figure 5.14.52***). Consistent with the criteria for defining seismic sources (***Subsection 5.14.5.4.(a) i***), the characterisation of this zone was to a large degree based on geological data.

The crust underlying the ECC displays a common history and its geology can be attributed to repeated episodes of crustal compression and extension over a two-billion-year period. It is largely distinguished from its neighbouring zones by the intensity of most recent tectonic events and its structural fabric. A detailed description of the major structures and geological history of the ECC is given in Section 8.3.1 of ***Reference 5.14.17***. The Palaeoproterozoic to Mesoproterozoic Namaqua-Natal Mobile Belt (NNMB) makes up the largest portion of the continental crust underlying the ECC (***Figure 5.13.10***). As documented in ***Section 5.13***, the rock record of the ECC reflects the influence of five major geological events, including multiple phases of compression and extension:

- The Mesoproterozoic Namaqua orogeny that formed the Namaqua-Natal tectonic province comprising the igneous and metamorphic rocks that envelop the southern and western margins of the Kaapvaal Craton (see ***Subsection 5.13.5.1.(b) i***).

- Accumulation of the Cape Supergroup in a passive margin setting (Early Ordovician to Early Carboniferous; ***Subsections 5.13.5.1.(b) i and 5.13.5.1.(c) ii***).

- Permo-Triassic Cape Orogeny that formed the Cape Fold Belt (***Subsections 5.13.5.1.(b) i*** and ***5.13.5.1.(a) iii***).

- Continental breakup of Gondwana during the Mesozoic

© Eskom 2026/Rev 0a

(***Subsection 5.13.5.1.(b) ii***).

- Late Neogene to Quaternary coastal deposition (***Subsections 5.13.5.1.(b) iii*** and ***5.13.5.1.(c) v***).

The most recent tectonic event to affect the ECC zone was extension associated with the breakup of Gondwana during the mid to late Mesozoic (***Reference 5.14.170***). The ECC zone exhibits low levels of seismicity (***Figure 5.14.52***) that are slightly lower than the KAR zone to the north and significantly lower than the SYN zone to the west. Seismicity in the ECC zone is characterised by a few small-to-moderate magnitude events, which is in contrast to the more elevated levels of seismicity in the SYN source, which hosted the M_w 6.2 1969 Ceres earthquake (***Subsection 5.14.5.4.(d) ii***). As explained below, the ECC zone also differs from neighbouring zones in terms of the selection of the appropriate prior distribution for the assessment of Mmax, the assessment of the style of faulting, as well as expected rupture orientations.

Based on the evaluation of the geological and seismological databases (***Subsections 5.14.4.3 and 5.14.4.4***), the SSC TI Team developed the logic-tree shown in ***Figure 5.14.56***, the technical bases of which are summarised below, alongside those for the modelling of future earthquake characteristics modelled as aleatory distributions. Full details of the technical justifications can be found in Section 8.3.1 of ***Reference 5.14.17***).

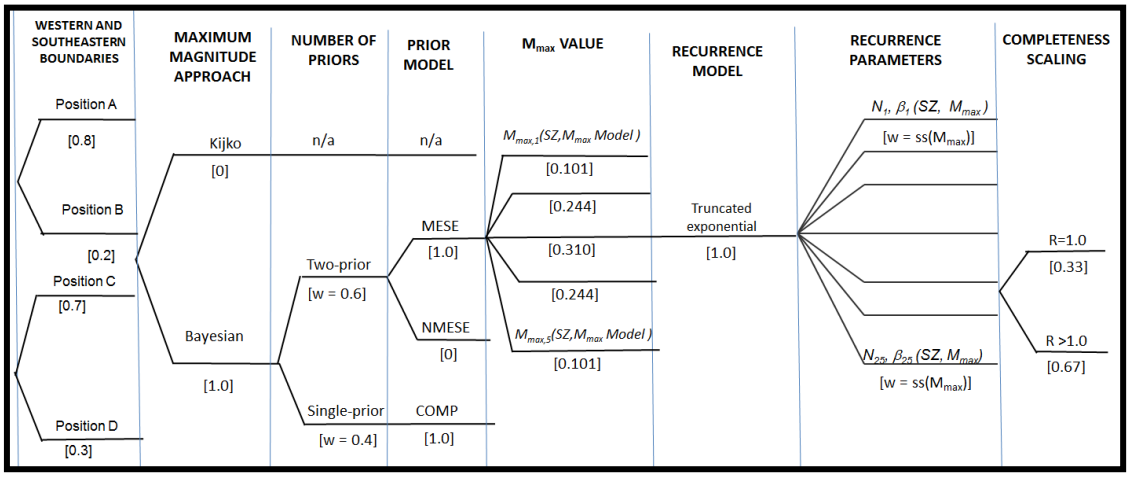


Figure 5.14-56 Logic Tree Summarising the Epistemic Uncertainties in the Characterisation of the ECC Source Zone.

Epistemic uncertainties that are common to multiple source zones such as seismogenic thickness are discussed in Subsection 5.14.5.4.(c).

Four alternative geometries were considered in order to incorporate the epistemic uncertainties regarding the position of the western and south-eastern boundaries of the ECC. The northern boundary for the ECC zone is delineated by the landward-most evidence for major Mesozoic crustal extension. This is supported by the progressive thinning that the crust displays towards the south (***Subsection 5.13.5.1.(d) ii***; see ***Figure 5.13.41***). As noted in ***Subsection 5.13.5.1.(c) iv***, the majority of onshore basins are half-grabens bounded by reactivated thrust faults along their northern margins. The Oudtshoorn Basin and the Sunday River Trough represent the northernmost limit of these extensional basins. Hence the northern limit of the ECC zone is placed along a line directly to the north of the Kango Fault (***Subsection 5.14.5.4.(e) i***), extending to the northern margin of the Sundays River Trough, before swinging south to the AFFZ.

The south-eastern boundary of the ECC source zone corresponds to the boundary separating the continental crust within the ECC zone from oceanic crust. Due to the thinning of the continental crust that resulted from plate separation and the transitional nature of the crust, the location of the boundary is uncertain. Two alternative locations (Locations C and D on ***Figure 5.14.52***) express the epistemic uncertainty in the location of the south-eastern boundary of ECC.

As noted in ***Subsection 5.13.5.1.(a) iii***, Parsiegla *et al*. (***Reference 5.14.171***) distinguished between a northern area that experienced one episode of extension, with stress directions perpendicular to the AFFZ, as a result of Gondwana rifting; and a southern area that underwent two phases of extension thinning associated with shear along the AFFZ (***Figure 5.13.42***). The division between these areas appears to correspond with the southern limit of the offshore faults in the Outeniqua Basin, as well as being in broad agreement with the southern limit of the continental shelf (***Reference 5.14.172***). Since the southern part of the Outeniqua Basin has been subjected to a different tectonic history from the rest of the ECC zone (including the Thyspunt site), the preferred south-eastern source zone boundary, with a weight of [0.7], is positioned along the southern limit of the visible fault traces (indicated by position D in ***Figure 5.14.52***).

At the AFFZ, the crust thins rapidly (***Figures 5.13.41*** and ***5.13.42***) to about 7 km on the oceanic side and is considered to represent a transition zone from continental to oceanic crust. An alternative south-eastern source zone boundary for the EEC source zone is therefore placed along the continental margin along the AFFZ (position C in ***Figure 5.14.52***). This alternative is given a lower weight of [0.3] because it would include what appears to be highly attenuated and transitional crust within ECC.

© Eskom 2026/Rev 0a

The Agulhas-Columbine Arch is a basement arch composed of Cape Supergroup metasediments that forms the western boundary of the offshore Outeniqua Basin (***Figure 5.13.42***; ***Reference 5.14.172***). It also separates this basin (***Figures 5.13.3*** and ***5.13.15***) from the north-south-oriented, passive, volcanic continental margin and elongated extensional basins that developed to the west (***References 5.14.172 and 5.14.173***). The south-western boundary of the ECC zone is therefore placed along the same boundary of the Outeniqua Basin and extended in the same direction until it intersects the western zone boundary.

The western boundary of the ECC is defined by the western termination of east-west crustal fabric within the ECC source against the north-northwest-/south-southeast–striking crustal fabric of the SYN. On a regional scale this happens where the east–west trend of the southern branch of the Cape Fold Belt (***Figures 5.13.13*** and ***5.14.57***) coalesces with the north-northwest-trending western branch in the syntaxis, which is characterised by complex faulting and folding (see ***Subsection 5.14.5.4.(d) ii***).

The extent of the syntaxis and, by implication, its boundary with the ECC zone is poorly defined. For the SSC model, uncertainty in the western boundary of the ECC is represented by two alternative boundary locations (positions A and B in ***Figure 5.14.52***). Traditionally, the centre of the syntaxis is considered to extend from Ceres to the eastern limb of False Bay near Cape Town (***References 5.14.175 and 5.14.176***). This core displays a strong northeast-directed structural grain (Figure 8.36) and the limit of the east–west structural grain, and the preferred alternative boundary between the EEC and SYN source zones, is placed immediately to the east of the syntaxis core (position A, see ***Figure 14.52***). This location is assessed to have a weight of [0.8].

In contrast to the western boundary of the syntaxis, the eastern boundary represents a much more gradual transition from northeast-trending syntaxial folds to the east–west structural orientation of the southern branch of the CFB (***References 5.14.174 and 5.14.177***). An alternative boundary between the ECC and SYN source zones therefore traces the eastern limit of the northeast-oriented, syntaxial trend of faults and secondary folds (position B; see ***Figure 14.52***). Due to the more diffuse nature of this boundary, it is assessed to have lesser weight of [0.2].

© Eskom 2026/Rev 0a

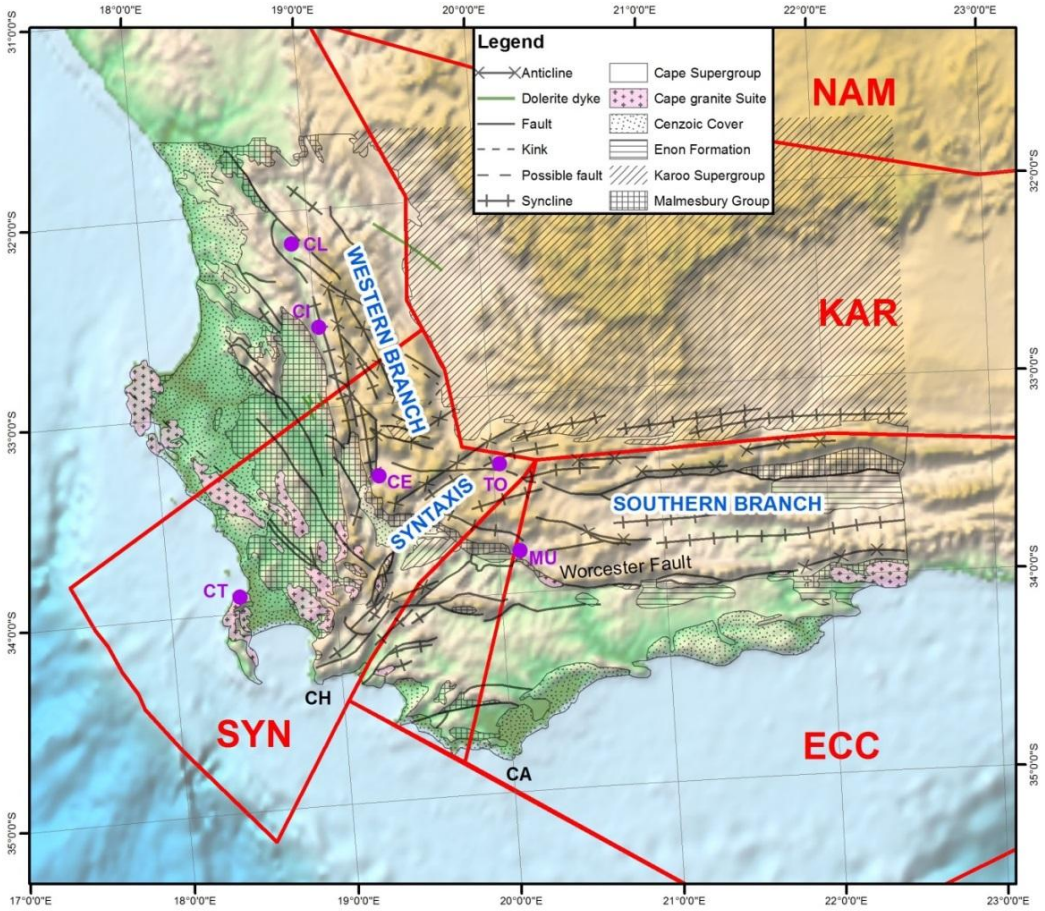


Figure 5.14-57 Map Showing the Two Structural Branches in the Cape Fold Belt, the Setting of the Syntaxis, and Alternative Source Zone Boundaries Superimposed Upon a Regional DEM.

Location names are as follows: CA = Cape Agulhas; CE = Ceres; CH = Cape Hangklip, MG = McGregor; MU = Montagu; TO = Touwsrivier (Modified from Reference 5.14.174).

The ECC zone is dominated by an east-west-oriented structural trend, with the majority of large faults displaying this orientation (***Figure 5.14.53***). As they approach the continental margin, sections of the major faults swing southeast (***Figure 5.13.42***) and to the south (***Figure 5.13.49***), which is interpreted to be the result of drag that occurred along the AFFZ (***Reference 5.14.171***). The SSC TI Team considered identifying a source zone boundary based on this change in trend, but concluded that such a boundary was not necessary given the continuity of the structures across the change in trend. As a result, the change in trend is reflected in the variation in the rupture orientations within the ECC source. Smaller, northeast-southwest-oriented transfer faults are common in

the southern branch of the Cape Fold Belt (***Reference 5.14.178***). Given the interpretation by the SSC TI Team of the orientation of structures and structural trends, the strike of future earthquake ruptures within the ECC source zone is modelled as an aleatory distribution having the following azimuths and percentages: 45° (15%), 80° (25%), 95° (25%) and 110° (35%).

The faults in the ECC zone have a complex history, but their current geometries primarily reflect events that took place during extension related to Mesozoic breakup of Gondwana. The majority of the large east-west-striking faults are interpreted to be inverted thrust faults that subsequently underwent normal displacement (***Reference 5.14.179***) that may be on the order of several kilometres (***References 5.14.180 to 5.14.183***). There is little to no evidence for strike-slip movement on any of the onshore traces of the major fault systems of the ECC zone (***References 5.14.184 to 5.14.186***). However, the proposed southwards rotation that these faults experienced at their eastern ends, supposedly as a result of shear along the AFFZ (***References 5.14.187 and 5.14.188***) suggests that some strike-slip movement may have taken place in the eastern fault segments. This is supported by evidence for strike-slip movement in various offshore faults ***References 5.14.170, 5.14.189 and 5.14.190***). In addition, strike-slip displacements have been recorded in the smaller northeast-oriented faults that occur between the larger fault systems (***References 5.14.191 and 5.14.192***).

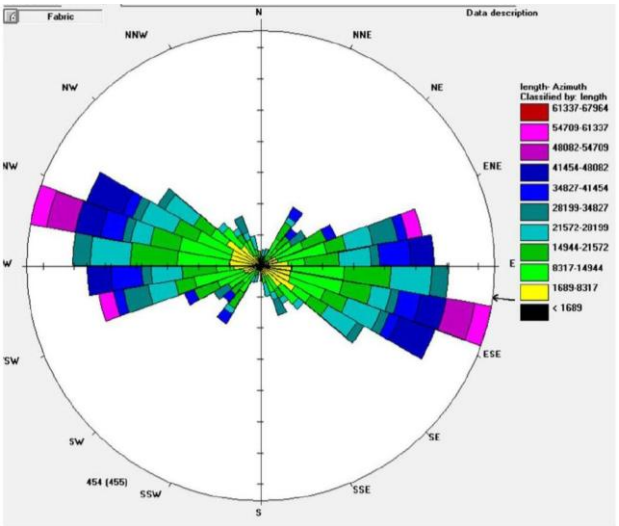


Figure 5.14-58 Rose Diagram of the ECC Zone Showing the Prominent West-Northwest Structural Trends.

The diagram was developed by measuring the average orientation and approximate lengths of structural trends within the ECC zone.

There are no focal mechanisms for earthquakes within the ECC zone that might provide direct evidence of the contemporary style of faulting, but the evaluation of the regional tectonic regime based on focal mechanisms shows a mix of normal and strike-slip faulting (***Subsection 5.13.5.1.(d) i***). Geological data support both normal and strike-slip faulting, but clear evidence for Late-Quaternary normal faulting on the Kango Fault (***Subsection 5.14.5.4.(e) i***) indicates that normal faulting may more dominantly characterise contemporary processes. Based on the available evidence, the style of faulting of future earthquake ruptures within the ECC zone is defined by the following aleatory (relative frequency) distribution: normal (60%), strike-slip (40%).

Since there are no earthquake focal mechanisms and few independent observations of the downdip geometry of most structures, the proposed dips of faults are dependent on the style of faulting and observations within the ECC zone. Normal faults within ECC are known to dip to the south (***References 5.14.193 and 5.14.194***; ***Figure 5.13.50***), becoming listric at depth. As is evident from the discussion in ***Subsections 5.14.5.4.(e) i***, ***5.14.5.4.(e) iii***, and ***5.14.5.4.(e) iv***, there is uncertainty about the variation in the dips of individual faults, both as mapped near the surface and at depth based on geophysical data. In the absence of source-specific information, the assessment of the dips associated with normal and strike-slip earthquake ruptures is based on a consideration of fault dips documented for earthquakes in the worldwide database (***Subsection 5.14.5.4.(c) v***). Based on that evidence, and giving due consideration to the limited observations within the ECC zone itself, the following aleatory distributions were assessed for the ECC source as a function of the style of faulting:

- Normal faulting events are assumed to all dip to the south, with the generic aleatory distribution of dip angles for such events defined in ***Subsection 5.14.5.4.(c) v***: 45º (20%), 60º (60%), 70º (20%).

- Strike-slip faulting events are assumed to dip to the north or south in equal proportions (50% each), with dip angles described by the following distributions: 75º (30%), 90º (70%).

The aleatory assessments of the characteristics of future earthquake ruptures within the ECC source zone are summarised in ***Figure 5.14.59***.

The Mmax value for the ECC was assessed using the seismicity catalogue (***Subsection 5.14.4.4***) and the approaches described in ***Subsection 5.14.5.4.(c) ix***. This requires the assessment of source-specific weights for the MESE and NMESE priors. Progressive thinning of the ECC crust to the continental margin to the south and presence of major Mesozoic rift-basins and associated faults provide ample evidence that the ECC zone has

© Eskom 2026/Rev 0a

undergone Mesozoic crustal extension. Hence, on the two-prior branch of the Mmax logic tree, the MESE prior distribution is assigned a weight of [1.0]. Only small-to-moderate magnitude earthquakes and sparse levels of seismicity have been recorded for the ECC seismic source zone (***Figure 5.14.52***). The largest observed event of M_w 4.8± 0.5 was recorded near the town of Heidelberg in the Western Cape Province on 11 September 1969. Using the weighting scheme discussed in ***Subsection 5.14.5.4.(c) ix***, a weight of zero was assessed for the Kijko approach (*i.e.*, there is insufficient data for this approach to give stable results). Combining the Mmax distributions from the various approaches considered resulted in the Mmax distribution shown in ***Figure 5.14.53***. The recurrence curves developed using this Mmax distribution and the approach discussed in ***Subsection 5.14.5.4.(c) vii*** are shown in ***Figure 5.14.55***. These recurrence curves include a completeness correction factor to account for the fact that part of the ECC source zone is located offshore, where completeness of small-to-moderate earthquakes is more difficult to assess than in the onshore region, and hence more uncertain (***Figure 5.14.60***).

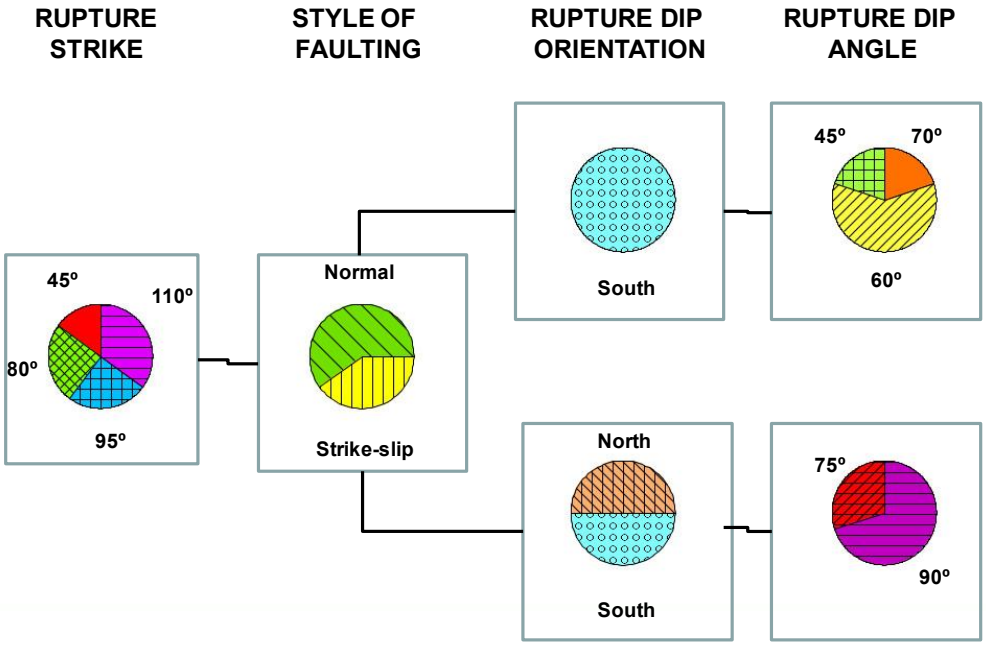


Figure 5.14-59 Summary of Aleatory Assessments for the ECC Source Zone.

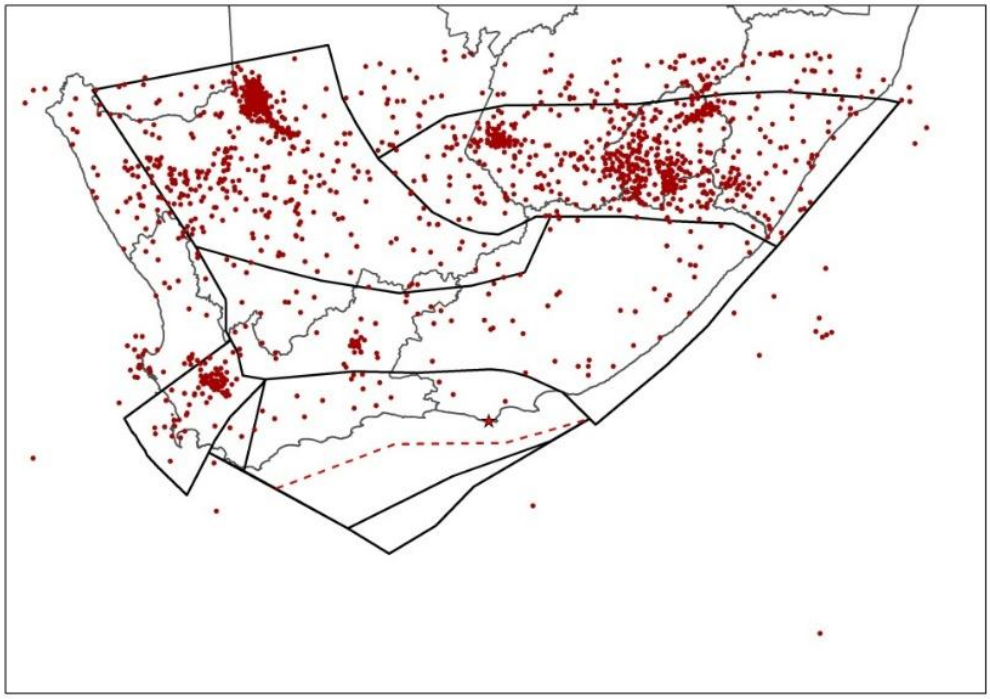


Figure 5.14-60 Location of a Possible Completeness Boundary Within the ECC Source Zone (*dashed red line*).

ii Syntaxis Source Zone (SYN)

The Syntaxis source zone (SYN) is located at the intersection of the western and southern branches of the Cape Fold Belt (***Subsection 5.13.5.1.(a) iii***) where an abrupt change in structural orientation occurs that is known as the 'syntaxis' (***Figure 5.14.57***). The SYN neighbours the Karoo seismic source zone (KAR; ***Subsection 5.14.5.4.(d) iii***) to the northeast and the Extended Continental Crust host zone (ECC; ***Subsection 5.14.5.4.(d) i***) to the east. To the northwest lies a region that is structurally and geologically different from the SYN, but is not characterised for the PSHA due to its distance from the Thyspunt site.

The syntaxis is the most fractured part of the Cape Fold Belt. Most faults in the area trend northeast–southwest in parallel with fold trends, but some east–west and northwest–southeast faults also are present (***Reference 5.14.195***). The major structures within the SYN formed during the Permo-Triassic Cape Orogeny and were subsequently reactivated in the Mesozoic during the

© Eskom 2026/Rev 0a

breakup of Gondwana. Many workers have proposed that tectonic inversion (normal faulting) in the Mesozoic localised along steep ramps of thrust faults formed during the Cape Orogeny (***References 5.14.170, 5.14.175, and 5.14.195 to 5.14.197***). While the major structures within the SYN have deformational histories similar to structures in neighbouring zones, the SYN contains structural complexities that are unique to the region.

Major basement-involved structures associated with the syntaxis include the Worcester Fault (***Subsections 5.13.5.1.(d) iv*** and ***5.14.5.4.(e) v***), the Hex River Anticline, and the Ceres Arc with its associated faults and fractures. The Hex River Anticline subdivides the syntaxis north of the Worcester Fault into two distinct subdomains (***Figure 5.14.61***). South of the anticline, the east-trending southern Cape Fold Belt branch and the northeast-trending folds of the syntaxis merge and intersect (***Reference 5.14.198***). North of the anticline lies the Ceres Arc, a zone of intensely deformed rocks that can be characterised by the termination of the north-trending western Cape Fold Belt branch folds against the northeast-trending folds of the syntaxis (***Reference 5.14.199***). The Ceres Arc is considered the structural centre of the syntaxis. The M_w 6.2 Ceres earthquake on 29 September 1969 may have occurred along the Groenhof Fault within the Ceres structural arch (***Reference 5.14.21***). However, a number of neighbouring faults have similar orientations, no coseismic surface rupture was documented, and no particular fault source has been definitively associated with the Ceres earthquake.

Based on the evaluation of the geological and seismological databases ***(Subsections 5.14.4.3*** and ***5.14.4.4***), the SSC TI Team developed the logic-tree shown in ***Figure 5.14.62***, the technical bases of which are summarised below, alongside those for the modelling of source-specific future earthquake characteristics modelled as aleatory distributions. Full details of the technical justifications can be found in Section 8.3.2 of ***Reference 5.14.17***.

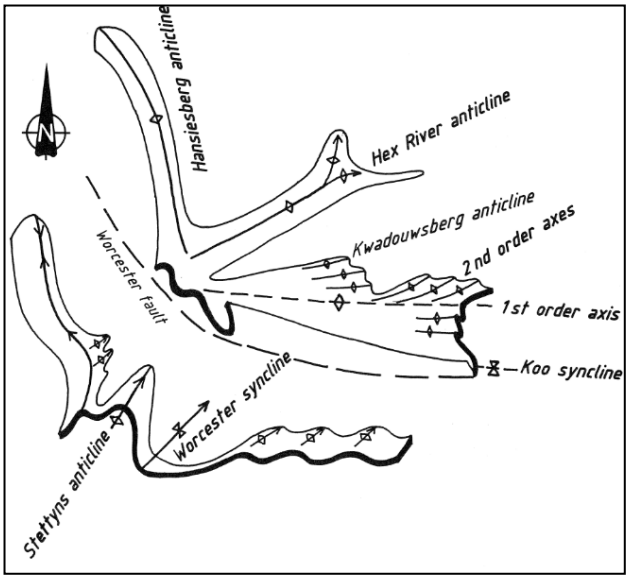


Figure 5.14-61 Schematic Interpretation of the Syntaxial Core Showing the Differences in Structural Subdomains to the North and South of the Worcester Fault (*Reference 5.14.174*).

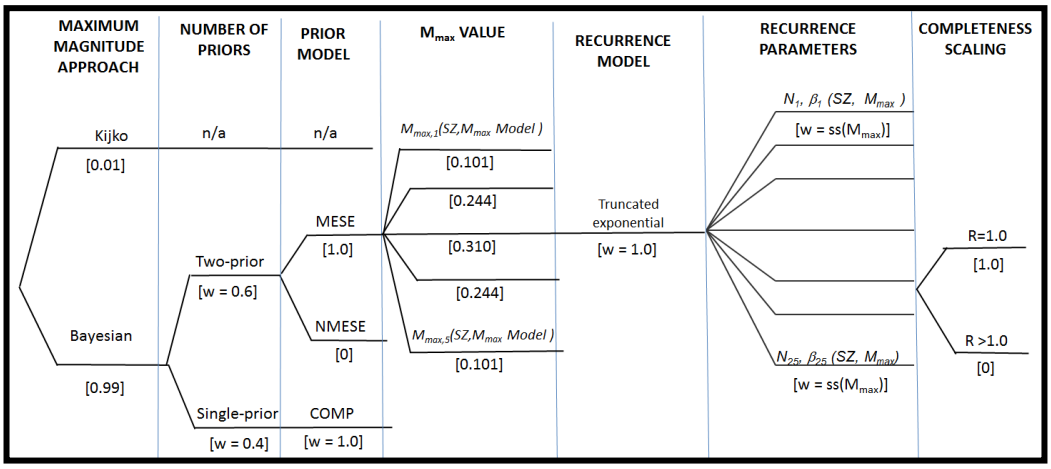


Figure 5.14-62 Logic Tree Summarising the Epistemic Uncertainties in the Characterisation of the SYN Source Zone.

Epistemic uncertainties that are common to multiple source zones such as seismogenic thickness are discussed in Subsection 5.14.5.4.(c).

The identification of the SYN was based on the criteria for defining seismic sources summarised in ***Subsection 5.14.5.4.(a) i***. The SYN is defined by differences in levels of seismicity from its neighbours, the applicable Mmax prior distribution, the style of faulting, and the assessed orientation of future ruptures.

The north-eastern boundary for the SYN with the KAR is delineated by the evidence for Mesozoic extended crust. The Ceres-Kango-Baviaanskloof-Coega Fault system (***Subsection 5.13.5.1.(d) i***), is considered to represent the northernmost evidence for extension (see also discussion in ***Subsection 5.14.5.4.(d) i***). This boundary changes orientation from north–south to east–west consistent with the northeast boundary of the Mesozoic faulting as mapped by Toerien (***Reference 5.14.200***) and Toerien & Hill (***Reference 5.14.201***). This is supported by the progressive thinning that the crust displays towards the south, with the change in thickness being coincident with the boundary between non-MESE to MESE crust.

The north-western boundary of the SYN marks the northern limit of deformation characteristic of the syntaxis as mapped by De Beer (***Reference 5.14.199***). The north-western boundary marks also the northern limit of elevated seismicity (***Figure 5.14.63***) concentrated in the Ceres region within the Ceres Arc, which corresponds to the most intensely deformed zone of Mesozoic crust. The elevated levels of seismicity are roughly correlated with the trend of the northeast–southwest zone of deformation in the syntaxis where the southern and western branches of the Cape Fold Belt meet. Moving north, away from the zone of mergence, there are fewer earthquakes as the structure becomes more consistent in orientation and less intensely deformed.

The south-western boundary of the SYN marks the western edge of continental Mesozoic rifting and is positioned at the edge of the continental shelf (***Figure 14.52***). Finally, the eastern boundary is defined by the western termination of east-west crustal fabric within the ECC source against northwest-southeast-striking crustal fabrics. As discussed in ***Subsection 5.14.5.4.(d) i***, the position of this boundary is uncertain and, because of its potential hazard significance as the closest boundary to the site, uncertainty in its position is included in the SSC model. The alternative positions for this boundary (indicated by positions A and B in ***Figure 5.14.52***) and their associated weights ([0.8] and [0.2], respectively), have already been discussed in ***Subsection 5.14.5.4.(d) i***.

The core of the SYN is characterised by the structural syntaxis that is defined as a localised northeast-trending zone of weakened crust at the intersection of large-scale structural fabrics. The east-west structures of the ECC to the east change to a north-northwest orientation in the SYN. Thus the orientation of future ruptures is assessed to be different in the SYN from that of the ECC.

© Eskom 2026/Rev 0a

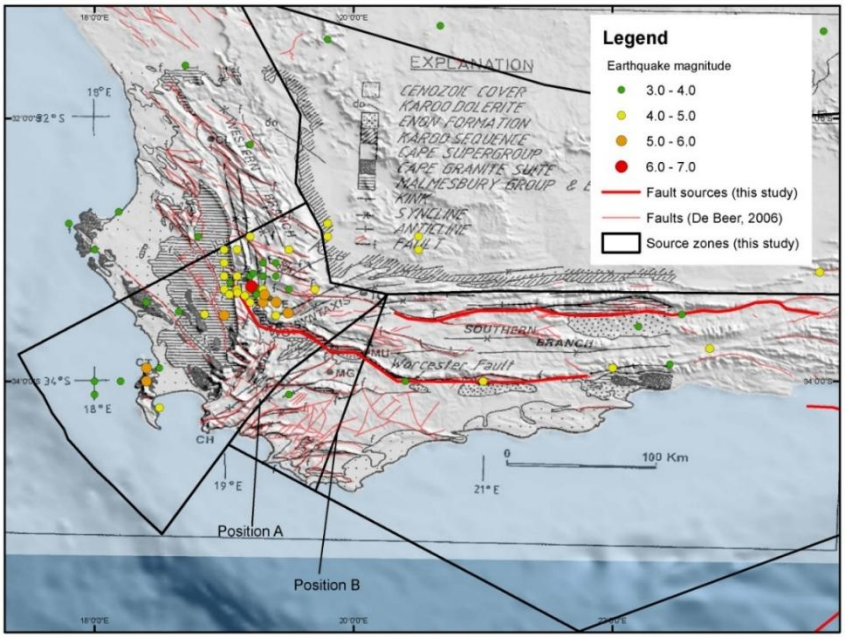


Figure 5.14-63 Map Showing the Two Structural Branches in the Cape Fold Belt, the Setting of the Syntaxis, Distribution of Seismicity, and Alternative Source Zone Boundaries Superimposed Upon a Regional DEM.

Location names are as follows: CH = Cape Hangklip, MG = McGregor; MU = Montagu; TO = Touwsrivier (Modified from De Beer, 1998).

Local structures within the SYN can be subdivided into four major orientations of northwest-, west/northwest-, northeast-, and east-striking faults, and northeast-, northwest-, and east-trending associated folds (***Reference 5.14.198***). The pattern of aftershocks for the 1969 Ceres earthquake strikes to the northwest and is nearly vertical. Given the wide range of geometries of structures that have been documented and the uncertainties, the strike of future earthquake ruptures is modelled as a uniform aleatory distribution. Because of the large distance of the SYN to the site, the dip of ruptures is not modelled explicitly but is assumed to be vertical.

The style of faulting within the SYN is assessed to be strike-slip [1.0], which differs from the styles of faulting for the ECC and KAR. Major faults such as the Worcester Fault change orientation abruptly within the source zone, becoming less continuous, fragmented, and steeply dipping. The primary evidence for

strike-slip faulting is the focal mechanisms from the 1969 Ceres earthquake and a number of aftershocks (***Table T-5.13.4***), as well as the near-vertical distribution of aftershocks at depth. Assuming the aftershocks define the primary rupture plane, the focal mechanism for the Ceres event indicates left-lateral faulting on a near-vertical (south-dipping) plane striking N56W (124 degrees).

The Mmax value for the SYN was assessed using the seismicity catalogue (***Subsection 5.14.4.4***) and the approaches described in ***Subsection 5.14.5.4.(c) ix***. This requires the assessment of source-specific weights for the MESE and NMESE priors. As discussed previously in this section, the SYN displays abundant evidence of Mesozoic and younger crustal extension, including thinning of the crust towards the continental margin and the presence of major Mesozoic extensional faults. Hence, on the two-prior branch of the Mmax logic tree, the MESE prior distribution is assigned a weight of [1.0]. The largest observed earthquake within the source is the 29 September 1969 Ceres event with M_w = 6.2 ± 0.2. Using the weighting scheme discussed in ***Subsection 5.14.5.4.(c) ix***, a weight of [0.01] was assessed for the Kijko approach. Combining the Mmax distributions from the various approaches considered resulted in the Mmax distribution shown in ***Figure 5.14.53***. The recurrence curves developed using this Mmax distribution and the approach discussed in ***Subsection 5.14.5.4.(c) vii*** are shown in ***Figure 5.14.55***. Given the relatively limited spatial extent of this source and its onshore location, no completeness correction was deemed necessary.

iii Karoo Source Zone (KAR)

The Karoo seismic source zone (KAR) is situated in the southern part of South Africa encompassing the Great Escarpment (***Subsection 5.13.5.1.(a) iii***; ***Figure 5.13.8***). This zone is bounded to the north by the Namaqua (NAM; ***Subsection 5.14.5.4.(d) v***) and the Cedarville-Koffiefontein (CK; ***Subsection 5.14.5.4.(d) iv***) zones and to the south by the Extended Continental Crust (ECC; ***Subsection 5.14.5.4.(d) i***) zone (***Figure 5.14.52***).

Consistent with the criteria for defining seismic sources (***Subsection 5.14.5.4.(a) i***), the characterisation of this zone was based on geological considerations and differences in levels of seismicity from its neighbours. The KAR can be correlated to the Cape Low zone and Spesbona microplate of the Du Plessis (***Reference 5.14.202***) and Hartnady (***Reference 5.14.203***) seismotectonic models, respectively. It is also equivalent to part of the Southern, South Eastern and Eastern Hinterland of the seismotectonic model by Partridge (***Reference 5.14.204***).

© Eskom 2026/Rev 0a

A detailed description of the major structures and geological history of the ECC is given in Section 8.3.3 of ***Reference 5.14.17***. The KAR is characterised by the geology of the Late Carboniferous to Middle Jurassic Karoo Supergroup (***Subsection 5.13.5.5.(a) iii***), which overlies the Cape Supergroup (***Subsection 5.13.5.5.(a) iii***). Both these geologic entities rest on the Proterozoic Namaqua-Natal basement. Tectonic activity in the KAR started with the orogeny of the Namaqua-Natal Mobile Belt (NNMB) when colliding with the Kaapvaal Craton around 1.1 Ga (***Figure 5.14.64***). The Namaqua-Natal metamorphic province stabilised and behaved like a craton, and now forms the basement to the Karoo Supergroup and the Cape Orogen. This metamorphic province composes the NNMB, which is draped along the western and southern margin of the Kaapvaal Craton. Tectonism in the KAR is recorded by widespread dykes and volcanic intrusions. Major structures that are exposed show brittle deformation. According to Chevallier & Woodford (***Reference 5.14.205***), in the northwest part of the KAR is an inferred failed transform fault or rift with a dextral sense of shear. Within this 800 km long east-west-trending right-lateral shear corridor, there are north-northwest-striking dolerite dykes that have been displaced because of the movement along the shear corridor. Beside a few short faults along the east coast of South Africa and the dolerite intrusions, the KAR is almost devoid of known brittle deformation.

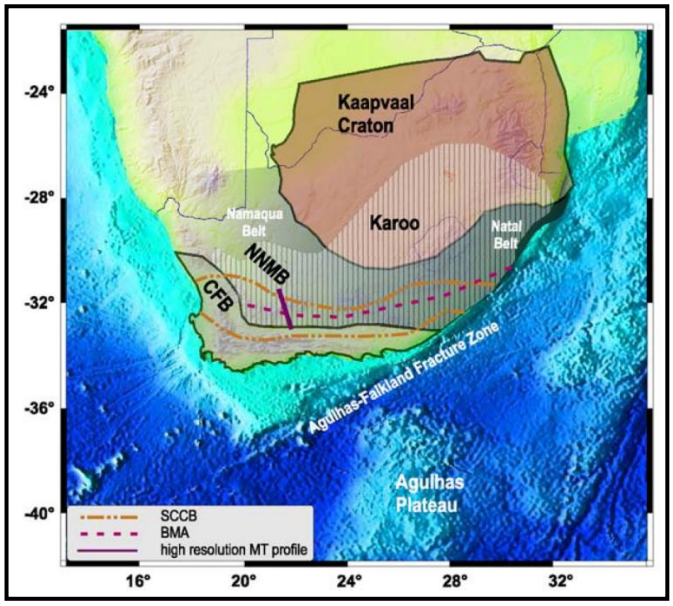


Figure 5.14-64 Positions of the Kaapvaal Craton and the Namaqua-Natal Mobile Belt (NNMB). The Southern Cape Conductive Belt (SCCB) and the

Beattie Magnetic Anomaly (BMA) Are Also Shown.

The vertical hatches show the extent of the Karoo Basin (Reference 5.14.206).

Based on the evaluation of the geological and seismological databases (***Subsections 5.14.4.3*** and ***5.14.4.4***), the SSC TI Team developed the logic-tree shown in ***Figure 5.14.65***, the technical bases of which are summarised below alongside those for the modelling of source-specific future earthquake characteristics modelled as aleatory distributions. Full details of the technical justifications can be found in Section 8.3.3 of ***Reference 5.14.17***.

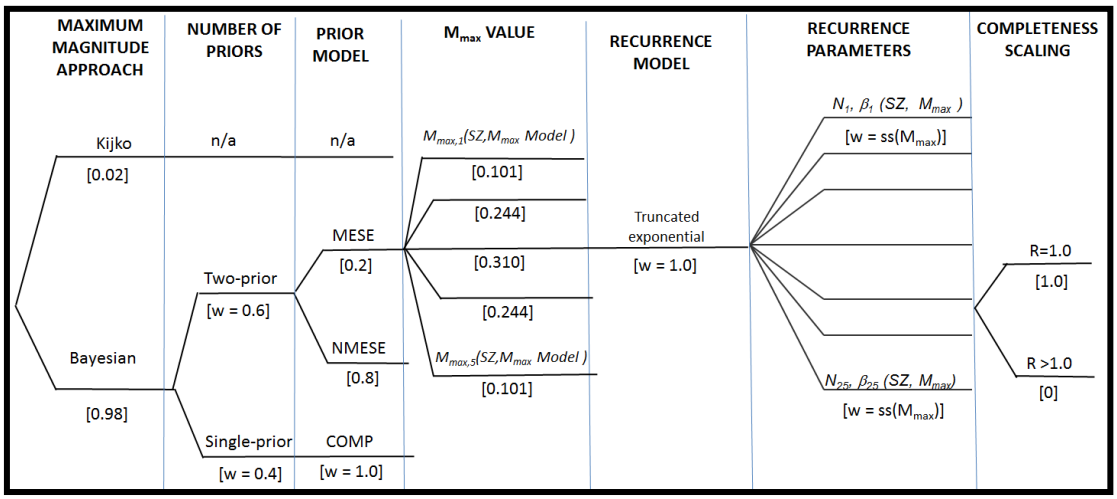


Figure 5.14-65 Logic Tree Summarising the Epistemic Uncertainties in the Characterisation of the KAR Source Zone.

Epistemic uncertainties that are common to multiple source zones such as seismogenic thickness are discussed in Subsection 5.14.5.4.(c).

As discussed in ***Subsection 5.14.5.4.(d) i***, the southern boundary of the KAR, which separates it from the ECC host zone, is placed at the northernmost margin of crustal extension to the north of the Ceres-Kango-Baviaanskloof-Coega fault system (***Subsection 5.13.5.1.(d) iv***). The north-western boundary of the KAR, the Williston magnetic anomaly (***Figure 5.14.66***), separates the magnetically neutral crust of the Saldanian belt from the Namaqua crust, which is typified by small but randomly oriented anomalies (***Reference 5.14.207***). In the eastern part of the zone, the Doringberg-Hartbees fault zone (see ***Figure 5.14.68***) is truncated by the Williston magnetic anomaly. The eastern

section of the northern boundary of the KAR follows the margin of the Kaapvaal Craton, also delineating a contrast in the level of seismicity. The eastern boundary is parallel and in line with the northeast-southwest-trending strike-slip Agulhas-Falkland Fracture Zone (AFFZ***; Subsection 5.13.5.5.(a) iv***). The western boundary of the KAR corresponds to the limit of the Mesozoic (Cretaceous) extension of the west coast of South Africa from Springbok to Port Nolloth (***Reference 5.14.208***). The western boundary is also where the Williston and Beattie magnetic anomalies are truncated by the magnetically neutral crust of the Saldanian province (***Reference 5.14.207***). Mapped structures within the KAR do not appear to extend into adjacent zones, thus the boundaries of the KAR are interpreted to be strict.

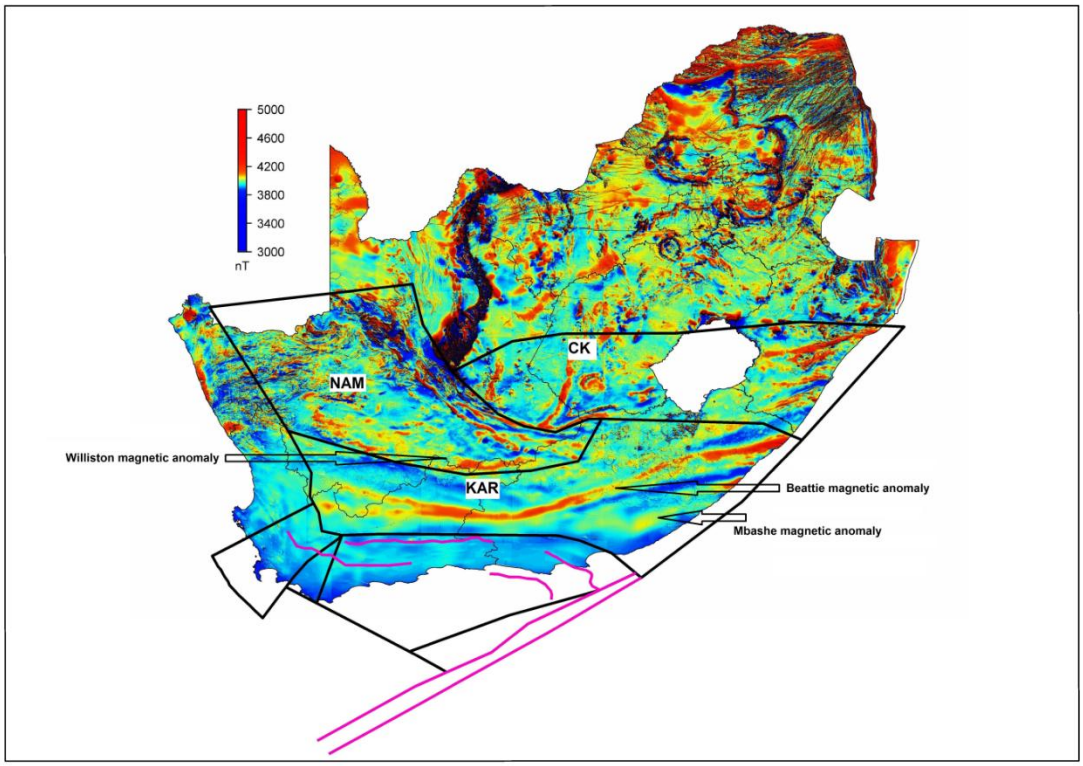


Figure 5.14-66 The Beattie Set of Magnetic anomalies in the KAR Source Zone Shown on the Magnetic Map of South Africa (*Subsection 5.13.5.1.(d) ii*). The Source Zones and Fault Sources developed in the Thyspunt PSHA SSC Model are also shown.

The major structure inferred as a failed rift that was identified by Chevallier and Woodford (***Reference 5.14.205***) in the west of KAR zone shows right-lateral strike-slip sense of shear. Two earthquakes with focal mechanisms lie within the KAR (***Table T-5.13.4***) and have strike-slip and normal faulting mechanisms. The style of faulting in the KAR is therefore defined by the following aleatory distribution: Strike-slip faulting (50%), normal faulting (50%).

In general, the KAR has an east-west structural grain (***Figure 5.14.67***), parallel to that of the NNMB. This is deduced from the major shear zone and the alignment of the Beattie-set magnetic anomalies within this zone. Towards the east of the KAR, the Beattie-set anomalies change strike direction and trend towards the northeast. The few short faults on the east coast are also parallel to this direction. The east-west structures in the major shear zone are exploited by Jurassic dolerite dykes. There are also north-northwest-trending dykes which may have exploited relict zones of weakness. Some dip angles and directions are difficult to assess because of the arcuate nature of some structures (specifically dykes). Chevallier & Woodford (***Reference 5.14.205***) report dips of 25° and 50° N in the Williston area. Almost vertical dips are reported in the Fraserburg sill area, south of the Northern Cape Province. Specific dips of 85°E (and 35°E) are observed in some regions (***Reference 5.14.205***).

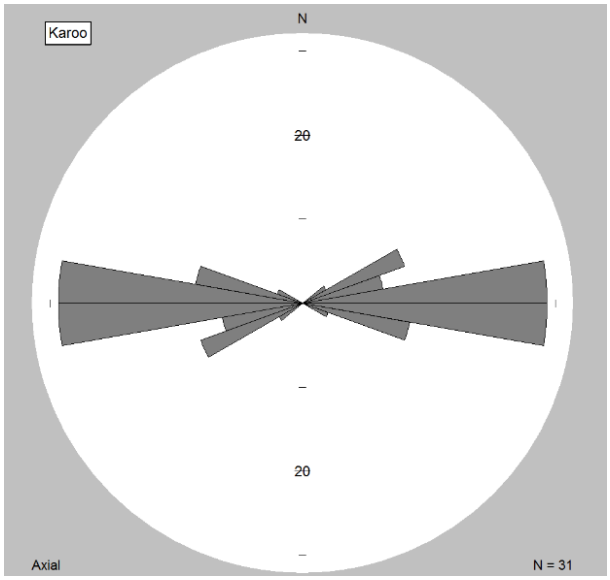


Figure 5.14-67 Rose diagram of the KAR showing the prominent east-west structural grain in the KAR zone. The diagram was developed by measuring the average orientation of structural trends within the KAR.

Given the interpretation by the SSC TI Team of the orientation of structures and structural trends inferred from geophysical data, the strike of future earthquake ruptures within the KAR is modelled as an aleatory distribution having the following azimuths and percentages: 30°(15%), 70°(20%), 90°(30%), 110°(20%), 160° (15%). Due to the distance of the KAR source to the site and the resulting insensitivity to site hazard, the dip of future earthquake ruptures is assumed to be vertical in the hazard analysis.

The Mmax value for the KAR was assessed using the seismicity catalogue (***Subsection 5.14.4.4***) and the approaches described in ***Subsection 5.14.5.4.(c) ix***. This requires the assessment of source-specific weights for the MESE and NMESE priors. Strong geologic evidence of extensional tectonics, such as the development of large basins and associated major faulting, is absent in the KAR. The southern boundary of this zone serves as the limit of clearly extended crust south of the zone within the ECC. Apart from the few faults along the east coast of South Africa north of East London, there are very few mapped faults or other structures mapped either at the surface or interpreted in the subsurface. However, despite the lack of strong structural evidence for extension, the presence of the Jurassic dykes does provide weak evidence for Mesozoic extension (MESE) in the KAR. Hence, on the two-priors branch of the logic tree, a weight of [0.2] is assigned to MESE and [0.8] for non-Mesozoic extended crust (NMESE). The largest observed earthquakes in the KAR were two earthquakes of about the same size that occurred on 21 May 1850 and 09 August 1932. These are situated north of Butterworth and in Grahamstown with magnitudes M_w 5.7 ± 0.4 and 5.7 ± 0.35, respectively. Using the weighting scheme discussed in ***Subsection 5.14.5.4.(c) ix***, a weight of [0.02] was assessed for the Kijko approach. Combining the Mmax distributions from the various approaches considered resulted in the Mmax distribution shown in ***Figure 5.14.53***. The recurrence curves developed using this Mmax distribution and the approach discussed in ***Subsection 5.14.5.4.(c) vii*** are shown in ***Figure 5.14.55***. Given the onshore location of this source, no completeness correction was deemed necessary.

iv Cedarville-Koffiefontein Source Zone (CK)

The Cedarville-Koffiefontein Source Zone (CK) is situated in the southern portion of the Kaapvaal Craton, also covering a portion of the NNMB in the KwaZulu-Natal Province. The southern margin of the Kaapvaal Craton extends across Lesotho and is marked by the Doringberg-Hartbees fault zone (***Figure 5.14.68***). Much of the fault zone is covered by the Karoo Supergroup and its associated volcanic rocks and is therefore interpreted from geophysical maps. The Natal Group which was deposited in the Natal Trough representing

a graben parallel to the coast of KwaZulu-Natal (***Reference 5.14.209***) is also present in the CK.

The identification of the CK source was based on the criteria for defining seismic sources summarised in ***Subsection 5.14.5.4.(a) i***. The CK source is defined by differences in levels of seismicity with its neighbours, differences in the Mmax prior distribution, and differences in the assessed orientation of future ruptures.

When combined with the NAM zone (***Subsection 5.14.5.4.(d) v***), the CK zone corresponds to the Cedarville/Koffiefontein/O'Kiep zone in the seismotectonic model by Partridge (***Reference 5.14.204***). Although the boundaries are somewhat different, the CK is also analogous to the Free State/Lesotho/Natal zone in the model by Du Plessis (***Reference 5.14.202***), and the Cedarville/Ulwandle zone in the model of Hartnady (***Reference 5.14.203***).

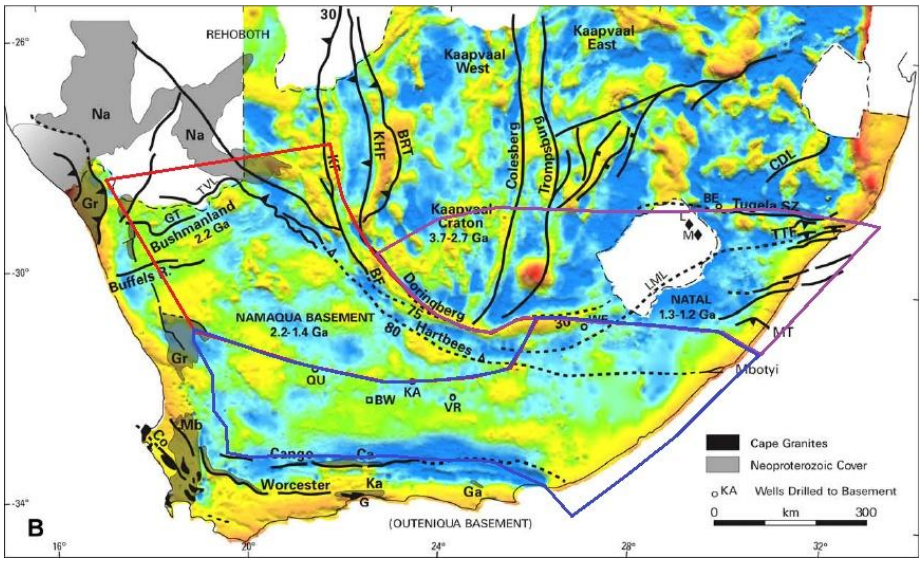


Figure 5.14-68 Doringberg-Hartbees Fault Zone, Marks the Western and Southern Margin of the Kaapvaal Craton and the Southwestern Boundary of the CK Source Zone.

Other faults on the Kaapvaal Craton such at the Brakbos (BF), Colesberg, and Trompsburg Faults are shown. The three source zones polygons; NAM (red), CK (purple), and KAR (blue) are superimposed on this gravity map (Reference 5.14.210).

A detailed description of the major structures and geological history of the CK is given in Section 8.3.4 of ***Reference 5.14.17***). Apart from the southern margin of the Kaapvaal Craton that runs through Lesotho, which is believed to be the position along which the NNMB obliquely collided with the craton at 1.1 Ga (***Reference 5.14.211***), the CK is host to several faults, thrusts and lineaments. This part of the Natal sector of the NNMB accommodates 3 discontinuous tectonostratigraphic domains; the Tugela, Mzumbe and Margate terranes, which are part of a juvenile orogen (***Reference 5.14.212***). In the eastern part of the CK, the southern edge of the Kaapvaal Craton is marked by the Lilani-Matigulu lineament, which represents the leading edge of the imbricated Tugela terrane and also marks the division between the Tugela and the Mzumbe terranes. Several episodes along northeast to east-northeast-trending left-lateral transcurrent shear zones significantly deformed the Mzumbe and Margate terranes. In the Tugela terrane, which rests on the Kibaran Natal belt, at least three episodes of deformation occurred and resulted in the obliteration of primary structures by subsequent deformation to high grade metamorphism within folds, faults, and shear zones (***Reference 5.14.213***).

Based on the evaluation of the geological and seismological databases (***Subsections 5.14.4.3*** and ***5.14.4.4***), the SSC TI Team developed the logic-tree shown in ***Figure 5.14.69***, the technical bases of which are summarised below, alongside those for the modelling of source-specific future earthquake characteristics modelled as aleatory distributions. Full details of the technical justifications can be found in Section 8.3.4 of ***Reference 5.14.17***.

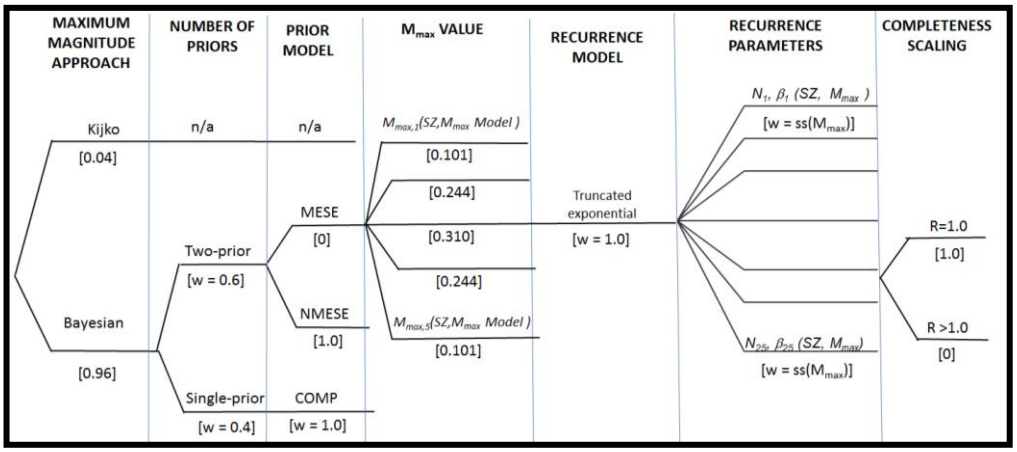


Figure 5.14-69 Logic Tree Summarising the Epistemic Uncertainties in the Characterisation of the CK Source Zone.

Epistemic uncertainties that are common to multiple source zones such as seismogenic thickness are discussed in Subsection 5.14.5.4.(c).

The northern boundary of the CK in the west is placed along the east-northeast-trending Tugela shear zone. In the western part of the CK, the northern boundary is defined by a contrast in the level of seismicity, as well as by differences in crustal thickness between the southern and northern Kaapvaal Craton (***Reference 5.14.214***). The eastern boundary is placed along the AFFZ (***Subsection 5.13.5.1(d) iv***), which represents the boundary between crustal and oceanic crust. The southern boundary of the CK is situated south of Lesotho and divides regions of elevated seismicity in the CK from low seismicity regions in the KAR. In the east, this boundary also marks the southern extent of thrusts and shear zones on the Natal sector of the NNMB. The western boundary rests on the Doringberg-Hartbees fault zone (***Figure 5.14.68***), which is a major zone that dips at high angles of 75 to 85° and offsets the Moho by approximately 16 km (***References 5.14.23*** and ***5.14.210***). This fault zone also separates the thin old Kaapvaal Craton from the younger thick Namaqua crust (***Reference 5.14.210***). The Colesberg and Trompsburg Faults are terminated at the Doringberg-Hartbees fault zone (***Figure 5.14.68***).

The Colesberg and Trompsburg Faults incise both the northern and southern boundary, and the southern boundary is furthermore cut by one of the Margate terrane shear zones, therefore the boundaries of the CK are assessed to be leaky.

The assessment of the future style of faulting within the CK comes primarily from earthquake focal mechanisms (***Table T-5.13.4***), which suggest a mixture of both strike-slip and normal faulting. In the eastern part of the CK, east-west and east-northeast left-lateral strike-slip faults (transcurrent shear zones) are observed, and these may be seismogenic faults. Based on the available evidence, the following aleatory percentages for the style of faulting are the following: strike-slip (50%), normal (50%).

Prominent strike directions in the CK are east-west and east-northeast (***Figure 5.14.70***). This is especially noted in the eastern part of the zone where the Natal sector of the NNMB is host to three tectonostratigraphic domains. A large number of faults and shear zones dip at steep angles. A few normal faults are identified that trend to the northeast and east-west to west-northwest with moderate to steep dips reported (***Reference 5.14.215***). The steep Colesberg and Trompsburg Faults west of the CK have a north-northeast strike. The Doringberg-Hartbees fault zone defining the western boundary of the CK (***Reference 5.14.210***) trends to the northwest. Given the range of geometries of structures and structural trends that have been documented in the CK, the strike of future earthquake ruptures is modelled by the following aleatory distribution of azimuths and percentages: 45° (30%), 65° (35%), 85° (25%), 155° (10%).

© Eskom 2026/Rev 0a

The Mmax value for the CK zone was assessed using the seismicity catalogue (***Subsection 5.14.4.4***) and the approaches described in ***Subsection 5.14.5.4.(c) ix***. This requires the assessment of source-specific weights for the MESE and NMESE priors. Thomas *et al.* (***Reference 5.14.212***) reported Mesoproterozoic intrusions that tectonically affected the Mzumbe and Margate terrains in the eastern part of the CK. According to De Wit & Tinker (***Reference 5.14.216***), the Colesberg-Trompsburg fault zone is a Neoarchaean palaeosuture. The CK is also host to a significant number of Karoo dykes and basalts belonging to the Drakensberg Group capping the Karoo Supergroup. These intrusions are Jurassic in age (***Reference 5.14.217***). However, this is insufficient evidence to conclude that either Kaapvaal or Natal crusts, which are stable parts of South Africa have undergone Mesozoic and younger extension. For this reason, a weight of [1.0] is given to the NMESE nature of this seismic source zone on the two-prior branch.

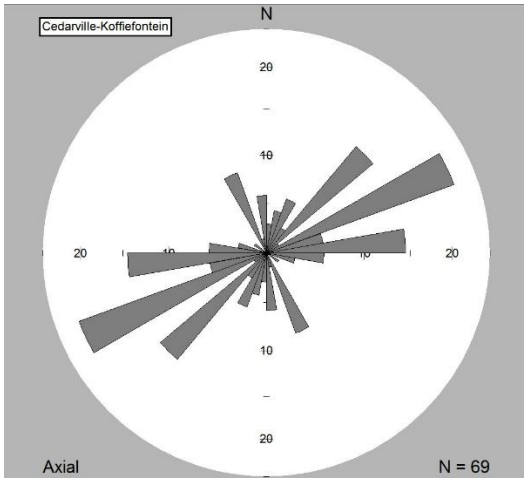


Figure 5.14-70 Rose Diagram Showing the Orientation of Major Structures and Structural Trends Within the CK Source Zone.

The diagram was developed by measuring the average orientation of faults and structural trends within the CK source zone

The CK shows elevated levels of seismicity (***Figure 5.14.52***) and the largest observed earthquake is the Koffiefontein event (20 February 1912) with magnitude M_w 6.2 ± 0.25 (***Figure 5.14.54***). This event occurred within the Koffiefontein cluster and is one of the largest earthquakes in any of the source

zones for the Thyspunt SSC model. Using the weighting scheme discussed in ***Subsection 5.14.5.4.(c) ix***, a weight of [0.04] was assessed for the Kijko approach. Combining the Mmax distributions from the various approaches considered resulted in the Mmax distribution shown in ***Figure 5.14.53***. The recurrence curves developed using this Mmax distribution and the approach discussed in ***Subsection 5.14.5.4.(c) vii*** are shown in ***Figure 5.14.55***. Given the onshore location of this source, no completeness correction was deemed necessary.

v Namaqua Source Zone

The Namaqua Source Zone (NAM) covers most of the Northern Province in South Africa and is underlain by rocks that form part of the Namaqua sector of the Namaqua-Natal Metamorphic Province. The zone shares boundaries with CK to the east (***Subsection 5.14.5.4.(d) iv***), and KAR (***Subsection 5.14.5.4.(d) iii***) to the south.

The identification of the NAM source was based on the criteria for defining seismic sources summarised in ***Subsection 5.14.5.4.(a) i***. The NAM source is defined by differences in levels of seismicity with its neighbours, differences in the Mmax prior distribution, and differences in the assessed orientation of future ruptures.

In the seismotectonic model by Partridge (***Reference 5.14.204***), the NAM is equivalent to part of the Cedarville/Koffiefontein/O'Kiep zone. In the models of Du Plessis (***Reference 5.14.202***) and Hartnady (***Reference 5.14.203***), the NAM is comparable to the Karoo/Namaqualand and Orange zones, respectively.

A detailed description of the major structures and geological history of the ECC is given in Section 8.3.5 of ***Reference 5.14.17***. The oldest structures in the NAM are Proterozoic in age (***Reference 5.14.208***). This zone is separated along its western margin from an area of younger Cretaceous structures adjacent to the NAM in the west coast of South Africa. The Proterozoic structures in the NAM are mostly low-angle thrusts and almost vertical shear zones (***Reference 5.14.211***). Along the eastern margin, the high-angle Doringberg-Hartbees fault zone separates the Mesoproterozoic Namaqua block from the Archaean Kaapvaal Craton (***Reference 5.14.210***) and is interpreted to be an area of crustal weakness along the Kaapvaal Craton (***Reference 5.14.218***). Along this major vertical structure, the Namaqua basement block was juxtaposed causing a displacement of the Mohorovicic discontinuity (***Reference 5.14.210***). Other major structures include the Brakbos and the Brakfontein shear zones. These are truncated at the Doringberg-Hartbees fault zone (***Reference 5.14.219***). The most recent movement along

© Eskom 2026/Rev 0a

the Doringberg-Hartbees fault alongside the margin of the Kaapvaal Craton occurred about 1.0 Ga, after the collision of the Kaapvaal Craton and the NNMB. The Transvaal-Griqualand Axis runs across the NAM in a northeast-southwest direction. This tectonic axis is related to the subsidence of the Kalahari Basin (Partridge, cited in ***Reference 5.14.220***). Slight movements along this axis led to the disruption of drainage networks and resulted in new networks (***Reference 5.14.221***). Singh *et al.* (***Reference 5.14.220***) suggested low levels of seismicity along this axis.

Based on the evaluation of the geological and seismological databases (***Subsections 5.14.4.3*** and ***5.14.4.4***), the SSC TI Team developed the logic-tree shown in ***Figure 5.14.71***, the technical bases of which are summarised below, alongside those for the modelling of source-specific future earthquake characteristics modelled as aleatory distributions. Full details of the technical justifications can be found in Section 8.3.5 of ***Reference 5.14.17***

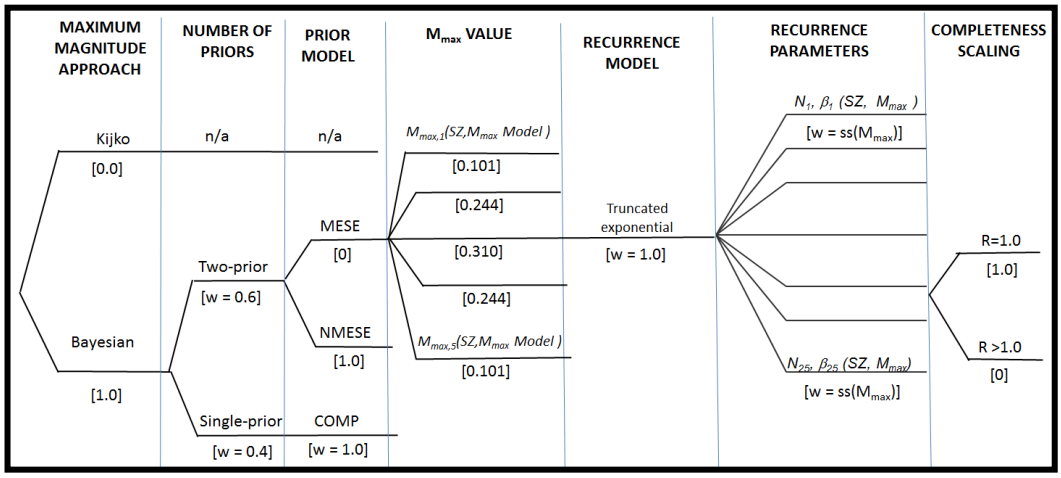


Figure 5.14-71 Logic Tree Summarising the Epistemic Uncertainties in the Characterisation of the NAM Source Zone.

Epistemic uncertainties that are common to multiple source zones such as seismogenic thickness are discussed in Subsection 5.14.5.4.(c).

The eastern boundary of the NAM is the Doringberg-Hartbees fault zone which separates the thin old Kaapvaal Craton crust from the thick and younger Namaqua crust (***Reference 5.14.210***; see discussion in ***Subsection 5.14.5.4.(d) iv*** and ***Figure 5.14.68***). Structures such as the Brakbos and Brakfontein Faults as well as the Kheis-Magondi mobile belt (west

of the Kaapvaal Craton) are terminated at the Doringberg-Hartbees Fault zone. Transcurrent shear zones close to the Kheis-Magondi orogenic belt (***Reference 5.14.212***) also terminate at the Doringberg-Hartbees Fault zone. The northern boundary follows the northern extent of seismicity in South Africa. The western boundary separates an area of structures that were reactivated in the Late-Cretaceous (***Reference 5.14.208***) close to the west coast of South Africa from a region that hosts Proterozoic structures (*e.g.*, Brakbos shear zone). The southern boundary is placed along the west-northwest-trending Williston magnetic anomaly (see discussion in ***Subsection 5.14.5.4.(d) iii*** and ***Figure 5.14.66***). Since there are no major structures or structural trends that transect the boundaries of NAM, particularly the southern and eastern boundaries closest to the site, all boundaries of the NAM are considered to be strict in the hazard calculations.

Assessment of the future style of faulting within the NAM comes primarily from earthquake focal mechanisms within the Augrabies earthquake cluster (see ***Table T-5.13.4***). The focal mechanisms show normal-oblique strike-slip motion, suggesting a mixture of both strike-slip and normal faulting. From the standpoint of the geologic history of the development of major faults, both dextral and sinistral strike-slip faulting is present in the NAM. Some of the structures such as the Brakbos shear zone were initially left-lateral and were later reactivated as dextral transcurrent shear zones (***Reference 5.14.212***). The Doringberg-Hartbees fault zone was initially normal, but was alter reactivated as strike-slip (***Reference 5.14.210***). Based on this evidence, the SSC TI Team assessed the following aleatory distribution for the style of faulting in the NAM: strike-slip (50%), normal (50%).

In general, major right- and left-lateral faults and thrusts in the NAM trend in the northwest-southeast direction (***Figure 5.14.72***). Minor faults strike in the northeast-southwest direction. The Brakbos shear zone and Brakfontein Fault (at the margin of the Kaapvaal Craton) in the NAM strike in the northwest-southeast direction and swing towards the east following the margin of the Kaapvaal Craton. Given the geometries of structures and structural trends that have been documented in the NAM, the strike of future earthquake ruptures is modelled by the following aleatory distribution of azimuths and percentages: 35°(10%), 85°(25%), 135°(55%), 175°(10%).

© Eskom 2026/Rev 0a

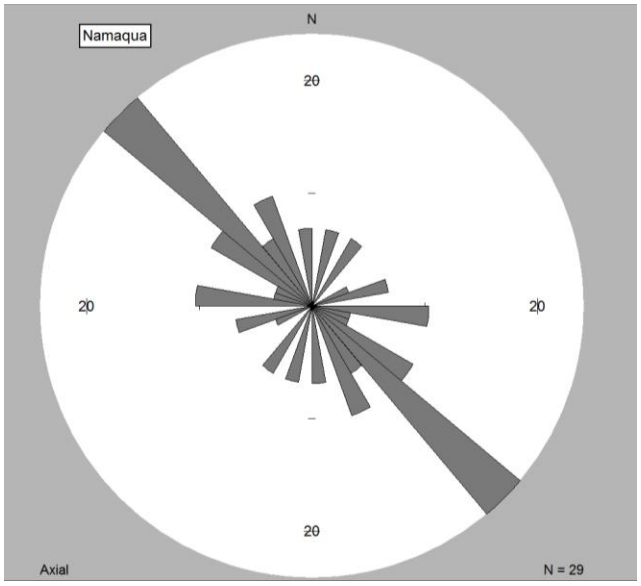


Figure 5.14-72 Rose Diagram Showing the Orientation of Major Structures and Structural Trends within the NAM Source Zone.

The diagram was developed by measuring the average orientation of faults and structural trends within the NAM.

The Mmax value for the NAM zone was assessed using the seismicity catalogue (***Subsection 5.14.4.4***) and the approaches described in ***Subsection 5.14.5.4.(c) ix***. This requires the assessment of source-specific weights for the MESE and NMESE priors. Geologic structures in the NAM differ from the Late Cretaceous Faults adjacent to the zone along the west coast of the Northern Cape Province of South Africa, which show Cenozoic extension (***Reference 5.14.208***). Structures in the north-eastern part of NAM are all Precambrian and as old as the Proterozoic. No structures are exposed in the southern part of the NAM due to the concealment of the Namaqua crust by the younger Karoo Sequence, but the interpretations of geophysical data do not suggest major basins or other evidence of continental-scale extension. In summary, there is no evidence of Mesozoic or younger extension in the NAM; therefore, the NMESE prior distribution is given a weight of [1.0]. The two largest observed earthquakes in the NAM both have magnitude M_W 5.0 ± 0.4. The 11 February 1979 event is situated southwest of Kenhardt and the 15 September 1996 event in north of Loeriesfontein. Using the weighting scheme discussed in ***Subsection 5.14.5.4.(c) ix***, a weight of zero was assessed for the Kijko approach (*i.e.*, there is insufficient data for this method to give stable

© Eskom 2026/Rev 0a

results). Combining the Mmax distributions from the various approaches considered resulted in the Mmax distribution shown in ***Figure 5.14.53***. The recurrence curves developed using this Mmax distribution and the approach discussed in ***Subsection 5.14.5.4.(c) vii*** are shown in ***Figure 5.14.55***. Given the onshore location of this source, no completeness correction was deemed necessary.

e) Fault Sources

This section summarises the characteristics of fault sources identified for the SSC model. Using the criteria discussed in ***Subsection 5.14.5.4.(a) i*** for defining seismic sources and for evaluating their seismogenic probability, five fault sources are identified, as shown in ***Figure 5.14.73***.

The faults characterised here are those assessed to have a seismogenic probability that is greater than zero. Those faults that were evaluated as potential fault sources and that were assessed to have a seismogenic probability equal to zero are discussed in ***Subsection 5.14.5.4.(f)***.

Global assessments that relate to multiple seismic sources (*e.g.*, seismogenic crustal thickness) are discussed above in ***Subsection 5.14.5.4.(c)***. In ***Subsections 5.14.5.4.(e) i*** through ***5.14.5.4.(e) v***, each of the fault sources that are part of the SSC model is described along with a summary of its characteristics. The discussion includes the technical bases that support the assessments included in the model as well as the uncertainties given in the source logic trees. ***Table T-5.14.7*** summarises the source zone–specific assessments that make up the SSC model. Full details of the technical justifications are given in Section 8.4 of ***Reference 5.14.17***. The recurrence curve distributions developed for the various seismic source zones using the approach described in ***Subsection 5.14.5.4.(c) viii*** are shown in ***Figure 5.14.74***.

© Eskom 2026/Rev 0a

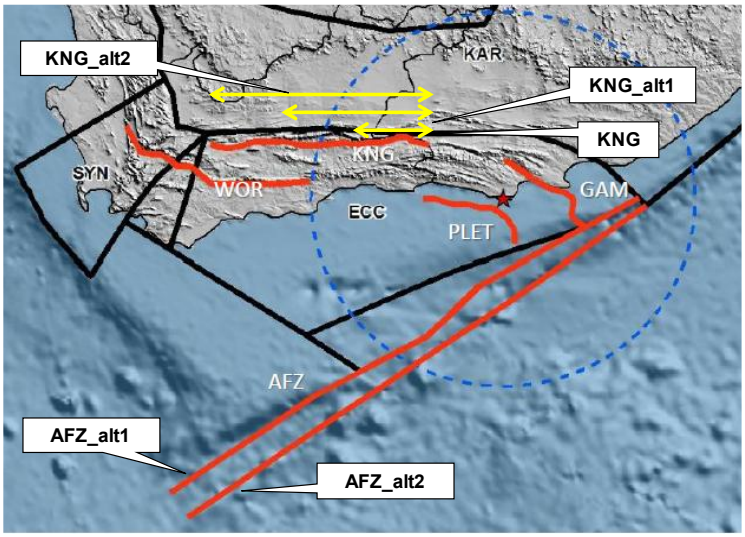


Figure 5.14-73 Overview of the Fault Sources Included in the SSC Model, With Alternative Coordinates for KNG and AFZ Highlighted.

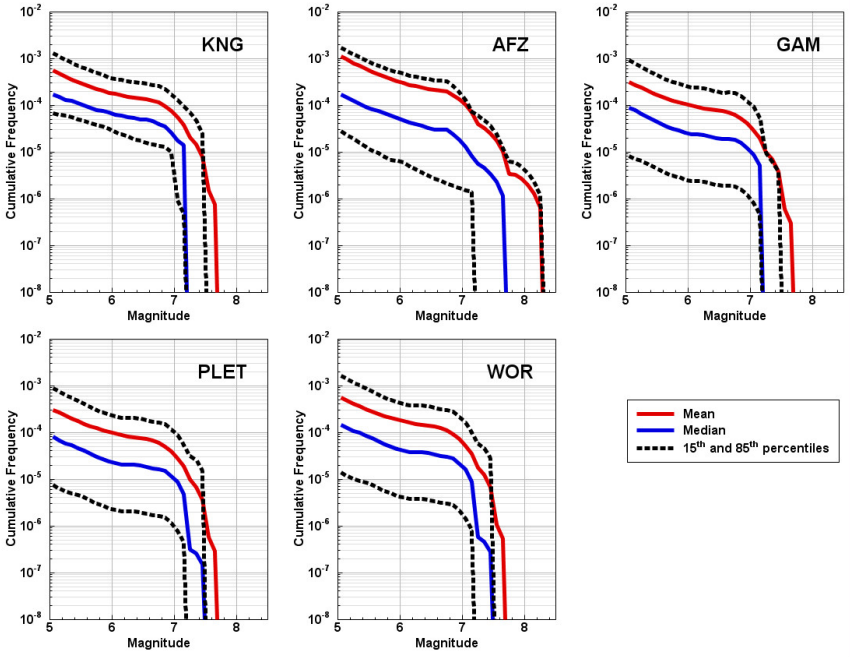


Figure 5.14-74 Summary of Earthquake Recurrence Relationships for the Fault Sources Included in the SSC Model

© Eskom 2026/Rev 0a

Table 5.14.7
Summary of Fault Source Characteristics Included in the SSC Model

	Kango	Agulhas	Gamtoos	Plettenberg	Worcester
Seismogenic probability, p[S]	[1.0][1]	[0.2]	[0.2]	[0.2]	[0.2]
Temporal clustering[2]	In cluster [0.8] Out of cluster [0.2]	Not assessed	Not assessed	Not assessed	Not assessed
Alternative Total Lengths/Mapped Location	In cluster 110 km [1.0] Out of cluster 101 km [0.4] 250 km [0.3] 313 km [0.3]	AFZ_alt1 [0.5] AFZ_alt2 [0.5]	No alternatives	No alternatives	No alternatives
Style of Faulting	Normal [1.0]	Strike-slip [1.0]	Normal [1.0]	Normal [1.0]	Normal [1.0]
Dip	South 45° [0.3] 60° [0.6] 70º [0.1]	90° [0.5] 70° [0.5] North [0.5] South [0.5]	Southwest 45° [0.3] 60° [0.6] 70º [0.1]	South 45° [0.2] 60° [0.6] 70º [0.2]	South 45° [0.2] 60° [0.6] 70º [0.2]
M_{char}	6.75 [0.1] 7 [0.4] 7.25 [0.4] 7.5 [0.1]	7 [0.3] 7.5 [0.4] 8.1 [0.3]	6.75 [0.1] 7 [0.4] 7.25 [0.4] 7.5 [0.1]	6.75 [0.1] 7 [0.4] 7.25 [0.4] 7.5 [0.1]	6.75 [0.1] 7 [0.4] 7.25 [0.4] 7.5 [0.1]
Recurrence Approach	Recurrence Intervals [0.5] Slip Rate [0.5]	Slip Rate [1.0]	Slip Rate [1.0]	Slip Rate [1.0]	Slip Rate [1.0]
Magnitude Distribution Model	Characteristic [0.8] Max moment [0.2]	Characteristic [0.8] Max moment [0.2]	Characteristic [0.8] Max moment [0.2]	Characteristic [0.8] Max moment [0.2]	Characteristic [0.8] Max moment [0.2]
Rec. Interval Rates (events/yr)	In cluster 1.67E-4 [0.2] 1.25E-4 [0.8] Out of cluster 2.00E-5 [0.2] 1.00E-5 [0.3] 3.33E-6 [0.3] 2.00E-6 [0.2]	n/a	n/a	n/a	n/a
Slip Rates	In cluster 0.1 mm/yr [0.2] 0.2 mm/yr [0.6] 0.3 mm/yr [0.2] Out of cluster 0.001 mm/yr [0.2] 0.01 mm/yr [0.4] 0.02 mm/yr [0.4]	0.005 mm/yr [0.5] 0.05 mm/yr [0.4] 0.5 mm/yr [0.1]	0.001 mm/yr [0.3] 0.01 mm/yr [0.4] 0.1 mm/yr [0.3]	0.001 mm/yr [0.3] 0.01 mm/yr [0.4] 0.1 mm/yr [0.3]	0.001 mm/yr [0.3] 0.01 mm/yr [0.4] 0.1 mm/yr [0.3]

[1] Epistemic weights are given as probabilities in [brackets].
[2] The term "in cluster" refers to the fault being within a period of higher activity; "out of cluster" refers to the fault being out of a period of higher activity

i Kango Fault Source (KNG)

The Kango Fault source (KNG) is approximately 129 km from the site at its closest approach (***Figure 5.14.73***). As discussed in ***Subsection 5.13.5.1.(d) v***, the Kango Fault is the only recognised Quaternary fault in South Africa and several detailed palaeoseismic investigations were conducted with the specific aim to develop data for the characterisation of the Kango Fault in terms of its recency of activity, sense of slip, slip rate, recurrence behaviour, and magnitude. Based on these investigations, the logic-tree shown in ***Figure 5.14.75*** was developed by the SSC TI Team.

The first node of the logic tree addresses the probability that the KNG is seismogenic in the contemporary tectonic environment. Since the geological investigations summarised in ***Subsection 5.13.5.1.(d) v*** found clear evidence of late Pleistocene and Holocene activity on this fault, KNG was judged to be seismogenic with a weight of [1.0]. However, it was noted that there is uncertainty regarding the extent of the reactivation and the segmentation of the fault, with evidence for reactivation being confined to the eastern part of the fault (see ***Subsection 5.13.5.1.(d) v*** for details). This uncertainty was addressed by considering three alternative lengths of 101, 250 and 313 km for KNG (***Figure 5.14.76***). The estimate of the length of the fault is influenced by the issue of temporal clustering of earthquakes in the present tectonic stress regime.

As noted in ***Subsection 5.13.5.1.(d) v***, the Kango Fault lies within a seismically quiescent region of South Africa, but has evidence for three latest Pleistocene to Holocene surface-faulting events preceded by a long period of several tens of thousands of years of no activity (***Reference 5.14.222***), indicating that the Kango Fault may be within a period of higher activity. Low cumulative neotectonic displacement on the reactivated Kango Fault also suggests that the recent rate of activity is not typical of the long-term behaviour of the fault. This pattern of behaviour is typical of the long-term behaviour of recognised active faults in other stable continental regions (***References 5.14.166, 5.14.223 and 5.14.224***). Based on these geologic and geomorphic lines of evidence, which are described in detail in ***Reference 5.14.222***, the relatively high rate of late Pleistocene to Holocene activity along the reactivated Kango Fault is not interpreted to be a long-lived phenomenon. There is no evidence, however, to suggest that the Kango Fault is out of a period of activity (temporal cluster). Based on empirical observations of the number of events in clustered sequences elsewhere (***Reference 5.14.166***) and on the palaeoseismic record for the Kango Fault, a weight of [0.8] was given for the 'in-a-period-of-higher-activity' branch of the logic tree for the KNG, and a weight of [0.2] for the 'out-of-a-period-of-higher-activity' branch (***Figure 5.14.75***).

© Eskom 2026/Rev 0a

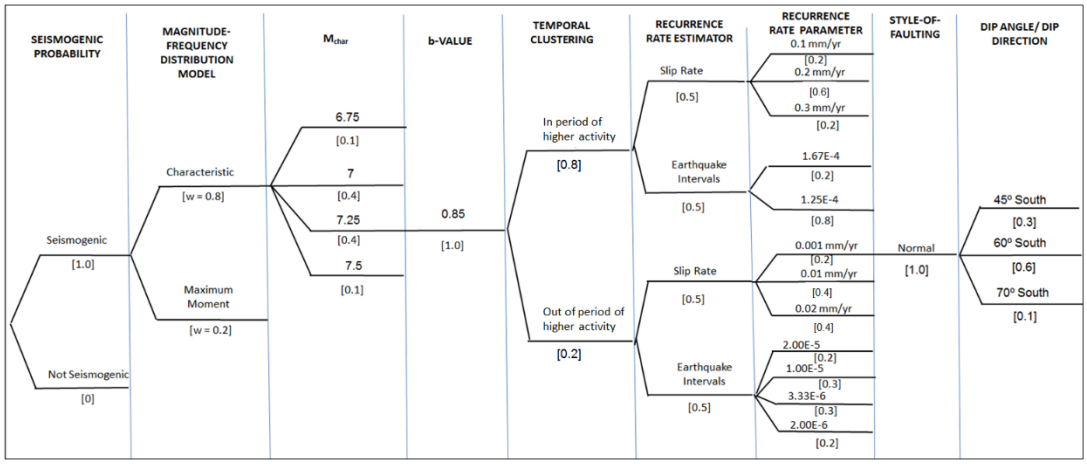


Figure 5.14-75 Logic Tree for the Kango Fault Source (KNG), Including the Source-Specific Epistemic Uncertainties.

Epistemic uncertainties that are common to multiple fault sources are the magnitude-frequency distribution model and the b-value, discussed in Subsection 5.14.5.4.(c)

.

The absence of evidence for recent surface faulting therefore does not preclude the possibility that the western part of the fault is seismogenic. Consequently, the alternative lengths of 101, 250 and 313 km are assigned weights of [0.4], [0.3] and [0.3], respectively on the 'out-of-a-period-of-higher-activity' branch, allowing the active segment to rupture farther to the west. On the 'in-a-period-of-higher-activity' branch, the activity is assumed to be confined to the eastern part of the fault, so the 101 km length is given a weight of [1.0] and the other alternatives are not considered.

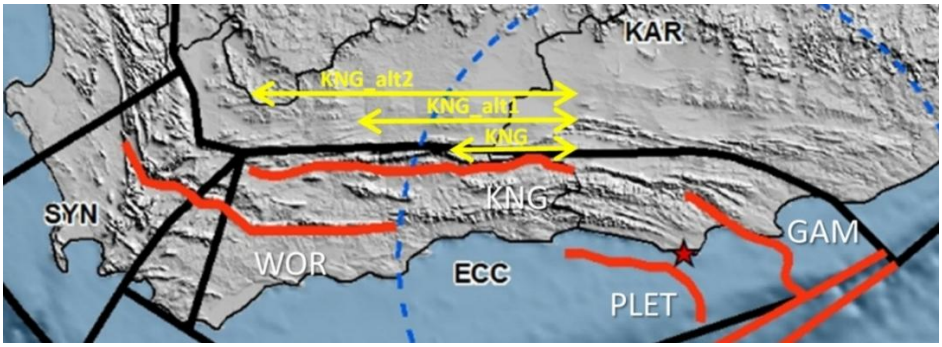


Figure 5.14-76 Map Showing Three Alternative Lengths for the KNG.

Dashed blue line represents a distance of 320 km from the site, which is indicated by the red star.

The style of faulting assigned to the KNG is normal, with a weight of [1.0]. Goedhart (***Reference 5.14.184***) notes that the simple geometry of the recent fault scarp across the region suggests surface rupture by dominantly normal slip. The attitude of the faults exposed in the trench excavations and the lack of indicators of strike-slip (***References 5.14.185 and 5.14.222***) also indicate down-to-the-south normal faulting during the two most recent surface ruptures. Based on a desk study of aerial photos, Goedhart (***Reference 5.14.181***) considered the en-echelon arrangement of scarps at the M1.130 site to indicate left-lateral shear. However, both eastern and western margins of the silcrete cap on high pediment gravels (Tg) demonstrate equal amounts of dip-slip, and not a strike-slip offset (***Reference 5.14.184***). Hill (***Reference 5.14.225***) also concluded that because of the restricted occurrence of the en-echelon scarps, an alternative explanation may be that the incoherent and inhomogeneous cover material may be responsible for differential transmission of youngest fault to the surface.

The limited data available to assess the downdip geometry of the KNG (see ***Subsection 5.13.5.1.(d) v***) indicates that the global default distribution assigned for normal faulting ***(Subsection 5.14.5.4.(c) v***) is used to capture the range of dip values; the weights are slightly modified for the KNG to give more weight to the lowest dip, based on observations described in ***Subsection 5.13.5.1.(d) v***. The uncertainty in fault dip on the KNG is defined by the following epistemic alternatives: 45° [0.3], 60° [0.6], and 70° [0.1]. The direction of the fault dip is to the south.

As discussed in ***Subsection 5.14.5.4.(c) x***, the data from palaeoseismic investigations along the Kango Fault pertaining to possible rupture segments, rupture areas, and displacements per event are used to estimate the magnitude of prehistoric surface ruptures along the reactivated Kango Fault (***Reference 5.14.222***). These data suggest that the expected M_{char} earthquake on the reactivated Kango Fault ranges from a minimum of approximately M_w 6.6 to a maximum of M_w 7.6; values in the range of M_w 7.0 to M_w 7.4, based on rupture areas defined by seismogenic depths of 15–17 km and average displacement-per-event data, are preferred estimates.

The temporal clustering behaviour also influences the recurrence behaviour of the fault, with the ‘out-of-a-period-of-higher-activity’ branch model leading to lower seismic activity rates than the ‘in-a-period-of-higher-activity’ branch. Two approaches are used to estimate recurrence for the KNG, using the results of the geological investigations discussed in ***Subsection 5.13.5.1.(d) v***: earthquake recurrence intervals (weight [0.5]) and slip rate (weight [0.5]); see discussion of approaches in ***Subsection 5.14.5.4.(c) viii***). The recurrence data and resulting parameters for the recurrence approaches are based on the

KNG's currently being either in or out of a temporal cluster (period of higher activity).

The earthquake recurrence intervals for the characteristic magnitude (M_{char}) 'in-a-period-of-higher-activity' rate [0.8] are as follows:

- 1.67E-4 events/yr (based on two earthquakes 10–15 ka or four earthquakes 24 ± 1.4 ka) [0.2].
- 1.25E-4 events/yr (based on three earthquakes 24 ± 1.4 ka) [0.8].

For the slip rate approach [0.5], the uncertainty in the slip rate assigned for M_{char} 'in-a-period-of-higher-activity' rate is as follows:

- 0.1 mm/yr [0.2]
- 0.2 mm/yr [0.6]
- 0.3 mm/yr [0.2]

On the 'out-of-a–period-of-higher-activity' branch [0.2], the earthquake recurrence intervals for M_{char} are as follows:

- 2.00E-5 events/yr (interval of 50 kyr) [0.2]
- 1.00E-5 events/yr (interval of 100 kyr) [0.3]
- 3.33E-6 events/yr (interval of 300 kyr) [0.3]
- 2.00E-6 events/yr (interval of 500 kyr) [0.2]

Several observations were considered in estimating these intervals (see ***Figure 5.13.76*** for locations of the sites). On the western end of the fault, the minimum interval between time of the PE event and age of oldest deposits at the M1.26 site (~64–76 kyr) and the M1.42 site (~53 and 100–113 kyr) suggests long intervals of at least 50 kyr to perhaps over 100 kyr. At the eastern end of the fault, an assumed average recurrence interval based on an estimated four to six palaeoearthquakes (cumulative vertical separation of 6.5–8.5 m; average displacement of 1.5 m) in the past approximately 370 kyr (CN exposure age) gives a range of possible intervals:

- 370 kyr/4 = 92.5 kyr
- 370 kyr/5 = 74 kyr

© Eskom 2026/Rev 0a

- 370kyr/6 = 62 kyr
- 370kyr/7 = 53 kyr (assumes an additional earthquake will occur in the near future to close the interval)

At the M1.42 site, if the long-term cumulative offset of 26–30 m in 2–3 Ma occurred in temporal clusters of 2–4 events with average displacement per event of 1–1.5 m, the cumulative displacement during clusters would be approximately 2–6 m. Based on these assumptions, there may have been 5–15 clusters with an average interval between 125 kyr (2 Ma/16 clusters, including an open interval) and 600 kyr (3 Ma/5 clusters). A long interval of up to 500 kyr is consistent with this observation and with recurrence assessments for analogue faults in other stable continental regions (*e.g.*, the Meers and Criner Faults in the United States, discussed ***Reference 5.14.69***; Australian faults as discussed in ***Reference 5.14.222***).

Using the slip rate approach [0.5] for the 'out-of-a-period-of-higher-activity' branch, the uncertainty in the slip rate assigned for KNG is as follows:

- 0.001 mm/yr [0.2]
- 0.01 mm/yr [0.4]
- 0.02 mm/yr [0.4]

This distribution reflects the long-term slip rate for the western part of the reactivated segment (0.008 mm/yr to 0.018 mm/yr) based on data from the M1.42 site, and the more uncertain long-term slip rate for the eastern part, which ranges from as little as 0.0007–0.001 mm/yr to 0.012–0.025 mm/yr (***Reference 5.14.222***).

Incorporating all of the recurrence-related epistemic uncertainties shown in the logic tree and using the fault-specific recurrence models discussed in ***Subsection 5.14.5.4.(c) viii***, earthquake recurrence relationships were developed for the Kango Fault, as shown in ***Figure 5.13.74***.

ii Agulhas Fracture Zone Fault Source (AFZ)

The Agulhas Fracture Zone fault source (AFZ) is approximately 91 km from the site at its closest approach (***Figure 5.13.73***). The geological characterisation of the Agulhas Fracture Zone is summarised in ***Subsection 5.13.5.1.(d) iv***, with details provided in Section 8.4.2 of ***Reference 5.14.17***. The Agulhas Fracture Zone is part of the Agulhas-Falkland fracture zone, an approximately 1 200 km long transform fault extending across the southern Atlantic, and forms the

boundary between continental and oceanic crust along southern Africa. The logic-tree developed for the AFZ source is shown in ***Figure 5.13.77***.

As discussed in ***Subsection 5.13.5.1.(d) iv***, evidence for possible neotectonic reactivation of the Agulhas Fracture Zone coming from seismic profiles and evidence of recent volcanism is not conclusive, and several observations suggest that there is little or no compelling evidence for neotectonic reactivation. Based on these observations, the AFZ is assigned a low probability of being seismogenic, p[S] of [0.2]. The strongest evidence of neotectonic reactivation is the interpretation of post–early Pliocene faulting on seismic reflection line AWI-20050101 by Parsiegla *et al.* (***Reference 5.14.226***) and Uenzelmann-Neben & Huhn (***Reference 5.14.227***). However, the largest apparent vertical offsets (up to 600 m) of the early Pliocene marker horizon across an individual fault trace imply a rate of vertical displacement that does not appear to be consistent with onshore Pliocene to Quaternary uplift rates.

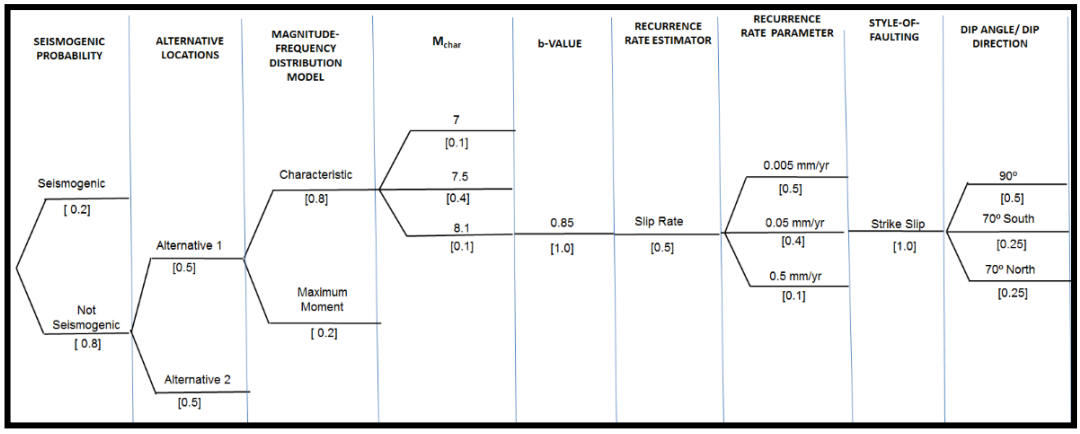


Figure 5.14-77 Logic Tree for the AFZ Fault Source, Including the Source-Specific Epistemic Uncertainties.

Epistemic uncertainties that are common to multiple fault sources are the magnitude-frequency distribution model and the b-value, discussed in Subsection 5.14.5.4.(c)

Two alternative locations (***Figure 5.14.73***) are included in the model with equal weight of [0.5] each, based on a review of existing interpretations (see ***Subsection 5.13.5.1.(d) iv***, in particular ***Figure 5.13.70*** for the location of the segments discussed below). The northern option (AFZ_alt1), with a total length of 756 km, is defined by the locations of the northernmost faults within the zone as interpreted by Uenzelmann-Neben & Huhn (***Reference 5.14.227***) and Parsiegla *et al.* (***Reference 5.14.226***) in the regional seismic reflection lines AWI-20050101 and AWI-20050201 (***Figures F-5.13.72*** and ***F-5.13.73***). This location roughly corresponds to the outer limit of the Diaz Ridge at the upper

part of the continental slope near the shelf break. The southern option (AFZ_alt2), with a similar total length of 753 km, coincides with the general location of the Mallory Trough and Diaz Ridge segments of the Agulhas Fracture Zone transform as shown by Ben-Avraham *et al.* (***Reference 5.14.228***). This location at the base of the continental slope coincides with the northern edge of prominent magnetic anomalies inferred to represent oceanic crust.

The north-eastern ends of the both AFZ_alt1 and AFZ_alt2 generally coincide with the north-eastern limit of Mesozoic rift basins. This location is generally consistent with the mapped extent of the Agulhas Fracture Zone as shown by other authors (*e.g.*, ***References 5.14.171, 5.14.226, 5.14.227 and 5.14.229***). No reported evidence of Tertiary or younger deformation is reported for the AFZ to the northeast of the Diaz Ridge segment. This and the evidence to suggest that the East London segment may have been modified during late-stage movement of the Agulhas Fracture Zone by thermal processes related to the spreading centre near the eastern boundary of the Diaz Ridge segment (***Reference 5.14.228***) are the basis for truncating the possible AFZ fault source at this location. The south-western ends of both AFZ_alt1 and AFZ_alt2 coincide with the western limit of the Mallory Trough segment as defined by Ben-Avraham *et al.* (***Reference 5.14.228***); this location generally marks the western margin of the Agulhas Arch (***Figure 5.13.70***).

As discussed in ***Subsection 5.14.5.4.(c)***, the continental crust that is adjacent to the AFZ is attenuated, and is significantly thinner than the crust to the north. This is expected to also be reflected in a thinner seismogenic crust at the location of the AFZ. Therefore, smaller values of the seismogenic crustal thickness are assumed for this source, compared to those assumed for the other sources (see ***Subsection 5.14.5.4.(c)*** for details).

The Agulhas Fracture Zone originated as a high-angle strike-slip fault and is favourably oriented within the modern stress regime (***Figure 5.13.27***) to be reactivated as a strike-slip fault. McMillan *et al.* (***Reference 5.14.230***) cite evidence for strike-slip motion in the Outeniqua Basin near the Agulhas Fracture Zone. Faults within the Agulhas Fracture Zone have steep to near-vertical dips; some faults within the zone dip approximately 70°, based on seismic profile data (***References 5.14.226 and 5.14.227***; ***Figures F-5.13.72*** and ***F-5.13.73***). North- and south-dipping geometries are equally weighted with a weight of [0.25] each, and a dip of 90° is given a weight of [0.5]. Given these steep dips, it is assumed that the fault, if reactivated, would exhibit strike-slip behaviour with a possible minor component of oblique slip.

The M_{char} magnitude distribution for the AFZ is defined based on analogy to historical earthquakes that have occurred on other large transforms and

© Eskom 2026/Rev 0a

fracture zones. The largest such events observed worldwide included the following:

- M_w 8.6 2012 Sumatra earthquake (***References 5.14.231 and 5.14.232***)
- M_w 8.1 2004 Tasman Sea earthquake (***Reference 5.14.233***)
- M_w 8.1 1946 Queen Charlotte Island (***References 5.14.234 and 5.14.235***)
- M_w 8.0 1942 Southwest Indian Ridge (***Reference 5.14.236***)

The largest of these, the M_w 8.6 Sumatra earthquake was likely related to nearby deformation along the Sunda trench. Although generally considered intraplate, this event was associated with strongly oblique deformation, and its large magnitude has been interpreted as potentially indicative of association with a diffuse or incipient plate boundary (***References 5.14.230, 5.14.231, 5.14.237 and 5.14.238***). This case is thus not analogous to AFZ in terms of tectonic setting; therefore, the M_w 8.6 earthquake was not used as a potential analogue for the AFZ. The two postulated segments of the Agulhas Fracture Zone as defined by Ben-Avraham *et al.* (***Reference 5.14.228***) that are considered as part of the AFZ (the Mallory Trough and Diaz Ridge segments) are 350 km and 360 km in length, respectively. These lengths and related fault areas are of sufficient size to generate earthquakes of these magnitudes using empirical magnitude relationships (*i.e.*, ***References 5.14.158 and 5.14.159***).

Earthquakes on active transforms between ridges tend to be smaller. Boettcher & McGuire (***Reference 5.14.239***) conclude that, in contrast to continental strike-slip faults, slip on mid-ocean ridge transform faults is largely aseismic, and magnitudes of the largest earthquakes are small ($6 \leq M_w \leq 7.1$). Furthermore, according to Bird *et al.* (***Reference 5.14.240***), some large earthquakes near ridge transform junctures are thought to have occurred on intraplate fracture zones, rather than active ridge transform faults (*e.g.*, the M_w 7.6 2003 Central Indian Ridge earthquake, the M_w 7.2 1977 earthquake on a fracture zone 130 km west of the Bullard ridge transform fault, and the 1942 Indian Ridge earthquake near the Andrew Bain ridge transform fault in the Southwest Indian Ocean).

The M_{char} probability distribution used in this study encompasses the general range of the earthquakes discussed above. The characteristic magnitude probability distribution assigned to the AFZ is M_w 7.0 [0.3], M_w 7.5 [0.4], and M_w 8.1 [0.3].

There are no palaeoseismic data to evaluate either earthquakes per interval or recurrence intervals for the AFZ. Therefore, slip rate estimated from both

© Eskom 2026/Rev 0a

regional and fault-specific data are used to estimate the occurrence rates of earthquakes. There are few data that can be used to directly measure a slip rate for the AFZ. The AFZ lies close to the estimated poles of rotation (***Figure 5.13.25***) and, therefore, a low rate of slip along the AFZ would be expected. As noted above, the primary observation used to infer possible neotectonic activity is the faults imaged in seismic reflection line AWI-20050101 (***Figure 5.13.73***) that displace early Pliocene and younger sediments and extend to the seafloor bottom (***References 5.14.226 and 5.14.227***). The apparent maximum vertical displacement of the early Pliocene marker horizon across a single fault observed on this profile is approximately 600 m, implying a long-term average rate of vertical slip implied by this apparent vertical displacement is 600 m/~5 Ma = 0.12 mm/yr. However, this leads to vertical slip rate that is higher by over an order of magnitude than onshore rates of rock uplift over a similar time frame, inferred from low long-term rates of erosion or denudation (***References 5.14.222, 5.14.241, 5.14.242 and 5.14.243***). Relatively uniform low rates of uplift of marine terraces (consistent with the inferred rock uplift rates) inferred to be Pliocene in age along much of the southern coastal region between the Western Cape and Eastern Cape also suggest that there is not a significant vertical component of uplift along the southern margin of South Africa (***Reference 5.14.186***).

The probability distribution for slip rate assigned to the AFZ is 0.005 mm/yr [0.5], 0.05 mm/yr [0.4], and 0.5 mm/yr [0.1]. The two-order difference in the rate of slip represents the broad uncertainty in the slip rate for the AFZ in the present tectonic environment. The lowest value assumes that the rate of uplift on the AFZ is at the low end of the estimated uplift rate suggested by the cosmogenic analysis of sediment samples, and that the ratio of horizontal to vertical slip is at the low end of what would qualify as a strike-slip fault (*i.e.*, approximately H:V = 1.8:1). For a 70-degree or steeper dipping fault, a H:V ratio of approximately 1:8 or greater would suggest that the fault is a strike-slip fault (***Reference 5.14.244***). The intermediate value of 0.05 mm/yr assumes that the average rate of uplift (on the order of 4 m/Myr to 5 m/Myr) represents the vertical component of slip and that the H:V ratio is on the order of 10:1. The highest value of 0.5 mm/yr allows for the possibility that the AFZ is accommodating some of the relative motion between the Nubian and Lwandle Plates, but at a significantly lower rate than the plate boundary, which is assumed to range from approximately 0.5 mm/yr to <2.0 mm/yr and be located along alternative boundaries to the western margin of the Lwandle microplate, as presented by Stamps *et al.* (***Reference 5.14.245***), De Mets *et al.* (***Reference 5.14.246***), Argus *et al.* (***Reference 5.14.247***), Lemaux *et al.* (***Reference 5.14.248***), and Hartnady (***Reference 5.14.249***).

Incorporating all of the recurrence-related epistemic uncertainties, the earthquake recurrence curves shown in ***Figure 5.14.74*** were developed for the AFZ.

iii Gamtoos Fault Source (GAM)

The Gamtoos Fault source (GAM) is approximately 47 km from the site at its closest approach (***Figure 5.14.73***). The geological characterisation of the Gamtoos Fault is summarised in ***Subsection 5.13.5.1.(d) iv***, with details provided in Subsection 8.4.3 of ***Reference 5.14.17***). The Gamtoos Fault is the main basin-bounding fault along the eastern margin of the Gamtoos Basin, with a trace extending both onshore and offshore. The logic-tree developed for the GAM source is shown in ***Figure 5.13.78***.

Although the Gamtoos and other Mesozoic basin-bounding faults have long been recognised (***Reference 5.14.250***), most studies of these faults were related to basin formation and did not specifically address evidence for recent activity (*e.g.*, ***References 5.14.172, 5.14.230 and 5.14.250***). There is no direct evidence to indicate that the Gamtoos Fault is seismogenic, but based on possible structural association with Kango Fault (***Reference 5.14.183***), which has experienced multiple latest Pleistocene to Holocene surface-faulting earthquakes (see ***Subsection 5.14.5.4.(e) i***) and possible seafloor scarps along the northern part of the offshore section identified by Roux (***Reference 5.14.229***), the Gamtoos Fault is assigned a seismogenic probability p[S] of [0.2]. The possibility that the GAM may be seismogenic reflects to a large degree uncertainty in assessing recent activity based on the available data. These data do not provide sufficient resolution to preclude small amounts (*e.g.*, a few metres) of neotectonic displacement. Higher weight [0.8], however, is given to the assumption that the fault is not seismogenic based on the evidence for seismic inactivity summarised in ***Subsection 5.13.5.1.(d) iv***.

© Eskom 2026/Rev 0a

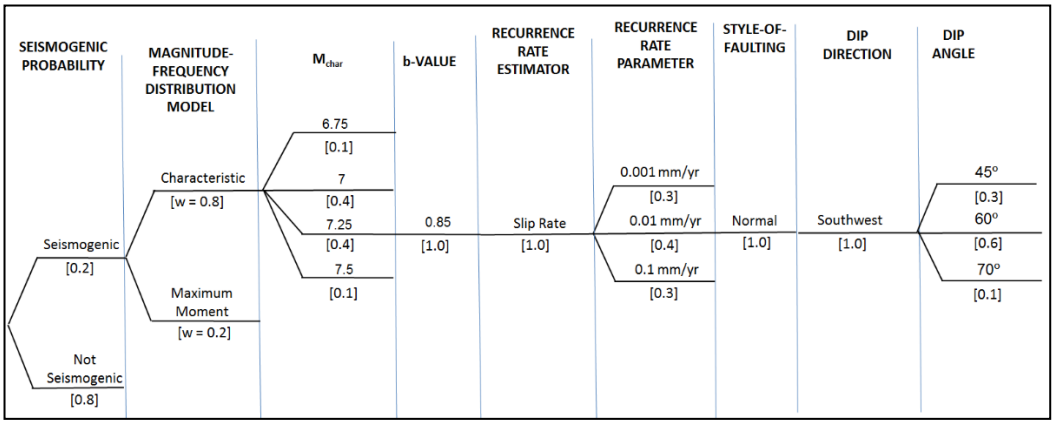


Figure 5.14-78 Logic Tree for the GAM Fault Source, Including the Source-Specific Epistemic Uncertainties.

Epistemic uncertainties that are common to multiple fault sources are the magnitude-frequency distribution model and the b-value, discussed in Subsection 5.14.5.4.(c)

The Gamtoos Fault trends northwest–southeast onshore and bends to a more north–south trend ~10 km south of Cape Recife (***References 5.14.230, 5.14.250 and 5.14.251***). The observed (minimum) total length of the Gamtoos Fault is 170 km, including both onshore (90 km) and offshore (80 km) reaches (***Reference 5.14.183***); the geometry of the GAM source as modelled based on the evaluation of the information available in the geological database (***Subsection 5.14.4.3***) is shown in ***Figure 5.14.73***. Based on the offset of Tertiary and older sediments, the Gamtoos Fault was most recently active as a normal fault; and, based on analogy to the Quaternary Kango Fault, the GAM is modelled as a normal fault [1.0].

As noted in ***Subsection 5.13.5.1.(d) iv***, the Gamtoos Fault displays listric geometry in many, but not all, subsurface images. The dip of the fault ranges from ~26 degrees to the southwest onshore (***Reference 5.14.252***) to 34 degrees on the northwest-trending portion of the offshore fault (***Reference 5.14.184***), but alternative interpretations of the data suggest that the fault could be much steeper (60 degrees) down to seismogenic depth. Therefore, the generic distribution of normal fault dip as discussed in ***Subsection 5.14.5.4.(c) iv*** is modified slightly for GAM to give more weight to the lowest dip: 45° [0.3], 60° [0.6], 70° [0.1].

In the absence of structural, geologic, or behavioural data that can be used to segment the approximately 170 km long fault, the characteristic magnitude for the GAM is inferred by analogy to the Kango Fault. Therefore, the following M_{char} distribution is assessed: M_w 6.75 [0.1], M_w 7.0 [0.3], M_w 7.25 [0.3], and M_w 7.5 [0.3].

There are no palaeoseismic data to evaluate either earthquake count per interval or recurrence intervals for the GAM. Therefore, constraints on slip rate estimated from both regional and fault-specific data are used to estimate the occurrence rates of earthquakes. The compilation of regional marine terrace data for the entire southern coastal region of South Africa provides information to assess whether there has been differential uplift across the Gamtoos Fault (***Reference 5.14.186***). Sequences of terraces at elevations of 18 m, 30 m, and 60 m can be correlated along the entire length of the southern coastline (***Figure 5.13.7***). There is no apparent vertical displacement of the 18 m and 30 m terraces across the Gamtoos Fault within a resolution of about 5 m or less. The regional marine terrace data were compiled from a number of different sources, and the accuracy and uncertainty in the reported elevations of the marine terraces vary. The observations as reported suggest that the long-term slip rate on the Gamtoos Fault would be on the order of 0.001 (5 m/3.3 Myr) to less than 0.003 (5 m/1.8 to 2.6 Myr).

If, however, the Gamtoos Fault had experienced one or two surface-rupturing earthquakes comparable to the latest Pleistocene and Holocene events on the Kango Fault (*i.e.*, ~1–1.5 m displacement per event, ***Reference 5.14.222***), a higher slip rate could not be precluded. Available data from interpretation of onshore aerial photographs and 10 m DEM data and higher-resolution offshore DEM data are used to constrain maximum slip rate based on younger deposits and geomorphic features leading to an estimated slip rate of approximately 0.1 mm/yr under this assumption. In the offshore region, there is no expression of surface displacement of seabed features on the continental shelf at and below the LGM lowstand (~120–125 m isobath). The nature of sediment erosion and deposition on the shelf in this area is unknown, and a single event of 1–1.5 m post-transgression of sea level across the continental shelf from the LGM of ~120–125 m below present level at ~21 ka may be possible within the resolution of the available data.

Based on these lines of reasoning, the probability distribution for slip rate assigned to the GAM is 0.001 mm/yr [0.3], 0.01 mm/yr [0.4], and 0.1 mm/yr [0.3]. The two-order difference in the rate of slip represents the broad uncertainty in the slip rate for the GAM in the present tectonic environment. Incorporating all of the recurrence-related epistemic uncertainties, earthquake recurrence curves were developed for the GAM as shown on ***Figure 5.14.74***.

iv Plettenberg Fault Source (PLET)

The Plettenberg Fault source (PLET) is approximately 20 km from the site at its closest approach (***Figure 5.14.73***). The geological characterisation of the Plettenberg Fault is summarised in ***Subsection 5.13.5.1.(d) iv3***, with details provided in Subsection 8.4.4 of ***Reference 5.14.17***). The Plettenberg Fault is

the main basin-bounding fault along the eastern margin of the Pletmos Basin, and lies completely offshore. The logic-tree developed for the PLET source is shown in ***Figure 5.14.79***.

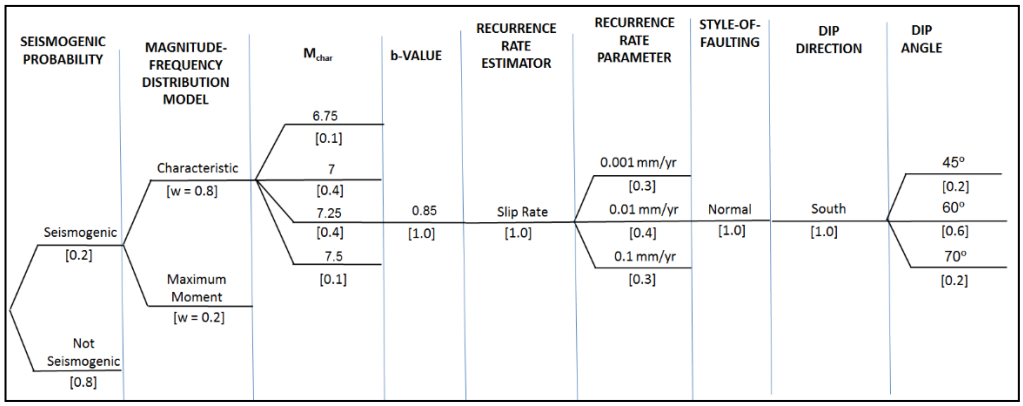


Figure 5.14-79 Logic Tree for the PLET Fault Source, Including the Source-Specific Epistemic Uncertainties.

Epistemic uncertainties that are common to multiple fault sources are the magnitude-frequency distribution model and the b-value, discussed in Subsection 5.14.5.4.(c)

Similarly to the Gamtoos Fault (see ***Subsection 5.14.5.4.(e) iii***), most studies of the Plettenberg Fault do not specifically address evidence for neotectonic reactivation (*e.g.,* ***References 5.14.172, 5.14.197 and 5.14.230***). There is no direct evidence to indicate that the PLET is seismogenic in the present tectonic regime. Other nearby Mesozoic basin–bounding faults such as the Baviaanskloof, Coega, and Kouga Faults show evidence of no displacement in Quaternary/late Pliocene time, and in some cases, no displacement since deposition of the Grahamstown Formation gravel deposits in the Miocene (see ***Subsection 5.14.5.4.(e) vi***). Offshore seismic data show evidence for no post-Cretaceous activity on some seismic profiles across the Plettenberg Fault and equivocal evidence for Tertiary displacements on other lines. The origin and timing of possible Tertiary displacement observed in the seismic data are not well constrained. The apparent vertical displacement may have occurred in the early Tertiary or may be due to nontectonic processes. For these reasons, the PLET is considered likely to be nonseismogenic. The small weight given to the option that PLET is seismogenic (p[S] = [0.2]) allows for the possibility that detection of minor displacement (a few metres in 1–2 surface-rupturing events like the surface-rupturing events observed along the Kango Fault to the north) may be beyond the resolution of the available offshore data.

The Pletmos Basin is a half graben that exhibits a change in trend from approximately west-northwest/east-northeast to north–south in the east of the basin and the main boundary fault. The fault is traced on seismic reflection lines and as the contact between Mesozoic basin sediments and basement rocks. The total length of the PLET (159 km) is based on the location of the fault as shown by Du Toit (***Reference 5.14.250***), Paton (***Reference 5.14.183***), and Roux (***Reference 5.14.229***). No evidence for an en-echelon configuration of segments or overlapping segments was observed by Paton (***Reference 5.14.183***), and the geometry shown in ***Figure 5.14.73*** was adopted for the PLET source.

The Plettenberg Fault is a Cape Fold Belt thrust reactivated as a normal fault during Mesozoic extension (***References 5.14.171, 5.14.226, 5.14.227 and 5.14.229***). If the Plettenberg Fault is seismogenic, it is interpreted to behave as a normal fault (weight of [1.0]), based on Mesozoic offset, evidence for post-Cretaceous displacements, and analogy to the reactivated Kango Fault. The downdip geometry of the Plettenberg Fault is interpreted from seismic lines to be planar and dipping at 65 degrees to the southwest on the northwest-southeast-trending portion, and at 50 degrees to the west on the north-south-trending portion (***References 5.14.171, 5.14.226, 5.14.227 and 5.14.229***). The fault extends to at least 12,000 m depth (***Reference 5.14.249***). Based on these observations, the following dip values and associated weights are used for the Plettenberg Fault: 45°S [0.2], 60°S [0.6], and 70°S [0.2]. These values are consistent with generic values used for normal fault dips based on worldwide data (see ***Subsection 5.14.5.4.(c) iv***).

In the absence of structural, geologic, or behavioural data that can be used to segment the approximately 160 km long fault, the characteristic magnitude for the PLET is inferred by analogy to the Kango Fault. The following M_{char} distribution, therefore, is assessed: M_w 6.75 [0.1], M_w 7.0 [0.3], M_w 7.25 [0.3], and M_w 7.5 [0.3].

There are no palaeoseismic data to evaluate either earthquakes per interval or recurrence intervals for the PLET. Therefore, constraints on slip rate estimated from both regional and fault-specific data are used to estimate the occurrence rates of earthquakes. The PLET lies completely offshore. There is no evidence of differential uplift of marine terraces across the projected trend of the PLET to indicate that the fault extends onshore or has been reactivated in Pliocene or younger time (***Reference 5.14.186***).

The long-term average post-Cretaceous (post-22At1 sequence boundary) slip rate is on the order of thousandths of a millimetre per year (*i.e.*, 22 m/6,700 kyr = 0.003 m/kyr [mm/yr]), similar to the resolution of post-Pliocene vertical

© Eskom 2026/Rev 0a

deformation for the GAM (***Subsection 5.14.5.4.(e) iii***) provided by the onshore marine terrace data.

If the PLET had experienced one to a few Quaternary surface-rupturing earthquakes comparable to the latest Pleistocene and Holocene events on the Kango Fault (*i.e.*, ~1–1.5 m displacement per event; ***Reference 5.14.222***), a higher slip rate could not be precluded based on the resolution of the available offshore data. The possibility that a few metres of slip may have occurred on the PLET in the latest Pleistocene, giving rise to a slip rate on the order of 0.1 mm/yr, is not precluded by the available data. Although there is no expression of surface displacement of seabed features on the continental shelf at and below the lowstand position (***Figure 5.14.80***), the nature of sediment erosion and deposition on the shelf in this area is unknown, and a small displacement of 1–1.5 m post-transgression of sea level across the continental shelf from the Last Glacial Maximum of approximately 120–125 m below present level at approximately 21 ka may be possible within the resolution of the available data.

The probability distribution for slip rate assigned to the PLET based on these observations is 0.001 mm/yr [0.3]; 0.01 mm/yr [0.4]; and 0.1 mm/yr [0.3]. The two-order range in the rate of slip represents the broad uncertainty in the slip rate for the PLET due to the resolution of the offshore data available to evaluate timing of most recent movement on the fault. Incorporating all of the recurrence-related epistemic uncertainties, earthquake recurrence curves were developed for the PLET as shown in ***Figure 5.14.74***.

© Eskom 2026/Rev 0a

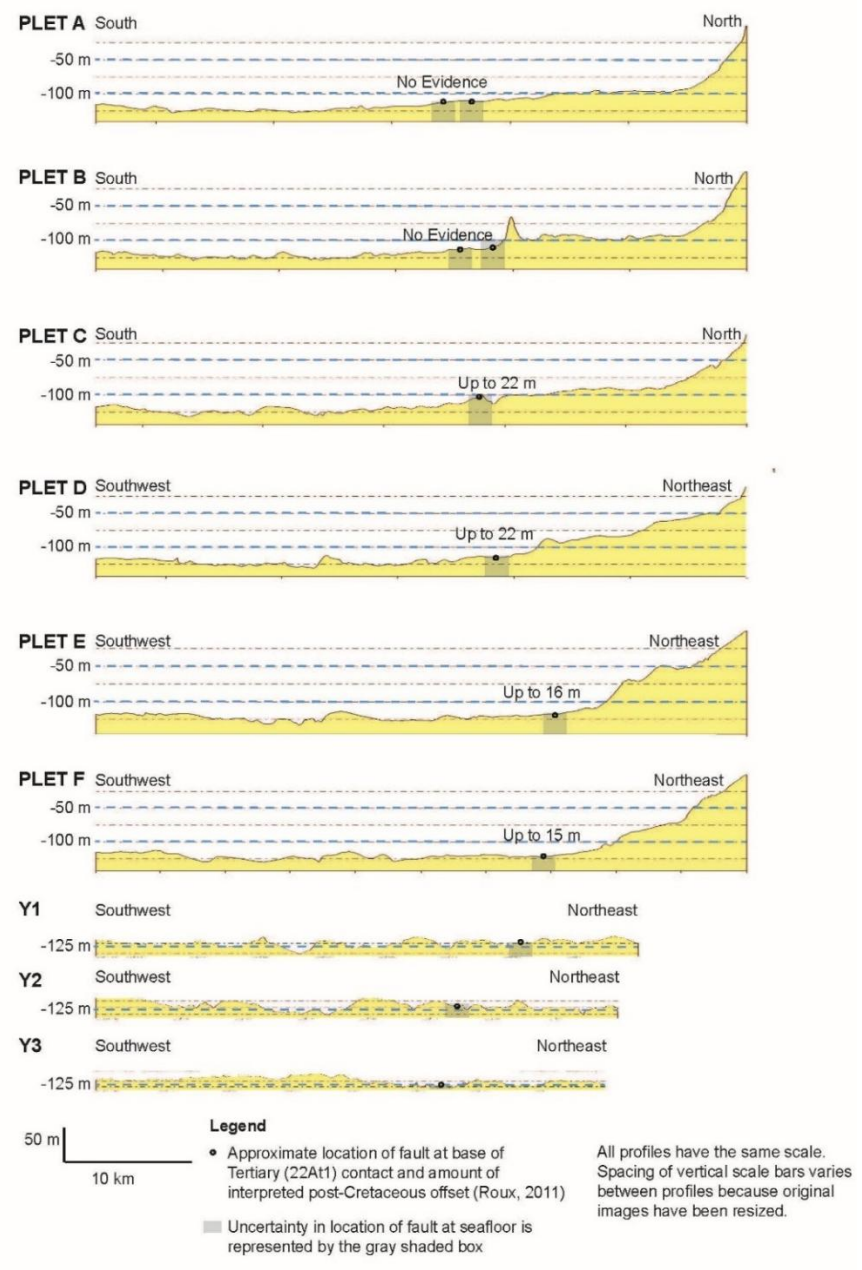


Figure 5.14-80 Topographic Profiles Showing the Morphology of the Seafloor Across the Plettenberg Fault (*Reference 5.14.254*).

The Late Glacial Maximum (LGM) shoreline is expressed as a planed surface at a depth of ~125 m or slightly lower. East-west-trending seafloor ridges observed at depths of between ~100 m and 125 m are interpreted to be aeolian dunes formed during the LGM, or possibly much older Pleistocene/Pliocene aeolianites.

iv Worcester Fault Source (WOR)

The Worcester Fault source (WOR) is approximately 269 km from the site at its closest approach (***Figure 5.14.73***). The geological characterisation of the Worcester Fault is summarised in ***Subsection 5.13.5.1.(d) iv***, with details provided in Subsection 8.4.5 of ***Reference 5.14.17***). The Worcester Fault is part of the Worcester Fault zone, a series of faults trending north-south in the Western Cape and east-west in the Eastern Cape, with a broad bend at the Cape Fold Belt syntaxis (***Figure 5.13.64***). The logic-tree developed for the WOR source is shown in ***Figure 5.14.81***.

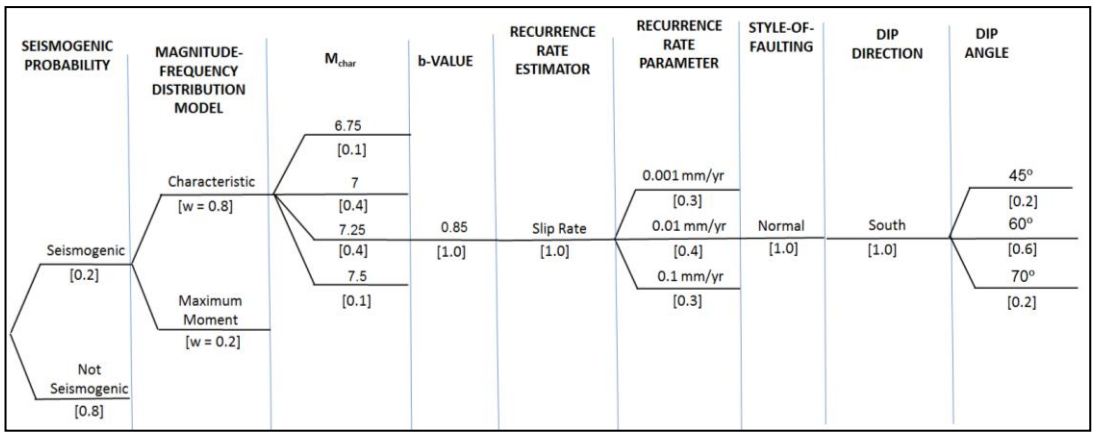


Figure 5.14-81 Logic Tree for the WOR Fault Source, Including the Source-Specific Epistemic Uncertainties.

Epistemic uncertainties that are common to multiple fault sources are the magnitude-frequency distribution model and the b-value, discussed in Subsection 5.14.5.4.(c)

There is no direct evidence to indicate that the WOR is seismogenic based on the criteria outlined in ***Subsection 5.14.5.4.(a) ii***. Based on limited reconnaissance mapping and office-based interpretation of aerial photographs and DEMs, De Beer (***Reference 5.14.182***) notes that there was no conclusive evidence for Pliocene to Quaternary activity on the Worcester Fault zone east of the syntaxis, although older scarps may be unrecognisable due to weathering and slope processes.

The Worcester Fault subparallels the Kango Fault, which has experienced multiple latest Pleistocene to Holocene surface-faulting earthquakes (see ***Subsection 5.14.5.4.(e) i***). The Worcester Fault is structurally associated with the Kango Fault in that both faults share a common geologic history of Mesozoic reactivation of an older Palaeozoic compressional structure. The

Worcester Fault, therefore, may be favourably oriented to be reactivated in the present tectonic regime. There also is a possible association between the Worcester Fault zone and seismicity in the Ceres area. Near Ceres, the Groenhof Fault, which is considered a possible source for the 1969 M 6.4 Ceres earthquake, may be the structural step-over between the Worcester and De Hoek Faults (***Reference 5.14.21 and 5.14.186***; see ***Figure 5.14.82***).

Based on these observations, there is some likelihood that the WOR is seismogenic (*i.e.*, p[S] is greater than zero). The relatively low weight [0.2] assigned to this probability is based on other lines of evidence and observations outlined in ***Subsection 5.13.5.1.(d) iv*** that show that the Worcester Fault does not appear to have been active in late Pliocene to Quaternary time.

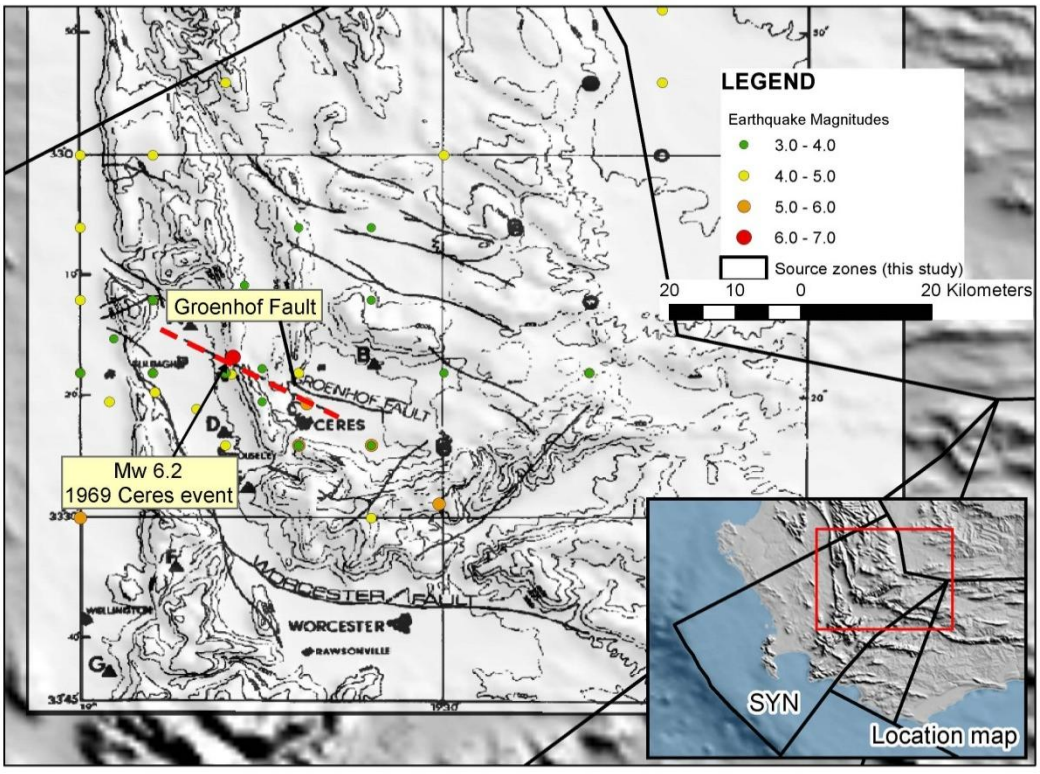


Figure 5.14-82 Location of 1969 Ceres Aftershocks (*red dashed line*) relative to the Groenhof and Worcester Faults ***(Modified from Reference 5.14.249)***.

The location and total length (291 km) of the WOR generally follows the CGS fault map compilation (***Figure F-5.13.64***). The western extent of the fault source is consistent with the fault as shown by Green & Bloch (***Reference 5.14.21***;

Figure 5.14.82). Although De Beer (***Reference 5.14.182***) suggests that the fault could extend to the coastline east of Mossel Bay and perhaps link up with the offshore Plettenberg Fault (***Subsection 5.14.5.4.(e) iv***), the fault is not shown as a continuous structure on geologic maps (***Reference 5.14.255 and 5.14.256***; ***Figure F-5.13.65***). The eastern endpoint of the WOR is designated as the eastern end of the relatively continuous fault as shown by De Beer (***Reference 5.14.182***) and on the Ladismith 1:250 000 geologic map (***Reference 5.14.255***). ***Figure F-5.13.65*** shows that the fault does not displace extensive Tg pediment remnants farther to the east.

Like the Kango Fault, the Worcester Fault was reactivated in the Mesozoic as a steep normal fault with a southerly throw. The eastern part of the fault, the part of the fault zone closest to the Thyspunt site, is subparallel to the Quaternary-reactivated part of the Kango Fault. It is assumed that if the fault were seismogenic, it would have a style of faulting similar to that of the Kango Fault. Therefore, the expected style of faulting is normal [1.0]. The generic distribution for normal fault dip as described in ***Subsection 5.14.5.4.(c) iv*** is used to characterise the WOR source: 45°S [0.2], 60°S [0.6], and 70°S [0.2].

No detailed palaeoseismic studies have been conducted along the Worcester Fault that can be used to assess parameters such as displacement per event or individual event rupture length. In the absence of structural, geologic, or behavioural data that can be used to define rupture segments, the characteristic magnitude for the WOR is inferred by analogy to the Kango Fault based on palaeoseismic studies summarised in Hanson *et al*. (***Reference 5.14.222***). Therefore, the following M_{char} distribution is used: M_w 6.75 [0.1], M_w 7.0 [0.3], M_w 7.25 [0.3], and M_w 7.5 [0.3].

Similarly, there are no palaeoseismic data from which to evaluate either earthquake count per interval or recurrence intervals for the WOR. Therefore, constraints on slip rate estimated from both regional and fault-specific data are used to estimate the occurrence rates of earthquakes. The rationale used to assess a range of possible slip rate for the Gamtoos Fault source (GAM) applies also to the Worcester Fault (see discussion in ***Subsection 5.14.5.4.(e) iii***). In both cases there is no evidence to suggest that the faults have experienced Quaternary reactivation comparable to the Kango Fault (***Subsection 5.14.5.4.(e) i***). However, there is not sufficient information available to preclude one or two surface-rupturing events in the late Pleistocene, the surface expression of which has subsequently been eroded or obscured. As described above, there is no indication in the regional data sets to suggest there has been significant differential uplift in the Eastern Cape region from either marine terrace or cosmogenically derived denudation rate data. The probability distribution for slip rate assigned to the GAM, therefore, is

© Eskom 2026/Rev 0a

also used to characterise recurrence for the WOR: 0.001 mm/yr [0.3], 0.01 mm/yr [0.4], and 0.1 mm/yr [0.3]. The two-order difference in the rate of slip represents the broad uncertainty in the slip rate for the WOR in the present tectonic environment.

Incorporating all of the recurrence-related epistemic uncertainties, earthquake recurrence curves were developed for the WOR as shown in ***Figure 5.14.74***.

e) Fault assessed to be Non-Seismogenic

Several potential fault sources were investigated as part of the Geological Investigations programme for the Thyspunt SSHAC PSHA (see discussion in ***Subsection 5.14.5.13***; ***Figure 5.14.83***). The Baviaanskloof, Coega (western and eastern segments), Kouga, and Cape St Francis Faults formed around the same time as the Kango Fault, the only fault in South Africa known to have an associated Quaternary scarp ***(Subsection 5.14.5.4.(e) i***), and are structurally related, having been reactivated as major basin-bounding normal faults in the Mesozoic. The geological investigations therefore focused specifically on the issue of their seismogenic potential in the current tectonic regime.

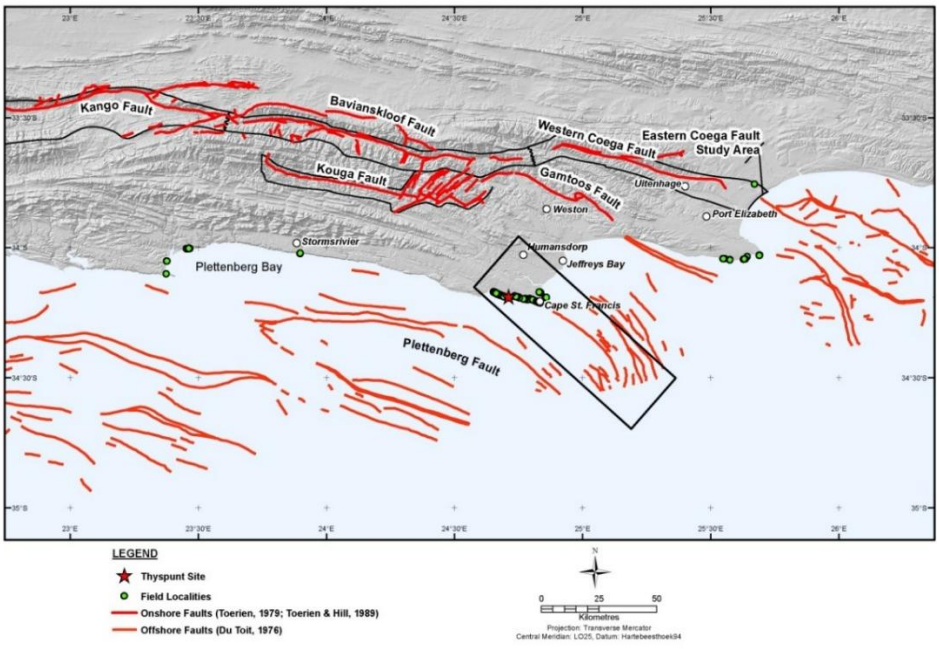


Figure 5.14-83 Map Showing Locations of Fault Corridor Study Areas (*outlined in black*) Investigated to Assess the Seismogenic Probability of the Baviaanskloof, Coega, Kouga, and Cape St Francis Faults.

Using the criteria described in ***Subsection 5.14.5.4.(a) ii*** and the results of the geological investigations summarised in the geological database (***Subsection 5.14.4.3***), the faults listed above were assessed to have a p[S] of zero. The Baviaanskloof, Western Coega, and Kouga Faults, whose traces are 40–60 km inland from the coast and, along with the Kango Fault, represent the northernmost Mesozoic extensional features in South Africa (see ***Subsection 5.13.5.1.(d) iv***), were evaluated using high-level terrace datum. The river drainages in these regions have incised approximately 150 m into the Palaeozoic Table Mountain Group quartzite, which has resulted in the abandonment of high-level pediment surfaces. The deposits on these remnant surfaces are known as the Tertiary Grahamstown Formation (Tg) and are often composed of fluvial and alluvial fan cobbles and boulders in a sandy matrix that have been cemented with silica (silcrete) or iron (ferricrete). The Tg and underlying pediment surface at the bedrock alluvium contact are generally considered to be Miocene in age (***Reference 5.14.257***). Thus, the lack of vertical offset on these surfaces indicates that the faults have not been reactivated during the Pliocene and Quaternary, leading to a p[S] of 0 according to the criteria described in ***Subsection 5.14.5.4.(a) ii***.

The results of the regional marine terrace studies (see ***Subsection 5.13.4.2*** and ***References 5.14.186 and 5.14.258*** for details), published geological observations and analysis of a recently compiled high-resolution near-shore bathymetry data set (***Reference 5.14.254***) were similarly used to assess possible vertical offset across the Eastern Coega (see ***Subsection 5.13.5.1.(d) iv***) and Cape St Francis Faults (see ***Subsection 5.13.5.1.(d) iv***) and thus evaluate the p[S] of the Eastern Coega and Cape St Francis Faults. The assessments of the individual faults are summarised below. Further details can be found in Section 8.5 of ***Reference 5.14.17***.

i Baviaanskloof Fault

The Baviaanskloof Fault extends 110 km and is positioned along strike with and directly east of the Kango Fault (***Figure 5.14.83***); at the closest distance, this fault comes within 60 km of the Thyspunt site. No apparent vertical offset of the Tg surface was observed at the four sites investigated along the fault. Further, geochronology samples collected from the silcrete surfaces indicate that the exposed surfaces have been stable for a minimum of 0.8–1.0 Myr or have experienced maximum erosion rates of 0.32–0.51 m/Myr, based on cosmogenic nuclide dating (***Reference 5.14.241***). Observations and information related to the mapping at specific sites is documented in ***Reference 5.14.259***. In view of the lack of deformation features within the

© Eskom 2026/Rev 0a

deposits overlying the Baviaanskloof Fault, and given the exposure ages of these surfaces, the SSC TI team has assessed the p[S] of this fault as zero.

ii Western Coega Fault

The Western Coega Fault trace extends 30 km and is positioned along strike with the Kango and Baviaanskloof Faults (***Figure 5.14.83***). The fault trace at the closest distance comes within 65 km of the Thyspunt site. No apparent vertical offset of the Tg surface was observed at the seven sites investigated along the fault. Further, geochronology samples collected from the Tg surfaces indicate that the exposed surface has been stable for a minimum of 2.0–3.7 Myr or has experienced a maximum erosion rate of 0.11–0.21 m/Myr, based on cosmogenic nuclide dating (***Reference 5.14.241***). At the SWC-06 locality along the fault, the unconformity between Palaeozoic bedrock and the overlying Tg deposits shows evidence of no surface faulting. This suggests that the Western Coega Fault has not been reactivated since initial abrasion of the bedrock surface and deposition of the Tg deposits in the Miocene. Detailed observations and information related to the specific mapping at each site are documented in ***Reference 5.14.260***. In view of the lack of deformation features within the deposits overlying the Western Coega Fault, and given the exposure ages of these surfaces, the SSC TI team has assessed the p[S] of this fault as zero.

iii Kouga Fault

The Kouga Fault, which is positioned parallel to and directly south of the Baviaanskloof Fault, extends approximately 80 km east to west (***Figure 5.14.83***). This fault at the closest distance comes within 40 km of the Thyspunt site. The western 30 km of the fault is offset by the Paul Sauer Faults, a series of 15–20 km long north-northeast-striking cross faults. No apparent vertical offset of the Tg surface was observed at the six sites investigated along the Kouga Fault. Further, geochronology samples collected from the silcretised Tg surfaces indicate that the exposed surface has been stable for a minimum of 1.9 Myr or has experienced erosion at maximum rates of 0.14–0.20 m/Myr, based on cosmogenic nuclide dating (***Reference 5.14.222***). At one location along the fault (Tafelberg site M2.60), exposures of unconformity between Palaeozoic bedrock and the overlying silcretised Tg show evidence for no surface faulting of the contact over a trace of the Kouga Fault. The age of the unconformity is unknown; it is likely to be considerably older than the minimum exposure ages estimated from the cosmogenic nuclide analyses and may be as old as Miocene. Detailed observations and information related to the specific mapping at each site is documented in ***Reference 5.14.260***. In view of the lack of deformation features within the deposits overlying the Kouga Fault (***Figure 5.14.84***), and given the exposure ages of these surfaces, the SSC TI team has assessed the p[S] of this fault as zero.

© Eskom 2026/Rev 0a

iv Coega Fault

The Coega Fault, a bounding fault of the Algoa Basin half-graben (***Reference 5.14.170***), is described in ***Subsection 5.13.5.1.(d) iv***. The fault at its closest distance comes within 75 km of the Thyspunt site (see ***Figure 5.14.83***), and comprises two sections. In contrast to the Western Coega Fault zone, which is geomorphically well expressed as an escarpment, the Eastern Coega Fault zone is buried under younger Tertiary to Recent sediments and is not exposed or geomorphically well expressed at the surface.

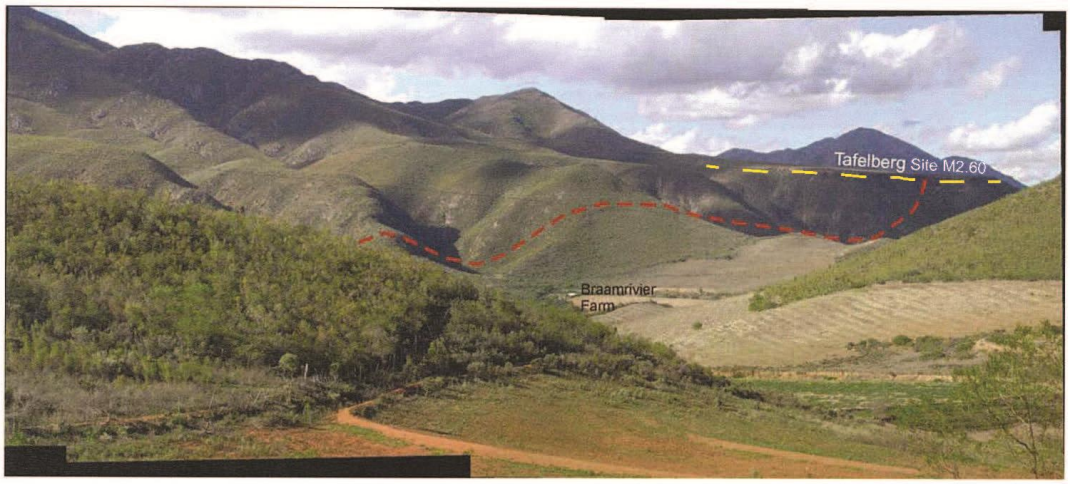


Figure 5.14-84 Unfaulted Tg Surface at Site M2.60 (*Reference 5.14.258*). The Unconformity Between the Tg Surface and Underlying Palaeozoic Bedrock (*dashed yellow line*) is Unfaulted.

The chronology and altitude of the marine deposits described in the Eastern Coega Fault study area (***Reference 5.14.258 and 5.14.186***) are tentatively correlated with other marine deposits along the southern African coast (***Figure 5.14.85***). Information on the top of bedrock surface and overlying lithologies indicates that one or more marine platforms occur at elevations ranging from 40 m to 60 m amsl and that these surfaces are correlated across the Coega Fault zone with little or no vertical displacement. The Pliocene age previously proposed for these terraces (***Reference 5.14.262***) is supported by the cosmogenic burial age data obtained from the Algoa Brick Quarry (***Reference 5.14.263***) and suggests that the broad marine platforms across the Coega Fault zone at approximately 50 m to 60 m amsl elevations have not

© Eskom 2026/Rev 0a

undergone deformation since the earlier Pliocene (~4.0 Ma). Additional evidence from borehole data suggest that within a resolution of about 2 ± 1 m, there is no vertical displacement of the seaward portion of the leading edge (~40 ± 3 m amsl) of the broad high platform across the Eastern Coega Fault zone in the vicinity of the N2. The age of this marine terrace platform is estimated to be late Pliocene (~3.6–2.6 Ma; ***Reference 5.14.186***). The presence of a probable marine terrace abrasion platform, which is estimated to be no younger than MIS 9 (approximately 330 ka; ***Reference 5.14.264***) extending across the Coega Fault zone with no apparent vertical offset, is consistent with the evidence for no apparent deformation of the older Pliocene platform(s).

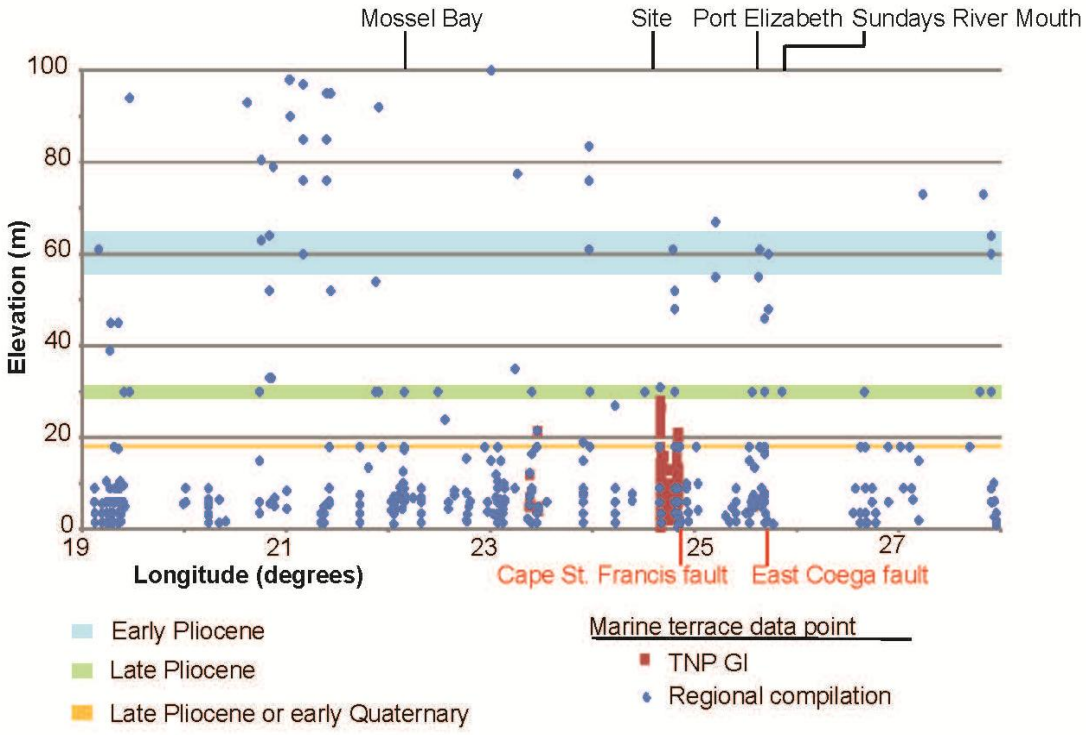


Figure 5.14-85 Summary Diagram Showing Correlations of Pliocene and Quaternary Marine Terraces from West of Mossel Bay to East of Port Elizabeth Based on Hanson *et al.* (*Reference 5.14.186*).

The locations of the Eastern Coega Fault and Cape St Francis Fault at the coastline are shown.

The lack of apparent deformation of marine terraces across the Coega Fault on both a regional and a local basis, as described above, implies that the most recent movement on the Eastern Coega Fault near the coastline predates formation of Pleistocene and Pliocene terraces, which are estimated to range in age from older than approximately 330 ka to approximately 3 Ma or older. These observations are consistent with evidence for the Western Coega Fault, which also indicates no reactivation in the past approximately 3.7 Myr. The SSC TI team has therefore assessed the p[S] of the Eastern Coega Fault as zero.

v Cape St Francis Fault

The Cape St Francis Fault is entirely offshore and has an approximate mapped length of 40 km. This fault at its closest distance comes within 17 km of the Thyspunt site (***Figure 5.14.83***). The fault was initially identified as a possible nearby fault source because of its proximity to the Thyspunt site and the possibility of an onshore extension (see ***Subsection 5.13.5.2***), as well as the similarity in tectonic age and style between this fault and associated faults along the Cape St Francis Arch and major onshore faults, such as the Kango-Baviaanskloof-Coega and Kouga Faults (***Reference 5.14.222***). The geological characterisation of this fault is summarised in ***Subsection 5.13.5.1.(d) iv***, which also includes a discussion of previously published interpretations based on a number of seismic reflection profiles that image the St Francis Arch from offshore petroleum exploration surveys (***References 5.14.229 and 5.14.230***). A detailed re-examination of these results as part of the evaluation of the geological database (***Subsection 5.14.4.3***), considering the results of the marine terrace investigations (see ***Subsections 5.13.4.2.(c)*** and ***5.13.5.1.(d)v***) as well as independent evidence from recently collected high-resolution bathymetry of the offshore region of the seafloor (***Reference 5.14.222***) concluded that the sea floor scarps observed in industry seismic profile data are likely related to shoreline erosional processes, rather than tectonic movement on the mapped faults.

A possible onshore extension of the Cape St Francis Fault is discussed by Goedhart (***Reference 5.14.178***), who postulated that, because of the gap in the data set in the nearshore, the use of the offshore survey data alone is not sufficient to preclude an onshore extension of the fault at Cape St Francis Bay. A detailed marine terrace mapping programme was conducted in the Oyster Bay to Cape St Francis study area (***Reference 5.14.186***) that addressed the seismogenic probability of potential onshore extensions of the Cape St Francis Fault and other structures within the Cape St Francis fault zone, as well as minor northeast-trending secondary faults documented by onshore bedrock mapping and interpretation of offshore seismic data (***References 5.14.265 to 5.14.267***).

© Eskom 2026/Rev 0a

The onshore marine terrace study in the 8 km region around the Thyspunt site indicated that a 13 ± 1 m shoreline angle can be mapped and correlated from Oyster Bay to Seal Point near Cape St Francis (***Reference 5.14.186***). The 13 ± 1 m shoreline angle is correlated to the MIS 11 sea level, indicating an age of approximately 400 ka. As shown on ***Figure 5.14.85***, There is no indication that terraces inferred to be Pliocene in age are deformed across the onshore projected trends of any of the faults within the Cape St Francis Fault zone (***Figure 5.14.85***).

In view of the lack of post-Cretaceous deformation within the deposits overlying most of the Cape St Francis Fault offshore, the evidence indicating that postulated sea floor scarps observed in industry seismic profile data are likely related to shoreline erosional processes, and the evidence for no vertical deformation of the MIS 11 shoreline angle across the project trace of the Cape St Francis Fault and other related faults within the zone, the SSC TI team has assessed the p[S] of the Cape St Francis Fault as zero.

5.14.5.5 Ground Motion Characterisation (GMC) Model

The purpose of the GMC model is provide predictions of ground motions, expressed in terms of ordinates of response spectral acceleration at a range of oscillator periods, at the surface reference horizon, which was defined as the top of the Goudini formation below the footprint of the nuclear island at the Thyspunt site. As noted in ***Subsection 5.14.4.5***, the decision was taken to develop ground-motion predictions at a deep horizon with the Goudini bedrock at the site, and perform the PSHA calculations at this horizon. The hazard estimates at bedrock would then be transferred to the reference surface horizon using the measurements of shear-wave velocity at the site (***Subsection 5.14.4.5***).

A choice was then required as to how to incorporate the response of the Goudini formation above the reference bedrock horizon. McGuire *et al*. (***Reference 5.14.16***) proposed five different approaches to the incorporation of site response effects—generally for soil layers overlying bedrock—into PSHA. These approaches are labelled as 1, 2A, 2B, 3 and 4, representing increasing accuracy as the number increases. The most accurate method, therefore, is Approach 4, in which the site amplification is represented probabilistically and is convolved directly with bedrock hazard to obtain surface motions that fully preserve the probabilities (or the annual frequencies of exceedance) obtained from the PSHA calculations at the bedrock level. The application of Approach 4 requires a large database of earthquake ground-motion recordings from the site in question, and therefore it represents an ideal situation that is very unlikely to be achieved in practice. Approach 3, which is essentially based on the work of Bazzurro & Cornell (***Reference 5.14.268***), is a practical approximation to

© Eskom 2026/Rev 0a

Approach 4, based on using site response analyses for the site in question and also retaining the correct annual exceedance frequencies (AFEs) at the ground surface.

In order to incorporate the dynamic site response characteristics as accurately as possible in the estimation of the surface motions, and also to ensure that these surface motions have accurately determined AFEs, the decision was taken to adopt Approach 3.

The first focus of the TI Team was to therefore build a model for the prediction of ground-motions in the bedrock Goudini. Ground-motion prediction equations (GMPEs) express the logarithm of spectral acceleration at a specific oscillator frequency as a function of various explanatory parameters such as earthquake magnitude, style-of-faulting, source-to-site distance, and V_{s30} at the site. Using large collections of ground-motion recordings, empirical equations are obtained fitting a suitable functional form, relating spectral accelerations to the variables listed above.

A very important feature to note with such equations is that the data always show a large scatter around the best fit obtained through regression analyses, an example of what is referred to as aleatory variability (***Subsection 5.14.7***). Residuals are calculated as the difference between recorded and predicted values of spectral acceleration, and the distribution of these residuals represents the scatter in the predictions. This scatter exists for several reasons, including the influence of variables that are not included in the equations (*e.g.*, stress drop, fault rupture directivity effects, azimuthal variations in energy propagation from the source, differences in the deeper geological structure) and the fact that the explanatory variables employed, such as V_{s30}, can yield identical values for very different sites with markedly distinct dynamic response characteristics. Several studies have shown that when the equations are derived in terms of the logarithmic value of spectral acceleration, the residuals conform to a standard normal (Gaussian) distribution, which is fully characterised by the standard deviation, σ (sigma) (***Figure 5.14.86***). GMPEs therefore predict not unique values of spectral acceleration but rather probabilistic distributions of this parameter. Viewed from this perspective, when a GMPE is employed by entering the magnitude, distance and other parameter values pertinent to the scenario in question, it is also necessary to select the number, ε, of standard deviations above or below the median prediction.

To develop a complete GMC model, it is therefore necessary to develop models for both the median predictions (***Subsection 5.14.5.5.(a)***) and the associated sigma (***Subsection 5.14.5.5.(a)***). For the specific approach adopted for the Thyspunt site, incorporating site response effects using USNRC Approach 3, it is also necessary to develop a model for the dynamic response characteristics

of the site (***Subsection 5.14.5.5.(a)***). As is explained in the following subsections, the three components are correlated, and in particular decisions regarding the modelling of the median bedrock motions and the site response characteristics influenced the sigma model developed for the Thyspunt PSHA.

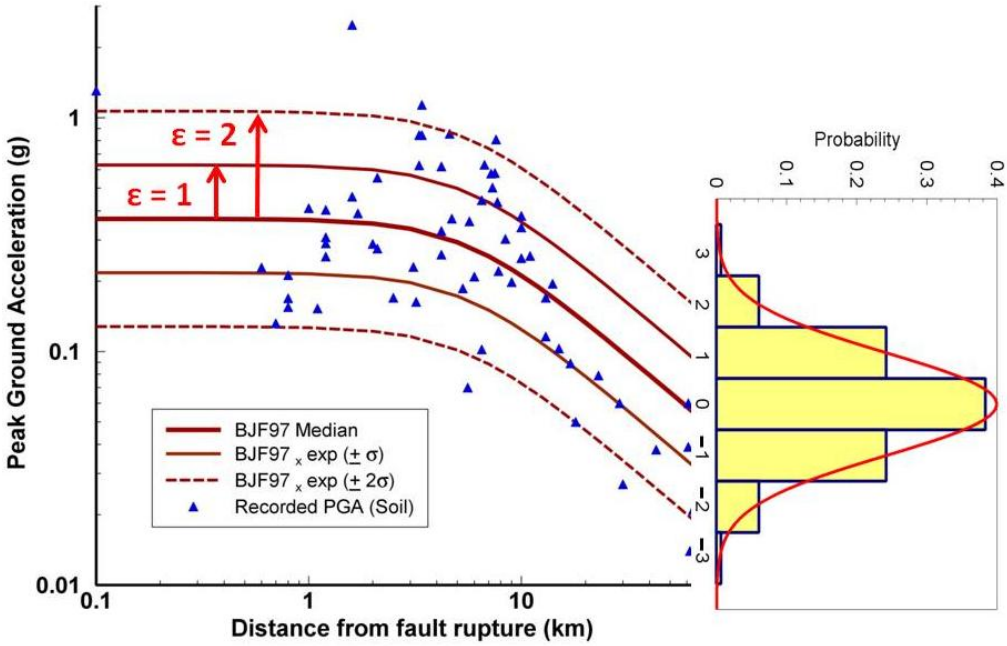


Figure 5.14-86 Peak Ground Acceleration (PGA) Values (*blue triangles*) Recorded on Soil Sites During the Magnitude 6.0 Earthquake that Occurred in Parkfield, California, in September 2004, Plotted as a Function of Distance, and Compared with Predictions From a Californian GMPE.

The predicted PGA values are shown for the median values and for one and two standard deviation above and below the logarithmic mean. Figure adapted from Reference 5.14.269.

a) Logic-tree for median ground motions

In the absence of instrumental recordings of strong ground-motion from moderate-and-large magnitude earthquakes in South Africa, the uncertainty in median predictions of ground motions at Thyspunt would inevitably be subject to large epistemic uncertainty. The GMC TI Team decided at an early stage that simply adopting a large numbers of GMPEs to populate a logic-tree was unlikely to capture a sufficiently wide range of uncertainty. Indeed, the opposite

effect could result by having several equations that produce comparable levels of predicted motions, thus leading to narrow distributions on epistemic uncertainty. Instead, the approach adopted was to use three GMPEs selected on the basis of their inherent quality (***Subsection 5.14.4.5***) to generate a suite of alternative models that would capture a wide range of potential future ground-motion amplitudes (i.e., capture the CBR of the TDI). The first stage was to adjust the models to the bedrock condition at the Thyspunt site.

i Vs-kappa adjustments

The first adjustment to be applied to the three selected backbone GMPEs was to render them applicable to the very hard rock conditions at the target bedrock horizon (V_s ~3 km/s). Since none of the selected backbone GMPEs is applicable to such high values of shear-wave velocity, a transformation is necessary to make the predictions applicable to the bedrock at the site. However, applying only an adjustment for differences in the host (GMPE) and target (Thyspunt bedrock) V_s profiles would lead to de-amplification of the motion across the entire frequency range, which is known not to be a realistic representation of what would be expected in nature. The very hard rock will also have a very low kappa (κ_0) value, meaning that only a weak filter is applied in terms of near-surface attenuation of the upcoming motions. Consequently, while the transformation from a lower to a higher V_{s30} may result in a decrease of predicted spectral ordinates at most oscillator periods, at very short periods it is likely that the motions would actually increase. This can be appreciated from figures illustrating the inverse operation, namely transforming ground-motion predictions from a very hard rock site to softer site conditions. ***Figure 5.14.87*** shows site amplification functions calculated for different target shear-wave velocities for motions in very hard rock, all of which show a monotonic increase with oscillator frequency. If the effect of the kappa filter is added in, then the amplification functions take on the form of those shown in ***Figure 5.14.88***, where the amplification diminishes at the highest frequencies because of the effect of the kappa filter.

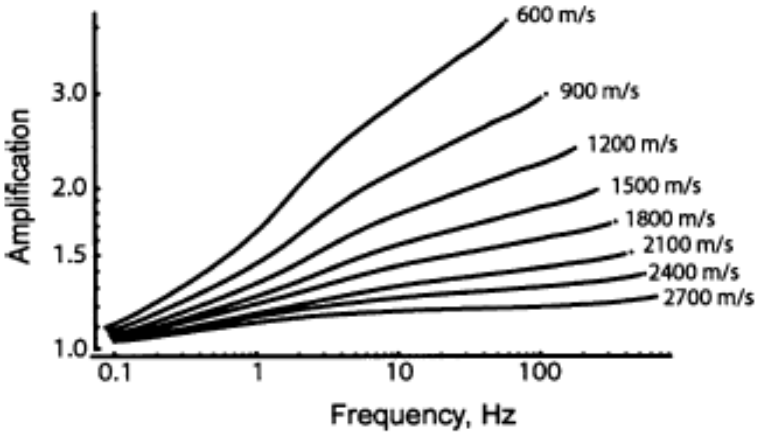


Figure 5.14-87 Site Amplification Functions for Generic V_s Profiles, Anchored to the V_{s30} Values Indicated, Relative to a Very Hard Rock Condition (*Reference 5.14.124*).

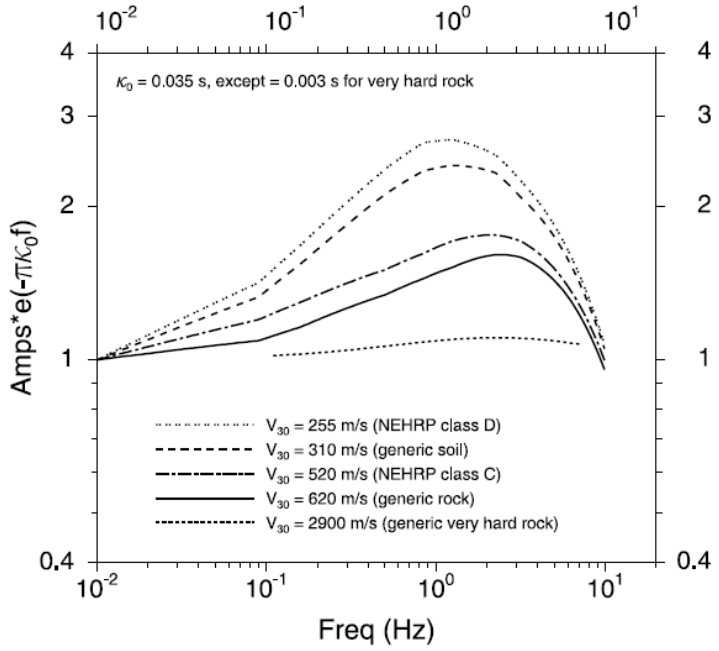


Figure 5.14-88 Fourier Spectra Site Effect Operators Obtained by Multiplying Site Amplification Operators for Various Sites With a Kappa Filter (*Reference 5.14.120*).

© Eskom 2026/Rev 0a

As was already noted in ***Subsection 5.14.4.7***, the generic California rock profile of Boore & Joyner (***Reference 5.14.138***) was adopted as the host profile of the NGA models (AS08, CY08), and also shown to be applicable to the Turkish model (AC10). The developers of the three backbone GMPEs claim that they are applicable to rather high V_{s30} values: 1 300 m/s (AC10), 1 500 m/s (CY08) and 2 000 m/s (AS08). However, it is known that the degree of constraint is actually very limited and although it may appear tempting to use the largest possible value so that the transition covered by the adjustment is minimised, starting from these very high V_{s30} values would actually add uncertainty. Instead, the anchoring value of the generic Californian rock profile (620 m/s), which is well constrained in all of the models, is chosen as the host value of V_{s30}.

For the target profile, the generic ENA rock profile of Boore & Joyner (***Reference 5.14.138***) was adopted, but adjusted—by simply truncation at the top—so that it had a shear-wave velocity of 3 000 m/s at the surface. The available data to explore the consistency of this model with upper crustal velocities in South Africa are limited. Midzi *et al*. (***Reference 5.14.270***) present the revised 1D model in terms of P-wave velocities used for routine earthquake locations by CGS. Kgaswane *et al*. (***Reference 5.14.15***) performed joint inversions of receiver functions and Rayleigh wave group velocities for 89 broadband stations deployed in Southern Africa. ***Figure 5.14.89*** compares the generic rock model adopted as the target for the V*s*-kappa adjustments with the average V_s profile from the Kgaswane *et al*. results (***Reference 5.14.150***), together with a few of the profiles from their study, including the profile from the station closest to the Thyspunt site, GRM. The average profile from Kgaswane *et al*. (***Reference 5.14.150***) indicates slightly lower velocities than the target profile, but the differences are small, and target profile provides an approximate fit to some of the individual profiles. In summary, the selected profile appears to be compatible with V_s measurements in South Africa.

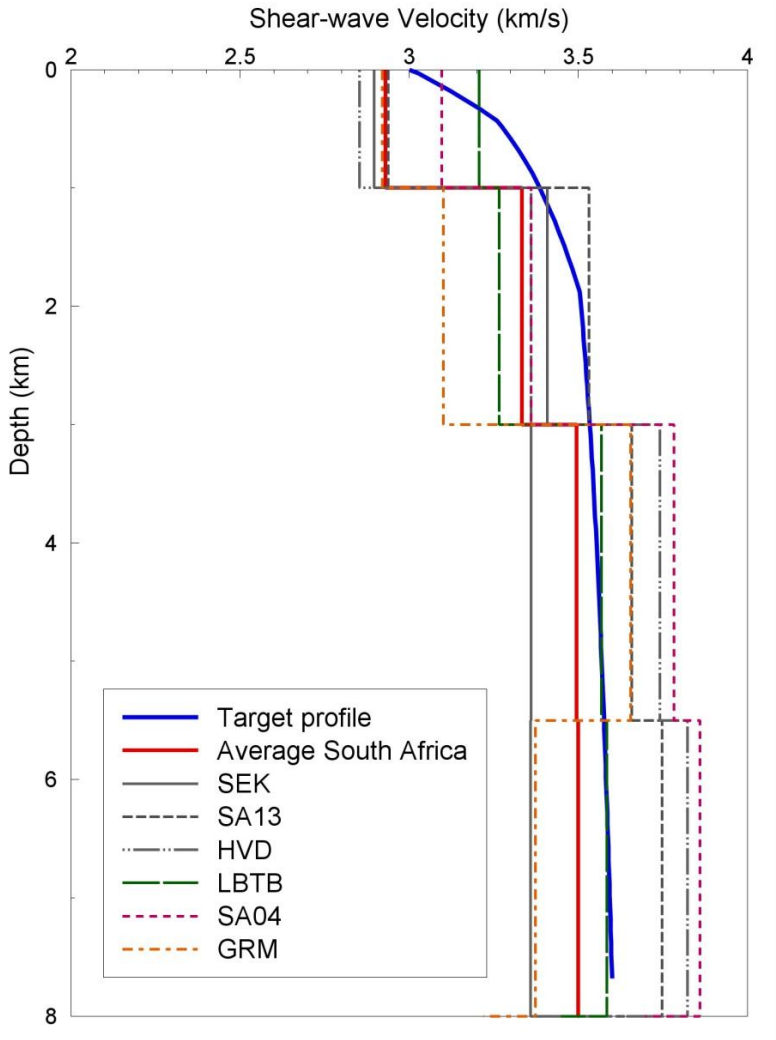


Figure 5.14-89 Comparison of the Target V_s profile with Selected Profiles and the Average V_s From Kgaswane *et al.* (*Reference 5.14.150*)

The V_s-kappa adjustment factors are anchored to a single earthquake scenario, which was selected as an earthquake of magnitude 5.75 at a horizontal distance from the site, based on disaggregation of the preliminary hazard results (***Subsection 5.14.9.3***). Using this scenario, the predicted response spectra for the three selected GMPEs were generated and then transformed to Fourier amplitude spectra using Inverse Random Vibration Theory (IRVT) (*e.g.*, ***Reference 5.14.271***). The IRVT spectra were then corrected for the differences between the attenuation filters for the host and target regions—using the Q-models of Campbell (***Reference 5.14.121***) and Rietbrock (***Subsection 5.14.5.5***)—at the scenario distance, in order to isolate the

influence of the site kappa (κ_0) on the spectra. The Q-model adjusted IRVT spectra were then plotted against frequency on a linear x-axis to identify the high-frequency portion where the spectrum is linear, which is interpreted as being indicative of the average host region κ_0 value (***Reference 5.14.119***). The frequency range over which the behaviour is linear was inferred to be 5 to 15 Hz . The host κ_0 value for each GMPE is then determined by regression, and the results obtained were: 0.0386 s for AC10, 0.0397 s for AS08, and 0.0372 for CY08. There is, of course, some epistemic uncertainty associated with the estimation of the host kappa values and the use of the unique values does not imply that these are considered to be determined with absolute uncertainty. Rather, what is important to capture is the total epistemic uncertainty in the V_s-kappa adjustments, and rather than create nine versions, for example, by selecting three host values as well as three target values, it is assumed that with the wide range of uncertainty in the target values, the uncertainty in this adjustment can be adequately captured.

In terms of the target site kappa values for the Thyspunt site, the analyses of weak-motion recordings presented in ***Subsection 5.14.4.4 (l)*** indicated a range between 0.001 s and 0.005 s could be considered reconcilable with the data. The frequency limit of 40 Hz on the recordings would suggest a limiting upper value of 0.0028 s for site kappa, but there were several reasons for the GMC TI Team to consider the possibility of higher values. One consideration was that none of the recording sites from which recordings were being used to infer site kappa values was actually the reference horizon within the Goudini formation at the Thyspunt site, and this in itself was interpreted as implying some uncertainty in the estimated maximum value. Although the measured shear-wave velocity in this horizon is very high, rock cores recovered from boreholes at the site show extensive fracturing. Campbell (***Reference 5.14.272***) cites several studies that have found that fracturing can significantly increase the damping of a rock mass and consequently the κ_0 value.

The possibility of a larger upper estimate of the site kappa value is also indicated by correlations between V_{s30} and κ_0 (***Figure 5.14.90***). Although the number of data points available for sites with shear-wave velocities as high as the Thyspunt bedrock elevation is very small, two of the three κ_0 values plotted in Figure 9.16 at this level of V_{s30} are greater than 0.0028s. The median value of κ_0 predicted by the equation Van Houtte *et al.* obtain by regression analysis for a V_{s30} of 3 000 m/s is 0.0067s (***Reference 5.14.273)***. Recently, Knetidou *et al*. (***Reference 5.14.274***) have suggested that for hard rock sites the Van Houtte *et al.* equations (***Reference 5.14.273***) may underestimate κ_0, which lends even greater support to arguments for the GMC logic-tree including a higher maximum value for the site kappa parameter.

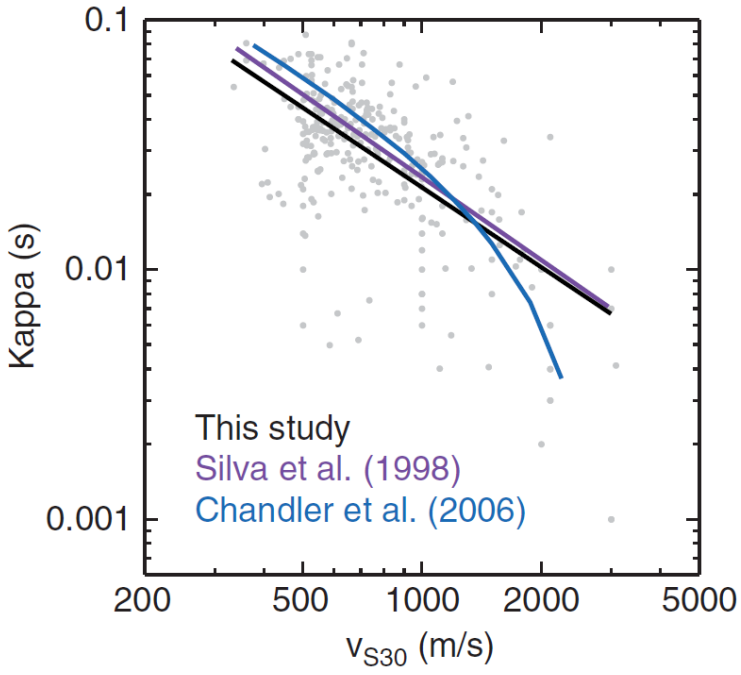


Figure 5.14-90 Data Compiled From Various Studies for Pairs of V_{s30}-κ_0, and Three Correlations Proposed Between These Two Parameters (*Reference 5.14.273*).

The final choice of the GMC TI Team was to adopt three values, with their associated weights indicated in parentheses: 0.0011 s (0.12), 0.0030 s (0.51), and 0.0050 s (0.37). Using the host kappa values associated with each of the three GMPEs and these three target values, a total of 9 adjustment factors were defined. The adjustment for the differences in V_s profiles (the host V_s profile from California was used, and the target V_s model shown in ***Figure 5.14.89***) was made using the quarter-wavelength approach of Joyner *et al.* (***Reference 5.14.275***). The nine sets of adjustment factors (three backbone GMPEs and three target site kappa values) at the 10 target oscillator periods are plotted in ***Figure 5.14.91***, from which some important observations can be made. The first observation is that the V_s-kappa adjustment factors have a very pronounced effect, as would be expected, at short oscillator periods (<0.1 s), in terms of amplifications. At longer periods (≥0.2 s) the effect is an appreciable de-amplification as a result of transformation from a low (620 m/s) to a very high (3 000 m/s) V_{s30} value, with no sensitivity to the target kappa value at all.

Analyses presented in Bommer *et al.* (***Reference 5.14.17***) explored the sensitivity of the V_s-kappa adjustments to the selection of the controlling earthquake scenario, showing that the choice was a reasonable compromise to the computationally prohibitive option of varying the adjustment factors with magnitude and distance, and at the same time was slightly conservative (thereby avoiding underestimation of the spectral ordinates at high oscillator frequencies).

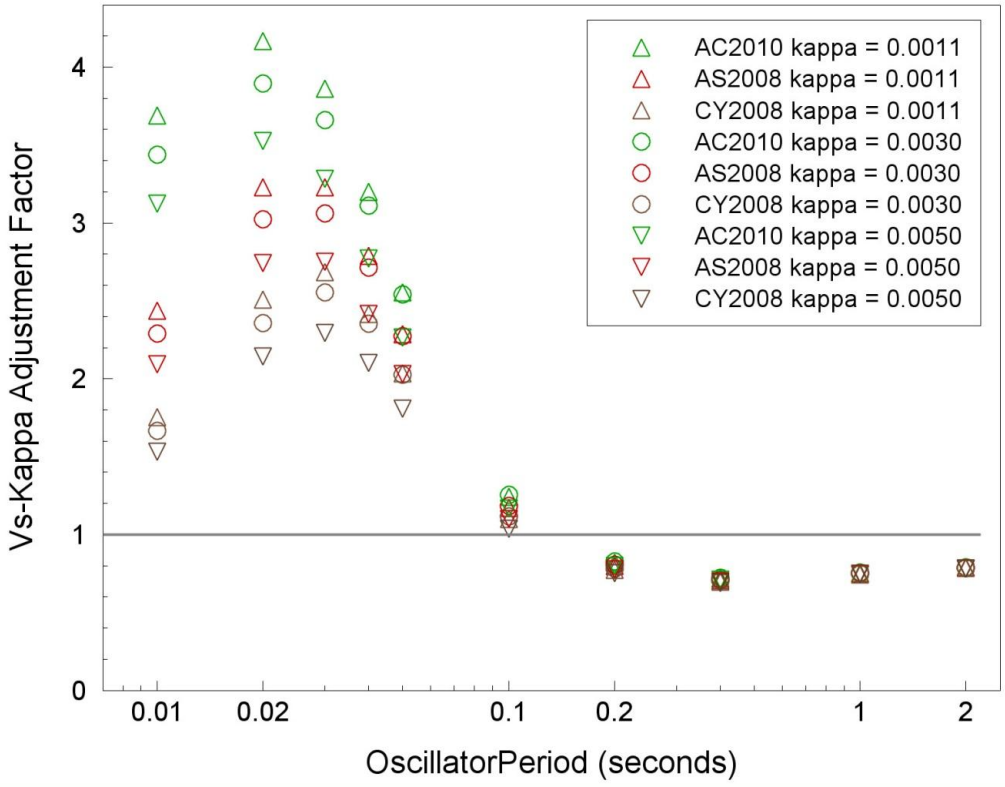


Figure 5.14-91 Final V_s-Kappa Adjustments for the Three Backbone GMPEs (*indicated by colours*) and the Three Target Site Kappa Values (*symbols*)

Although ***Figure 5.14.91*** only shows the adjustment factors at selected periods, plots of the full suite of values shows that they decay at high frequencies up to, and beyond, 100 Hz, which means that the transformed response spectra do not reach constant acceleration levels until frequencies considerably greater than 100 Hz. One consequence of this observation is that the spectral acceleration at 0.01s cannot be considered as equivalent to the peak ground acceleration (PGA). This may come as a surprise given than historically it was

often assumed that the response spectral acceleration at frequencies as low as 40 Hz were equivalent to PGA. However, it is now widely recognised that such an assumption is not appropriate for hard rock sites in stable continental regions (*e.g,.* ***Reference 5.14.276***).

ii Scaling factors and logic-tree for median motions

Having transformed the three originally selected GMPEs into 9 new equations adjusted to the Goudini bedrock horizon, the next stage was to scale these new models to create additional branches of the logic-tree that would encompass the full range of epistemic uncertainty. The primary basis for potential amplitude differences between the host regions of the GMPEs and the target region of South Africa was considered to be the stress drop parameter. For host values of the GMPEs in active regions, the TI Team adopted typical values of 80-100 bar. As discussed in ***Subsection 5.14.4.4 (I)***, the stress drop parameters determined from the stochastic inversions of South African weak-motion recordings were not considered reliable as indicators of the value this parameter would take for large magnitude earthquakes. Therefore, ranges of values were inferred from published studies used to generate predictive models in stable continental regions, leading to a range of target stress drop values of about 100-200 bar.

Adjustment scaling factors were estimated for spectral accelerations to account for host-to-target differences in stress drop parameter values using the model of Fukushima (***Reference 5.14.277***). These scaling factors were estimated for many different host-to-target stress drop differences, and for many combinations of oscillator period and earthquake magnitude (***Figure 5.14.92***).

The host-to-target scaling factors for increased stress drop (from 100 to 200 bar) shown in ***Figure 5.14.92*** indicate that the only departures from this constant scaling occur for long response periods and for small earthquakes. Given that the dominant scenarios identified in disaggregation of the hazard at longer response periods are typically associated with larger magnitude events, it seemed reasonable to adopt constant scaling factors across all periods.

© Eskom 2026/Rev 0a

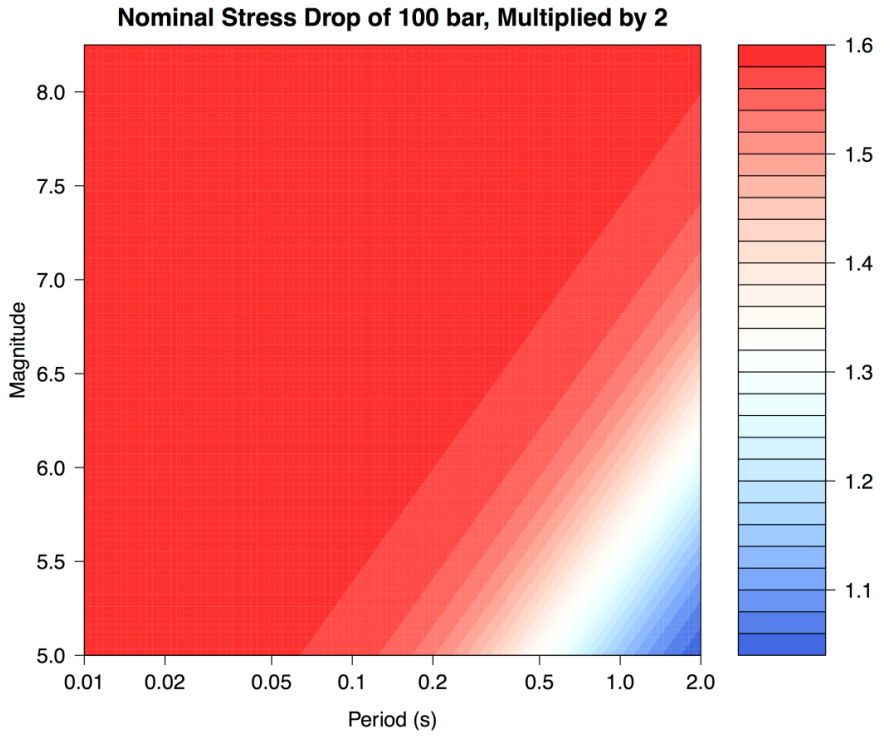


Figure 5.14-92 Factors to Be Applied to Ground-Motion Amplitudes in Order to Account for an Increase in Stress Drop from an Initial Value of 100 Bar to a New Value of 200 Bar.

The amplitude scaling factors that are applied to the backbone GMPEs are 0.75, 1.0, 1.25 and 1.5. The lower value is used to account for the fact that South Africa is an extensional stable region and one can expect lower than average stress drops in extensional regions. This point is also coupled with the fact that two NGA backbone models were derived from databases with very few extensional events. However, as all three backbone models are from active shallow crustal regions, the overriding thinking was that as South Africa is a stable region stress drop values are likely to be higher than the values implicitly represented by the original GMPE amplitudes. The amplitude scaling factors of 1.25 and 1.5 roughly correspond to factors on the stress drop of about 1.5 and just over 2 respectively. Therefore, starting with host stress drop values of around 80-100 bar for the three starting GMPEs implies that the amplitude scaled backbones represent median stress drop levels from around 60 bar to just over 200 bar. While there is precedent for ground-motion modellers to adopt larger median stress drops than this ~200 bar level, all such studies have

been within compressional regimes rather than the extensional environment relevant for Thyspunt.

Figure 5.14.93 shows the resulting logic-tree for median ground-motions. The logic-tree consists of a total of 36 branches, the weights on which are obtained from the product of the weights applied to the sequence of three branches through which the logic-tree is constructed:

- Choice of starting GMPE, all of which were considered to be of equal merit and therefore had the same weights applied (with one very minor exception to ensure summation to unity);
- The choice of target site values, represented by three target kappa values;
- The choice of scaling factors, inferred from four different ratios of host-to-target region stress drop differences.

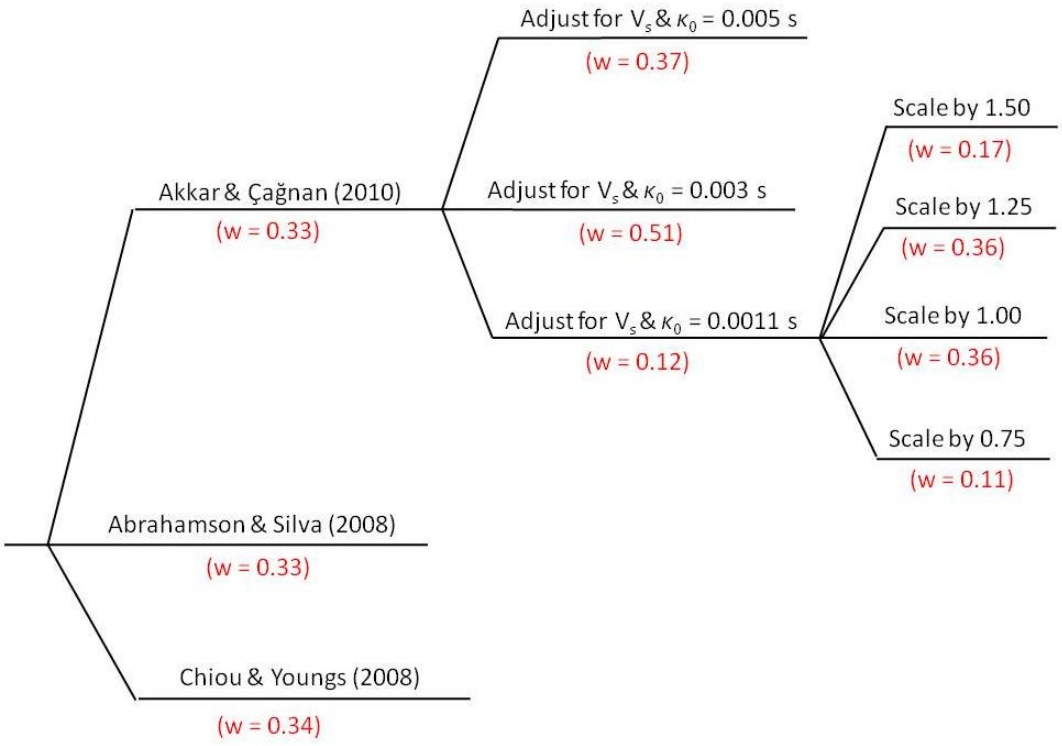


Figure 5.14-93 Logic-Tree for Median Ground Motions

(*branch weights in red*)

Although there are no strong-motion recordings from even moderate-magnitude, there is an extensive database of intensity data points (IDPs) especially compiled for this project (***Subsection 5.14.4.4***). The GMC TI Team decided to conduct an exercise using these data to explore the range of amplitudes predicted by the final GMC models, notwithstanding the considerable uncertainties associated with such an exercise. On the basis of being the most reliably determined data, in terms of both intensities and magnitudes, and also being among the larger earthquakes in the intensity database, the 1969 Ceres and 1976 Koffiefontein earthquakes were chosen for this purpose, with 87 and 103 IDPs, respectively. An important issue was to decide whether to use the backbone models before or after the application of the V_s-kappa adjustments. Although South Africa is a rocky environment, and moreover an attempt had been made to remove soft soil IDPs from the database, it was considered unlikely that a shear-wave velocity of 3,000 m/s would be representative of the locations from which intensity observations had been obtained. Therefore, the TI Team considered it more appropriate to use the GMPEs without adjustment and to set them to a V_{s30} of 620 m/s as being representative of stiff soil and soft rock sites. After reviewing and evaluating several available relationships between intensity and spectral accelerations, the Californian model of Dangkua & Cramer (***Reference 5.14.278***) was judged to be the most suitable for this application. The procedure adopted was to predict median spectral accelerations at each IDP location and then use this relationship to transform the predicted value to an equivalent intensity.

The TI Team did not consider it worthwhile to attempt to make inferences regarding regional attenuation rates from the intensity data. Consequently, it was decided to use only IDPs at distances from the earthquake source of less than 200km, partly because this is the upper limit of applicability of the GMPEs, and also because IDPs from greater distances are likely to be a biased sample by definition (reporting of felt shaking at large distances is much more likely than negative reporting). The IDPs from the two earthquakes (37 from Ceres and 41 from Koffiefontein with the distance limitation) were combined, and residuals calculated using the three backbone GMPEs multiplied by the three amplifying scale factors (1.0, 1.25 and 1.5). Linear trend lines were fitted to each set of residuals. The residuals and best fit trends are presented in ***Figure 5.14.94*** for Sa(0.3s), the spectral acceleration at 0.3 second. Similar comparisons were made for the spectral accelerations at 1.0 second.

The manner in which these comparisons were performed makes their interpretation very straightforward. The residuals are calculated as the observed minus predicted value of intensity, so a negative residual means that the models over-predict the IDPs (and a zero value implies a perfect match). If the focus is on the average residual over the chosen distance range of 200 km,

an indication of whether a specific branch (GMPE plus scaling factor combination) is under- or over-predicting the IDPs can be ascertained from whether the trend line is above or below the zero line at a distance of 100 km. Considering a 'success' all those cases where the trend line is equal to or below zero at 100 km, there are five successes at 0.3s and 6 at 1.0s. The total weights on the 'success' branches at 0.3s is 0.47 and at 1.0s the sum is 0.53.

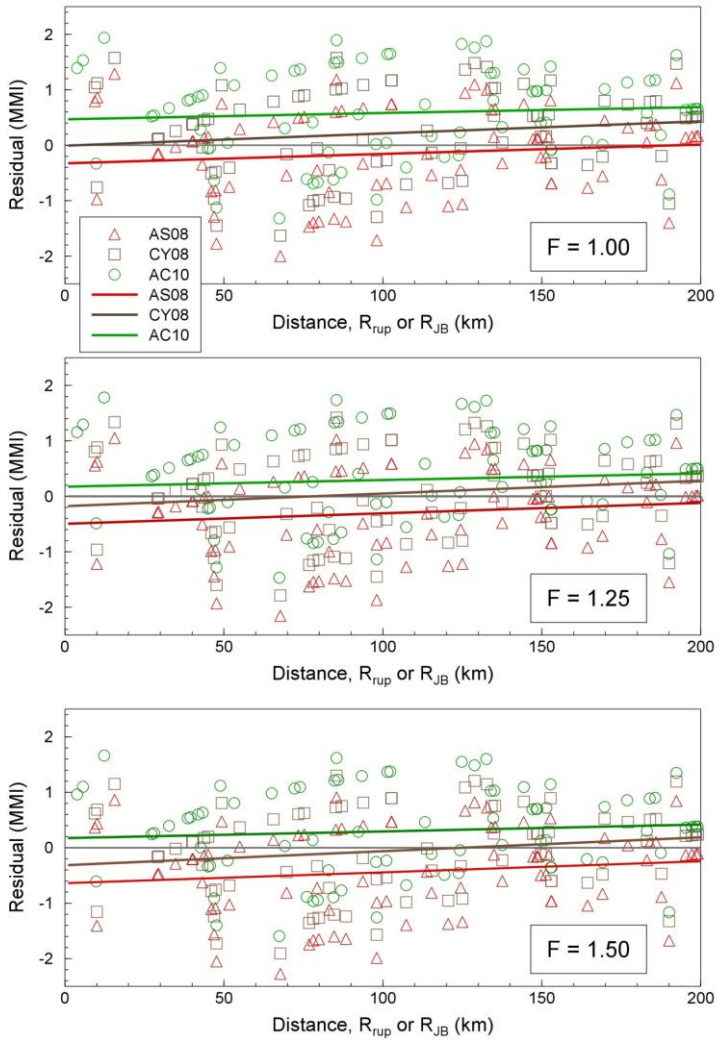


Figure 5.14-94 Intensity Residuals Calculated for the IDPs From the 1969 Ceres and 1976 Koffiefontein Earthquakes.

The residuals are calculatedfrom predictions of Sa(0.3s) from the three backbone GMPEs (with V_{s30}=620m/s) multiplied by three scaling factors as indicated on the plots. The predicted accelerations are transformed to intensities **using the North American GMICE of Dangkua & Cramer (Reference 5.14.278)**

There is no requirement that all of the branches envelope the observed motions, but the fact that half of the weight of the logic-tree corresponds to models that match or exceed the average levels of motion from these two earthquakes is interpreted as confirmation that the levels of predicted median motions are sufficient, as far as these data are concerned. Given the scatter of the residuals in these two plots, these results cannot be interpreted as conclusive validation of the GMC model, but they also do not reject the model.

Plots of the predicted median spectral accelerations from the 36 logic-tree branches for different magnitude-distance combinations suggested that a wide range of amplitudes were covered, which can be interpreted to show that ample epistemic uncertainty was captured in the logic-tree. However, for a more robust examination whether the epistemic uncertainty implicit in the GMC median logic-tree was sufficient, the spread of the predictions was compared with those from a suite of GMPEs currently in use in Central and Eastern United States (CEUS). Since CEUS is also a stable continental region with only sparse ground-motion datasets and very few recordings from moderate-to-large earthquakes, the epistemic uncertainty in ground-motion prediction in South Africa and CEUS are expected to be comparable (and certainly could not be smaller in South Africa with the currently available information). ***Figure 5.14.95*** provides a way of examining the spread of epistemic uncertainty captured by the median GMC model. This figure is a Sammon's map generated for the branches of the median GMC logic-tree, the South Africa stochastic models, and the suite of CEUS models listed in ***Subsection 5.14.7.4.(b)***. The 'distances' between points on this Sammon's map are Kullback-Leibler distances in bit; for more guidance on interpreting such figures the reader is referred to Scherbaum *et al*. (***Reference 5.14.279***). The Sammon's map is generated for oscillator periods of 0.1s and greater, to avoid the part of the spectrum where the V_s-kappa adjustments have their most pronounced effect, and for limited ranges of magnitude and distance: M_w 5-6.5, R 20-50 km. The magnitude range is selected to be relevant to the scenarios that have a dominant influence on the hazard, as well as avoiding excessive extrapolations of the South African models based on weak-motion inversions. The distance range is selected to capture the scenarios that are likely to contribute strongly to the hazard while avoiding the very near-source region where stochastic models tend to be poorly constrained (and thus to avoid influencing the plot with any erratic behaviour of the CEUS or South African models at short source-to-site distances).

The first observation that can be made is that the South African stochastic models lie within the space occupied by the GMC median models, confirming that the latter are not inconsistent with the forward modelling inferred from the weak-motion inversions. Another important observations is the spread of the

© Eskom 2026/Rev 0a

GMC models is comparable to—and slightly greater than—that of the CEUS stochastic and hybrid-empirical models, confirming that epistemic uncertainty captured for South Africa ground motions is not smaller than that generally considered for ground motions in Eastern North America.

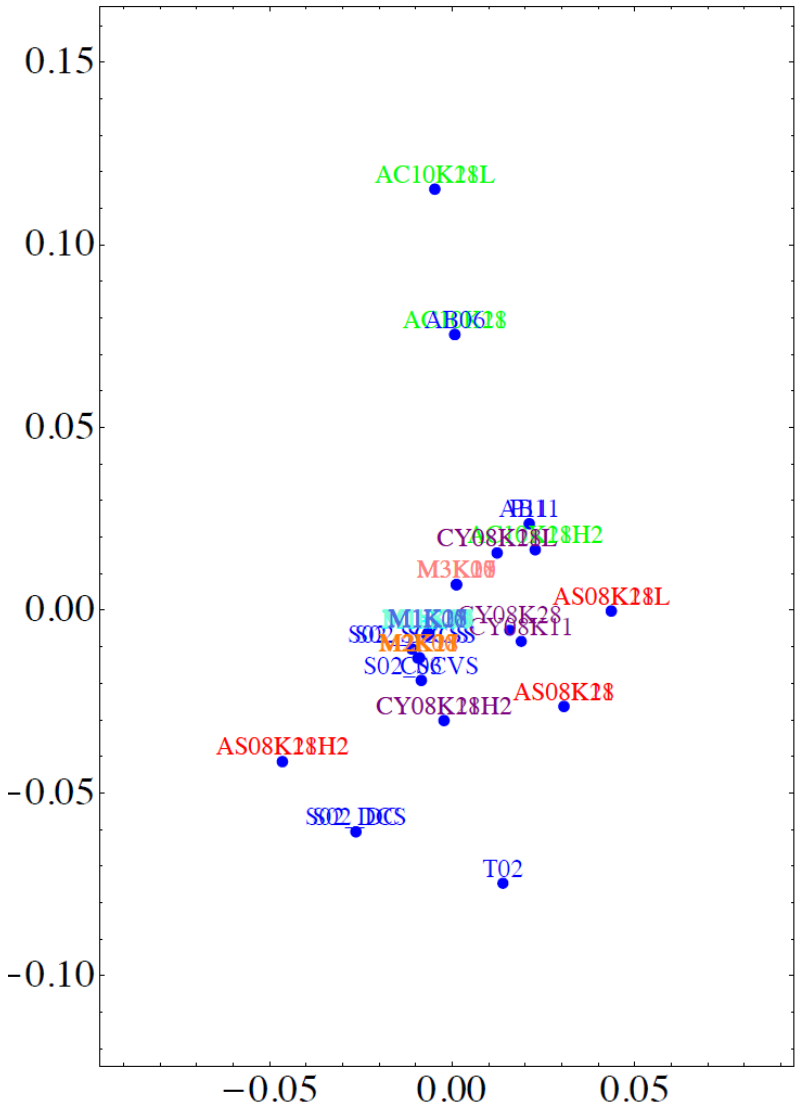


Figure 5.14-95 Sammon's Map of the GMC Median Models (*green, red and purple*) and the South African (*pink/salmon, orange and light blue*) and CEUS (*dark blue*) Stochastic Equations for Spectral Accelerations at Periods above 0.1s, of M_w 5-6.5, and Distances of 20 to 50 km.

iii Attenuation characteristics of median motions

Ground-motion prediction equations represent the influence of the earthquake source, the source-to-site travel path, and the site itself on the resulting motions. In developing the logic-tree for median motions presented in the previous subsections, adjustments were made for host-to-target differences between the regions from which the original GMPEs were selected (California, Turkey) and in which they are being applied (South Africa). The scaling factors informed by stress drop differences (***Subsection 5.14.5.5.(a) ii***) reflect a host-to-target source adjustment, and the V_S-kappa adjustment factors (***Subsection 5.14.5.5.(a) ii***) a host-to-target site correction. Before finalising the model, the GMC TI Team also considered the potential need for adjustments for path differences between the host and target regions.

Predictions from the median models over distances of 1 000 km were compared with the attenuation characteristics in South Africa inferred from the stochastic inversions of weak-motion recordings (***Subsection 5.14.4.6***). The purpose of these comparisons was to determine whether any adjustments were required to the attenuate rates in the median models, given that it is often found that in SCRs the attenuation rates are slower than in more active regions. The conclusion from such comparisons was that the adjusted and scaled GMPEs collectively encompassed the attenuation rates indicated by the stochastic model at most oscillator periods, with a slight tendency to slower attenuation rates for some branches at longer period (***Figure 5.14.96***). Since the equations in the GMC logic-tree were not found to predict excessively fast attenuation of the ground shaking, which could lead to underestimate of the hazard contributions from more remote but seismically active sources, it was concluded that no additional adjustments were required.

b) Site response model

Site response analyses require the characterization of the near surface materials in terms of the shear-wave velocity (V_S) and the nonlinear variation of shear modulus and damping ratio with shear strain (i.e., the nonlinear shear modulus reduction and damping curves). The site response analyses include Monte Carlo simulations that statistically vary the shear-wave velocity profile and nonlinear modulus reduction and damping curves.

The statistical generation of shear-wave velocity profiles involves a layering model and a velocity model. The layering model describes the variation of layer thickness (or layer transition rate) and is used to generate the thicknesses of layers within a simulated velocity profile. The shear-wave velocity model describes the statistical variation of shear-wave velocity within each layer. The layering model is based on the model developed by Toro

© Eskom 2026/Rev 0a

(***Reference 5.14.280***), which is a non-homogenous Poisson model where the mean layer thickness is depth dependent.

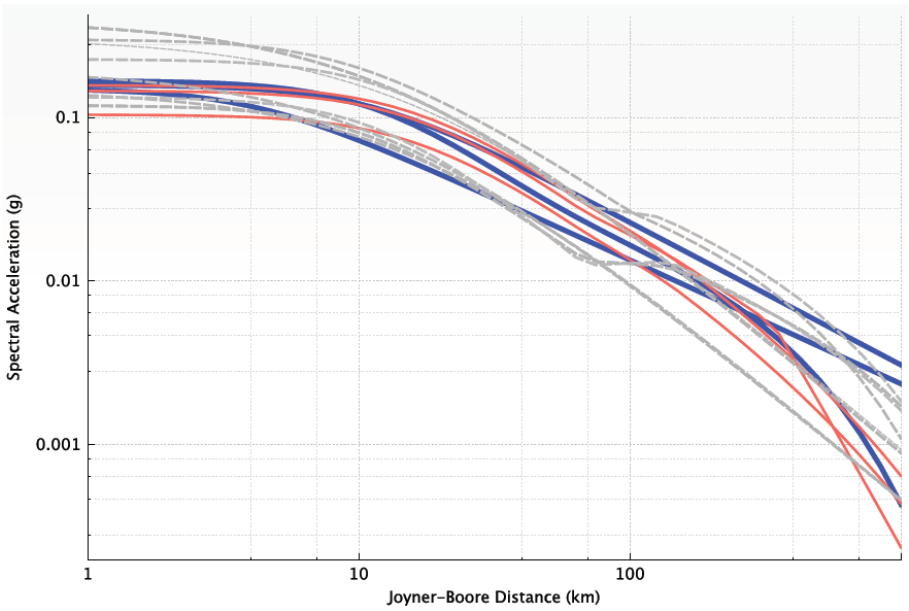


Figure 5.14-96 Comparison of Distance Attenuation from the Vs-Kappa Adjusted Backbone GMPEs for Sa(1.0s) (*blue*), the South African Stochastic Models (*red*) and a Suite of GMPEs in Current Use in the Central and Eastern US (*grey*).

The curves are for a scenario defined by the following parameters: V_{s30}=620m/s and M_w 6.5.

The median velocity profile and its standard deviation (in natural log units) as a function of depth for the Thyspunt site are developed based on the measured velocity profiles across the site. The velocity profiles measured by PS logging in the Goudini and Cederberg formations (***Subsection 5.14.4.4 (m)***) are shown in panel (a) of ***Figure 5.14.97***. The median V_s profile is shown based on all of the Goudini/Cederberg data and the proposed layered model is also shown that fits the median. The model basically increases from V_s = 1 200 m/s at the top of rock to V_s = 3 000 m/s at a depth of 80 m. The standard deviation of lnV_s (*i.e.*, σ_{lnVs}) as a function of depth is shown in panel (b) of ***Figure 5.14.97***. σ_{lnVs} is only shown for depths that have five or more profiles.

The Monte Carlo simulations of V_s may generate unrealistically larger or small V_s for a layer. The lognormal distribution is truncated to avoid these unrealistic

values. The proposed maximum and minimum values of V_s for each layer are shown in panel (a) of ***Figure 5.14.97***). These values were assigned as +/- 2.5 σ_{lnVs} values with an additional physical constraint of a maximum of 3 800 m/s. Generally these proposed maximum and minimum values bound the range of measured V_s values.

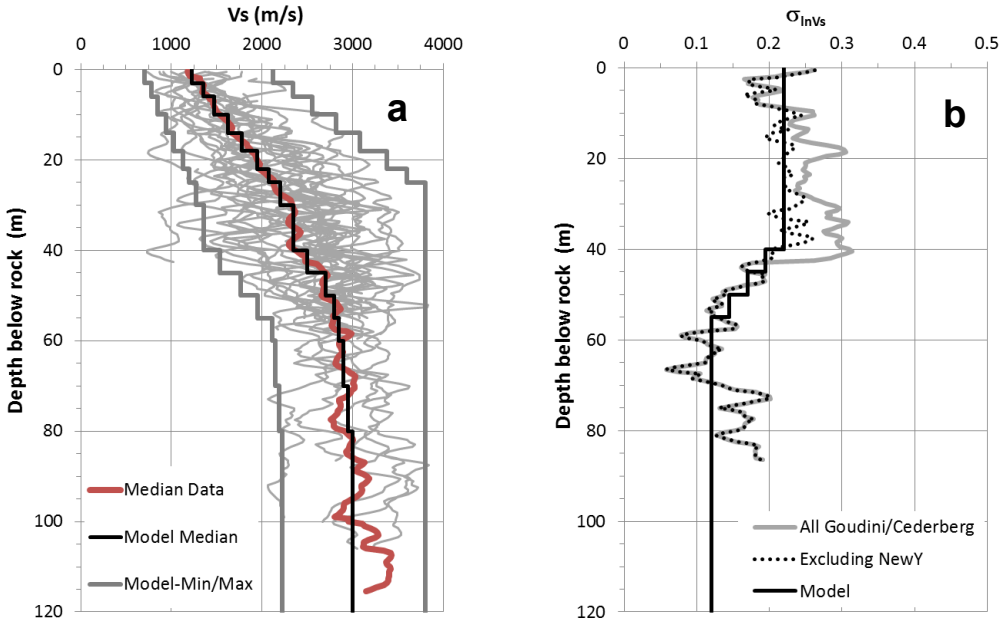


Figure 5.14-97 (a) Median Shear-Wave Velocity Profile (b) Associated Standard Deviation.

The final part of the velocity model is the model for interlayer correlation. The interlayer correlation coefficient (ρ) is used to assign shear-wave velocities in a layer based on the assigned value in the previous (*i.e.*, upper) layer. Toro (***Reference 5.14.280***) developed a ρ model that is dependent on depth and the distance between the mid-point of adjacent layers; analyses were performed to evaluate the interlayer correlation for the velocity data from the Thyspunt site using the Toro approach (***Reference 5.14.280***). To illustrate the velocity profiles generated using the models described, a subset of 10 shear-wave velocity profiles are plotted versus depth in ***Figure 5.14.98***. These 10 realizations show that the layer thicknesses vary from profile to profile and the thickness generally increases with depth. The simulated profiles are located both above and below the median V_s model and a single profile may be above the median at some depths and below the median at others.

© Eskom 2026/Rev 0a

Ten simulated velocity profiles are not enough to ensure that the median and standard deviation of the shear-wave velocity model are captured. Using 100 simulations, both the median velocity profile and the variation of σ_{lnVs} with depth are captured by the Monte Carlo simulations, as illustrated in ***Figure 5.14.99***.

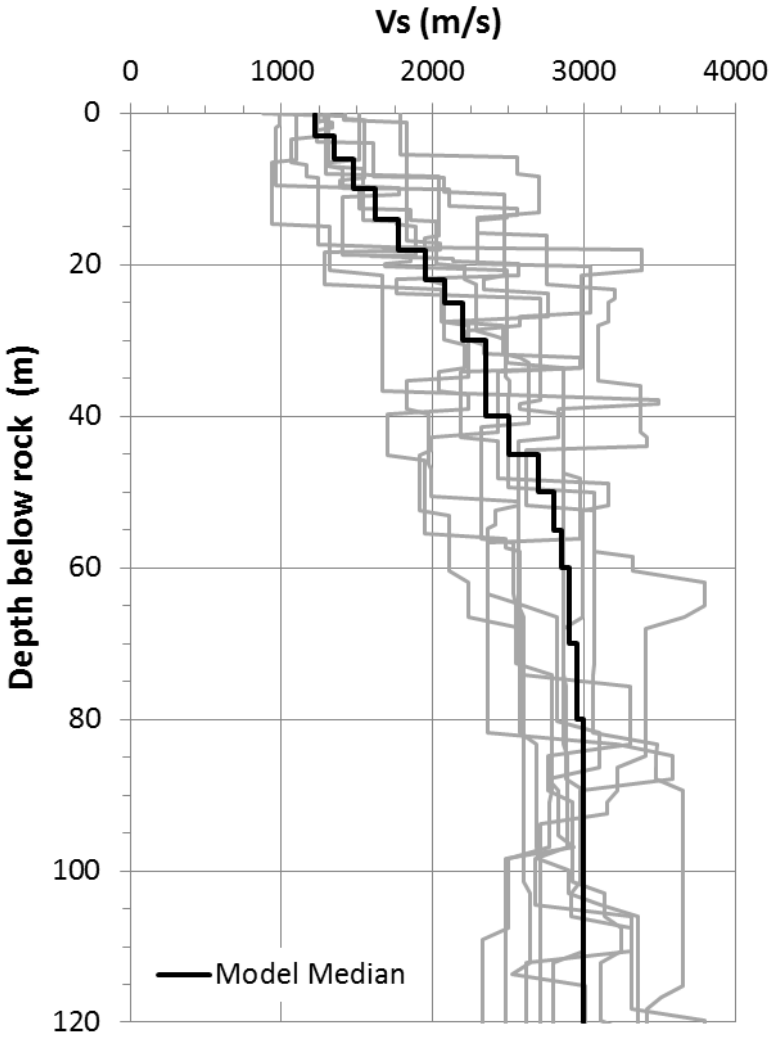


Figure 5.14-98 Examples of Simulated Shear-Wave Velocity Profiles

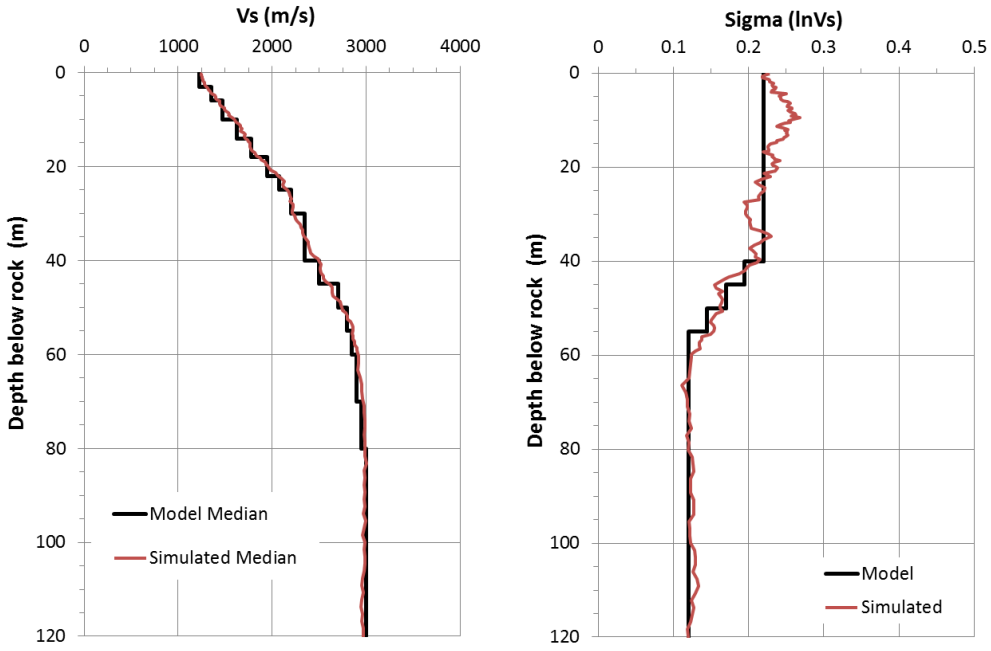


Figure 5.14-99 Median Shear-Wave Velocity and σ_{lnVs} Profiles of Simulated Shear-Wave Velocity Profiles.

The nonlinear properties of the rock describe the reduction in shear modulus (G/G_{max}) and the increase in damping ratio (D) with shear strain. It is difficult to measure the nonlinear properties of rock in the laboratory because of the influence of discontinuities and jointing on the results. Because of the significant jointing in the geologic units at the Thyspunt site, no dynamic laboratory testing was performed on rock cores from the site. However, relevant studies from the literature were identified to inform the selection of the nonlinear rock properties.

Most of the published laboratory studies on rock focus on measuring the small-strain shear modulus (G_{max}) and small-strain damping ratio (D_{min}) rather than the variation of these properties with shear strain. One notable exception is ***Reference 5.14.281***, a study that measured the modulus reduction and damping curves of welded volcanic tuff formations from Nevada and New Mexico, USA. While volcanic tuff formations are different from the sedimentary formations at Thyspunt, the measured shear-wave velocities of the tuff specimens are similar to those measured at Thyspunt and are considered applicable to the sedimentary units at Thyspunt. An additional source of information regarding the nonlinear properties of rock is ***Reference 5.14.282***). The Schnabel curves (***Reference 5.14.282***) generally are consistent with the

range reported by Choi (***Reference 5.14.281***) and thus are used as the basis for the curves used in the analyses for Thyspunt. However, the original Schnabel damping curve (***Reference 5.14.282***) is adjusted to larger damping values based on the highly weathered and fractured nature of the rock at Thyspunt and the observed increase in damping due to cracking reported by Choi (***Reference 5.14.281***).

The Darendeli & Stokoe (2001) models for nonlinear property variability (***Reference 5.14.283***) are used for the Monte Carlo simulations. The Darendeli & Stokoe model (***Reference 5.14.283***) assumes that the parameters G/G_{max} and D are normally distributed at each strain level and that the standard deviation for each is a function of the magnitude of G/G_{max} and D, respectively. To avoid the simulation of unphysical G/G_{max} and D values, the normal distributions were truncated at 0.05 and 1.0 for G/G_{max}, and 0.1% and 15% for D. A correlation coefficient of -0.5 was used to model the negative correlation between the G/G_{max} and D curves. Examples of modulus reduction and damping curves generated by the Monte Carlo simulations are shown in ***Figure 5.14.100***.

The site response analyses were performed using the program *Strata* (***Reference 5.14.284***). The program *Strata* performs one-dimensional equivalent-linear site response analysis in which the nonlinear response of the soil and rock is modeled through strain-compatible properties. The site response can be computed using either input time series or the RVT approach (*e.g.*, ***Reference 5.14.285 and 5.14.286***). The RVT approach was used in this project because the input excitation can be defined from a response spectrum using inverse RVT (*e.g.*, ***Reference 5.14.287***), which avoids the need of generating time-domain input motions and also results in a significant reduction in computational costs. *Strata* also allows users to perform Monte Carlo simulations that statistically vary the site layering, the shear-wave associated with each layer, and the nonlinear properties.

© Eskom 2026/Rev 0a

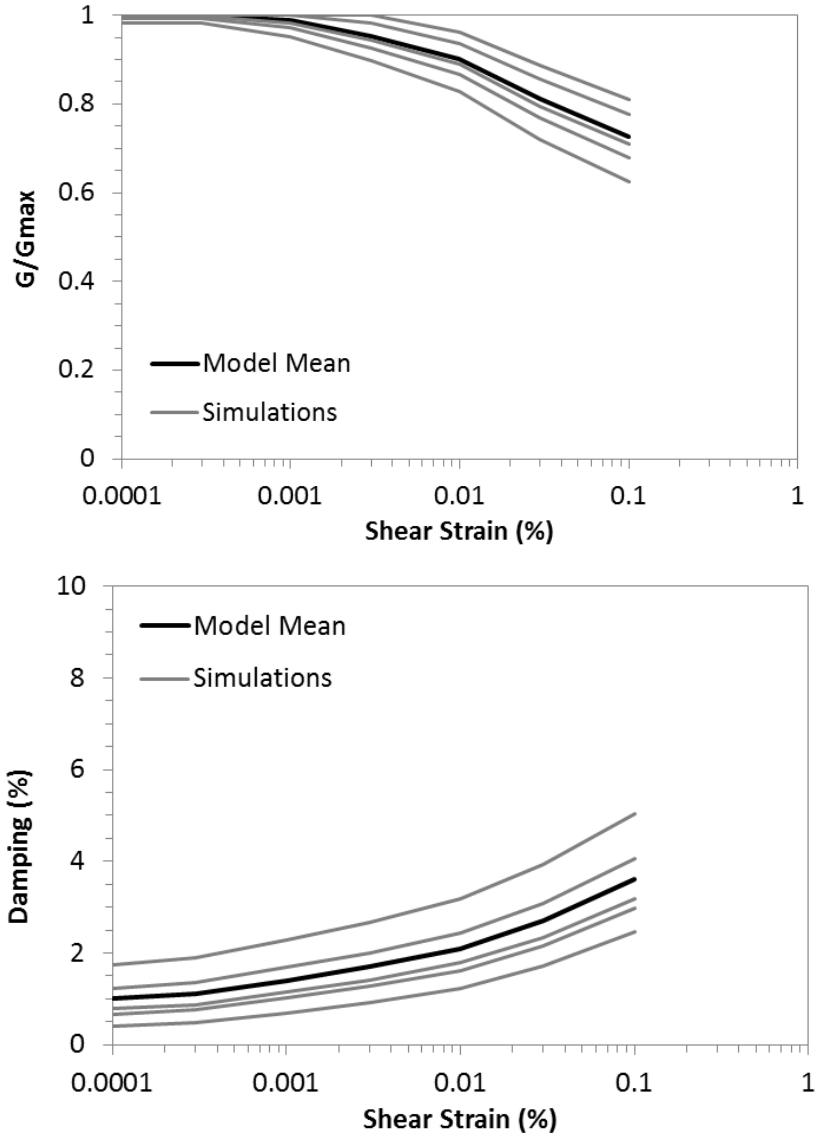


Figure 5.14-100 Simulated Modulus Reduction (*upper*) a and Damping (*lower*) Curves.

The input motions for the site response analyses were developed using uniform hazard spectra (UHS) for the reference rock condition. Following RG 1.208 (***Reference 5.14.3***) high-frequency (HF) and low-frequency (LF) scenario spectra were generated for the UHS at three hazard levels (annual frequencies of exceedance (AFE) equal to 10^{-4}, 10^{-5}, and 10^{-6}) resulting in 6 different input response spectra. The HF spectra were scaled to the UHS at a frequency of 7.5 Hz, and the LF spectra were scaled to the UHS at a frequency of 1.75 Hz.

Each scenario spectrum was developed using the magnitude and distance disaggregation for each AFE in either the HF or LF range.

For each magnitude and distance scenario, a weighted response spectrum was defined from the nine V_s-kappa corrected GMPEs developed as part of this project and scaled linearly to match the UHS. The resulting scenario spectra are plotted in ***Figure 5.14.101***; the intensity of these spectra span about one order of magnitude. A suite of input motions associated with only three hazard levels was deemed sufficient for the Thyspunt site because it is very stiff and the amplification factors will not vary significantly with the bedrock accelerations. For each input motion, 100 Monte Carlo simulations were performed on the site properties (*i.e.*, shear-wave velocity profile and nonlinear property curves).

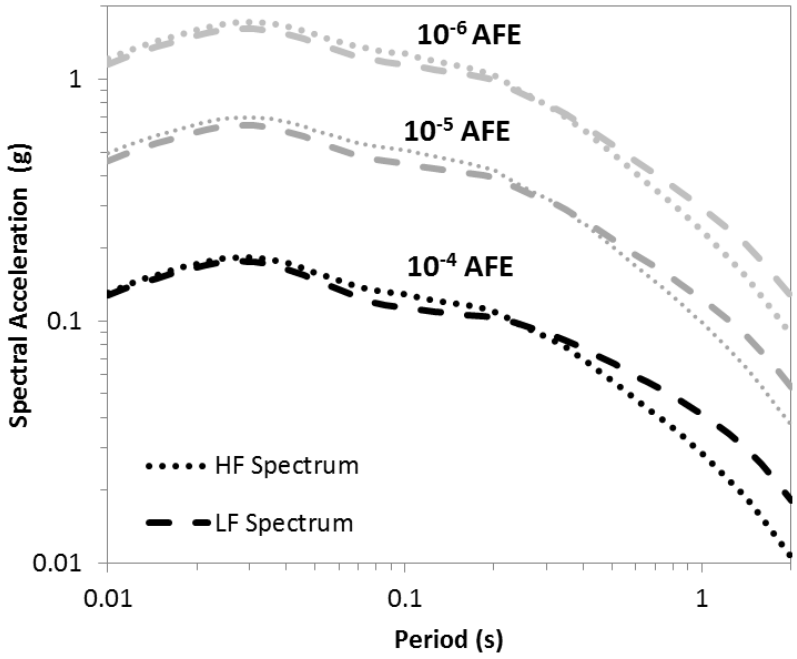


Figure 5.14-101 Scenario Spectra for AFE = 10^{-4}, 10^{-5}, and 10^{-6} Used as Input Into the Site Response Analyses

The amplification factors (AF) computed from the 10^{-5} LF scenario spectrum are plotted in panel (a) of ***Figure 5.14.102***. The median AF indicates amplification of about 1.2 to 1.5 at periods less than 0.25 s, with decreasing values of AF towards 1.0 at periods greater than 0.25 s. There is variability in the computed AF because of the variability in the site properties modeled

through the Monte Carlo simulations. This variability is largest at periods less than 0.1 s. The standard deviation of the natural logarithm of AF (σ_{lnAF}) is plotted in panel (b) of ***Figure 5.14.102***. The σ_{lnAF} varies from about 0.2 at short periods to close to 0.0 at periods greater than 1.0 s.

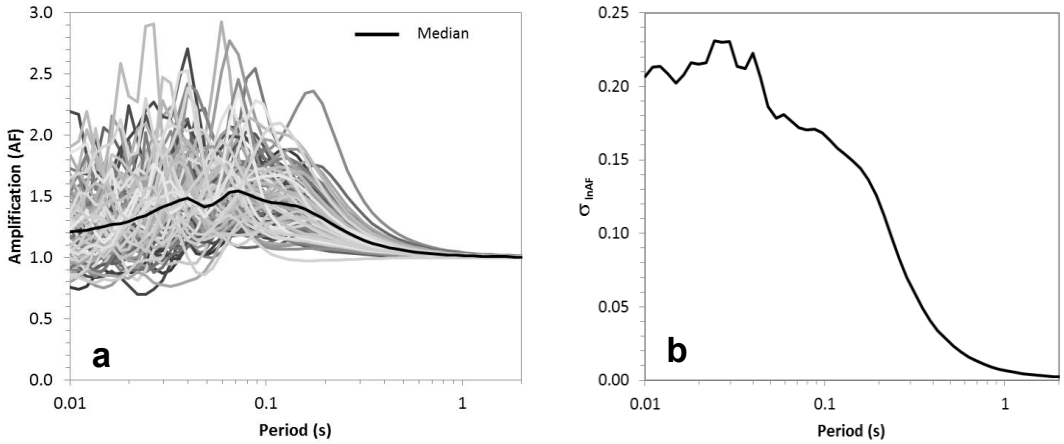


Figure 5.14-102 (a) Computed Amplification Factors for 100 Monte Carlo Simulations and the AFE 10^{-5} LF Scenario Spectrum (b) Standard Deviation of the Natural Logarithm of AF (σ_{lnAF}).

The site response results were used to develop AF relationships that describe the variation of AF with input Sa_r and provide an associated σ_{lnAF}. Plots of the computed AF data vs. bedrock spectral accelerations showed that the large stiffness of the site resulted in a very minor dependence for AF. A linear relationship was fit between the natural logarithm of AF and the natural logarithm of bedrock spectral acceleration to model the median AF, and an associated σ_{lnAF} was computed for each period.

Epistemic modeling uncertainty, as defined by Toro *et al.* (***Reference 5.14.288***) as the uncertainty in the true bias of a model, is associated with all types of site response models used in engineering seismology. One-dimensional site response analysis does not capture all aspects of wave propagation at a site, and this issue potentially results in a bias with respect to the true site amplification. Currently, there are no published estimates of the uncertainty in the bias of site amplification estimates. Therefore, an analysis of a small set of Japanese KiK-net borehole array sites was used to inform the selection of this

epistemic uncertainty. The mean bias between predicted equivalent-linear amplification factors and recorded amplification factors was computed for nine KiK-net soil sites. The standard deviation of the mean bias values across the nine sites (σ_μ) is a measure of the epistemic uncertainty associated with the one-dimensional equivalent linear analyses at those sites. The computed σ_μ was about 0.15 at short periods, increased to about 0.4 for periods between 0.1 and 0.5 s, and decreased towards 0.25 at a period of 2.0 s.

Because the Thyspunt site is a rock site and the levels of site amplification are relatively small, it is expected that σ_μ is smaller than those for soil sites. Additionally, because the site amplification approaches 1.0 at longer periods, σ_μ is expected to decrease with increasing period. Using this reasoning σ_μ was taken as 0.15 at periods less than 0.1 s and decreasing to 0.05 at periods greater than 1.0 s. The values of σ_μ were combined with the σ_{lnAF} values using the square root of the sum of the squares to generate a total standard deviation (σ_{total}) used in the convolution calculations of the bedrock hazard with the site amplification functions.

The site amplification factors at different oscillator periods, and their insensitivity to the intensity of the bedrock accelerations, are shown in ***Figure 5.14.103***.

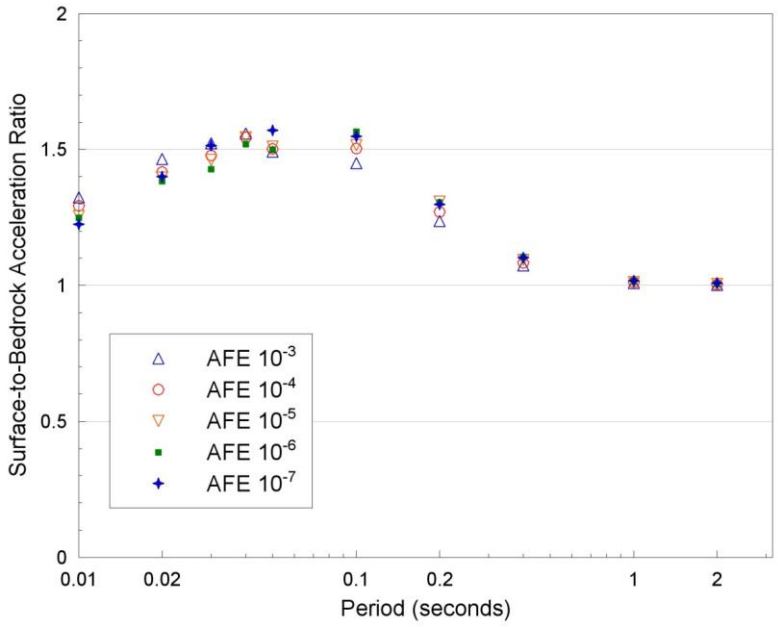


Figure 5.14-103 Ratios of Surface-to-Bedrock Spectral Accelerations at Various Mean Annual Exceedance Frequencies

c) Logic-tree for Aleatory Variability

The final element of the GMC logic-tree was a model for the aleatory variability, which represents the standard deviation (or sigma value) associated with the median predictions. In applying a GMPE to the assessment of seismic hazard at a specific location, the interest is in the variation of motions at this site due to different earthquakes that could occur over time. Since it is rare to have recording from the location under study, and even in the few cases where such recordings exist they will cover at most a few decades, PSHA generally invokes what is referred to as the ergodic assumption (***Reference 5.14.289***). The ergodic assumption essentially states that variability over space can be used as a substitute for variation of time, and it is invoked in practice since the sigma values calculated from regression analyses to develop GMPEs represent the variability across many different sites (and sometimes many regions). Where there are multiple recordings from individual sites, they display lower variability than indicated by the sigma values of GMPEs (*e.g.*, ***Reference 5.14.290***), the reason being that there are components of the behaviour at an individual site that are repeated in all cases and therefore do not contribute to variability. The effect is even more pronounced when there are multiple recordings from a single site of earthquakes associated with a single seismogenic source because in that case there are repeatable effects of both the path and the site.

If the repeatable contributions to the seismic motion at the site of interest can be modelled through an appropriate adjustment to the median predictions, then the sigma value can be reduced—to a value referred to as 'single-station sigma' (***Reference 5.14.290***)—by an amount that reflects the variability of the site term. The single-station sigma concept can also be invoked if epistemic uncertainty in the site term is incorporated into the logic-tree for the PSHA. In such a case, the net effect on the mean hazard is expected to be zero since the increased epistemic uncertainty balances the decreased aleatory variability, but it does mean that the division between randomness and uncertainty is being applied more completely. The ergodic assumption effectively folds the epistemic uncertainty regarding individual site terms into the sigma value of the GMPE, representing it as aleatory variability.

The concept of single-station sigma (or, more accurately, partially non-ergodic sigma) was invoked for the Thyspunt GMC model because of two factors which are interpreted as removing from the aleatory variability the component associated with the repeatable site term. The first is the use of multiple target kappa values to define site adjustment factors (***Subsection 5.14.5.5.(a)***) and the second the randomisations of the dynamic site properties in the site response analyses (***Subsection 5.14.5.5.(b)***). If the variability associated with the site term is removed and accounted for elsewhere, as was the case for

Thyspunt, the remaining components of the variability are the between-earthquake sigma and the single-station within-earthquake sigma (***Reference 5.14.291***). Values for the latter have been found to be relatively constant across different regions and tectonic environments. ***Figure 5.14.104*** shows a comparison of the values of single-station within-event sigma and ergodic within-event sigma for five different regions. Observe that the variability of the ergodic values across tectonic regions are higher than the variability observed in the single-station values. The lack of regional dependence of the single-station within-event components implies that they are more readily "exportable" to different regions, and that global datasets can be used to estimate their values.

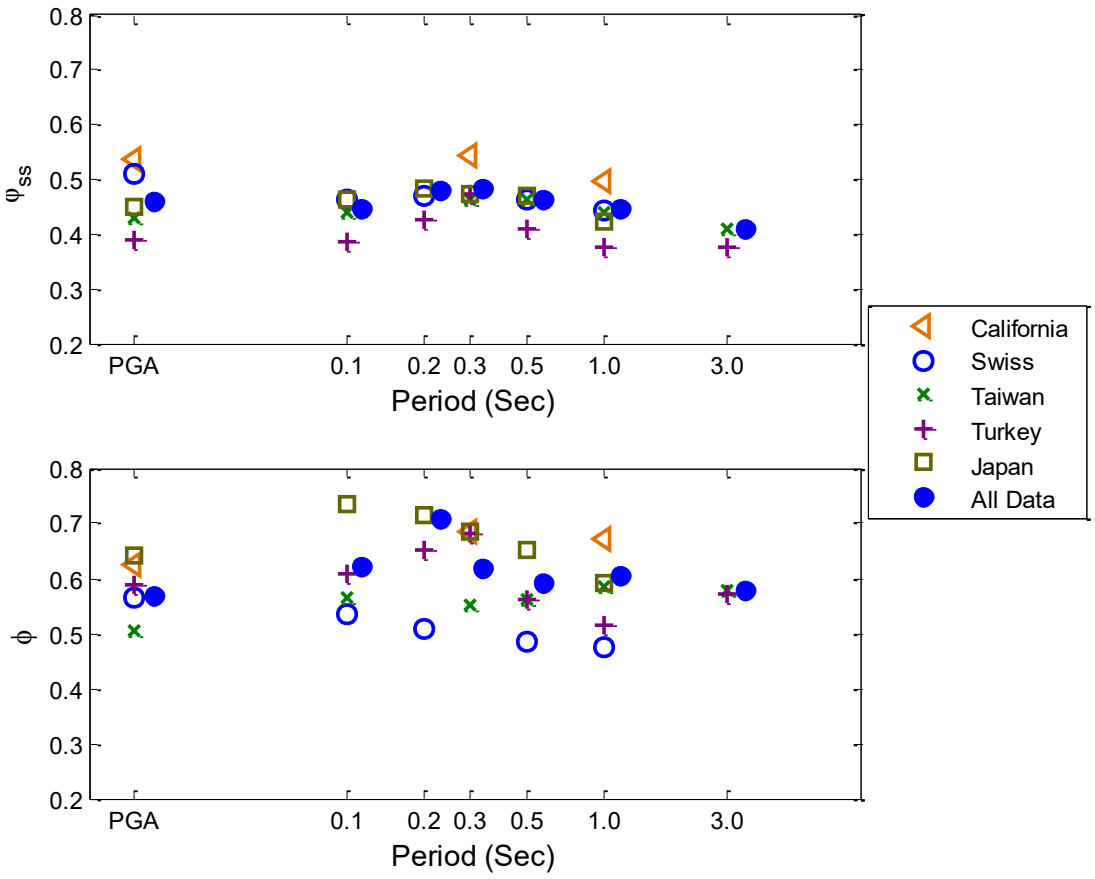


Figure 5.14-104 Values of Single-Station phi (ϕ_{ss}) and Ergodic phi (ϕ) for Different Regional Data Sets (*Reference 5.14.268*).

Data is for records from earthquake of magnitude higher than 4.5, and for distances lower than 200 km

The sigma logic-tree has two branches for the median sigma models: one for a magnitude-independent (homoskedastic) model, one for a magnitude-dependent (heteroskedastic) model. The two branches represent the differing views of the scientific community on magnitude dependency of sigma (e.g. ***Reference 5.14.268***). Moreover, the two branches represent a trade-off between model simplicity (*e.g.*, constant sigma) and an ability to properly constrain the values of sigma for a magnitude-dependent model. The GMC TI gave a higher weight (0.6) to the heteroskedastic model than to the homoskedastic model (0.4). The rationale for this 60:40 weighting in favour of the heteroskedastic model is that the GMC TI Team's evaluation concluded that the technical community remains divided over the issue of possible magnitude dependence of sigma, but there is slightly greater support in favour of heteroskedastic sigma. This weight distribution applies to both the single-station within-event variability model and between-event variability model. Median values of these two components of sigma and their associated epistemic uncertainty bounds were then inferred from published studies and the specific details of the site response modelling at Thyspunt to create three alternative branches for both the homoskedastic and heteroskedastic models.

his included consideration of the fact that the V_s-kappa adjustment factors are practically identical for response periods of 0.2 s and greater (***Figure 5.14.91***) and that there is almost no variability in the site amplification factors at periods of 0.5 s and above (***Figure 5.14.102***). The resulting uncertainty in the logic-tree for median ground motions is very low at long periods, which is akin to stating that there is no epistemic uncertainty on the site term at long periods. This result is not unreasonable when considering that very stiff sites are unlikely to be affected by long period seismic waves. On the other hand, the GMC TI Team considered that some degree of site-to-site epistemic uncertainty for the site terms at long periods was desired. The approach taken to correct this was to increase somewhat the single-station within-event standard deviation to represent the influence some of the epistemic uncertainty in the site term. This corrective term was applied to ensure a minimum level of epistemic uncertainty in the site-related component of sigma, and consequently was added only at periods greater than 0.2 s (***Figure 5.14.105***).

Weights were then assigned to these alternatives to yield the final sigma logic-tree (***Figure 5.14.106***). Details of the branch models are presented in ***Reference 5.14.17***. The higher values of sigma for both the heteroskedastic and homoskedastic cases approximated very closely to fully ergodic sigmas, thus assigning a 20% probability to the possibility that the option of no reduction in sigma for the capture of uncertainty in site terms in the V_s-kappa adjustments and the randomisations in the site response analyses.

© Eskom 2026/Rev 0a

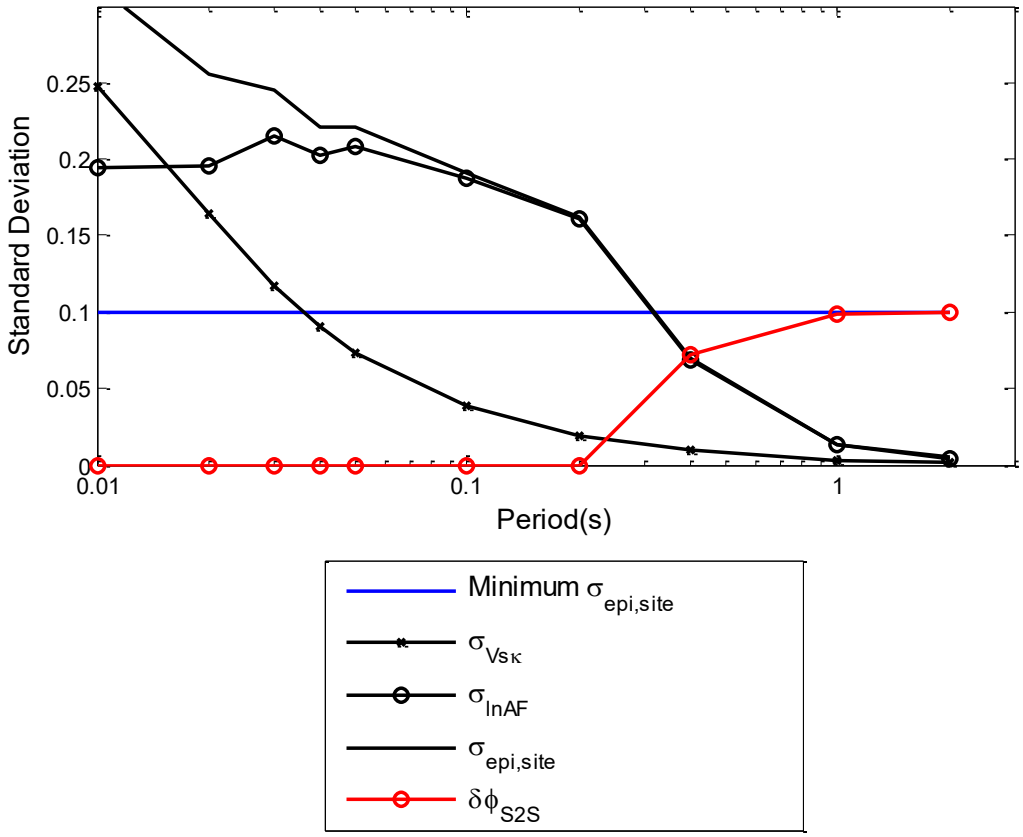


Figure 5.14-105 Different Components of the Epistemic Standard Deviation. **$\sigma_{Vs\kappa}$ is the standard deviation implicit in the median logic tree branches for the Vs-kappa correction. σ_{lnAF} is a preliminary estimate of the standard deviation of the site amplification function. These two standard deviations are combined in the $\sigma_{epi,site}$ term. The blue line represents a minimum target value for the epistemic uncertainty in the site term chosen by the GMC TI team. The red line ($\delta\phi_{S2S}$) is the additional component to single-station within-event standard deviation needed to reach this target**

The six branches of the sigma logic-tree were used in conjunction with each of the 36 branches on the logic-tree for median ground motions, leading to a total of 216 braches on the final GMC logic-tree.

d) PPRP Review and Final Evaluation

In a SSHAC Level 3 process, the Participatory Peer Review Panel (PPRP) fulfils a very important role. Following the issue of the final PSHA report, a SSHAC Level 3 project may be deemed successful if the PPRP concurs that the project has conformed to the requirements of a SSHAC Level 3 process and that all technical assessments have been adequately defended and documented.

From the preceding paragraph and consistent with the SSHAC guidelines, the PPRP fulfils two roles, the first being technical review. This means that the PPRP is charged with ensuring that the TI Teams have duly considered the full range of available data, methods and models in the hazard assessment, and adequately documented and justified all technical decisions. The second role of the PPRP is process review, which means ensuring that the project meets all the requirements of a SSHAC Level 3 process. These requirements include the recruitment of suitably qualified individuals to all the key roles in the project and the need to adhere to the responsibilities that are attendant to each role, particularly for the TI Teams, which are required to act as impartial evaluators.

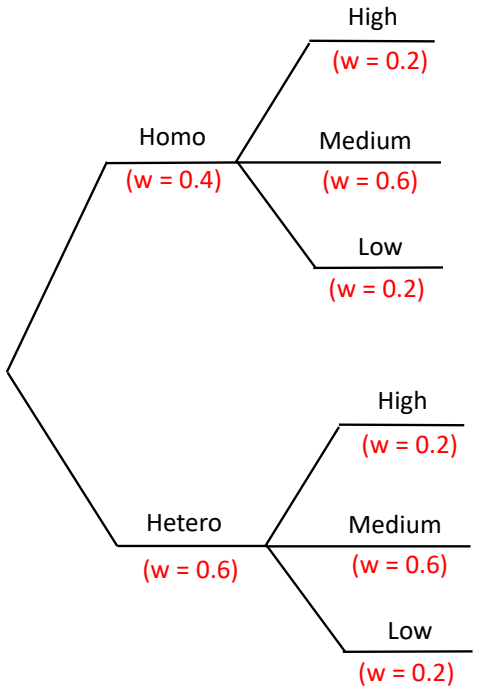


Figure 5.14-106 Schematic Representation of the Sigma Logic-Tree

© Eskom 2026/Rev 0a

As ***Figure 5.14.41*** indicates, the PPRP is required to possess deep knowledge of PSHA as well as technical expertise in SSC and GMC subject matters and extensive experience of the SSHAC process. This requirement must be filled collectively rather than individually by the members of the Panel, although it would generally be the case that each member would be expected to be fully conversant with the mechanics of PSHA and to also be a recognised expert in either SSC or GMC issues. The PPRP members are also expected to act as entirely impartial in terms of their assessment of the technical bases for the models developed by the TI Teams. This means that the PPRP is charged with judging whether the evaluation phase of the project identified all relevant data, methods and models, and whether these were all given due consideration. Equally, the PPRP must assess whether the technical bases for the final logic-tree are adequately documented and justified, both with regards to models incorporated into the final SSC and GMC models, and those that are excluded. The PPRP must also be satisfied with the rationale presented by the TI Teams for the weights on the logic-tree branches. This does not mean, however, that the PPRP members must necessarily agree entirely with the choices of models and parameter values that populate the final logic-tree branches or with the weights assigned to these branches; the Panel need only be convinced that the explanations given by the TI Teams for the logic-tree branches and weights are sufficiently detailed and also defensible. In this regard, the PPRP is charged with remaining objective in their assessments. Towards this end, all members of the PPRP must serve in a personal capacity in the project, and not as representatives of the organisations for which they work. This is a very important stipulation since PPRP members must stay focused on fulfilling the requirements of technical and SSHAC process review, which may not align with their usual duties within their organisations.

Another requirement of the PPRP is that they reach consensus positions and common conclusions. Ensuring that these goals are finally attained is one of the duties of the PPRP chairman, who must also ensure that Panel members remain objective in their assessments. The PPRP Chairman is the point of contact between both the sponsor and the Project Manager for the Panel, and is expected to take the lead in ensuring timely production and delivery of the PPRP reports after each Workshop and for the review of this final report. The PPRP Chairman is also expected to communicate to the Project Manager in a timely manner any concerns that may arise during the project, and to energetically pursue these concerns until a satisfactory response or resolution is received. The chairman of the PPRP was Dr Hilmar Bungum, who met all these requisites and filled all the requirements of the role. Dr Bungum's curriculum vitae, together with those of the other PPRP members (and all the technical participants in the project) is included in Appendix 1 of the final PSHA report (***Reference 5.14.17***).

© Eskom 2026/Rev 0a

The PPRP for the Thyspunt PSHA consisted of five renowned individuals who are all distinguished experts in the field of seismic hazard assessment. The PPRP members collectively have produced hundreds of widely-cited publications on tectonics, seismicity, ground-motion prediction, seismic hazard analysis and site response. The PPRP members also all have extensive professional experience of participating in PSHA projects worldwide, including many studies in regions of low seismic activity and also in projects conducted within a nuclear regulatory context. All of the members of the PPRP had prior experience of participating in SSHAC Level 3 or 4 projects.

The PPRP fulfilled its review role through a number of actions throughout the project, engaging from the initial stages of the work so that there were ample opportunities to raise issues of concern early in the study to allow these to be addressed well before the models and hazard calculations are finalised. Specifically, in the Thyspunt PSHA project, the PPRP engaged in the following ways to conduct their review and provide feedback:

- Review and comment on proposed lists of Resource Experts invited to participate in Workshop #1;
- Attendance as observers at Workshop #1;
- Review and comment on proposed lists of Resource and Proponent Experts invited to participate in Workshop #2;
- Attendance as observers at Workshop #2;
- Panel representative present as an observer at each SSC and GMC Working Meeting (eight meetings in total);
- Active participation in Workshop #3, including interrogation of the TI Teams on the bases for the SSC and GMC models;
- Private meetings the day before and day after Workshops;
- Informal feedback meetings with PMT and TI Leads at the end of each day of all Workshops;
- Written feedback reports at the end of each Workshop, and review of the written responses to these reviews from the TI Leads;
- Review of the draft version of this report, including compilation of individual panel member comments at a meeting in March 2013;

© Eskom 2026/Rev 0a

- Review of TI Leads' responses to review of draft final report and review of the final report.

The continuous engagement of the PPRP throughout a SSHAC Level 3 project makes it possible for the Panel to judge whether the SSHAC process was correctly followed. In particular, the PPRP needed to be assured that there was open exchanges among the members of each TI Team, so that the final consensus models were established through extensive technical challenge and defence rather than through coercion. Equally, the PPRP were charged with establishing the degree to which all members of each TI Team assumed ownership of the final models. From the perspective of technical review, the advantage of the continuous engagement by the PPRP was that issues, questions and concerns—whether relating to data or models that had not been considered, or technical issues that were unresolved—could be raised at an early stage. This allowed such issues to be effectively addressed by the TI Teams before the completion of the final models and execution of the final hazard calculations. However, the final verdict of the PPRP regarding the acceptability of the hazard study as having captured the CBR of the TDI is determined by the review of the final PSHA report, and associated documentation.

A complete draft report was submitted to the PPRP in mid-February 2013. The PPRP members made individual reviews of the document, and then met for three days (in London, 19-21 March 2013) to produce a single unified set of comments and feedback .At the end of the meeting in London, the PPRP made available their review, which consisted on a total of 394 comments, covering all 10 chapters of the draft final report, which were classified into one of the three categories as follows:

- RE (Response Expected): The PPRP explicitly required written responses to these comments, of which there were 29, all referring to Chapters 8 and 9, in which the SSC and GMC models are presented.

- NR (No Response): These were 135 comments for consideration by the TI Teams but for which explicit responses were not required, but were offered as suggestions for the improvement of the report.

- ED (Editorial): The remaining 259 comments were of an editorial nature and were primarily related to minor errors and inconsistencies.

After receipt of the PPRP review comments, the TI Teams wrote responses to all of the 394 comments, regardless of their classification, and revised all 10 chapters of the report in response to these suggestions, questions and recommendations of the PPRP. Where suggested changes were not made, the

responses clearly explained the TI Teams reasons for the decision not to make that particular modification. The full revised report, including the Executive Summary, the listing of Acronyms, Abbreviations and Symbols, the merged list of all references and Appendix 1 containing the CVs of the key project participants, was delivered to the PPRP in early May 2013, together with the responses to the PPRP review comments. Following its final review of both the revised documentation and the TI Teams' responses to the original review, the PPRP issued its closing letter, which is included as Appendix 4 of the final report (***Reference 5.14.17***). The letter, signed by all five members of the PPRP, conveys the following conclusions, cited here *ad verbatim*:

- "*The commendable implementation of a Senior Seismic Hazard Analysis Committee (SSHAC) Level 3 process in this Project allows the PPRP to endorse its procedural aspects*."

- "*The PPRP concurs that the full ranges of relevant data, models, and methods were duly considered in the TI Teams' assessments*."

- "*The PPRP concurs that assessments and decisions comprising the Seismic Source Characterization and Ground Motion Characterization (including site response) models, and their implementation in a PSHA are adequately defended and justified in the Final Report*."

- "*The PPRP concurs, based on its observation of the implementation of the SSHAC Level 3 process and its review of the technical bases and justifications provided by the TI Teams for their representations of the centre, body, and range (CBR) of technically defensible interpretations (TDI), that the final PSHA for the TNSP appropriately captures the CBR of TDI*."

The unqualified concurrence of the PPRP expressed in their closure letter, is the basis for acceptance of a SSHAC Level 3 PSHA according to NUREG-2117 (***Reference 5.14.2***).

5.14.6 Monitoring Programmes

In the context of the characterisation of the seismic hazard of the Thyspunt site, monitoring consists primarily of ongoing monitoring of earthquake activity in the region and the incorporation of new geological information derived from the geological investigations conducted for the PSHA (***Subsection 5.14.6.1***). Consideration is also given to the integration of new information both during the course of the PSHA project and beyond its completion (***Subsection 5.14.6.2***).

© Eskom 2026/Rev 0a

This subsection also discussed the monitoring of the hazard characterisation itself, in terms of model building and calculations to ensure that the PSHA model adequately considers all available data and models, and that the PSHA results are rigorously checked. The SSHAC Level 3 process contributes significantly to these aspects of monitoring (***Subsection 5.14.6.3***) but independent technical checks are required, and were carried out, on all calculations directly influencing the final results (***Subsection 5.14.6.4***).

5.14.6.1 Seismic Monitoring

Seismic monitoring is performed by sensitive recording instruments called seismographs which record the motion of the ground as a function of time during the passage of seismic waves propagating through the instrument location. Data are freely available from global networks of highly sensitive seismographs, and such sources were used in the compilation of the earthquake catalogue for the PSHA (***Subsection 5.14.4.4***). The primary source of instrumental earthquake information, however, is the South African National Seismograph Network, SANSN, operated by CGS (***Reference 5.14.20***). The SANSN covers the entire territory of South Africa and records earthquakes both within the borders of the country and in surrounding oceanic and continental regions. The network is in continuous operation, with CGS routinely determining earthquake source parameters (origin time, epicentral coordinates, focal depth and magnitude) for all events. The earthquake catalogue developed for the PSHA (***Subsection 5.14.4.4***) includes earthquakes recorded up to and including December 2011. Since the seismic monitoring is a routine activity, there is no expectation that the results of ongoing seismic monitoring will have a major effect on the assessment of seismic hazards at the site, unless a major earthquake were to occur with characteristics (location and magnitude) that are outside the range covered by the SSC model. The impact of such an event is discussed in ***Subsection 5.14.6.2***.

In order to enhance the detection capability and location accuracy of the SANSN in the vicinity of the Thyspunt site, a decision was taken to re-occupy the abandoned seismograph station at Buffelsbos (BUFB), located a few kilometres from the Thyspunt site. In addition to the purpose of monitoring seismic events to accurately estimate the epicentral locations and magnitudes of all earthquakes in the region, the monitoring of seismic waves also provided insight into ground-motion characteristics in the region and at the site (***Subsection 5.14.4.6***). With this in mind, it was decided that there would be value in installing instruments as close as possible to the Thyspunt site and, if possible, on outcrops of the Goudini formation on which the NPP footprint is now located. Finding suitable sites presented some challenge because in the immediate vicinity of the site there is generally thick sand cover over the

© Eskom 2026/Rev 0a

Goudini and coastal sites where the Goudini is exposed would be too noisy (as a result of wave and wind action) to serve as seismograph stations and such sites would also have a very high risk of inundation. REDACTED

The value of the seismic monitoring network, including the newly-installed stations, was enhanced by characterisation of the recording sites in terms of the shear-wave velocity, V_s, of the surface materials. Such a classification is particularly useful for the interpretation of the stochastic inversions of the weak-motion recordings used to determine source, path and site parameters (***Subsection 5.14.4.4 (l)***). The classification of the seismograph stations was also useful in helping to identify those stations—like HVD—that appear to be situated on very hard rock and therefore can be considered as potential analogues for the reference bedrock horizon for which the GMC model was developed. Three sources of information were used to infer the classification of the seismograph stations: geological maps and station books used to identify the surface geology; active MASW measurements at several of the stations, conducted by CGS staff specifically for this application; analysis of H/V (horizontal-to-vertical) ratios of recordings from the stations.

Since there is very little available information regarding typical shear-wave velocities of commonly encountered rock formations and other deposits in South Africa, the geological classification was not able to provide much more detail than identifying the site as being on rock, which was as expected. The active MASW measurements were conducted by the same CGS team that performed similar measurements at the Thyspunt site (***Subsection 5.14.4.4 (n)***). The advantage in this case is that unlike the Thyspunt site, where there is generally 20m or more of sand overlying the bedrock at most locations (and certainly within the proposed footprint of the proposed nuclear installation), at the locations of seismograph stations there are rock outcrops (or at most a thin layer of soil overlying rock). Such settings are much more favourable to the MASW measurements and even with a modest energy source (in this case a hammer blow), the waves are able to penetrate sufficiently into the ground to allow the shear-wave velocity (V_s) profile to be determined to a depth of several

tens of metres. The readings obtained in the field by the CGS team led by Denver Birch were analysed in-house by Dr Artur Cichowicz and then checked by Dr Choon Park, a specialist consultant based in the USA. For logistical reasons it was not possible to carry out active MASW measurements at all of the seismograph stations, primarily because of their distances from the CGS headquarters in Pretoria as well as some other considerations (for example, the MOPA station, which has only operated for a few years, is located within the Kruger National Park, which would present potential dangers for those conducting the field work). In view of this, a priority list was established based on a combination of proximity to Pretoria and the number of recordings available from each seismograph station, giving greater priority to obtaining measurements from those sites contributing abundantly to the weak-motion dataset. [redacted] By way of illustration, ***Figure 5.14.107*** shows the inferred dispersion curve for the fundamental mode from the measurements at the HVD station, and ***Figure 5.14.108*** the interpreted V_s profile at the same location.

Based on the V_s profiles developed at each station, the average shear-wave velocity over the uppermost 30 m (V_{s30}) was calculated, and used to assign a NEHRP (***Reference 5.14.268***) site classification.

The final tool used for site classification of the seismograph stations was the H/V ratios of the Fourier amplitude spectra (FAS) of the recorded motions. Only recordings with a signal-to-noise ratio of at least 3 in the frequency range 1-20Hz were used for this purpose, and each FAS was smoothed using 5 passes of a 7-point Parzen window. The H/V ratio from each record was calculated at each frequency as the ratio of the geometric mean of the two smoothed horizontal component FAS divided by the smoothed vertical component FAS. The H/V representative ratio for each seismograph station was then calculated as the logarithmic average of the ratios obtained from the recordings at that location. ***Figure 5.14.109*** shows the calculated horizontal-to-vertical spectral ratios (HVSR) for the HVD station, which are almost flat as would be expected for such a hard rock site.

The calculated HVSR were then used to assign site classification according to the scheme proposed by Zhao *et al*. (***Reference 5.14.295***), which is based on the period, or frequency, at which the HVSR displays a peak. In view of the uncertainty associated with assigning site classes on the basis of HVSR, this tool was only used to assign ‘rock’ or ‘soil’ classifications (*i.e.,* NEHRP A or B, on the one hand, or the soil categories on the other). The final classifications

© Eskom 2026/Rev 0a

were based on V_{s30}, if available, and the HVSR otherwise; of the 23 stations from which weak-motion recordings had been obtained, only two were unambiguously classified as being hard rock (NEHRP class A): HVD and GRM, although the latter has a much lower V_{s30} value at just 1 640 m/s compared to 2 750 m/s at HVD. Among the remaining stations, 13 were classified as rock (NEHRP A or B).

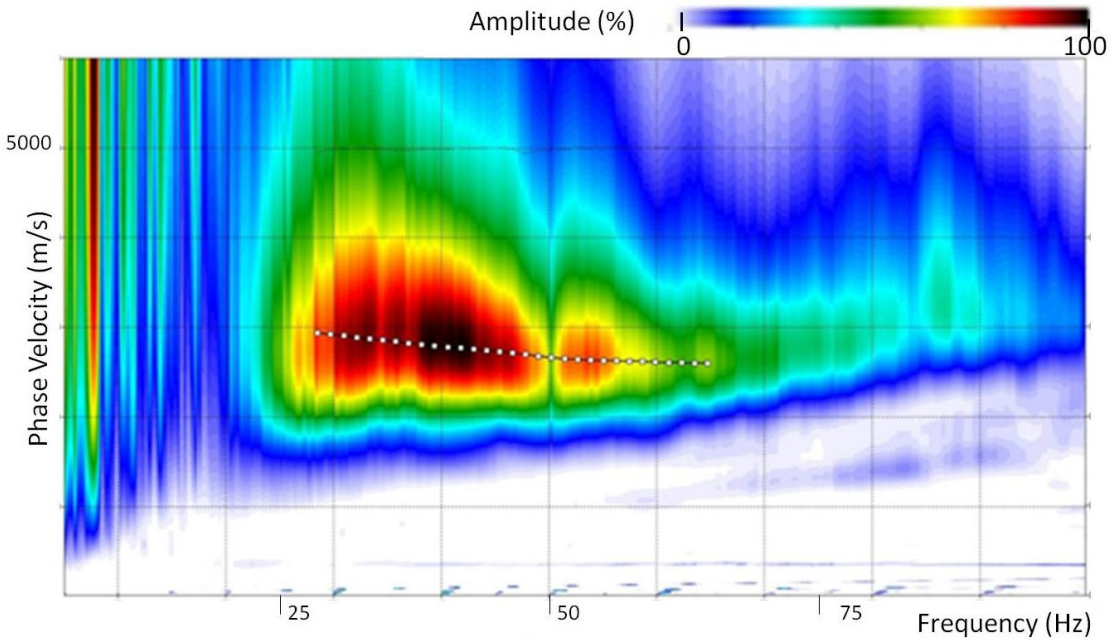


Figure 5.14-107 Active MASW Results and Inferred Dispersion Curve Corresponding to the Fundamental Mode at the HVD Seismograph Station

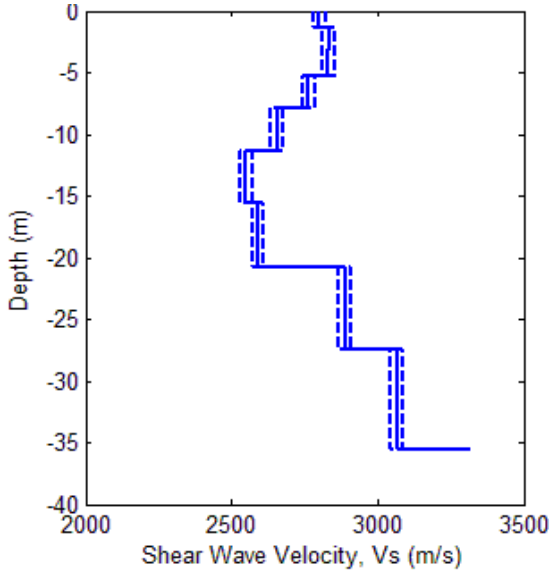


Figure 5.14-108 Shear-Wave Velocity Profile, and Associated Error Bounds, Inferred for the HVD Seismograph Station From the Dispersion Curve Shown in *Figure 5.14.107*.

Note the starting value on the x-axes. The V_{s30} value from this profile is 2 750 m/s.

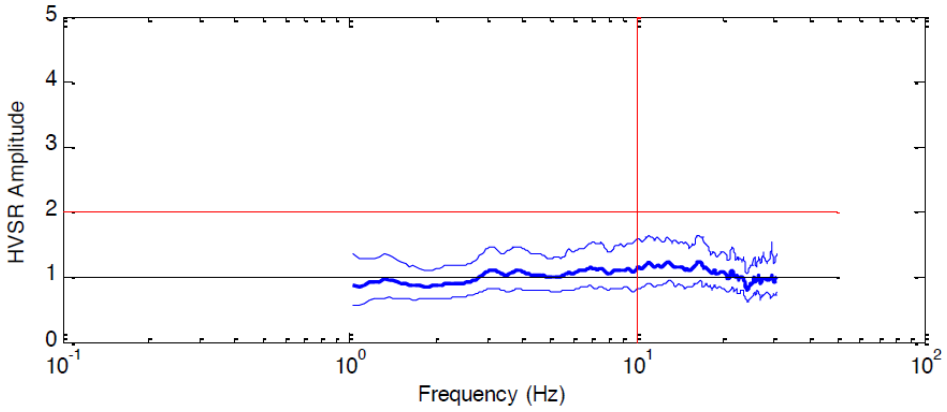


Figure 5.14-109 Calculated Mean HVSR for the HVD Seismograph Station Calculated From 138 Recordings at This Location.

The thinner blue lines correspond to ±1 standard deviation. The horizontal black and red lines indicate ratios of unity and 2.0 respectively; HVSR with a pronounced peak (usually meaning that it passes the horizontal red line) to the left of the vertical red line would be typical of soil or soft rock sites.

© Eskom 2026/Rev 0a

MASW measurements were made at the sites of the two newly-installed seismographs (KRON and ROSN). The V_{s30} values estimated for the two sites are 930 m/s at ROSN and either 830 m/s or 1 170 m/s (blue and red curves respectively) at KROM. Some recordings were obtained at these two stations and these were considered in the analyses to obtain constraint on the target kappa values. Although the velocity profiles precluded any chance of these highly-weathered outcrop sites being considered as analogues for the deep Goudini bedrock horizon, the recordings were considered when looking into the combined effects of kappa values at that lower horizon and damping models for the overlying rock (***Subsection 5.14.5.5***).

5.14.6.2 Integration of New Information

Throughout the time that the investigations for the PSHA were being conducted, results and data were being updated on a regular basis to ensure that the SSC and GMC models developed were based on the most up-to-date information. For example, as described in ***Subsection 5.14.4.3***, a number of geological investigations were conducted with the specific purpose of providing new information for use in the PSHA. Similarly, in situ measurements of V_s were made at the site, and the programme of investigations modified on the basis of the results obtained at each stage (***Subsection 5.14.4.4 (n)***). When it was found that MASW measurements were unable to resolve the velocity structure of the bedrock as a result of the thick sand cover at the site preventing the small energy sources achieving adequate depths of penetration, borehole-based PS suspension logging measurements were used instead. When the PS logging results from the first few boreholes showed a high degree of lateral heterogeneity in the velocity structure at the site, an expanded programme was designed and implemented, increasing by a factor of four the numbers of boreholes in which PS suspension logging was performed. This additional information allowed better constraint of both the velocity profile for the site and for the variability associated with this model (***Subsection 5.14.5.5.(b)***).

The participation of Resource Experts in the first and second Workshops of the project, and even more so the invitations to a large number of Proponent Experts to participate in the second Workshop (***Subsection 5.14.5.2***) particularly contribute to ensuring that the TI Teams were appraised of the most recent data, methods ad models of potential relevance to the seismic characterisation of the Thyspunt site.

All the geological, seismological, geophysical and geotechnical investigations were conducted, completed, and documented in a timely manner for their use as input information for the PSHA. An important factor in ensuring that adequate retrieval of available existing information and focused investigations to collect new information was the review of the database compilation and evaluation by

the PPRP (***Subsection 5.14.6.3***). The PPRP concurrence on the final conclusions of the study confirmed that the seismic characterisation of the Thyspunt site had given due consideration to all available information, including new data collected specifically within the framework of the project and publications and datasets that emerged during the course of the study (***Subsection 5.14.5.5***).

The intention of the SSHAC Level 3 process is to construct SSC and GMC logic-trees that reflect the current level of knowledge regarding the seismic hazard at the Thyspunt site (***Subsection 5.14.7.3***). The intention, as stated in NUREG-2117 (***Reference 5.14.2***), is to assure capture of the CBR of the TDI with regards to the estimation of seismic hazard in terms of vibratory ground motions at the site. With the passage of time and, potentially, the development of new information, there will likely be a need to assess whether that assurance still exists. This may be addressed either through fixed-term updates and/or through assessments following the development of new information in terms of data, methods or models (***Reference 5.14.2***). Examples of new information that might emerge could include the discovery of a previously unknown geological fault or the occurrence of a significant earthquake in the region. However, such developments do not automatically lead to a decision to revise the PSHA since the new information may well be fully represented within the multiple alternative models and parameter values already present in the logic-tree. Before a decision is taken to update a site-specific PSHA, an assessment should be made of the likely impact of the new information on the seismic hazard estimates at the site (***Reference 5.14.2***). McGuire (***Reference 5.14.296***) provides suggestions for assessing the need for revision of a PSHA in terms of the relative impact of new information on existing hazard estimates.

5.14.6.3 Role of the SSHAC Process

At the core of the SSHAC Level 3 process is the Technical Integration (TI) Team, usually divided into two TI Teams for the development of the SSC and GMC models. The first stage of a SSHAC Level 3 PSHA project must always be the compilation of a database of all existing data and models that are available to the TI Teams and which may be relevant to the characterization of the region and the site (***Subsection 5.14.4***). In order to provide additional constraint and thereby reduce uncertainties, it will also generally be the case that some new data will be collected, for example through geological (***Subsection 5.14.4.3***) and geotechnical (***Subsection 5.4.4.8***) investigations. Once the complete databases are assembled, these are evaluated by the TI Teams both in terms of their general quality and also their applicability to the region and site under study (***Subsection 5.14.5.3***). On the basis of this evaluation, the TI Teams then undertake the integration of the available data,

© Eskom 2026/Rev 0a

methods and models into logic trees that represent "*the center, the body, and the range of technically-defensible interpretations of available data, methods and models*" (***Reference 5.14.2***).

Calculations of two types may be performed in the development of the logic trees, some that provide information that informs the TI Teams in their decision-making process, and others that yield numerical outputs (for example, earthquake recurrence parameters or site amplification functions) that will be directly input to the hazard calculations. An example of the former type of calculation from the Thyspunt PSHA was estimating the implied recurrence rates of earthquakes of different magnitudes as a result of different combinations of recurrence model, M_{max} and slip rate to guide the final choices of slip rates on fault sources. An example from the GMC side was creating visualizations of the relative proximity of predictions from different ground-motion prediction equations under consideration, using the techniques developed by Scherbaum *et al.* (***Reference 5.14.279***), to inform the selection of models and inspect their implied range of epistemic uncertainty (***Subsection 5.14.5.5.(a) iii***). Finally, the hazard calculations are performed using a suitably qualified computer code, and the entire study documented to provide sufficient information regarding all of the technical bases of the hazard model. ***Figure 5.14.110*** provides an overview of this process, indicating those elements where formal Quality Assurance (QA) is required. A key role in high-level SSHAC studies is that of the Participatory Peer Review Panel (PPRP), which is charged with both technical and process review throughout the duration of the project (***Subsection 5.14.5.5***).

© Eskom 2026/Rev 0a

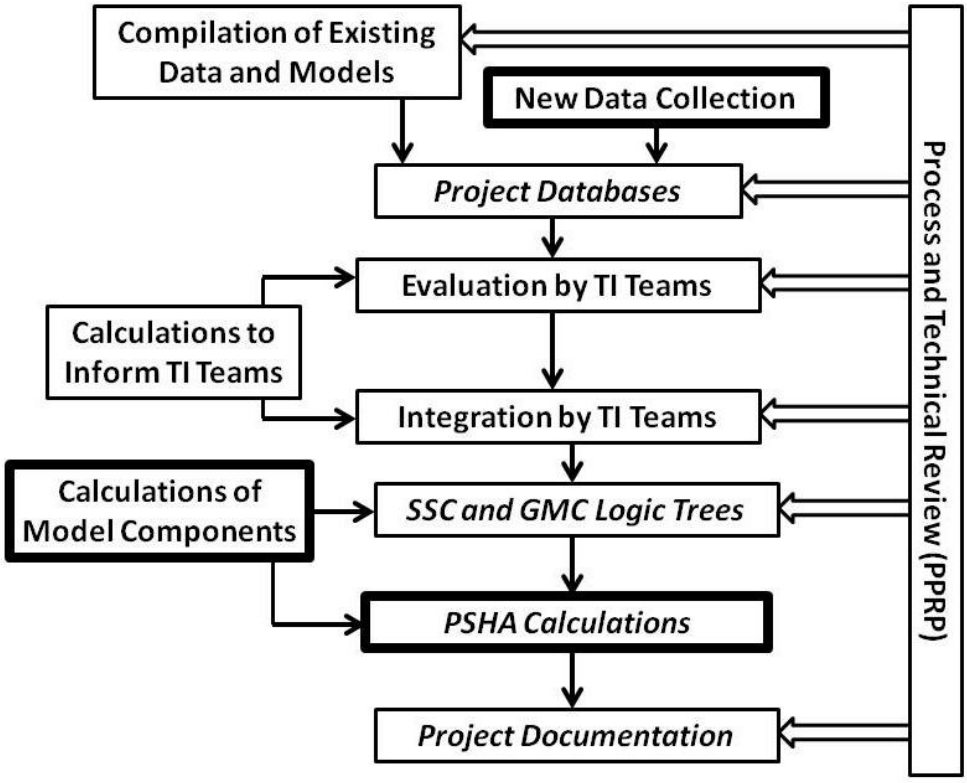


Figure 5.14-110 Phases of a SSHAC Level 3 PSHA, Indicating the Role of Technical and Process Review by the PPRP (*Reference 5.14.297*).

Items in normal fonts are processes, those in italic are products. Thick outlines indicate elements for which there are formal QA requirements.

As indicated in ***Figure 5.14.110***, the PPRP engages on several occasions with the project, from ensuring that all available data, methods and models are duly considered, to assessing if the final logic tree adequately captures the range of uncertainty and if its technical bases are properly documented (***Subsection 5.14.5.5***). Final concurrence by the PPRP, if forthcoming and given without reservations, is the basis for acceptance of the PSHA study as the characterization of the seismic hazard at the site. The position of the USNRC on how the PPRP contributes to the overall nuclear QA in SSHAC Level 3 project is stated as follows: "*Therefore, it is the collective, informed judgment of the TI Team (via the process of data evaluation and model integration) and the concurrence of the PPRP (via the participatory peer review process) as well as adherence to the national standards.....that ultimately leads to the assurance of quality in the process followed and in the products resulting from the SSHAC hazard assessment framework*" (***Reference 5.14.2***).

Nonetheless, as indicated by the boxes with thick outlines in the flowchart of ***Figure 5.14.110***, standard QA procedures do need to be applied to the collection of new data and to calculations that provide numerical input to the hazard calculations.

Quality Assurance is also required, as ***Figure 5.14.110*** indicates, for the actual hazard calculations, and this has two components. The first is to select a computer code that has undergone suitable validation and verification benchmarking. The second, and potentially much more challenging, component is to check that the logic trees representing the project-specific SSC and GMC models—which may have hundreds of branches and thus imply thousands of different combinations of the hazard inputs—have been correctly implemented. The focus of this paper is precisely this kind of check, illustrated with a practical example of a logic tree developed within a SSHAC Level 3 PSHA project for a nuclear site, as described in ***Subsection 5.14.6.4***.

5.14.6.4 Independent Technical Checks

As discussed in ***Subsection 5.14.6.3***, calculations that provide numerical inputs to the hazard calculations, as well as the hazard calculations themselves, need to be checked in terms of their correctness. This subsection documents the independent technical checks that were carried out on the numerical inputs to the SSC model and GMCM (***Subsection 5.14.6.4.(a)***), as well as those performed on the hazard calculations (***Subsection 5.14.6.4.(b)***). The full technical details of the checks are given in the report documenting Verification and Validation (V&V, see ***Subsection 5.14.8.4***) activities (***Reference 5.14.298***)). The checks on the hazard calculations are further discussed in ***Reference 5.14.297***.

a) Checks on Inputs to SSC and GMC models

Elements of the SSC (***Subsection 5.14.5.4***) and GMC (***Subsection 5.14.5.5***) models that contributed numerical inputs to the characterisation of these models as described in the HID (see ***Subsection 5.14.5.3***) were identified and independently checked by members of the project team, in accordance with the procedures included in the Integrated Management System (IMS; ***Reference 5.14.299 and 5.14.300***); see ***Subsection 5.14.8.1***). The checks are independent in the sense that the checker is a different member of the project team from the originator of the calculations.

These independent checks included direct review of software codes and spreadsheets used in the calculations, as well as independent implementations using alternative software code. The SSC and GMC model elements for which such checks were performed include the following:

© Eskom 2026/Rev 0a

- Mmax calculations (***Subsection 5.14.5.4.(c) ix***)
- Recurrence calculations ***(Subsection 5.14.5.4.(c) vii***)
- Host GMPE implementations (***Subsection 5.14.5.5.(a) ii***)
- IRVT-generated Fourier spectra ***(Subsection 5.14.5.5.(a) i***)
- Sigma values (***Subsection 5.14.5.5.(c)***)
- Site response calculations (***Subsection 5.14.5.5.(b)***)

Examples of such checks are shown in ***Figure 5.14.111*** for the V_s-kappa adjustments using the IRVT-generated Fourier spectra, and for the site response calculations in ***FigurF-5.14.112***.

All checks were documented using the appropriate forms developed as part of the IMS. These forms are included as appendices in the V&V report (***Reference 5.14.298***).

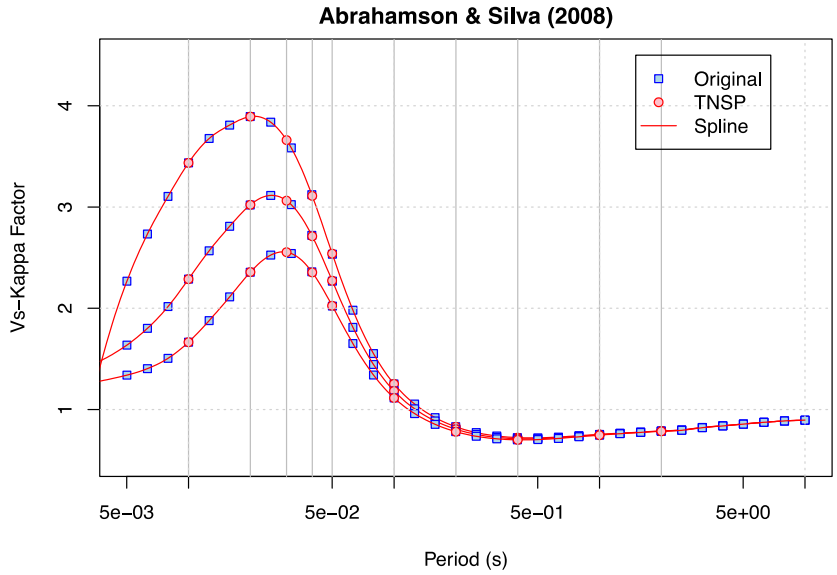


Figure 5.14-111 V_s-Kappa adjustment Factors developed by Frank Scherbaum (*blue*) for the Model of Abrahamson & Silva (*Reference 5.14.129*), and the Interpolated Values at the Thyspunt PSHA Response Periods (Peter Stafford).

The three curves, consistently from top to bottom are the factors for the target Kappa of 0.001,

0.003 and 0.005. Vertical grey lines denote the Thyspunt PSHA periods.

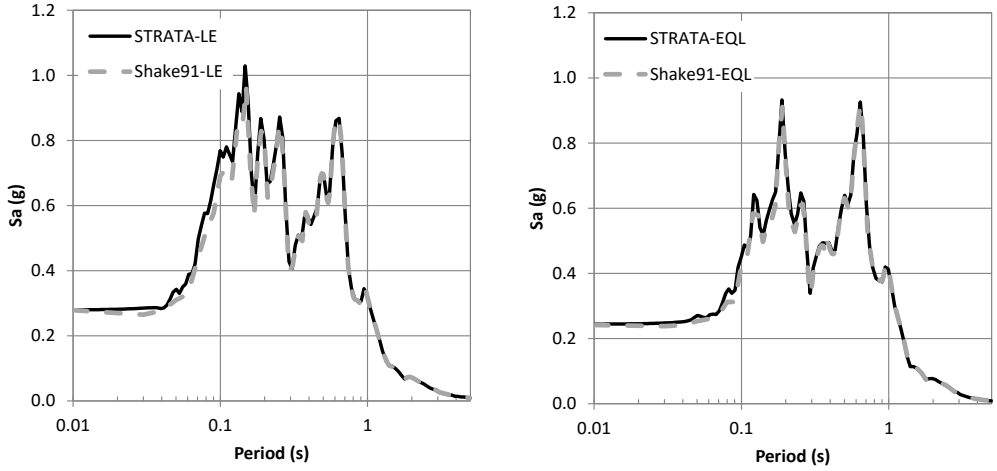


Figure 5.14-112 Surface Response Spectra Calculated by STRATA and Shake91 for Linear Elastic (LE) and Equivalent-Linear (EQL) Analyses

b) Checks on Hazard Calculations

The correct implementation of the SSC model and GMCM as described in the HID was done by simultaneously implementing the logic tree in two different, and entirely independent, software packages for the calculation of probabilistic seismic hazard. This exercise is described in more detail in the V&V report (***Reference 5.14.298***) and in ***Reference 5.14.297.***

i Choice of software

The FRISK88® software was selected for running the main seismic hazard calculations for the Thyspunt PSHA, on the basis of having all of the computational capabilities required for the SSC and GMC models, as well as having undergone extensive nuclear QA and having been used in several nuclear licensing projects. The question of which hazard software could be used for the independent checks then arose. A point that must be strongly emphasized here is that the purpose was not to check if the FRISK88® software performs the hazard calculations correctly, since this is already proven by its nuclear qualification, but rather to check the implementation of the logic trees in the FRISK88® software by obtaining comparable results when the same

logic tree was input to another hazard code. In order for this exercise to be meaningful, it is necessary that the second hazard software has also undergone rigorous QA and additionally has similar computational capacities as the primary program.

The *OpenQuake-engine* hazard program being developed as part of the Global Earthquake Model (GEM) project, a global collaborative effort aiming at the establishment of uniform, open standards for calculating and communicating earthquake risks worldwide (***Reference 5.14.301***), was identified as an ideal program for this purpose, since it fulfils all of the requirements listed above (***References 5.14.301*** and ***5.14.302***). From discussions of the software capabilities at Workshop 3, it was concluded that *OpenQuake-engine* could effectively mimic the calculations that were to be performed in FRISK88®.

ii Precision in Seismic Hazard Estimates

There are many software packages available, both commercially and freely, for performing PSHA calculations. Although in principle all these codes are essentially performing the same calculations—integrations over distribution of magnitude, *m*, distance, *r*, and conditional ground-motion exceedances, ε—the way the numerical integrations are coded will vary from one code to another, as will the modeling choices available to the analyst. For instance, the differences may reflect different discretization schemes for each of the variables above, which in combination with other specific features of the calculations (often intended to reduce the time required to execute each PSHA run), lead to the fact that for any specific input, the results obtained from different hazard codes are unlikely to be identical. This fact is amply demonstrated by the results presented in the study by Thomas *et al*. (***Reference 5.14.304***) for simple source-site configurations, where hazard curves obtained with different codes diverge even at annual frequencies of exceedance (AFE) as high as 10^{-3}. The expectation must be, therefore, that when comparing mean hazard curves obtained from the implementation of logic trees representing uncertainty in complex SSC models, exact coincidence is even less likely to be obtained.

However, this does not mean that the hazard results obtained from the different codes are erroneous or unreliable, simply that the estimation of seismic hazard is an inexact science. In the discussion of what impact on existing hazard estimates new models would need to have to warrant a revision, the final report of the *Central and Eastern United States Seismic Source Characterization* (CEUS SSC) project (***References 5.14.69*** and ***5.14.296***) provides insight regarding the precision with which mean seismic hazard at a site can be known, in view of the inherent uncertainty. The report suggests that for the CEUS, changes of less than ±25% in the AFE for ground-motion levels with a mean hazard of 10^{-4} may not be significant, and at 10^{-6} the tolerance is ±35%.

Therefore, before even starting the independent hazard runs, it was agreed that confirmation that the same model had been implemented correctly in both codes would be judged on the basis of moderate and consistent differences in the mean hazard curves, confirmed over a wide range of AFEs, including the range of AFEs of most interest to the project for nuclear applications, generally the 10^{-4} to 10^{-5} interval); exact agreement was neither expected nor required.

iii Checks on GMC model implementation

All hazard results generated are the outcome of combining the SSC logic-tree branches with the GMC logic-tree branches. In order to audit the correct implementation of both components, it is highly desirable to first check the coherent implementation of the GMC logic-tree branches, since any discrepancies therein will compound any differences in the implementation of the SSC logic-tree, making an observed difference in overall hazard results difficult to interpret. Moreover, since the output of the GMC model for specified scenarios are individual values of spectral acceleration, it was possible to run checks of its implementation for which exact agreement could be reached. This then allowed the independent hazard runs to be performed only for checking the implementation of the more complex SSC logic tree.

For this exercise, a blind three-way check was carried out whereby the GMC logic-tree was implemented in FRISK88® by the hazard analysts at CGS, in the *OpenQuake-engine* software by the GEM Hazard Team in Pavia, and in a separate application by Dr. John Douglas at BRGM, France. The PTI generated a list of almost 6 500 test scenarios based on different combinations of 'backbone' GMPE, oscillator period, magnitude, style-of-faulting, and distance. The combinations also sampled the branches of the sigma logic tree and the output specified both median and 84-percentile values of the spectral accelerations in order to test all the elements of the model. Specifications were given for the fixed parameters of the three GMPEs (V_{s30}, Z_{TOR}, *etc.*) and the equations were modified by the application of the V_s-kappa adjustment factors.

The three-way check involved the calculation of response spectral accelerations for all 6 500 scenarios in three different (and completely independent) implementations. The reason for a three-way check was to allow the source of any discrepancies to be located more easily (on the basis of the reasonable assumption that if two implementations were in agreement, any error was most likely to be encountered in the third implementation that differed). The exercise concluded with exact agreement in the predicted accelerations, to several decimal places, for all of the scenarios. At that stage it was possible to run hazard calculations that would serve as checks on the implementation of the SSC logic tree.

© Eskom 2026/Rev 0a

iv Checks of SSC model implementation

For the SSC logic tree implementation testing, mean hazard curves were generated for 15 sets of branches which collectively spanned the entire SSC logic tree (***Subsection 5.14.5.4.(b)***). Each hazard curve was generated for the contributions from a single seismic source using the full SSC logic tree for that source, but only a single branch of the GMC logic-tree, effectively providing the mean hazard for all of the SSC logic-tree branches within that source. One such run was performed for each of the sources except the host ECC zone within which the Thyspunt site is located, for which multiple runs were performed. The emphasis on checking the implementation of the model for ECC was made because it is generally found that in low seismicity regions, the hazard at a site is dominated by contributions from the host source.

In order to increase the chances of picking up on any problems, all three 'backbone' GMPEs were used in different runs. Three different response periods were used because of their different sensitivities to earthquake magnitude, which once again was designed to increase the chances of identifying any discrepancies. For the fault sources, which generally produce only larger magnitude events, the longest of the three response periods was chosen. For the critical ECC host zone, all three GMPEs and oscillator periods were used in the runs. The results for the fault source runs are shown in ***Figure 5.14.113*** and from area source calculations in ***Figures 5.14.114*** and ***5.14.115***.

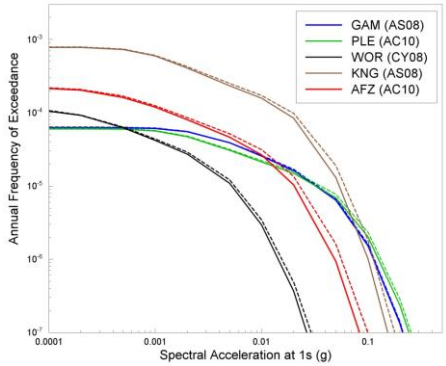


Figure 5.14-113 Mean Hazard Curves obtained for the Fault sources Using FRISK88® (*solid curves*) and *OpenQuake-engine* (*dashed curves*).

The sources are identified in Figure 5.14.73 (Subsection 5.14.5.4.(e)); the selected parent GMPE of the GMC logic-tree branch used in each case is indicated in parentheses: AC10 – Akkar and Çağnan (Reference 5.14.134), AS08 – Abrahamson and Silva

(Reference 5.14.129), CY08 – Chiou and Youngs (Reference 5.14.132).

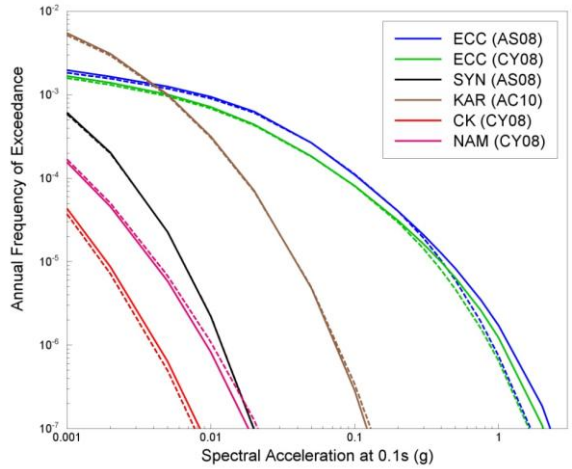


Figure 5.14-114 Hazard Curves for Sa(0.10s) Obtained for the Various Source Zones (see *Figure 5.14.52*; *Subsection 5.14.5.4.(d)*) and GMPE Combinations Using FRISK88® (*solid curves*) and *OpenQuake-engine* (*dashed curves*). See Caption of *Figure 5.14.113* for Details.

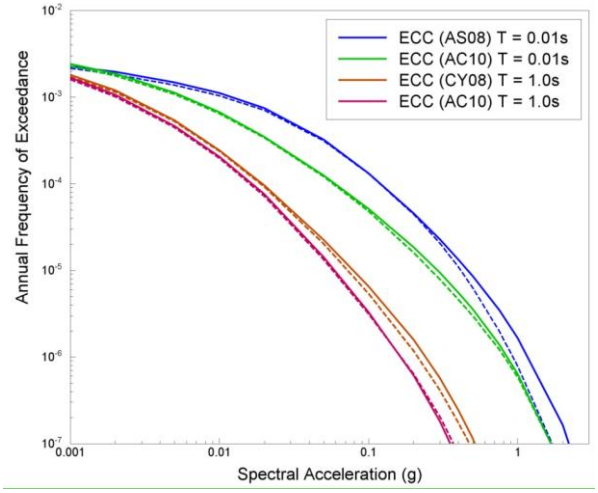


Figure 5.14-115 Hazard Curves Obtained for the Host ECC Source (see *Subsection 5.14.5.4.(d) i*) Using FRISK88® (*solid curves*) and *OpenQuake-engine* (*dashed curves*) for Different Combinations of GMPE and Response Period (See Caption of *Figure 5.14.113* for Details).

Several important observations can be made on the plots in these figures, the first being that the level of agreement is very high considering the complexity of some of the sources and the SSC logic-trees defining the ranges of activity and M_{max}. For the two faults sources closest to the site, PLET and GAM (***Figure 5.14.113***), the two pairs of hazard curves are almost identical. For the area sources, the agreement is generally even better, and neither of the hazard codes produces consistently higher or lower results. The most interesting, and probably most important, observations concern the hazard contributions from the host ECC source zone (***Figures F-5.14.114*** and ***F-5.14.115***). For the AC10 GMPE (Figure 5) the differences are very small, whereas using the other two backbone GMPEs larger differences are seen at low AFEs; these differences are attributed to differences in the modelling of extended fault ruptures in the two software packages used. The clear conclusion from these comparisons was that the hazard model was correctly implemented and therefore the final hazard results could be accepted with confidence.

v Independent Checks on Post-Processing Routines

In view of the large number of runs generated, the post-processing steps of the files output by FRISK88® software were automated using a set of MatLab routines developed specifically for the project, which were rigorously checked and tested by an independent reviewer, Dr John Douglas of BRGM. Details of these checks are given in ***Reference 5.14.298***).

These checks were documented using the appropriate IMS forms (***Reference 5.14.300***). The completed forms are included as appendices to the V&V report (***Reference 5.14.298***).

5.14.7 Management of Uncertainties

The basis for assurance regarding the characterisation of the seismic hazard at a site is two-fold. On the one hand, clear demonstration is required that all available data relevant to the seismic characterisation of the region and of the site were gathered and interpreted by suitably-qualified experts, using state-of-the-art approaches to construct models representing the spatial and temporal distribution of future earthquakes, and the ground motions expected at a given location due to such earthquakes. Demonstration is also required that the derivation of the models and the hazard calculations performed using these models were subject to rigorous checks (***Subsection 5.14.8.4***). On the other hand, it is also necessary to demonstrate that the full range of uncertainty in all elements of the models has been accounted for so that the consequent uncertainty associated with the final seismic hazard estimates are duly quantified. The ultimate objective is to provide seismic hazard estimates that can be used as the basis for design and for safety assessments that bound

appropriate levels of uncertainty so that there is can be confidence in the safety margins ensuring acceptable behaviour of nuclear installations under the shaking of possible future earthquakes.

Although arguments are presented below for the use of probabilistic seismic hazard analysis (PSHA) over deterministic seismic hazard analysis (DSHA), it may be noted that DSHA was not a viable option for the seismic characterisation of the Thyspunt site. The unique choice of PSHA was the result the governing regulatory requirements specify seismic design levels in terms of annual exceedance frequencies (***Subsection 5.14.3***), which cannot be reliably estimated using DSHA.

5.14.7.1 Types of Uncertainty

The primary objective of a PSHA is to produce a seismic hazard curve for each ground-motion parameter of interest. These curves express the relationship between different values of the parameter of interest and the associated annual frequency of that value being exceeded. However, an equally important aspect is that the uncertainty associated with each curve calculated is assessed. As stated in the original SSHAC Guidelines (***Reference 5.14.1***):

> *"The most important and fundamental fact that must be understood about a PSHA is that the objective of estimating annual frequencies of earthquake-caused ground motions can be attained only with significant uncertainty."*

Two fundamental types of uncertainty can be identified; and a variety of terms have been used for these two types of uncertainties in different fields. Some have argued that in classical decision theory, the distinction between the two types of uncertainty is unimportant and that only the total uncertainty matters (*e.g.*, ***Reference 5.14.305***). For practical application of PSHA, it is assumed in these guidelines that the distinction is important because the way in which the two classes of uncertainty are handled in seismic hazard analysis is very different. Clearly classifying each uncertainty and defining the procedure for its incorporation into the assessment of seismic hazard helps to ensure that no element of uncertainty is neglected.

The two classes of uncertainty have traditionally been referred to by the simple terms *randomness* and *uncertainty*. However, over the years, the usage of these terms has become lax and they have often been employed interchangeably, thereby blurring the distinction. For this reason, in PSHA, new terms have been introduced to encourage greater clarity when treating the uncertainties associated with the assessment of seismic hazard. The two types of uncertainty are now referred to as *aleatory variability* and *epistemic*

uncertainty (***Reference 5.14.1***); the original SSHAC guidelines referred to these as aleatory uncertainty and epistemic uncertainty, but the terminology adopted herein makes the distinction even clearer.

Aleatory variability is the inherent randomness in a process. Its name derives from *alea*, the Latin word for dice. This type of uncertainty has also been referred to as randomness, variability, irreducible uncertainty, inherent uncertainty, natural variability, type-A uncertainty, and stochastic uncertainty. In theory, aleatory variability cannot be reduced, because it is interpreted as representing an inherent quality of Nature. In terms of the practice of PSHA, it is more useful to consider aleatory variability explicitly in association with a particular model of Nature defined in the study because it is reflected in the calculation of random variability of observations specifically with respect to the model predictions. For this reason, it may be helpful to think of this type of uncertainty as “apparent” random variability, in which it is possible that some epistemic uncertainty has been included. Then, as more sophisticated models are developed that incorporate a greater number of explanatory variables—and perhaps a more complex functional form—the aleatory variability can be transformed to epistemic uncertainty on the explanatory variables.

Aleatory variability is represented by a probability distribution for known parameters. Once we have a model for a particular earthquake process, it is possible to define the range of values that the predicted variable is expected to take. However, the aleatory variability means that we do not know which value a parameter will take in any particular instance. An example of this is that we may define the expected distribution of focal depths of earthquakes in a given region based on well-determined depths in the earthquake catalogue; but we have no way of knowing at what depth within the seismogenic layer any individual future earthquake may occur. Similarly, we may be able to determine the average recurrence rate for earthquakes of different magnitudes in an earthquake catalogue, but this does not mean that we can know the magnitudes of the earthquakes that will occur in the next decade or the size of the next earthquake. The PSHA process integrates across the full distribution of each identified source of aleatory variability (***Subsection 5.14.7.2***).

Epistemic uncertainty arises because our analyses are conducted using models (mathematical and conceptual constructs of reality) rather than directly on real systems. The adjective epistemic is derived from the Greek *ἐπιστήμη* (epistêmê) meaning knowledge; and this uncertainty reflects our lack of knowledge regarding earthquake processes, both in general and in a specific location. Epistemic uncertainty has also been referred to as reducible uncertainty, subjective uncertainty, model form uncertainty, ignorance, type-B uncertainty, and specification error. Unlike aleatory variability, epistemic

uncertainty can—in theory at least—be reduced through the acquisition of additional data.

Whereas aleatory variability is always represented by probability distributions, there are more options for the representation of epistemic uncertainty. In PSHA, it is increasingly common for epistemic uncertainty to be expressed through the use of a logic tree (***Subsection 5.14.7.3***). The SSHAC process itself is primarily concerned with the capture of epistemic uncertainty, although both types of uncertainty must be fully expressed in the PSHA. A key focus of the SSHAC process is ensuring adequate incorporation of epistemic uncertainties (***Subsection 5.14.7.4***).

5.14.7.2 Aleatory Variability and the PSHA Integration Process

Aleatory variability reflects the inherent randomness in earthquake and ground-motion processes, including the location, the number, and the magnitude of future earthquakes that could occur during the useful life of the facility being designed. This was expressed by Cornell (***Reference 5.14.306***) in the landmark paper that introduced the basis for PSHA: "*In the determination of the distribution of maximum annual earthquake intensity at a site, one must consider not only the distribution of the size (magnitude) of an event, but also its uncertain distance from the site and the uncertain number of events in any time period."* Whereas deterministic seismic hazard analysis (DSHA) is focused on defining a small number of earthquake scenarios (for the design basis motions to be then set on the basis of the magnitude-distance combination generating the largest levels of acceleration at the site), PSHA considers all possible earthquake that could affect the site in order to calculate the overall rate at which different levels of acceleration are expected to be exceeded. Each earthquake is defined by its magnitude (or seismic moment), its location (which determines the distance from the site), and its average recurrence rate. The scenarios are defined by a seismic source characterisation (SSC) model, which is comprised of the geographical definition of seismic sources and recurrence models, which respectively define where future earthquakes are expected to occur and how frequently earthquakes of different magnitudes are expected (***Figure 5.14.116***).

The ground motions generated at the site of interest by each of the earthquakes is calculated by the ground motion characterisation (GMC) model, which is generally in the form of equations that predict a probabilistic distribution of accelerations for a given combination of magnitude, M, and distance, R. The predicted ground-motion amplitudes follow a log-normal distribution, defined by the median value and a standard deviation, sigma (σ) (*e.g.*, ***Reference 5.14.293***). For a given M-R pair, the predicted level of acceleration can be defined by the number of standard deviations above or below the

median; this number is expressed by epsilon (ε). In the original formulation of PSHA by Cornell (***Reference 5.14.306***) the sigma in the ground-motion prediction was a missing element of aleatory variability, but this was subsequently embedded in standard formulations of PSHA (***References 5.14.269 and 5.14.308***).

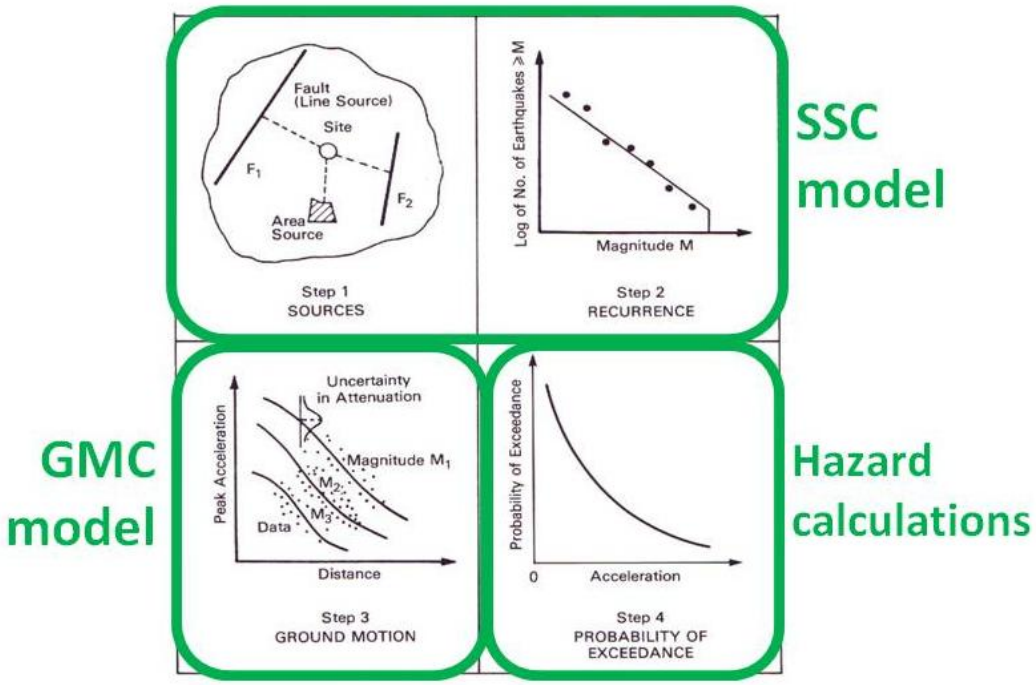


Figure 5.14-116 Overview of Steps Involved in a PSHA.

Adapted from *Reference 5.14.307*.

In the hazard calculations, all M-R-ε combinations are considered and the exceedance frequency of the resulting level of motion calculated as the product of the recurrence rate of the earthquake and the probability of exceeding ε as defined by the standard normal distribution. The total exceedance frequency for each level of acceleration is found by summing the frequencies of all M-R-ε combinations that generate that level of acceleration. Plotting these total exceedance frequencies against the corresponding levels of acceleration creates a seismic hazard curve, as illustrated in ***Figure 5.14.116***.

The probabilistic approach to seismic hazard analysis is specifically formulated to integrate all these sources of variability into the estimation of the annual exceedance frequency of different levels of each ground-motion parameter. Therefore, adoption of PSHA as the basis for determining the seismic design

loads, and executing the PSHA in terms of characterising design ground motions according to the specification of RG 1.208 (***Reference 5.14.3***) ensures adequate consideration of aleatory variability.

5.14.7.3 Epistemic Uncertainty and Logic Trees

Earthquakes are caused by tectonic processes that are defined by cycles of tens or even hundreds of years in length, whereas the periods for which there are detailed instrumental observations of seismic events is only a little longer than a century. Inevitably, the data available for the characterisation of the region and the site under consideration are never sufficient to unambiguously and uniquely define SSC and GMC models. There is always epistemic uncertainty in both the SSC and GMC models developed for PSHA for two simple reasons: the nature of the data available is such that there will always be several technically-defensible interpretations, and the PSHA calculations will invariably consider earthquake scenarios that are not covered by the available databases. The treatment of epistemic uncertainties in seismic hazard analysis therefore requires expert judgement to identify the best estimate for each component of the seismic hazard model, and then to estimate the range of uncertainty associated with each model or parameter in view of the limited and incomplete data available for its constraint. In stable regions such as South Africa, where moderate and large earthquakes are relatively infrequent, epistemic uncertainty becomes particularly important.

The tool most widely used in PSHA to incorporate epistemic uncertainties is the logic tree, which was first introduced to PSHA by Kulkarni *et al*. (***Reference 5.14.309***) and Coppersmith & Youngs (***Reference 5.14.310***). In a logic tree, alternative models or values for each elements of the SSC and GMC model are assigned to branches emanating from sequential nodes and assigned weights that reflect the relative confidence of each of the branches representing the best model for the application in question (***Figure 5.14.117***). The weights on the branches emerging from each node sum to 1.0, reflecting their subsequent treatment as probabilities. Once the logic tree is set up, the PSHA calculations are performed for all branch combinations (every route through the logic tree), each one leading to a hazard curve to which a total weight is assigned that is the product of the individual branch weights. Whereas the consequence of aleatory variability is to influence the shape of the seismic hazard curve, the consequence of considering epistemic uncertainty is to create suites of seismic hazard curves. From these results, a mean hazard curve and hazard curves for various fractiles (including the median) can be generated, which convey the uncertainty in the final hazard estimates as a result of the uncertainty considered in the individual elements of the SSC and

GMC models. Examples of mean and fractile hazard curves for the Thyspunt site are presented in ***Subsection 5.14.9.2***.

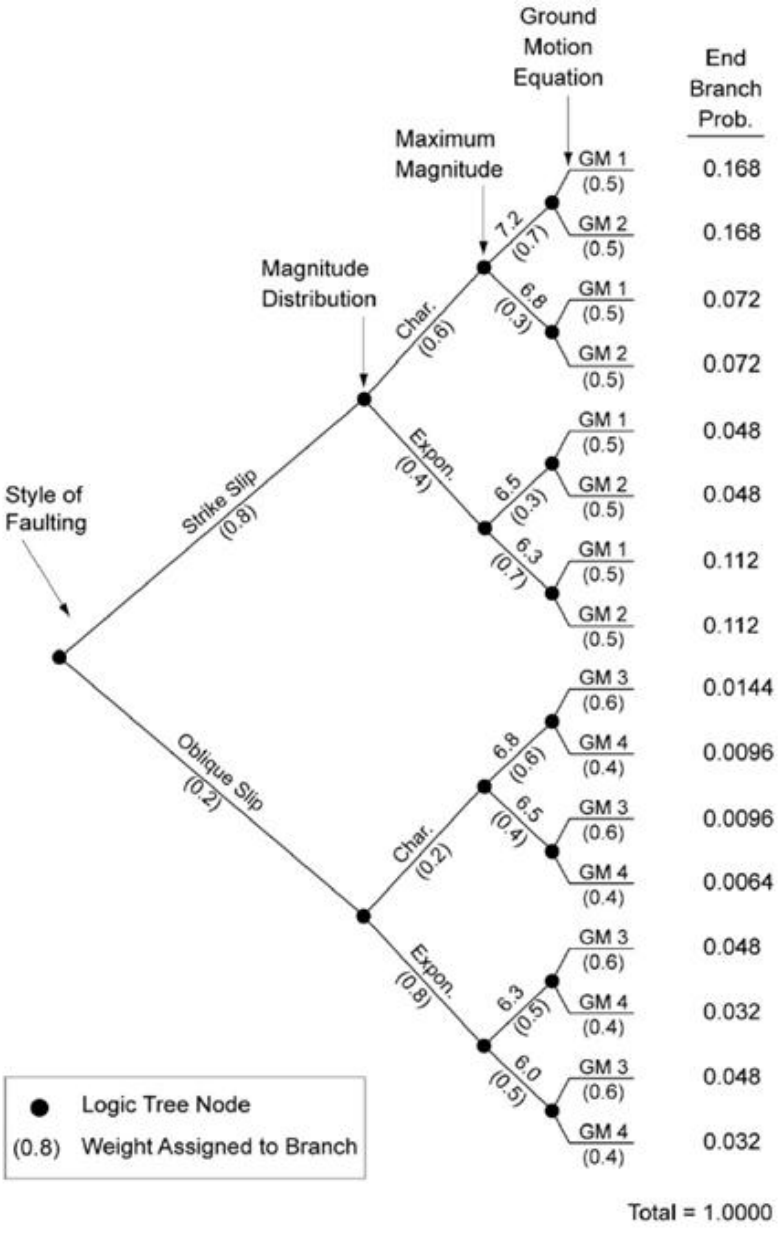


Figure 5.14-117 Example of a Simple Logic Tree for a Site-Specific PSHA (*Reference 5.14.311*).

The first three nodes from the left correspond to the SSC model, the final node is the GMC model. The numbers in the final column are the total weight, or probabilities, associated with the hazard curve obtained combining the branches leading to that end point, obtained from the product of the individual branch weights.

5.14.7.4 Role of the SSHAC Process

The correct incorporation of aleatory variability is ensured by adoption of PSHA and adherence to the guidelines in RG 1.208 (***Reference 5.14.2***), supplemented by systematic verification of calculations (***Subsections 5.14.6.4 and 5.14.8.4***). The tool for capturing epistemic uncertainty is the logic tree, and the central purpose of the SSHAC Level 3 process adopted for the Thyspunt PSHA is to provide assurance that the SSC and GMC logic-trees that were developed by the TI Teams captured the full extent of the epistemic uncertainty. To appreciate this role of the SSHAC Level 3 process, it is useful to recall how the SSHAC process came into being.

Identification, characterisation and quantification of epistemic uncertainty inevitably involves expert judgement. In order to ensure that all epistemic uncertainties are identified and adequately quantified, it is common to invoke the judgement of several experts. Two major PSHA studies for nuclear power plant sites in the Central and Eastern United States (CEUS) were conducted in the 1980s, both involving several experts in the fields of seismic source characterisation and ground motion prediction. The two studies, sponsored by the Electric Power Research Institute (EPRI) and Lawrence Livermore National Laboratory (LLNL), were published in the same year (***References 5.14.312 and 5.14.313***) and resulted in very different hazard estimates for several locations in CEUS. There were also very large variations amongst the hazard estimates from the experts within each project. In both projects, the problem arose as to how to combine the various expert models into a single hazard assessment. This led to reflection on how the views of multiple experts can be reconciled and the degree of interaction that the experts should have during the process. Concerns about the issues that arose in the EPRI and LLNL studies eventually led the US Nuclear Regulatory Commission (USNRC), EPRI, and the US Department of Energy (DOE) to form the Senior Seismic Hazard Analysis Committee (SSHAC) to review the state-of-the-art in PSHA and to formulate guidelines for greater stability in such studies. The findings of this review were published as NUREG/CR-6372 (***Reference 5.14.1***) and have become widely known as the SSHAC Guidelines. A key finding of the review was stated as follows: "*In the course of our review, we concluded that many of the major potential pitfalls in executing a successful PSHA are procedural rather than technical in character.…This conclusion, in turn, explains our heavy emphasis on procedural guidance*." (***Reference 5.14.1***). The first volume of the SSHAC Guidelines are consequently focused on describing procedures for conducting PSHA studies, in which four study levels were defined, with the simplest studies being classified as Level 1.

© Eskom 2026/Rev 0a

The SSHAC approach at all levels has the same intention, which is to present the best estimate of the seismic hazard (as supported by current data and models) together with an estimate of the full range of uncertainty (resulting from the limitations of the currently available data). In the original SSHAC Guidelines this intention was stated in terms of the "informed technical community", a term that caused considerable confusion. In the more recent application guidelines published as NUREG-2117 by USNRC (***Reference 5.14.2***), the objective has been stated more clearly as capturing "*the centre, the body, and the range of technically-defensible interpretations*", or the CBR of the TDI. This objective is achieved through a two-stage process: evaluation and integration. The evaluation phase consists of the consideration of all the data, methods, and models proposed by the larger technical community that are relevant to the hazard analysis. The integration phase builds a representation (generally in the form of a logic tree) of the centre, the body, and the range of technically-defensible interpretations in light of the evaluation process (***Subsection 5.14.5.3***).

The SSHAC process represents international best practice, and is specifically identified as an acceptable and appropriate framework for conducting a PSHA in RG 1.208 (***Reference 5.14.3***), in the standard ANSI/ANS-2.29-2008 (***Reference 5.14.314***), and in the USNRC Branch Technical Position on the Use of Expert Elicitation in the High-Level Radioactive Waste Program (***Reference 5.14.315***). The decision to adopt the SSHAC process as the framework for the Thyspunt PSHA was therefore completely consistent with current international best practice. In NUREG-2117, the USNRC explicitly states that for new nuclear sites, the seismic hazard assessment must be conducted as a Level 3 or 4 process, but makes no distinction between the two levels in terms of regulatory assurance. More recently, following the Fukushima Dai-ichi accident of March 2011 in Japan, the NRC issued the 50.54(f) letter to all nuclear power plant license holders in the United States to re-evaluate the seismic hazard at their sites, explicitly stating that a SSHAC Level 3 study should be developed for the PSHA at western US sites. For sites in CEUS, licensees were permitted to use the SSC model developed in the regional SSHAC Level 3 CEUS-SSC (Central and Eastern United States Seismic Source Characterization for Nuclear Facilities) Project (***Reference 5.14.69***). Through the issuance of the 50.54(f) letter, which is specifically required for all licensees, the USNRC stated that a SSHAC Level 3 provides an appropriate basis for the seismic design review of existing nuclear power plants. The benefits of SSHAC Level 3 studies are reflected in the fact the process is being widely applied currently (in addition to the studies noted above, a Level 3 PSHA is underway the US Department of Energy Hanford site in Washington state), and while there are discussions of applying the SSHAC Level 3 process in

several locations around the world, there are no plans currently to conduct Level 4 studies.

The SSHAC Level 3 process was applied to the Thyspunt PSHA in accordance with the guidelines and requirements listed in NUREG-2117 (***Reference 5.14.2***) in terms of selection of participants, organisation of workshops, and review process. The key feature of the SSHAC Level 3 process that assures that the PSHA study adequately characterised and accounted for uncertainties is the continuous technical and process review conducted by the Participatory Peer Review Panel (PPRP) as described in ***Subsection 5.14.5.5***. This is further reinforced by the technical challenge and defence within the SSC and GMC TI Teams required for the team members to arrive at consensus logic-trees of which each and every team member is prepared to assume full ownership.

5.14.7.7 Sensitivity Studies

Sensitivity studies were used extensively in the Thyspunt PSHA as a way of identifying and quantifying uncertainties. At the first and third Workshops (***Subsection 5.14.5.2***) hazard sensitivity calculations were presented that served, among other purposes, to identify the relative impact of different uncertainties on the hazard estimates in order to prioritise those elements of the SSC and GMC models warranting greatest effort and attention. In particular at Workshop #3, extensive hazard sensitivity calculations run using the preliminary SSC and GMC models were presented and discussed in order to identify elements requiring refinement towards the production of the final models (***Subsection 5.14.5.3***). The sensitivity calculations showed the contributions to the total hazard of individual branches of the logic-tree as well as contributions from individual seismic sources. Disaggregations, showing the relative contributions of different intervals of magnitude and distance to the total hazard at specific oscillator periods and AFEs, were also presented and discussed. Both the hazard sensitivity feedback and the disaggregation results presented at Workshop #3 were of fundamental importance to the revision of the preliminary SSC and GMC models (***Subsection 5.14.5.3***).

Hazard sensitivity analyses were also performed using the final SSC and GMC models as a way of both checking the internal consistency of the models and the PSHA results, and also obtaining insight into relative influences of different components of the final models on the hazard. The simplest sensitivity analyses showed the contributions from individual seismic sources to the total mean hazard, showing the hazard to be dominated, unsurprisingly, by contributions from the ECC source zone (***Figure 5.14.118***) within which the Thyspunt site is located (***Subsection 5.14.5.4.(c) i***).

© Eskom 2026/Rev 0a

The spectral accelerations at longer response periods scale more rapidly with increasing earthquake magnitude than those at shorter periods, with the consequence that they are more strongly influenced by the occurrence of larger earthquakes. The fault sources, on which the recurrence is represented by the characteristic earthquake model and which therefore generally produce more frequent large-magnitude earthquakes than the area sources (***Subsection 5.14.5.4.(d)***), would be expected to make greater contributions to the hazard as the response period increases. This pattern is confirmed in ***Figure 5.14.119***. This figure shows the total mean hazard and the total contributions by all area sources and all faults grouped together, at six oscillator periods. Although the area sources remain dominant at all response periods, the relative contribution from the fault sources increases appreciably beyond 0.10 second; at the longest period of 2.0 s, the total contribution from fault sources becomes almost equal to that from the area sources at AFEs in the range of 10^{-5}.

Other sensitivity analyses confirmed the relatively strong influence of the uncertainty included in key components of the SSC model, especially the recurrence parameters. The sensitivity of the hazard to the Mmax branches, for example, is illustrated ***Figure 5.14.120***. For the ECC source zone alone, there are seven branches for Mmax in the logic-tree with values ranging from 6.0 to 7.9. The plots in these figures show, as would be expected, a distinct influence of this parameter on the hazard due to the seismicity in the host source zone. The influence of Mmax increases as the AFE decreases, which is also to be expected since at lower AFEs there are more contributions from larger earthquakes. The hazard curves also show some separation at high AFEs, which at first may be a little surprising, but the separation of the curves corresponds to a 0.6 magnitude unit increment in Mmax values, and the lowest two branches (with Mmax estimates of just 6.0 and 6.1) do result in markedly low hazard simply because of this very low truncation of the recurrence relationship (and it should be borne in mind that the minimum magnitude considered in the calculations is just 5.0).

© Eskom 2026/Rev 0a

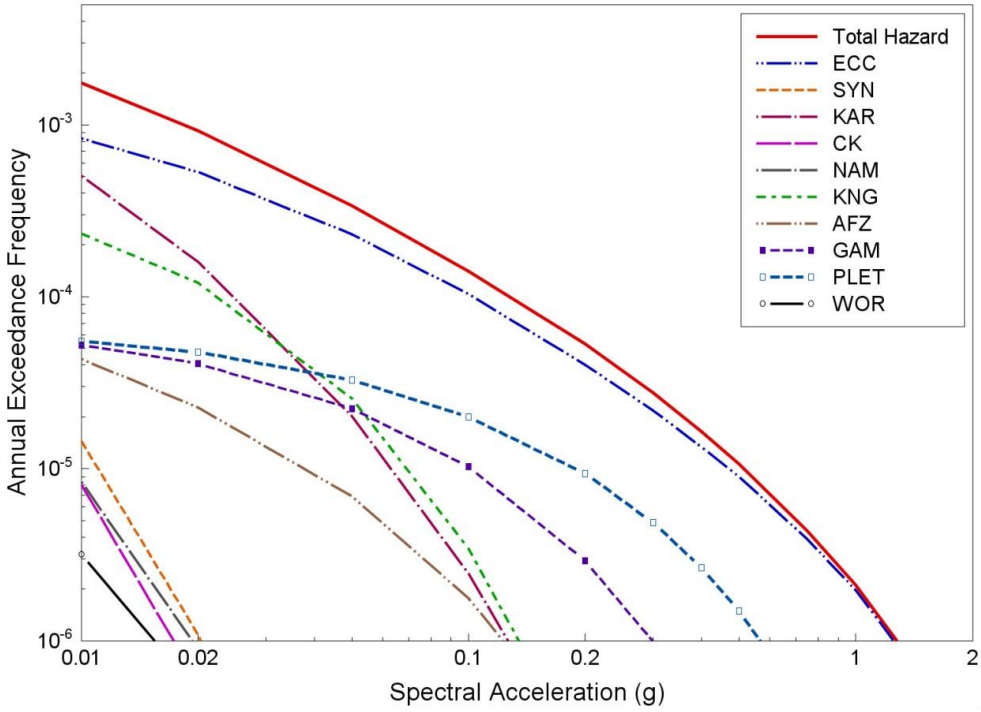


Figure 5.14-118 Mean Hazard Curves for Sa(0.10s) at the Bedrock Elevation and the Contributions from Individual Seismic Sources

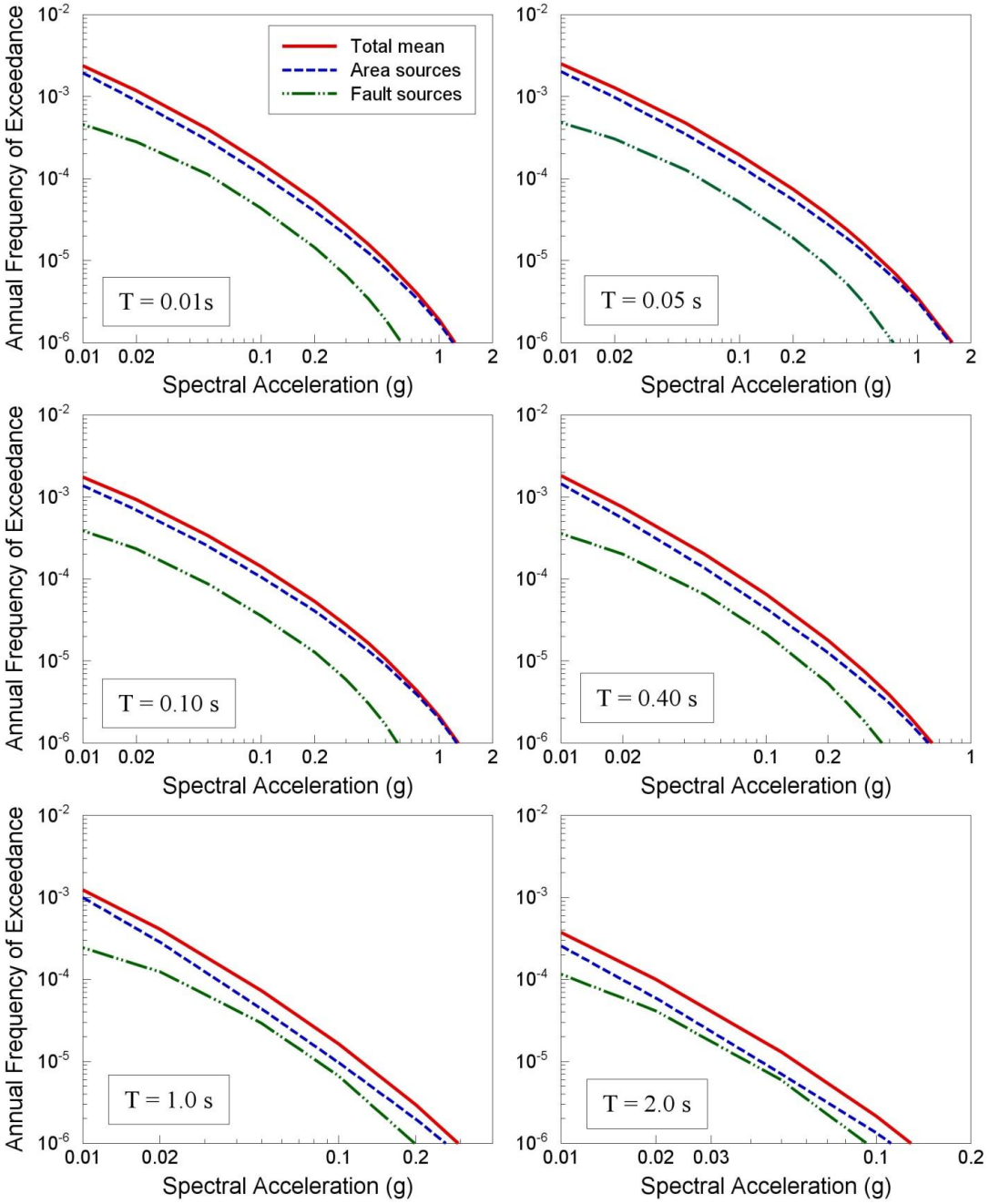


Figure 5.14-119 Mean Hazard Curves at Six Different Oscillator Periods (*labelled on each plot*), Showing the Relative Contributions From All of the Area Source Zones and All of the Fault Sources Grouped Together

Another component of the ECC SSC model explored was the *b*-value of the recurrence relationship. Since the *b*-values are conditional on the Mmax values (***Subsection 5.14.5.4.(c) vii***), plots have been generated for individual Mmax branches, showing the conditional mean hazard that would then have been obtained using each of the five *b*-value branches alone. The three selected Mmax values are the two end members and the central value, namely 6.0, 7.1 and 7.9, and the hazard sensitivity to the *b*-value is shown in ***Figure 5.14.121*** for the central value. The plots confirm the influence of Mmax already revealed in the previous figures, and also show a very pronounced sensitivity to the *b*-value, with lower b-values (indicating a greater relative proportion of larger magnitude earthquakes) leading to consistently higher hazard.

The influence of key elements of epistemic uncertainty in the GMC logic-tree was also explored in sensitivity analyses. ***Figures 5.14.122*** and ***5.14.123*** show the relative influence of the three backbone GMPEs. Since the three models are assigned (very nearly) equal weights, the curves are plotted in this case to show the appearance that the mean hazard curve would have had if each of the three GMPEs had been used alone (carrying a weight of 1.0 in the logic-tree). The AS08 equation consistently produces the highest hazard curve and is therefore seen to be the largest contributor to the total hazard at all both oscillator periods. Conversely, the AC10 equation generally yields the lowest hazard curve, with the exception of high AFEs and longer oscillator period, for which combination the CY08 equation produces the lowest hazard estimates. These observations are not surprising and are consistent with observations of the median predictions compared from the three equations. A reassuring observation is that the three equations consistently produce different hazard curves, confirming that the GMC logic-tree captures distribution of epistemic uncertainty in the median motions.

The influence of other key elements of the GMC model, such as the site adjustment factors (***Subsection 5.14.5.5.(a) i***) and the scaling factors for host-to-target stress drop differences (***Subsection 5.14.5.5.(a)*** **ii**) are self-evident from the size of these scaling factors applied to the median predictions. The individual branches representing epistemic uncertainty in the sigma model (***Subsection 5.14.5.5.(c)***) exerted a non-trivial influence on the hazard results, but these were almost insensitive to the choice between homoskedastic and heteroskedastic sigma models ***Figure 5.14.124***.

© Eskom 2026/Rev 0a

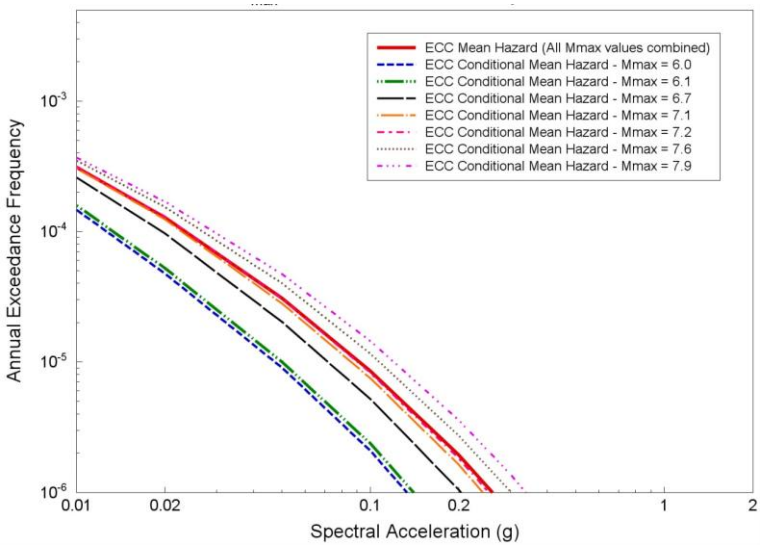


Figure 5.14-120 The Mean Hazard for Sa(1.0s) Due to the ECC Source Using the Full SSC Logic-Tree Compared With the Results That Would Be Obtained Using Each Mmax Branch Alone.

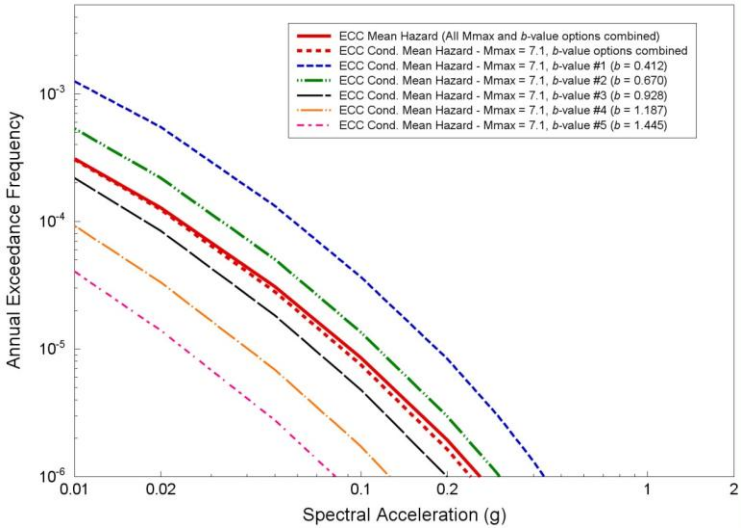


Figure 5.14-121 The Mean Hazard for Sa(0.10s) Due to the ECC Source Using the Full SSC Logic-Tree Compared With the Results That Would Be Obtained Using Each of the *b*-value Branches Associated with the Mmax = 7.1 Branch Alone.

© Eskom 2026/Rev 0a

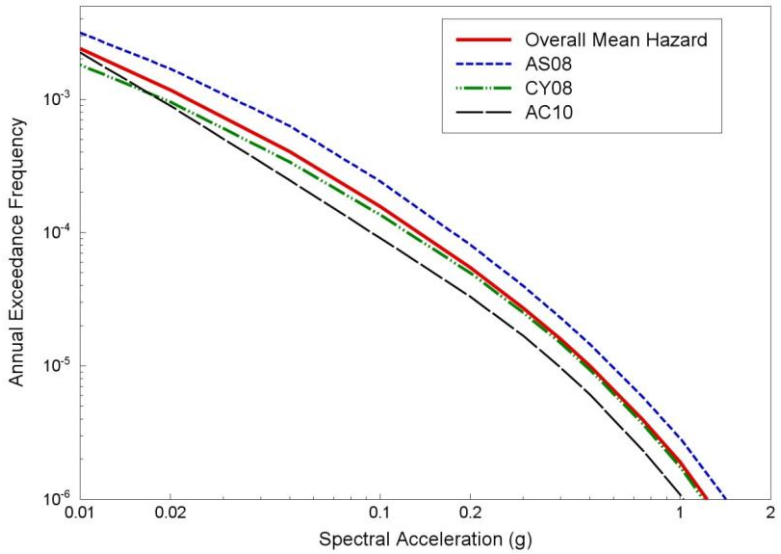


Figure 5.14-122 Mean Hazard Curves for Sa(0.01s) Obtained With the Full Logic-Tree and Assuming That Each of the Three Backbone GMPEs Was Used As the Sole Model.

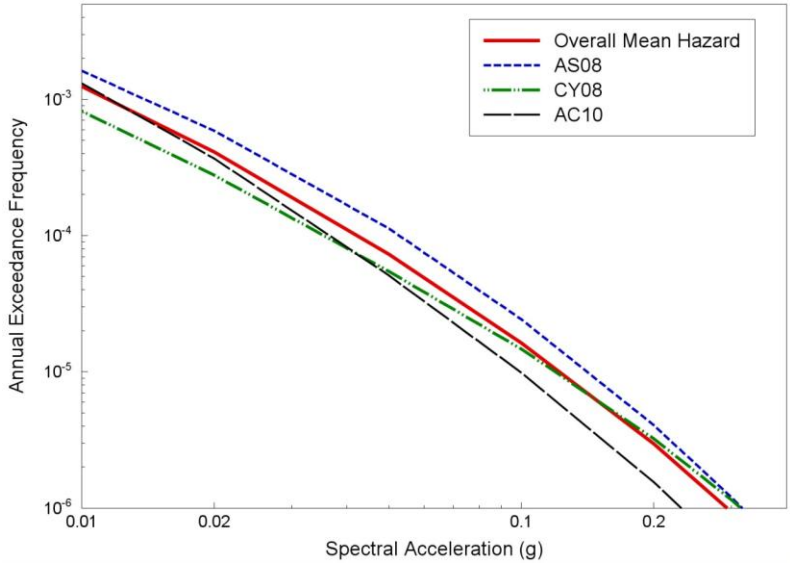


Figure 5.14-123 Mean Hazard Curves for Sa(1.0s) Obtained With the Full Logic-Tree and Assuming That Each Of the Three Backbone GMPEs Was Used as the Sole Model.

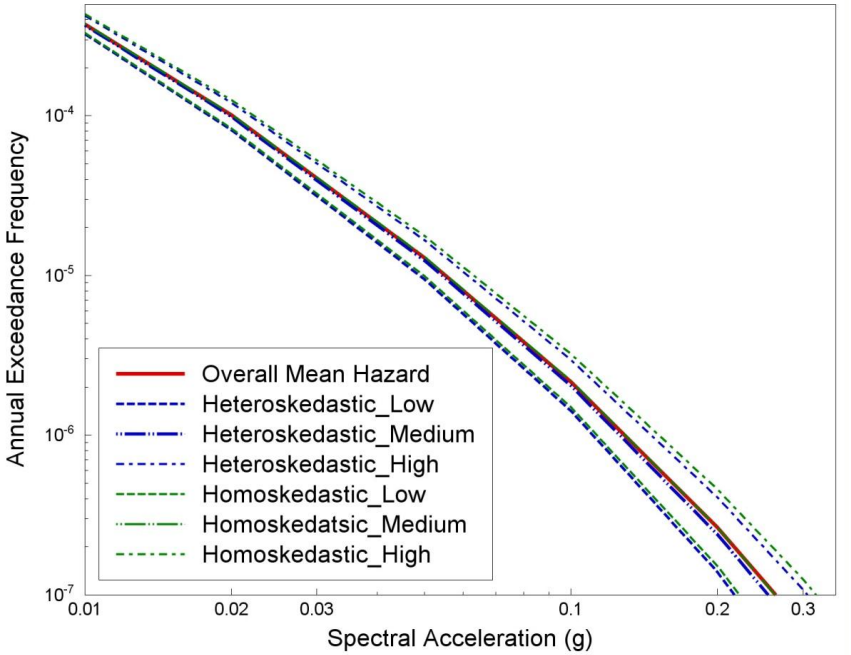


Figure 5.14-124 Overall Mean Hazard Curve for Sa(2.0s) and the Conditional Mean Hazard Curves Obtained Using Each of the Sigma Logic-Tree Branches Alone

Since PSHA is essentially a process of integrating the contributions to the hazard from different earthquake scenarios, the process can be inverted to quantify the relative contributions from different combinations of magnitude, distance and ground-motion exceedance, ε (***References 5.14.316 and 5.14.317***). This process, referred to as deaggregation or disaggregation, enables the contributions from individual bins of magnitude and distance to the spectral acceleration at a particular oscillator period and for a given AFE. Disaggregation information provides very useful insight into the combinations of magnitude (M), distance (R) and numbers of standard deviations (ε) that are driving the hazard. This information provides a check, in a very real sense, on the hazard calculations because the contributing scenarios must be consistent with the SSC model: large contributions would not be expected from sources with relatively low activity that are remote from the site, and the largest magnitude contributing from a given location should obviously not be larger than the maximum value of M_{max} assigned in the logic-tree for the source within which it lies. The number of epsilons (ε) contributing to the dominant scenarios conveys how hard the GMC model is having to work to reach the target hazard levels: in regions of low activity, much of the AFE is obtained directly from the

recurrence of the earthquake itself and it is not necessary to use multiple standard deviations to achieve rare levels of motion.

Figure 5.14.125 shows a typical pair of disaggregation plots, for a selected oscillator period of 0.1 s and an AFE of 10^{-5}. The upper plot shows a classic 3D disaggregation plot with contributions from M-R bins of 0.2 M_w units and 15km, with the shading of the vertical bars indicating the contribution from different intervals of ε. The lower plot shows a 2D representation of the M-R contributions, on which symbols are plotted to indicate the location of modal and the mean scenarios. As point representations of a complex 3D distribution, both of these measures have shortcomings, but they each are also capable of conveying useful information. The modal scenario is simply the M-R pair making the single largest contribution to the hazard. If the disaggregation plot has a single distinct peak, the importance and significance of the modal scenario is very clear. However, for distributions with broad 'ridges' or with multiple peaks of similar height, the modal scenario might not reveal important information. In such cases, the mean scenario has the benefit of capturing the influence of all peaks in the disaggregation plot, but it may correspond to an M-R combination that is not coincident with any of the peaks (indeed, it could conceivably be located at a distance that locates it within an area which an SSC model defines as being aseismic). The benefits and drawbacks of the modal and mean scenarios as the basis for seismic design are discussed by Harmsen *et al*. (***Reference 5.14.318***) and references therein.

Many additional hazard sensitivity and disaggregation plots are presented in ***Reference 5.14.17***.

5.14.8 Management System

This section draws information from another SSR section, ***Section 5.13*** (Geology). A management system in line with that described in ***Chapter 10*** is in place. This system is ISO-9001 certified.

Detailed records of the work carried out and databases established are kept by the consultant. Electronic records have been stored in a secure central repository. These records are backed-up and stored off site as per the consultant's procedures as approved by Eskom. All references cited are saved in the central repository.

© Eskom 2026/Rev 0a

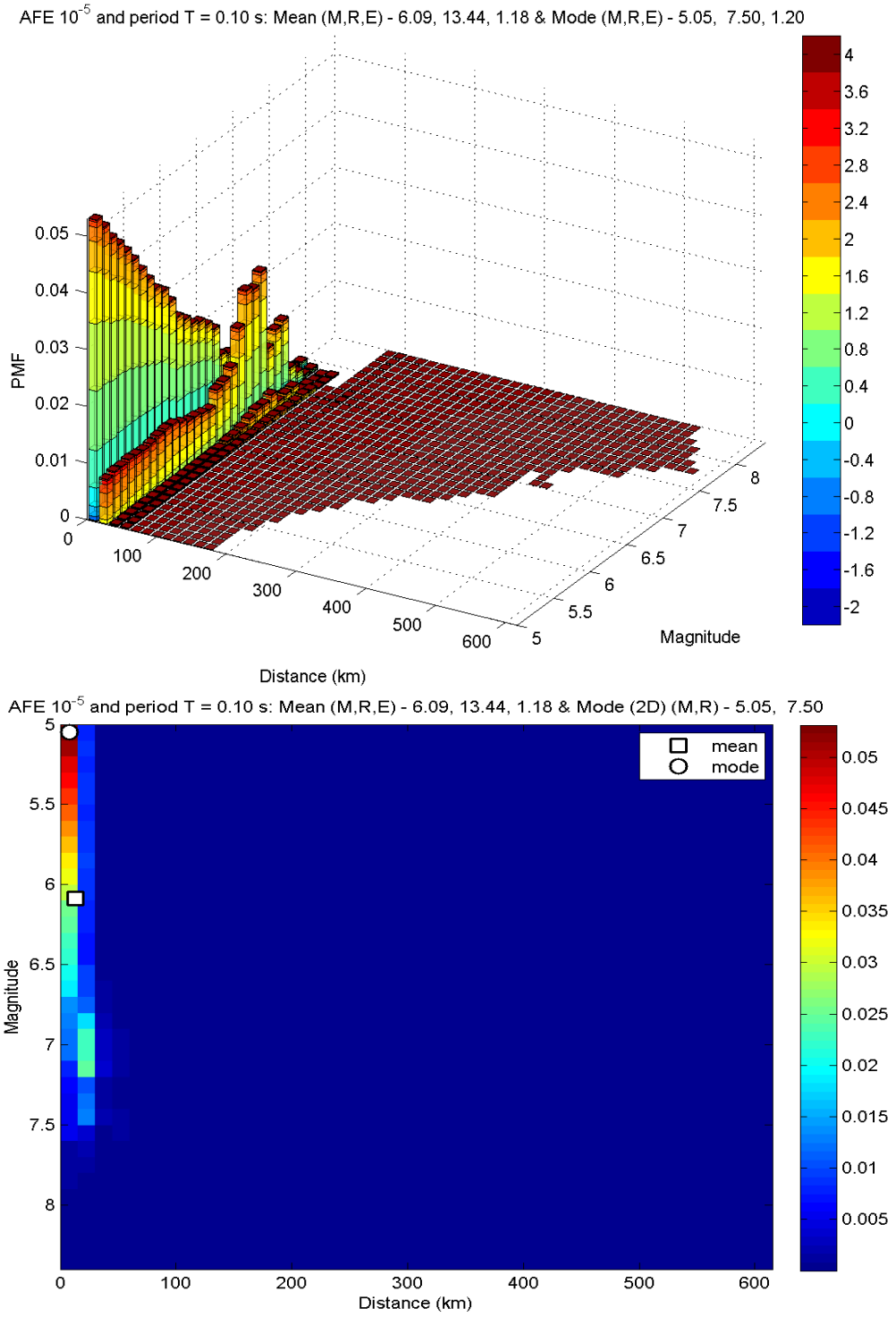


Figure 5.14-125 Disaggregation for Sa(0.10s) at an AFE of 10^{-5}

Site-specific seismic hazard analysis has been classified as Safety Class A activity according to Eskom's safety classification methodology (***Reference 5.14.319***. A Safety Class A classification means that the process is of high importance to nuclear safety and a quality management system compliant with RD-0034 Level 1 (***Reference 5.14.320***) is required, which includes the implementation of a Safety Culture Enhancement Programme.

The seismic hazard study for this SSR followed a SSHAC Level 3 process (***Subsection 5.14.5***) and entailed the following:

- Seismic Source Characterisation (SSC) model);
- Ground Motion Characterisation (GMC) model;
- Seismic hazard calculations using certified computer software.

A safety justification was developed for the SSHAC Level 3 PSHA methodology (***Reference 5.14.321***).

5.14.8.1 Integrated Management System

An Integrated Management System (IMS) manual and procedures were developed by the CGS (***Reference 5.14.299 and 5.14.300***) to control the effective execution of this analysis, which conforms to the overall management system for this SSR (***Chapter 10***). The methodology known as "Plan-Do-Check-Act" (PDCA) was applied to the SSHAC Level 3 processes as required in ISO 9001 (***Reference 5.14.322***) and NNR RD-0034 (***Reference 5.14.320***).

Prior to the start of the seismic hazard analysis the following documents were compiled and approved by Eskom to assist in quality assurance and ensure that work was carried out safely:

- Project Execution Plan (***Reference 5.14.323***),
- Project Quality Plan (***Reference 5.14.324***),
- Procedure for the Project Risk Register (***Reference 5.14.325***),
- Compliance Matrix (***Reference 5.14.326***),
- Safety Culture Enhancement Programme (***Reference 5.14.327***).

© Eskom 2026/Rev 0a

Table 5.14.8
Summary of Activities, Links, and Quality Requirements

Activity	Links		Quality Requirements
	Inputs	Outputs	
Database development	Published and newly gathered geoscientific information	***Sections 5.13***, ***5.14***, and ***5.15***.	Work done according to NNR- / Eskom-approved QMS appropriate for the classification of the activity.
SSC Model development	Data from geological and seismological databases, recurrence models and methods	***Sections 5.13***, ***5.14***, and ***5.15***.	Work done according to NNR- / Eskom-approved QMS appropriate for the classification of the activity.
GMC Model development	Weak-motion data, intensity database, geotechnical data, published ground-motion models and methods	***Sections 5.13***, ***5.14***, and *5.15*.	Work done according to NNR- / Eskom-approved QMS appropriate for the classification of the activity
Hazard Calculations	SSC model and GMCM as described in the HID	***Sections 5.14*** and ***5.15***. ***Chapter 6***	Work done according to NNR- / Eskom-approved QMS appropriate for the classification of the activity
Seismic Monitoring	Recordings of local and regional earthquakes	***Section 5.14*** and ***Section 5.2***	Work done according to internal CGS quality standards.

5.14.8.2 Safety Management

The nuclear industry safety management is concerned with the safety of all processes, including the reliability of the products with respect to their nuclear safety functions. The RD-0034 (***Reference 5.14.320***) requirement document prompts the incorporation of the safety reports INSAG 4 (***Reference 5.14.328***) and INSAG 15 (***Reference 5.14.329***) with the specific aim to establish and enhance a safety culture. Reliability is achieved through adequate management of the procedures as a supporting attribute for safety.

OHSAS 18001 (BSI, 1999) was incorporated into the IMS to control its occupational, health and safety risks and improve its performance.

During the SSHAC level 3 processes, the following safety activities were implemented:

© Eskom 2026/Rev 0a

- SCEP Workshops;
- monthly safety themes;
- monthly safety meetings including the discussion of nuclear safety;
- workshop event safety;
- an industrial psychologist specializing in health and safety awareness in the nuclear industry assessed the team on safety culture;
- safety awards.

5.14.8.3 Considerations for the Nuclear Installation Safety

It is required (***Reference 5.14.330***) that safety classified items of the nuclear installation are designed with reference to either the Operating Basis or Safe Shutdown Earthquake, according to their safety function. Usually safety classification is associated with the Safe Shutdown Earthquake and operational requirements for operability or licensing, with the Operating Basis Earthquake. Estimates for these two design ground motions will be determined after the completion of the PSHA calculations from the outputs that will be provided, as defined previously.

In order to provide a comprehensive representation of the potential seismic loading on the nuclear installation, the output from the PSHA includes all of the following:

- seismic hazard curves for five per cent-damped horizontal spectral accelerations at the following response frequencies: 0.5, 1.0, 2.5, 5.0, 10, 20, 33, 50 and 100 Hz, and for annual exceedance frequencies down to 1 x 10^{-8}. The mean hazard curves are presented, together with the median and fractiles from the 5th to the 95th percentiles.
- uniform hazard spectra (UHS) at various mean annual exceedance frequencies; disaggregations were performed to identify the dominant earthquake scenarios (in terms of magnitude-distance pairs) at defined response periods.
- the horizontal UHS extend to a response frequency of 0.1 Hz, informed by the magnitude scenarios identified by disaggregations and established relationships between the response period beyond which spectral displacement becomes constant and earthquake magnitude.

© Eskom 2026/Rev 0a

- vertical spectra were generated from the horizontal spectra and appropriate vertical-to-horizontal spectral ratios selected to be consistent with the characteristics of the disaggregated earthquakes scenarios.

5.14.8.4 Validation and Verification Exercises

The NNR document RD-0016 defines validation as follows (***Reference 5.14.331***; p.5):

> "*The evidence that demonstrates that the calculation method is fit for its purpose. When calculating physical processes it may mean showing that the calculation is bounding with a suitable degree of confidence rather than a best estimate*."

This has been interpreted to mean that in all parts of the Thyspunt PSHA, appropriate types of calculations have been adopted.

Verification is defined in the following way in RD-0016 (***Reference 5.14.331***; p.5):

> "*The process of ensuring that the controlling physical equations have been correctly translated into software coding, or in the case of hand calculations, correctly incorporated into the calculation procedure. For the purposes of this document verification is taken to be part of the validation submission*."

This has been interpreted to imply that measures are taken to demonstrate that the selected calculation approach is correctly implemented in the software used for the project.

The arguments to support the choices pertaining to validation made in the Thyspunt PSHA project, as well the independent technical checks carried out on numerical elements of the SSC model and GMC model, and on the hazard calculations themselves (see ***Subsection 5.14.6.4***), are described in ***Reference 5.14.298***.

All validation and verification activities were carried out using procedures and forms developed as part of the IMS (***References 5.14.299*** and ***5.14.300***). The completed forms are included as appendices in ***Reference 5.14.298***.

5.14.9 Conclusions

This section presents the final results of the seismic hazard assessment for the Thyspunt site.

© Eskom 2026/Rev 0a

5.14.9.1 Adequacy of the Technical Bases for the PSHA

Geological investigations that contribute to the knowledge base for the Thyspunt site have been conducted over more than the last 25 years. These studies include geological mapping, onshore and offshore geophysical studies, geochronological analyses, geomorphic studies, palaeoseismic studies, and geotechnical investigations. These studies were conducted as part of early screening studies to evaluate multiple nuclear sites, specific studies conducted by the CGS for the Thyspunt site, and geological investigations conducted specifically to address key issues of importance to the seismic hazard analysis. Consistent with all existing NNR guidance and international regulatory guidance and standards, the full range of methods and tools were exercised and the investigations included the recommended increasing levels of specificity ranging from the site region, site vicinity, and site area, to the site location. As is also recommended in the existing regulatory guidance, the results of the investigations conducted for the site were integrated with studies conducted by a large number of investigators within the geoscientific community and published in the professional literature. The available information was supplemented by focused studies conducted specifically to address uncertainties identified in the database compiled at the start of the site-specific PSHA conducted from 2011 to 2013, and included fault corridor mapping, trenching, marine terrace studies, and dating of field samples (***Subsection 5.14.4.3***).

The net result of integrating all the geological studies conducted with the interpretations offered by members of the community in technical publications is a strong, complete geological knowledge base for the site region, site vicinity, site area, and site location. Because the bulk of the studies were conducted according to international best practices for nuclear facilities according the regulatory guidance of the IAEA and the USNRC, the knowledge base is commensurate with the geological knowledge base at other nuclear facilities worldwide. As a result, the subsequent characterisation of seismic sources was able to make use of a complete, high-quality geological knowledge base (***Section 5.13***). The tectonic and geological setting of the region encompassing the Thyspunt site is well understood, being characterised as a stable region.

Seismic monitoring in South Africa has been carried out for many years, primarily by CGS, and a wealth of seismological information from both instrumental and historical sources was compiled and analysed for the Thyspunt site-specific PSHA. New data collection studies were also initiated to address uncertainties in the database, including extensive investigation of archive records of earthquake effects, particularly in the Eastern Cape. This investigation established thresholds of completeness in the historical

earthquake record, which provided assurance regarding the levels of seismicity in the region surrounding the Thyspunt site (***Subsection 5.14.4.4***). The historical earthquake investigations were complemented by collection of intensity data from earthquakes for which instrumental solutions are available (***Subsection 5.14.4.4***), which were used to calibrate the relationships employed to assign locations and magnitudes to historical earthquakes (***Subsection 5.14.4.4***). Consequently, the seismicity patterns in the southern part of South Africa are well understood.

There is no database of strong ground-motion recordings from earthquakes in South Africa, but use was made of weak-motion recordings (***Subsection 5.14.4.6***) and the intensity database (***Subsection 5.14.4.4***) to obtain insights into the nature and amplitude of ground motions in this region. There are no published ground-motion prediction equations (GMPEs) for South Africa, but care was taken to select state-of-the-art GMPEs for this application (***Subsection 5.14.4.7***) and then to adjust these to the target region and site (***Subsection 5.15.5.5.(a)***).

Extensive in situ measurements of shear-wave velocity were made at the Thyspunt site itself (***Subsection 5.14.4.4 (n)***), conducted in two phases after the first set of measurements was assessed to provide insufficient constraint on the dynamic characteristics of the site.

In all regards, therefore, excellent databases were assembled for the Thyspunt PSHA, and rigorously analysed by teams comprised of local experts in South African geology and seismology together with internationally-recognised experts in these fields and in the assessment of seismic hazard in terms of earthquake ground motions. The technical bases were further enriched through structured interactions with Resource and Proponent Experts at formal Workshops conducted in accordance with the specifications for a SSHAC Level 3 process (***Reference 5.14.2***).

5.14.9.2 Capture of Epistemic Uncertainties

While the geological, geophysical, seismological, and geotechnical databases compiled for the Thyspunt PSHA were extensive and developed in accordance with best international practice, it was acknowledged that there would be epistemic uncertainty associated with their interpretation. The SSHAC Level 3 process was adopted strictly for this purpose, to conduct the PSHA within a framework specifically designed to capture "*the centre, the body, and the range of technically-defensible interpretations*", or the CBR of the TDI, of available data, methods and models. The role of the SSHAC Level 3 process in ensuring that the epistemic uncertainty in the SSC and GMC was adequately represented is described in ***Subsection 5.14.7.4***. In the closing letter of the

PPRP, it was unambiguously stated that the CBR of the TDI was effectively captured in the Thyspunt PSHA (***Subsection 5.14.5.5***).

A clear indication of the degree of epistemic uncertainty represented in the logic trees developed for the SSC and GMC models is the spread of the fractiles of the resulting seismic hazard curves. In particular, the separation of the median and mean seismic hazard curves is a clear reflection of the PSHA having incorporated a wide range of epistemic uncertainty. The fractiles of the hazard curves for the spectral acceleration at an oscillator period of 0.2 second (at the deep bedrock horizon) are displayed in ***Figure 5.14.126***, in which the spread of the hazard estimates indicated by the fractile curves is considerable, with a factor on the order of 5 between the 95% and 5% curves at lower AFEs. The degree of epistemic uncertainty captured in the hazard estimates is also attested to by the clear and considerable separation of the mean and median hazard curves, with the former generally seen to be at or above the 70% fractile at the AFEs of relevance to design, and becoming very close to the 85% fractile at an AFE of 10^{-8}. Similar plots for the spectral accelerations at other response periods at both the bedrock horizon and at the surface of the Goudini are presented in ***Reference 5.14.17***.

5.14.9.3 Seismic Hazard Results

The seismic hazard results were obtained from PSHA calculations conducted using state-of-the-art software and subjected to rigorous QA (***Subsection 5.14.6.4***). The PSHA calculations were performed using the full SSC (***Subsection 5.14.5.4***) and GMC (***Section 5.14.6.5***) logic-trees for spectral accelerations at 10 specified oscillator periods (0.01, 0.02, 0.03, 0.04, 0.05, 0.1, 0.2, 0.4, 1.0 and 2.0 seconds). The PSHA calculations were performed to estimate the ground shaking hazard at a depth of about 80 m below the surface of the Goudini formation at the site, where the shear-wave velocity reaches 3 000 m/s (***Figure 5.14.98***). The mean seismic hazard curves for the spectral accelerations at the 10 specified oscillator periods for the bedrock horizon are shown in ***Figure 5.14.127*** and listed in ***Table T-5.14.9***. The bedrock hazard curves were then convolved with the site amplification factors calculated from the dynamic characteristics of the overlying 80 metres of the Goudini formation (***Subsection 5.14.5.5.(b)***) to obtain the seismic hazard curves at the reference surface horizon at the top of the Goudini (***Figure 5.14.128*** and ***Table T-5.14.10***).

Extracting the 10 corresponding spectral acceleration values at any specified annual exceedance frequency (AFE) from the mean seismic hazard curves allows the uniform hazard response spectra (UHRS) to be constructed at both the deep bedrock (***Figure 5.14.129***) and reference surface (***Figure 5.14.130***) horizons. The PSHA calculations were performed up to a limiting upper value

of 5g for the accelerations, which is why the UHRS are incomplete over a small range of oscillator periods for low AFEs.

The hazard calculations were only performed up to a maximum oscillator period of 2.0 seconds, but the UHRS were required to extend to a maximum period of 10.0 seconds. The UHRS were extrapolated by transforming the UHRS acceleration response spectra to relative displacement spectra, and then linearly extrapolating the displacement ordinates from 1.0 to 2.0 seconds. The displacement response spectrum becomes constant beyond a certain control period, TL, which seismological theory predicts to be a function of the controlling earthquake magnitude and the stress drop (***Figure 5.14.131***). The conservative decision was taken to use a value of 10 seconds for TL in all cases, which places the displacement plateau beyond the upper limit of the UHRS. After linearly extrapolating the displacement spectra to 10 seconds, the pseudo-spectral relationship is once again applied to transform the spectral ordinates back to accelerations.

© Eskom 2026/Rev 0a

Table 5.14.9
Seismic hazard curves for the 10 specified oscillator periods at the bedrock elevation

Sa (g)	0.01 s	0.02 s	0.03 s	0.04 s	0.05 s	0.10 s	0.20 s	0.40 s	1.0 s	2.0 s
0.0001	0.048193	0.050877	0.050478	0.048895	0.044978	0.038055	0.043146	0.059271	0.067768	0.049389
0.0002	0.040231	0.04376	0.043569	0.041953	0.038154	0.030754	0.034936	0.049517	0.056621	0.032453
0.0005	0.02709	0.031859	0.03205	0.030176	0.026543	0.019029	0.02174	0.032327	0.034171	0.015668
0.001	0.017404	0.021549	0.021893	0.020213	0.017314	0.011655	0.013121	0.019728	0.019438	0.008051
0.002	0.010262	0.012997	0.013307	0.012162	0.010281	0.006805	0.007424	0.010728	0.009782	0.003719
0.005	0.004647	0.005986	0.006182	0.005628	0.004739	0.003191	0.003316	0.004119	0.003279	0.001116
0.01	0.00239	0.003115	0.003236	0.002952	0.002504	0.001751	0.001756	0.001811	0.001241	0.000375
0.02	0.001174	0.001554	0.001624	0.001489	0.001283	0.000925	0.000887	0.000751	0.00041	0.000101
0.05	0.000403	0.000564	0.000598	0.000548	0.000474	0.000339	0.000304	0.000202	7.27E-05	1.29E-05
0.1	0.000156	0.000229	0.000247	0.000226	0.000196	0.000141	0.000118	6.51E-05	1.63E-05	2.16E-06
0.2	5.45E-05	8.34E-05	9.17E-05	8.46E-05	7.4E-05	5.32E-05	4.03E-05	1.8E-05	2.96E-06	2.64E-07
0.3	2.72E-05	4.36E-05	4.87E-05	4.51E-05	3.94E-05	2.77E-05	1.95E-05	7.56E-06	9.36E-07	6.34E-08
0.4	1.58E-05	2.63E-05	2.99E-05	2.77E-05	2.4E-05	1.65E-05	1.1E-05	3.8E-06	3.8E-07	2.06E-08
0.5	1,00E-05	1.72E-05	1.99E-05	1.84E-05	1.59E-05	1.06E-05	6.73E-06	2.13E-06	1.78E-07	8.06E-09
0.75	3.97E-06	7.33E-06	8.71E-06	8.04E-06	6.87E-06	4.33E-06	2.49E-06	6.52E-07	3.84E-08	1.23E-09
1	1.9E-06	3.7E-06	4.51E-06	4.16E-06	3.52E-06	2.11E-06	1.12E-06	2.5E-07	1.13E-08	2.83E-10
2	2.2E-07	5.12E-07	6.74E-07	6.18E-07	5.06E-07	2.54E-07	1.05E-07	1.46E-08	3.59E-10	5.09E-12
5	4.46E-09	1.34E-08	2.04E-08	1.85E-08	1.45E-08	5.5E-09	1.45E-09	9.78E-11	1.26E-12	8.58E-15

© Eskom 2026/Rev 0a

Table 5.14.10
Seismic hazard curves for the 10 specified oscillator periods at the surface elevation

Sa (g)	0.01 s	0.02 s	0.03 s	0.04 s	0.05 s	0.10 s	0.20 s	0.40 s	1.0 s	2.0 s
0.0001	0.048139	0.050846	0.050449	0.048859	0.044935	0.038003	0.042914	0.058931	0.067457	0.048811
0.0002	0.044642	0.048382	0.04812	0.04631	0.042069	0.034512	0.036611	0.049899	0.056429	0.032385
0.0005	0.032148	0.037588	0.03777	0.035749	0.031444	0.023361	0.023772	0.032961	0.034168	0.01566
0.001	0.022187	0.027887	0.028377	0.026398	0.022483	0.0154	0.015036	0.020479	0.019523	0.008058
0.002	0.013577	0.018055	0.018644	0.017102	0.014167	0.009265	0.008727	0.011287	0.009845	0.003724
0.005	0.00627	0.008665	0.009099	0.008322	0.006791	0.004439	0.003983	0.004406	0.003312	0.001118
0.01	0.003276	0.004628	0.004918	0.004522	0.00369	0.002475	0.002141	0.001967	0.001258	0.000376
0.02	0.001614	0.002333	0.002508	0.00233	0.001919	0.001337	0.001106	0.000824	0.000417	0.000102
0.05	0.000565	0.000863	0.000947	0.000893	0.000744	0.000528	0.000401	0.000226	7.44E-05	1.31E-05
0.1	0.000228	0.000371	0.000417	0.000398	0.000331	0.000236	0.000165	7.46E-05	1.67E-05	2.19E-06
0.2	8.09E-05	0.000141	0.000163	0.000158	0.000132	9.47E-05	6.01E-05	2.12E-05	3.06E-06	2.7E-07
0.3	4.16E-05	7.58E-05	8.95E-05	8.8E-05	7.36E-05	5.29E-05	3.12E-05	9.2E-06	9.8E-07	6.53E-08
0.4	2.49E-05	4.74E-05	5.7E-05	5.67E-05	4.74E-05	3.38E-05	1.87E-05	4.77E-06	4,00E-07	2.14E-08
0.5	1.62E-05	3.22E-05	3.94E-05	3.95E-05	3.29E-05	2.32E-05	1.21E-05	2.73E-06	1.89E-07	8.4E-09
0.75	6.85E-06	1.49E-05	1.89E-05	1.93E-05	1.59E-05	1.08E-05	4.99E-06	8.74E-07	4.11E-08	1.29E-09
1	3.45E-06	8.05E-06	1.06E-05	1.1E-05	8.92E-06	5.88E-06	2.47E-06	3.53E-07	1.23E-08	2.99E-10
2	4.65E-07	1.37E-06	2,00E-06	2.16E-06	1.69E-06	9.98E-07	3.04E-07	2.3E-08	3.97E-10	5.44E-12
5	1.24E-08	5.53E-08	9.93E-08	1.18E-07	8.59E-08	4.1E-08	7.09E-09	1.8E-10	1.08E-12	6.6E-15

© Eskom 2026/Rev 0a

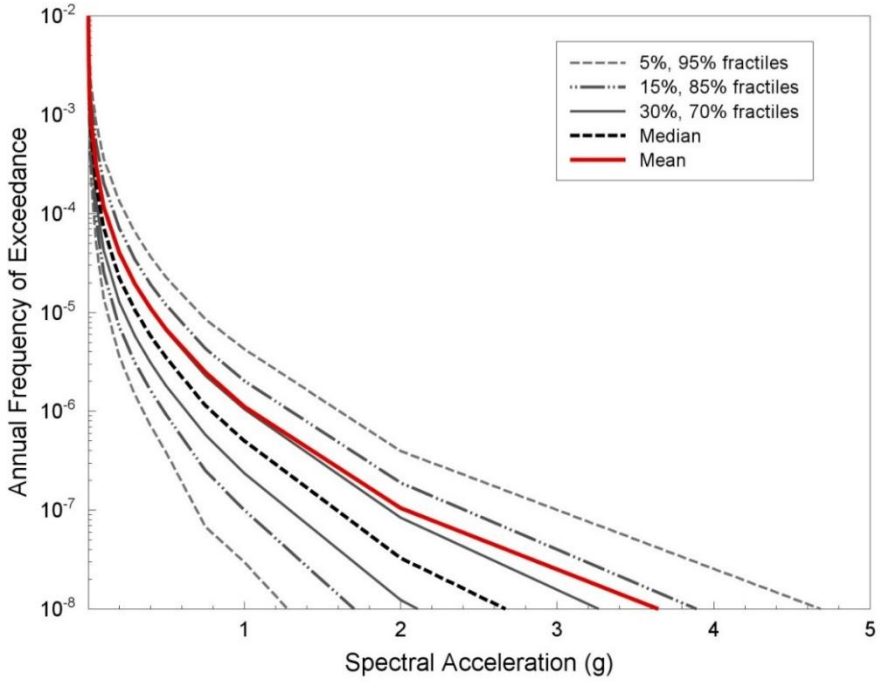


Figure 5.14-126 Mean and Fractile Hazard Curves for Sa(0.20s) at the Bedrock Elevation

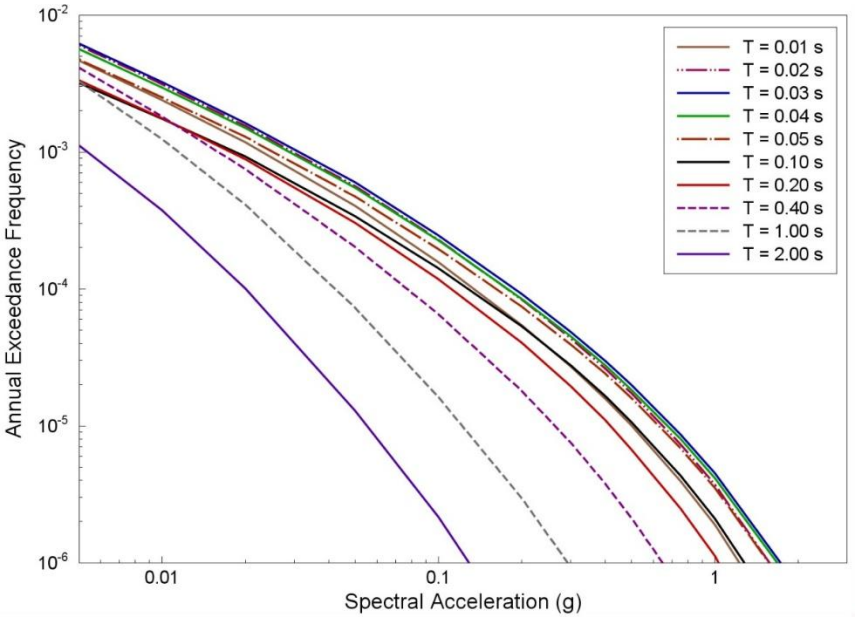


Figure 5.14-127 Mean Hazard Curves Calculated at the Bedrock Elevation

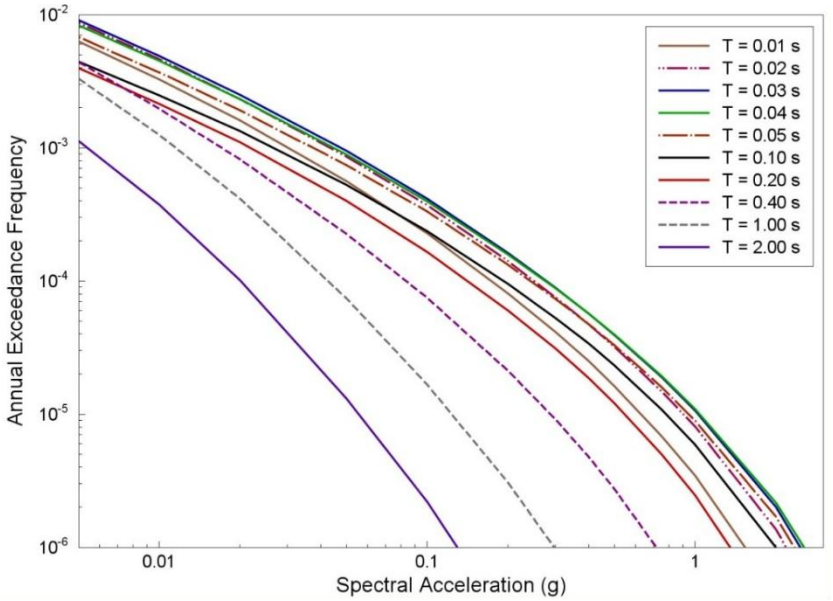


Figure 5.14-128 Mean Hazard Curves Calculated at the Surface Elevation

© Eskom 2026/Rev 0a

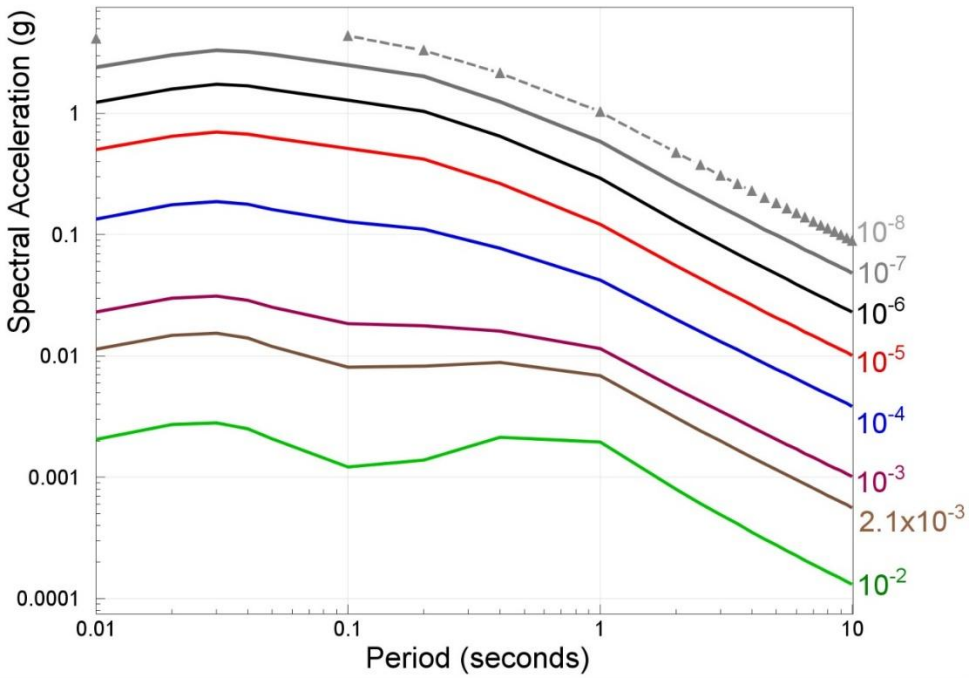


Figure 5.14-129 Uniform Hazard Spectra at the Deep Bedrock Level

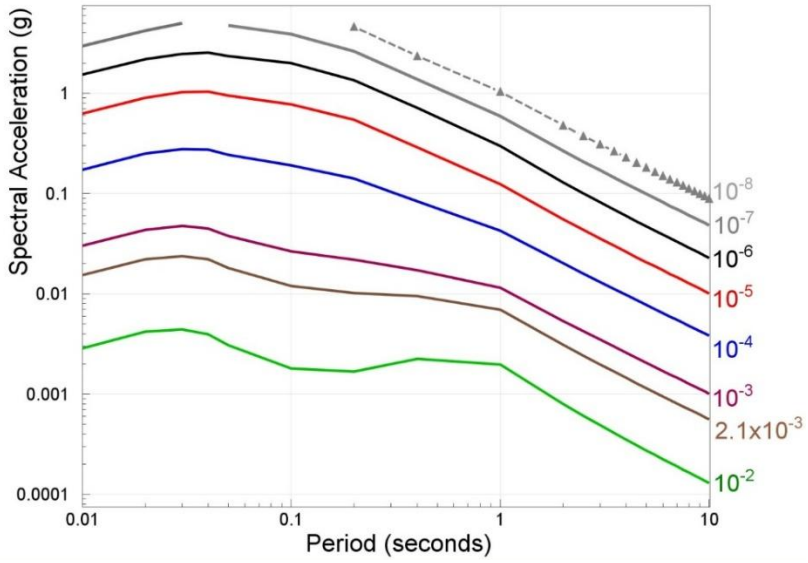


Figure 5.14-130 Uniform Hazard Spectra at the Surface Elevation Level

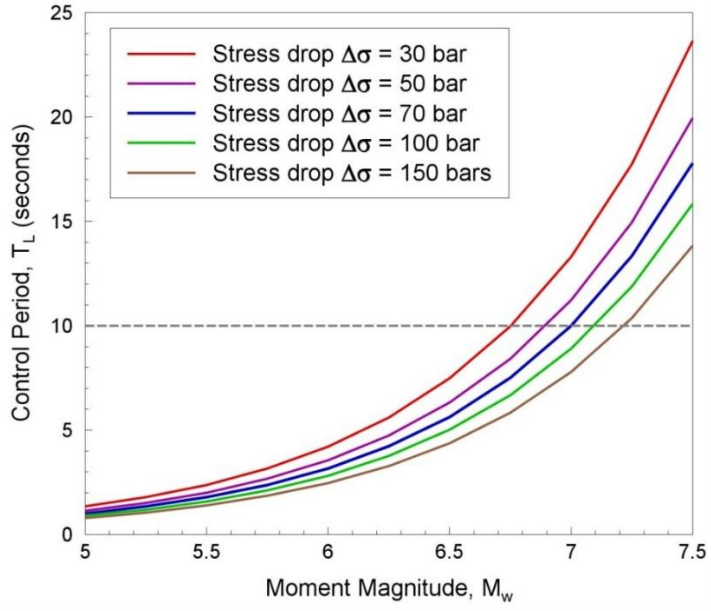


Figure 5.14-131 Predicted Values of the Control Period Defining the Start of Constant Displacement Plateau, From Seismological Theory, for Various Combinations of Magnitude and Stress Drop

The ground motion response spectrum (GMRS) is defined as the basic site demand in terms of ground shaking in RG 1.208 (***Reference 5.14.3***) and is the basis for seismic design of nuclear installations. The GMRS is defined in RG 1.208 and ASCE 43-05 (***Reference 5.14.13***) as the UHRS with a mean AFE of 10^{-4} multiplied by factor, DF, calculated at each oscillator period from the ratio of the UHRS ordinates at mean AFEs of 10^{-5} and 10^{-4}. The UHRS at the bedrock and surface levels at these two AFEs, and the resulting horizontal GMRS at the surface reference horizon are displayed in ***Figure 5.14.132***. The values of the surface UHRS, DF and GMRS are listed in ***Table T-5.14.11***.

The final requirement in terms of representation of the ground shaking hazard is the vertical response spectrum. In order to transform the horizontal response spectra into their vertical equivalents, the GMC TI Team adopted, as a conservative option, the vertical-to-horizontal spectral ratios proposed by McGuire *et al.* (***Reference 5.14.16***) for hard rock sites in CEUS. These factors were interpolated to obtain the values required at the target oscillator periods. The ratios are defined as function of the spectral accelerations at 0.01 s and values were linearly interpolated in the intermediate range of these values (***Reference 5.14.17***). The resulting vertical GMRS, together with the horizontal

GMRS, is shown in the plot in ***Figure 5.14.133***; the vertical ordinates are tabulated in ***Table 5.14.11***.

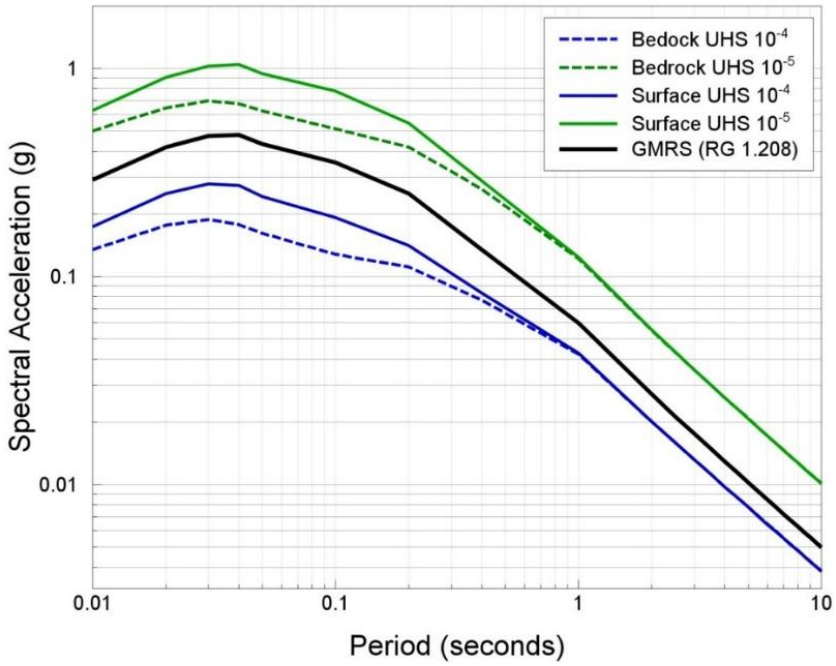


Figure 5.14-132 Uniform Hazard Spectra at the bedrock (*dashed*) and Surface (*solid*) Elevations for AFEs of 10^{-4} and 10^{-5}, and the Resulting GMRS

Table 5.14.11
UHS and GMRS at the surface elevation

Period (s)	UHS (10^{-4})	UHS (10^{-5})	DF	GMRS (H)	GMRS (V)
0.01	0.173506	0.627571	1.678147	0.291168	0.273123
0.02	0.250149	0.903614	1.676406	0.419351	0.397925
0.03	0.278203	1.024514	1.702457	0.473629	0.429882
0.04	0.274562	1.04142	1.74317	0.478608	0.412771
0.05	0.242447	0.944706	1.781129	0.431829	0.357229
0.1	0.191892	0.777815	1.838258	0.352747	0.260996
0.2	0.141104	0.545589	1.770163	0.249776	0.184808
0.4	0.08325	0.288093	1.619836	0.134851	0.099776
1	0.042712	0.123302	1.401147	0.059846	0.04428
2	0.020134	0.055475	1.349852	0.027178	0.020109
2.5	0.015912	0.043392	1.338774	0.021302	0.015761
3	0.013151	0.035611	1.331222	0.017507	0.012953
3.5	0.011206	0.030187	1.325745	0.014856	0.010992
4	0.009761	0.026193	1.32159	0.012901	0.009545
4.5	0.008647	0.023131	1.31833	0.011399	0.008434
5	0.00776	0.020708	1.315705	0.01021	0.007554
5.5	0.007039	0.018744	1.313545	0.009245	0.006841
6	0.00644	0.017119	1.311736	0.008447	0.00625
6.5	0.005935	0.015754	1.3102	0.007776	0.005753
7	0.005503	0.01459	1.308879	0.007203	0.005329
7.5	0.00513	0.013586	1.307731	0.006709	0.004964
8	0.004804	0.012711	1.306724	0.006278	0.004645
8.5	0.004517	0.011942	1.305834	0.005899	0.004365
9	0.004263	0.01126	1.305041	0.005563	0.004116
9.5	0.004036	0.010652	1.30433	0.005264	0.003895
10	0.003831	0.010107	1.303689	0.004995	0.003696

© Eskom 2026/Rev 0a

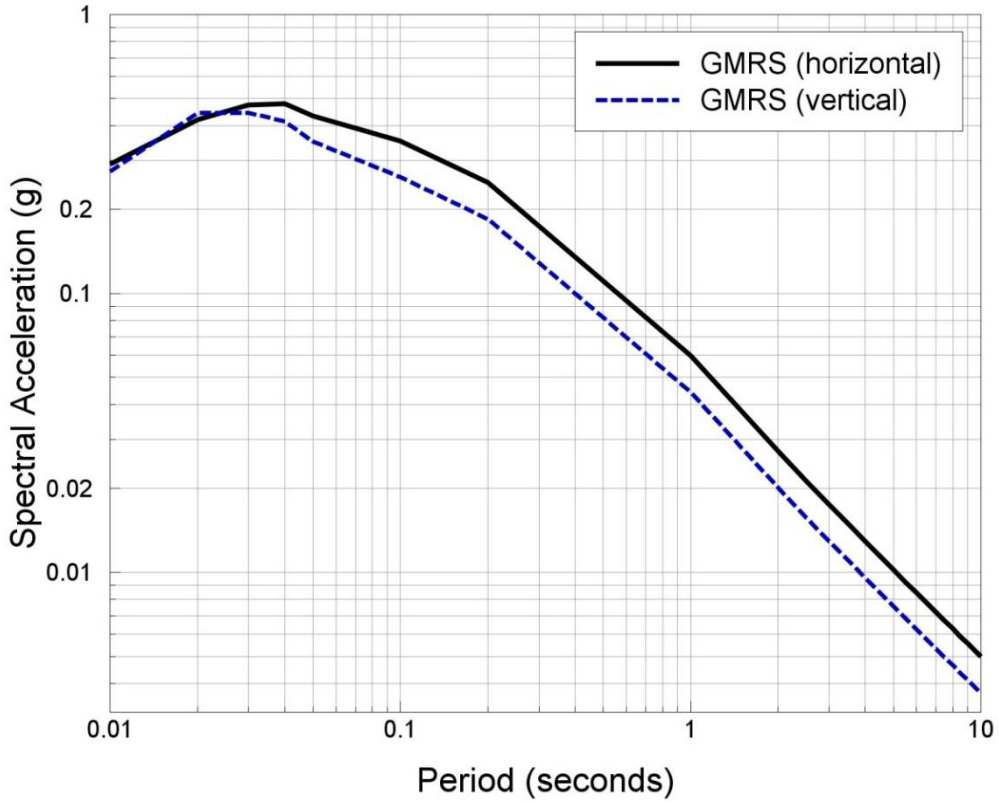


Figure 5.14-133 Horizontal and Vertical GMRS at the Surface Elevation

The full suite of mean, median and fractiles hazard curves, as well as horizontal and vertical UHRS are included in digital form in Appendix 5 of ***Reference 5.14.17***.

5.14.9.4 Use of Seismic Hazard Results

The seismic hazard curves and UHRS allow the spectral accelerations at the Thyspunt site, for both the deeper bedrock level and the reference surface horizon, corresponding to a wide range of annual exceedance frequencies to be determined. While the acceleration at the mean hazard level is the most widely used representation in seismic design for nuclear facilities, the full range of hazard fractiles are also made available for use in probabilistic risk assessments.

As explained in ***Subsection 5.14.5.5.(a)***, the transformation of the ground-motion predictions to the very hard rock conditions at the site means that the

spectral acceleration at the shortest oscillator period considered (0.01 s) is no longer equivalent to PGA, and therefore hazard estimates in terms of this parameter are not available. However, if a design basis PGA value is required, then Eskom recommend the adoption of the 0.01-second spectral acceleration as a surrogate for PGA (although it is noted that this would lead to overestimation of this parameter), which, it is also noted, is not required according to the specifications of RG 1.208 (***Reference 5.14.2***).

In order to provide a basis for generating additional representations of the seismic hazard at the Thyspunt site, such as scenario response spectra and acceleration time histories, disaggregation results are also presented. ***Tables T-5.14.12*** to ***T-5.14.14*** summarise the characteristics of both the mean and modal scenarios for three AFEs (10^{-4}, 10^{-5}, and 10^{-6}, respectively) and for all 10 target oscillator periods. The interpretation of the mean and model scenarios is discussed in ***Subsection 5.14.7.5***.

Acceleration time-histories generated for use in engineering analyses and design will need to be consistent with the hazard estimates, in terms of response spectral ordinates (whether these correspond to the uniform hazard response spectra, the GMRS, scenario spectra or other variations) at least in their ensemble average. Since the generation, scaling or adjustment of acceleration time-histories to conform to the shape and amplitude of a specified elastic response spectrum depends on the target period of vibration (which will be technology specific) and the numbers of analyses to be performed (and whether the desired output is the median structural response or the complete distribution of structural responses), the presentation of the full suite of accelerograms is outside the scope of the Site Safety Report. However, it is noted that the accelerograms must collectively be consistent with the seismic hazard estimates presented in this Section, namely in terms of the acceleration ordinates of their response spectra and also their duration (or effective number of cycles) which must be consistent with the dominant magnitudes identified through disaggregation.

© Eskom 2026/Rev 0a

Table 5.14.12
Disaggregated scenarios at AFE of 10^{-4}

Period	Mean Scenarios			Modal Scenarios		
(seconds)	Mw	R (km)	ε	Mw	R (km)	ε
0.01	6.16	41.07	0.79	5.05	22.5	0.8
0.02	6.15	39.49	0.79	5.05	22.5	0.8
0.03	6.14	38.57	0.80	5.05	22.5	0.8
0.04	6.12	37.42	0.80	5.05	22.5	0.8
0.05	6.09	36.38	0.80	5.05	22.5	0.8
0.1	6.05	33.65	0.78	5.05	22.5	0.8
0.2	6.15	38.78	0.82	5.05	22.5	0.8
0.4	6.41	56.70	0.91	5.35	22.5	0.8
1.0	6.84	122.88	1.13	7.45	127.5	0.8
2.0	7.01	151.63	1.21	7.15	157.5	1.2

Table 5.14.13
Disaggregated scenarios at AFE of 10^{-5}

Period	Mean Scenarios			Modal Scenarios		
(seconds)	Mw	R (km)	ε	Mw	R (km)	ε
0.01	6.20	15.61	1.12	5.05	7.5	1.2
0.02	6.18	15.10	1.13	5.05	7.5	1.2
0.03	6.17	14.74	1.15	5.05	7.5	1.2
0.04	6.14	14.37	1.16	5.05	7.5	1.2
0.05	6.12	14.16	1.17	5.05	7.5	1.2
0.1	6.09	13.44	1.18	5.05	7.5	1.2
0.2	6.22	15.07	1.19	5.15	7.5	1.2
0.4	6.45	20.50	1.20	7.15	22.5	0.8
1.0	6.84	44.40	1.35	7.15	22.5	0.8
2.0	7.02	61.47	1.45	7.15	22.5	0.8

© Eskom 2026/Rev 0a

Table 5.14.14
Disaggregated scenarios at AFE of 10^{-6}

Period	Mean Scenarios			Modal Scenarios		
(seconds)	Mw	R (km)	ε	Mw	R (km)	ε
0.01	6.17	9.56	1.55	5.45	7.5	1.6
0.02	6.15	9.27	1.58	5.35	7.5	1.6
0.03	6.13	9.10	1.61	5.35	7.5	1.6
0.04	6.10	8.95	1.63	5.15	7.5	1.6
0.05	6.08	8.90	1.65	5.05	7.5	1.6
0.1	6.05	8.77	1.68	5.05	7.5	2.0
0.2	6.21	9.32	1.69	5.95	7.5	1.6
0.4	6.48	11.12	1.64	6.65	7.5	1.2
1.0	6.85	18.47	1.71	7.15	22.5	2.0
2.0	7.03	25.10	1.76	7.15	22.5	2.0

© Eskom 2026/Rev 0a

5.14.10 References

5.14.1) Budnitz, R.J., Apostolakis, G, Boore, D.M., Cluff, L.S, Coppersmith, K.J., Cornell, A.C., & Morris, P.A. (1997), **Recommendations for Probabilistic Seismic Hazard Analysis: Guidance on the Uncertainty and Use of Experts**. NUREG/CR-6372. Two volumes. Washington D.C., United States Nuclear Regulatory Commision.

5.14.2) United States Nuclear Regulatory Commission (2012), **Practical Implementation Guidelines for SSHAC Level 3 and 4 Hazard Studies**. NUREG-2117, Rev. 1, Washington D.C. United States Nuclear Regulatory Commision, Office of Nuclear Regulatory Research.

5.14.3) United States Nuclear Regulatory Commission (2007), **A Performance-Based Approach to Define the Site-Specific Earthquake Ground Motion**. Regulatory Guide 1.208. US Nuclear Regulatory Commision, Washington DC.

5.14.4) United States Energy Information Administration (2011), **An Initial Assessment of 14 Regions Outside the United States.** United States Energy Information Administration, United States Department of Energy, Washington D.C.

5.14.5) De Wit, M.J. (2011), **The Great Shale Debate in the Karoo.** South African Journal of Science 107(7/8), doi: 10.4102/sajs.v107i7/8.791.

5.14.6) Majer, E., Baria, R., Stark, M., Oates, S., Bommer, J., & Asanuma, H. (2007), **Induced Seismicity Associated with Enhanced Geothermal Systems**. Geothermics 36(3), 185-222.

5.14.7) Davies, R., Foulger, G., Bindley, A., & Styles, P. (2013). **Induced Seismicity and Hydraulic Fracturing for the Recovery of Hydrocarbons**. Marine and Petroleum Geology 45, 171-185.

5.14.8) Klose, C.D. (2013), **Mechanical and Statistical Evidence of the Causality of Human-Made Mass Shifts on the Earth's Upper Crust and the Occurrence of Earthquakes**. Journal of Seismology 17, 109-135.

5.14.9) Green, C.A., Styles, P., & Baptie, B.J. (2012). **Preese Hall Shale Gas Fracturing: Review & Recommendations for Induced Seismic Mitigation**. Report prepared for the UK Department of Energy & Climate Change.

5.14.10) Department of Minerals and Energy (2011), **The Regulations on Licencing of Sites for New Nuclear Installations**. Government Gazette 34735. Pretoria.

5.14.11) National Nuclear Regulator (2008), **RD-0024: Requirements on Risk Assessment and Compliance with Principal Safety Criteria for Nuclear Installations**. Rev. 0., Centurion, National Nuclear Regulator.

© Eskom 2026/Rev 0a

5.14.12) National Nuclear Regulator (2012), **PP-0014: Considerations of External Events for New Nuclear Installations**. Rev. 0 (Draft). Centurion, National Nuclear Regulator.

5.14.13) American Society of Civil Engineers (2005), **Seismic Design Criteria for Structures, Systems, and Components in Nuclear Facilities**. ASCE/SEI 43-05. Reston, VA, American Society of Civil Engineers.

5.14.14) International Atomic Energy Agency (2003), **Site Evaluation for Nuclear Installations**. Safety Standard Series, Safety Guide No. NS-R-3. Vienna, International Atomic Energy Agency.

5.14.15) International Atomic Energy Agency (2010), **Seismic Hazards in Site Evaluation for Nuclear Installations**. Safety Standards, Specific Safety Guide No. SSG-9. Vienna, International Atomic Energy Agency.

5.14.16) McGuire, R.K., Silva, W.J. & Costantino, C.J. (2001), **Technical Basis for Revision of Regulatory Guidance on Design Ground Motions: Hazard- and Risk-Consistent Ground Motion Spectra Guidelines**. NUREG/CR-6728, Washington DC, United States Nuclear Regulatory Commission.

5.14.17) Bommer, J.J., Coppersmith, K.J., Coppersmith, R.T., Hanson, K.L., Mangongolo, A., Neveling, J., Rathje, E.M., Rodriguez-Marek, A., Scherbaum, F., Shelembe, R., Stafford, P.J., & Strasser, F.O. (2013), **Probabilistic Seismic Hazard Analysis for the Thyspunt Nuclear Site, South Africa**. Report 2013-0190, 900 pp. Pretoria, Council for Geoscience.

5.14.18) Strasser, F.O. & Mangongolo, A. (2013) **TNSP Earthquake Catalogue**. Report 2012-0166, Rev 0. Pretoria, Council for Geoscience.

5.14.19) Wright, C. & Fernández, L. M. (2003), **Chapter 79.48: South Africa**. In: Lee, W.H.K., Kanamori, H. & Jennings, P.C. (eds.), International Handbook of Earthquake and Engineering Seismology. International Geophysics 81(B), 1433-1434.

5.14.20) Saunders, I., Brandt, M., Steyn, J., Roblin, D., & Kijko, A. (2008), **The South African National Seismograph Network**. Seismological Research Letters 79(2), 203-210.

5.14.21) Green, R.W.E. & Bloch, S. (1971), **The Ceres, South Africa, Earthquake of September 29, 1969. I. Report on Some Aftershocks.** Bulletin of the Seismological Society of America 61(4), 851-859.

5.14.22) Havskov, J., & Ottemöller, L. (1999), **SeisAn Earthquake Analysis Software.** Seismological Research Letters 70(5), 532-534.

5.14.23) Nguuri, T.K., Gore, J.,James, D.E., Webb, S.J., Wright, C., Zengeni, T.G., Gwavava, O., Snoke, J.A., & Kaapvaal Seismic Group (2001), **Crustal Structure Beneath Southern Africa and Its Implications for the Formation and Evolution of the Kaapvaal and Zimbabwe Cratons.** Geophysical Research Letters 28(13), 2501-2504.

© Eskom 2026/Rev 0a

5.14.24) Brandt, M.B.C. & Saunders, I. (2011), **New Regional Moment Tensors in South Africa**. Seismological Research Letters 82(1), 69-80.

5.14.25) Gutenberg, B. & Richter, C.F. (1965), **Seismicity of the Earth and Associated Phenomena**. 2nd ed., Hafner Publishing Company New York and London.

5.14.26) Engdahl, E.R., Van der Hilst, R., & Buland, R. (1998), **Global Teleseismic Earthquake Relocation with Improved Travel Time-s and Procedures for Depth Determination**. Bulletin of the Seismological Society of America 88(3), 722-743.

5.14.27) Albini, P. (2012), **Investigating the Past Seismicity of the Eastern Cape Province, South Africa**. Report 2012-0099, Rev. 0, 453 pp. Pretoria, Council for Geoscience.

5.14.28) Midzi, V., Zulu, S.B., Flint, N., Prasad, K., Strasser, F.O., Albini, P. ,& Bommer, J.J. (2012), **Database of Intensity Data for South Africa. Report 2012-0019**, Rev.0. 493 pp. Pretoria, Council for Geoscience..

5.14.29) Ballore, F. de M. de (1896), **Seismic Phenomena of the British Empire**. Quarterly Journal of the Geological Society 52, 651-668.

5.14.30) Wood, H.E. (1913), **On the Occurrence of Earthquakes in South Africa**. Bulletin of the Seismological Society of America 11, 113-120.

5.14.31) Finsen, W.S. (1950), **The Geographical Distribution of Some South African Earthquakes**. Circular No. 110, Union Observatory, Johannesburg.

5.14.32) Sieberg, A. (1932), **Erdbebengeographie**. In: Gutenberg, B. (ed.), Handbuch der Geophysik, Vol. 4, Bornträger, Berlin, Germany.

5.14.33) Theron, J.N. (1974), **The Seismic History of the South-Western Cape Province**. In: Van Wyk, W.L. & Kent, L.E. (eds.), The Earthquake of 29 September 1969 in the South-Western Cape Province, South Africa. Seismological Series 4. Pretoria, Geological Survey of South Africa.

5.14.34) Fernández, L.M. & Guzmán, J.A. (1979), **Seismic history of Southern Africa**. Seismological Series 9, 22pp. Pretoria, Geological Survey of South Africa.

5.14.35) De Klerk, W.J. & Reed, J. du S. (1988), **An Account of Historical Seismic Activity in Southern Africa with Emphasis on the Southern and Eastern Cape**. Report NSIP-GEN-005732#P1-88. Rev. 0. Grahamstown, Albany Museum.

5.14.36) Ambraseys, N.N. & Adams, R.D. (1991), **Reappraisal of Major African Earthquakes, South of 20°N, 1900–1930**, Natural Hazards 4, 389-419.

5.14.37) Musson, R.M.W. (1994), **The BGS Sub-Saharan African Earthquake Catalogue**. Technical Report WL/94/28, 59 pp.. Edinburgh, British Geological Survey.

© Eskom 2026/Rev 0a

5.14.38) Midzi, V., Hlatywayo, D.J., Chapola, L.S., Kebede, F. Atakan, K., Lombe, D.K., Turyomurugyendo, G., & Tugume, F.A. (1999), **Seismic Hazard Assessment in Eastern and Southern Africa**. Annali di Geofisicia 42(6), 1067-1083.

5.14.39) Brandt, M.B.C., Bejaichund, M., Kgaswane, E.M., Hattingh, E., & D.L. Roblin (2005), **Seismic History of South Africa**. Seismological Series 37, 32 pp. Pretoria, Council for Geoscience, South Africa.

5.14.40) Krige, L.J. & Venter, F.A. (1933), **The Zululand Earthquake of the 31st December 1932**. Transactions of the Geological Society of South Africa 36, 101-112.

5.14.41) Krige, L.J. (1936), **The Swaziland and Fauresmith Earthquakes of January 1936**. Transactions of the Geological Society of South Africa 39, 429-40.

5.14.42) Krige, L.J, & Maree, B.D. (1951), **Earthquakes in South Africa**. Bulletin No. 20, 14pp. Pretoria, Geological Survey of South Africa, [first edition in Afrikaans, 1948].

5.14.43) Van Wyk, W.L. &. Kent, L.E. (1974), **The Earthquake of 29 September 1969 in the South-Western Cape Province, South Africa**. Seismological Series 4. Pretoria, Geological Survey of South Africa.

5.14.44) Krüger, F., Reichmann, S., & Scherbaum, F. (2011), **Moment Tensor Solution for the 29.9.1969 Ceres Earthquake**. Presentation at Thyspunt PSHA Workshop 1, April 2011.

5.14.45) Jensen, B.L. (1991), **Source Parameters and Seismotectonics of Three Earthquakes in the Stable Continental Interior of Africa**. MSc Thesis, Memphis State University.

5.14.46) Fairhead, J.D. & Girdler, R.W. (1971), **The Seismicity of Africa**. Geophysical Journal 24(3), 271-301.

5.14.47) Maasha, N. & Molnar, P. (1972), **Earthquake Fault Parameters and Tectonics in Africa**. Journal of Geophysical Research 77(29), 5731-5743.

5.14.48) Fairhead, J.D. & Stuart, G.W. (1982), J.D. **The Seismicity of the East African Rift System and Comparison With Other Continental Rifts**, In: Palmason, G. (ed.), Continental and Oceanic Rifts, American Geophysical Union Geodynamic Series 8, 41–61.

5.14.49) Shudofsky, G.N. (1985), **Source Mechanism and Focal Depths of East African Earthquakes Using Rayleigh-Wave Inversion and Body-Wave Modeling**. Geophysical Journal of the Royal Astronomical Society 83(3), 563-614.

5.14.50) Wagner, G.S. & Langston, C.A. (1988), **East African Earthquake Body Wave Inversion with Implications for Continental Structure and Deformation**. Geophysical Journal 94(3), 503-518.

© Eskom 2026/Rev 0a

5.14.51) Foster, A.N. & Jackson, J.A. (1998), **Source Parameters of Large African Earthquakes: Implications for Crustal Rheology and Regional Kinematics**. Geophysical Journal International 134, 422-448.

5.14.52) Somerville, P., McLaren, J.P., LeFevre, L.V., Burger, R.W., & Helmberger, D.V. (1987), **Comparison of Source Scaling Relations of Eastern and Western North American Earthquakes**. Bulletin of the Seismological Society of America 77(2), 322-346.

5.14.53) Johnston, A.C., Coppersmith, K.J., Kanter, L.R. & C.A. Cornell (1994), **The Earthquakes of Stable Continental Regions**. Five vols. Report EPRI TR-10226. Palo Alto, CA, Electric Power Research Institute.

5.14.54) McGarr, A., Bicknell, J., Sembera, E., & Green, R.W.E. (1989), **Analysis of exceptionally large tremors in two gold mining districts of South Africa.** Pure and Applied Geophysics 129(3-4), 295-307.

5.14.55) Fan, G. & Wallace, T. (1995), **Focal Mechanism of a Recent Event in South Africa: A Study Using a Sparse Very Broadband Network**. Seismological Research Letters 66(5), 13-18.

5.14.56) Bowers, D. (1997), **The October 30, 1994, Seismic Disturbance in South Africa: Earthquake or Large Rock Burst?** Journal of Geophysical Research 102(B5), 9843-9857.

5.14.57) Musson, R.M.W. (2009), **MEEP 2.0 User Guide**. Earth Hazards and Systems Programme Open Report OR/09/045, 16 pp. Edinburgh, British Geological Survey

5.14.58) Bakun, W.H. & Wentworth, C.M. (1997), **Estimating Earthquake Location and Magnitude from Seismic Intensity Data**. Bulletin of the Seismological Society of America 87(6), 1502-1521.

5.14.59) Kövesligethy, R. von (1907), **Seismischer Stärkegrad und Intensität der Beben**. Gerlands Beiträge zur Geophysik 8, 363-366.

5.14.60) Frankel, A. (1994), **Implications of Felt Area-Magnitude Relations for Earthquake Scaling and the Average Frequency of Perceptible Ground Motion**. Bulletin of the Seismological Society of America 84(2), 462-465.

5.14.61) Gasperini, P., Bernardini, F., Valensise, G., & Boschi, E. (1999), **Defining Seismogenic Sources from Historical Earthquakes Felt Reports**. Bulletin of the Seismological Society of America 89(1), 94-110.

5.14.62) Bakun, W.H. & Scotti, O. (2006), **Regional Intensity Attenuation Models for France and the Estimation of Magnitude and Location of Historical Earthquakes**. Geophysical Journal International 164, 596-610.

5.14.63) Gane, P.G. & Oliver, H.O. (1953), **South African Earthquakes - 1949 to December 1952**. Transactions of the Geological Society of South Africa 56, 21-33, Plates III-IV.

© Eskom 2026/Rev 0a

5.14.64) Oliver, H.O. (1956), **South African Earthquakes – January 1953 to December 1955**. Transactions of the Geological Society of South Africa 59, 123-129.

5.14.65) Goetz Observatory (1972), **A Seismological Study of Earthquakes in the Southwest Cape Province 1969-1970**. Technical Report, February 1972, 24pp. Bulawayo, Meteorological Department, Goetz Observatory.

5.14.66) Ma, S. & Atkinson, G.M. (2006), **Focal Depths for Small to Moderate Earthquakes (m_N =2.8) in Western Quebec, Southern Ontario, and Northern New York**. Bulletin of the Seismological Society of America 96(2), 609-623.

5.14.67) Hanks, T. & Kanamori, H. (1979), **A Moment Magnitude Scale**. Journal of Geophysical Research 84, 2348–2350.

5.14.68) Rietbrock, A. & Drouet, S. (2012), **Determination of Stochastic Simulation Parameters for South Africa Based on Weak Motion Recordings from the South African National Seismic Network**. Report 2012-0008. Pretoria, Council for Geoscience.

5.14.69) United States Nuclear Regulatory Commission (2012), **Central and Eastern United States Seismic Source Characterization for Nuclear Facilities**. NUREG-2115, Department of Energy DOE/NE-0140, and Electric Power Research Institute Report 1021097.

5.14.70) Saunders, I., Ottemöller, L., Brandt, M.B.C., & Fourie, C.J.S. (2013), **Calibration of an M_L Scale for South Africa Using Tectonic Earthquake Data Recorded by the South African National Seismograph Network: 2006 to 2009**. Journal of Seismology 17(2), 437-451.

5.14.71) Alsaker, A. Kvamme, L.B., R.A. Hansen, Dahle, A., & Bungum, H. (1991), **The M_L Scale in Norway**. Bulletin of the Seismological Society of America 81(2), 379-398.

5.14.72) Gaull, B.A., & Gregson, P.J. (1991), **A New Local Magnitude Scale for Western Australia**. Australian Journal of Earth Sciences 38, 251-260.

5.14.73) Grünthal, G., Wahlströhm, R. & Stromeyer, D. (2009), **The Unified Catalogue of Earthquakes in Central, Northern, and Northwestern Europe (CENEC) – Updated and Expanded to the Last Millenium**. Journal of Seismology 13(4), 517-541.

5.14.74) Goertz-Allmann, B.P., Edwards, B., Bethmann, F., Deichmann, N., Clinton, J., Fäh, D. & Giardini, D. (2011), **A New Empirical Magnitude Scaling Relation for Switzerland**. Bulletin of the Seismological Society of America 101(6), 3088-3095.

© Eskom 2026/Rev 0a

5.14.75) Edwards, B., Rietbrock, A., Bommer, J.J., & Baptie, B. (2008), **The Acquisition of Source, Path, and Site Effects from Microearthquake Recordings Using Q Tomography: Application to the United Kingdom**. Bulletin of the Seismological Society of America 98(4), 1915-1935.

5.14.76) Miao, Q. & Langston, C.A. (2007), **Empirical Distance Attenuation and the Local-Magnitude Scale for the Central United States**. Bulletin of the Seismological Society of America 97(6), 2137-2151.

5.14.77) Allen, T.I., Gibson, G., Brown, A., & Cull, J.P. (2004), **Depth Variation of Seismic Source Scaling Relations: Implications for Earthquake Hazard in Southeastern Australia**. Tectonophysics 390, 5-24.

5.14.78) Deichmann, N. (2006), **Local Magnitude, a Moment Revisited**. Bulletin of the Seismological Society of America 96(4A), 1267-1277.

5.14.79) Johnston, A.C. (1996a), **Seismic Moment Assessment of Earthquakes in Stable Continental Regions – I. Instrumental Seismicity**. Geophysical Journal International 124, 381-414.

5.14.80) Scordilis, E.M. (2006), **Empirical Global Relationships Converting M_S and m_b to Moment Magnitude**. Journal of Seismology 10(2), 225-236.

5.14.81) Nuttli, O.W. (1973), **Seismic Wave Attenuation and Magnitude Relations for Eastern North America**. Journal of Geophysical Research 78(5), 876-885.

5.14.82) Chow, R.A.C, Fairhead, J.D., Henderson, N.B., & Marshall, P.D. (1980), **Magnitude and Q Determinations in Southern Africa Using Lg wave Amplitudes**. Geophysical Journal of the Royal Astronomical Society 63, 735-745.

5.14.83) Fernández, L. M. (1974), **Geophysical implication of the 1969-1971 Ceres seismic sequence.** In: The earthquake of 29 September 1969 in the south-western Cape Province, South Africa. Van Wyk, W.L. & L.E. Kent (eds), Seismological Series 4, Pretoria, Geological Survey of South Africa.

5.14.84) Johnston, A.C. (1996b), **Seismic Moment Assessment of Earthquakes in Stable Continental Regions – II. Historical seismicity**. Geophysical Journal International 125, 639-678.

5.14.85) Wiemer, S (2001), **A Software Package to Analyze Seismicity: ZMAP**. Seismological Research Letters, 72, 373-382.

5.14.86) Gardner, J.K. & Knopoff, L. (1974), **Is the Sequence of Earthquakes in Southern California, With Aftershocks Removed, Poissonian?** Bulletin of the Seismological Society of the America 64(9), 1363-1367.

5.14.87) Reasenberg, P. (1985), **Second-Order Moment of Central Californian Seismicity, 1969-1982**. Journal of Geophysical Research 90, 5479-5495.

© Eskom 2026/Rev 0a

5.14.88) Veneziano, D. & Van Dyck, J. (1985), **Statistical Discrimination of Aftershocks and Their Contribution to Seismic Hazard**. In Seismic Hazard Methodology for Nuclear Facilities in the Eastern U.S., Volume 2, Appendix A-4, EPRI/SOG Draft 85-1.

5.14.89) Zhuang, J., Ogata, Y., & Vere-Jones, D. (2002), **Stochastic Declustering of Space-Time Earthquake Occurrences**. Journal of the American Statistical Association. 97, 369-380.

5.14.90) Hainzl, S., Scherbaum, F., & Beauval, C. (2006), **Estimating Background Activity Based on Interevent-Time Distribution**. Bulletin of the Seismological Society of the America 96(1), 313-320.

5.14.91) Stepp, J. C. (1972), **Analysis of Completeness of the Earthquake Sample in the Puget Sound Area and its Effects on Statistical Estimates of Earthquake Hazard**. Proceedings of the Microzonation Conference, Seattle, WA, 897-909.

5.14.92) Beauval, C. (2003), **Analysis of Uncertainties in Probabilistic Seismic Hazard Assessment: the Example of France**. PhD Thesis, Universite Joseph Fourier, Grenoble, France [in French].

5.14.93) Wiemer, S. & Wyss, M. (2000), **Minimum Magnitude of Complete Reporting in Earthquake Catalogs: Examples From Alaska, the Western United States, and Japan**. Bulletin of the Seismological Society of America 90(3), 859-869.

5.14.94) Stucchi, M., Albini, P., Mirto, C., & Rebez, A. (2009), **Assessing the Completeness of Italian Historical Earthquake Data**. Annali di Geofisica 47(2-3), 659-673.

5.14.95) Schorlemmer, D. & Woessner, J. (2008), **Probability of Detecting an Earthquake**. Bulletin of the Seismological Society of America 98(5), 2103-2117.

5.14.96) Brandt, M.B.C. (2011), **Regional Moment Tensors, Moment Magnitude, Completeness and National Network Expansion**. Presentation at Thyspunt PSHA Workshop 1, April 2011.

5.14.97) Willemann, R.J. (1999), **Regional Thresholds of the ISC Bulletin**. Seismological Research Letters 70(3), 313-321.

5.14.98) Midzi, V., Bommer, J.J., Strasser, F.O., Albini, P., Zulu, B.S., Prasad, K., & Flint, N.S. (2013) . **An Intensity Database for Earthquakes in South Africa from 1912 to 2011**. Journal of Seismology 17(4), 1183-1205.

5.14.99) Musson, R.M.W. & Cecic, I. (2002), **Macroseismology**. In: International Handbook of Earthquake and Engineering Seismology, W.H.K. Lee, H. Kanamori, P.C. Jennings & C. Kisslinger (eds.), International Geophysics 81, Part A, 49, 807-822.

© Eskom 2026/Rev 0a

5.14.100) Allen, T.I., Wald, D.J., Hotovec, A.J., Lin, K., Earle, P.S., & Marano, K.D.(2008), **An Atlas of ShakeMaps for Selected Global Earthquakes.** Open-File Report 2008-1236, United States Geological Survey.

5.14.101) Richter, C.F. (1958), **Elementary Seismology**. 768 pp. W.H. Freeman, San Francisco

5.14.102) Wood, H.O. & Neumann, F. (1931), **Modified Mercalli Intensity Scale of 1931**. Bulletin of the Seismological Society of America 21, 277-283.

5.14.103) Musson, R.M.W., Grünthal, G. & Stucchi, M. (2010), **The Comparison of Macroseismic Intensity Scales**. Journal of Seismology 14, 413-428.

5.14.104) Singh, S.K., Mena, E, & Castro R. (1988), **Some Aspects of Source Characteristics of the 19 September 1985 Michoacan Earthquake and Ground Motion Amplification In and Near Mexico City From Strong Motion Data.** Bulletin of the Seismological Society of America 78, 451-477.

5.14.105) Keyser, A.W. (1974), **Some Macroseismic Observations in the Meizoseismal Area of the Boland Earthquake of 29 September 1969 in the South-Western Cape Province.** In: The earthquake of 29 September 1969 in the south-western Cape Province, South Africa. Van Wyk, W.L. & L.E. Kent (eds), Seismological Series 4, Pretoria, Geological Survey of South Africa.

5.14.106) Park, J., Lindberg, C.R., & Vernon, F.L. (1987), **Mult itaper Spectral Analysis of High Frequency Seismograms**. Journal of Geophysical Research 92, 12 675 – 12 684.

5.14.107) Lees, J.M. & J. Park (1995),**Multi-Taper Spectral Analysis: A Standalone C Subroutine**. Computer & Geosciences 21, 199-236.

5.14.108) Aki, K. (1967), **Scaling Law of Seismic Spectrum**. Journal of Geophysical Research 72, 1217-1231.

5.14.109) Brune, J.N. (1970), **Tectonic Stress and the Spectra of Seismic Shear Waves from Earthquakes**. Journal of Geophysical Research 75(26), 4997-5009.

5.14.110) Brune, J.N. (1971), **Correction**. Journal of Geophysical Research 76(20), 5002.

5.14.111) Abercrombie, R.E. (1995), **Earthquake Source Scaling Relationships from -1 to 5 M_L Using Seismograms Recorded at 2.5-km Depth**. Journal of Geophysical Research 100(B12), 24015-24036.

5.14.112) Rietbrock, A., Strasser, F., & Edwards, B. (2013), **A Stochastic Earthquake Ground-Motion Prediction Model for the United Kingdom**. Bulletin of the Seismological Society of America, 103(1), 57-77.

5.14.113) Atkinson, G.M. (2004), **Empirical Attenuation of Ground-Motion Spectral Amplitudes in Southeastern Canada and the Northeastern United States**. Bulletin of the Seismological Society of America 94(3), 1079-1095.

© Eskom 2026/Rev 0a

5.14.114) Allen, T.I., Dhu, T., Cummins, P.R., & Schneider, J.F. (2006), **Empirical Attenuation of Ground-Motion Spectral Amplitudes in Southwestern Western Australia**. Bulletin of the Seismological Society of America 96(2), 572-585.

5.14.115) Archuleta, R.J., Cranswick, E., Mueller, C., & Spudich, P. (1982), **Source Parameters of the 1980 Mammoth Lakes, California, Earthquake Sequence**. Journal of Geophysical Research 87(B6), 4595-4607.

5.14.116) García-García, J.M., Romacho, M.D. & Jiménez, A. (2004), **Determination of Near-Surface Attenuation, With k Parameter, to Obtain the Seismic Moment, Stress Drop, Source Dimension and Seismic Energy for Microearthquakes in the Granada Basin (Southern Spain)**, Physics of the Earth and Planetary Interiors 141, 9-26.

5.14.117) Bressan, G., Kravanja, S., & Franceschina, G. (2007), **Source Parameters and Stress Release of Seismic Sequences Occurred in the Friuli-Venezia Giulia region (Northeastern Italy) and in Western Slovenia**. Physics of the Earth and Planetary Interiors 160, 192-214.

5.14.118) Moghaddam, H., Fanaie, N., & Motazedian, D. (2010), **Estimation of Stress Drop for Some Large Shallow Earthquakes Using Stochastic Point Source and Finite Fault Modeling**. Transaction A: Civil Engineering 17(3), 217-235.

5.14.119) Anderson, J.G. & Hough, S.E. (1984), **A Model for the Shape of the Fourier Amplitude Spectrum of Acceleration at High Frequencies**. Bulletin of the Seismological Society of America 74(5), 1969-1993.

5.14.120) Boore, D.M. (2003), **Simulation of Ground Motion Using the Stochastic Method**. Pure and Applied Geophysics 160, 635-676.

5.14.121) Campbell, K.W. (2003), **Prediction of Strong Ground Motion Using the Hybrid Empirical Method and its Use in the Development of Ground-Motion (Attenuation) Relations in Eastern North America**. Bulletin of the Seismological Society of America 93(3), 1012-1033.

5.14.122) Scherbaum, F. Cotton, F., & Staedtke, H. (2006), **The Estimation of Minimum-Misfit Stochastic Models from Empirical Ground-Motion Prediction Equations**. Bulletin of the Seismological Society of America 96(2), 427-445.

5.14.123) Papaspiliou, M., Kontoe, S., & Bommer, J.J. (2012), **An Exploration of Incorporating Site Response Into PSHA – Part I: Issues Related to Site Response Analysis Methods**. Soil Dynamics & Earthquake Engineering 42, 302-315.

5.14.124) Cotton, F., Scherbaum, F., Bommer J.J., & Bungum, H. (2006), **Criteria for Selecting and Adjusting Ground-Motion Models for Specific Target Regions: Application to Central Europe and Rock Sites**. Journal of Seismology 10(2), 137-156.

© Eskom 2026/Rev 0a

5.14.125) Douglas, J. (2011), **Ground-motion prediction equations 1964-2010**. BRGM/RP-59356-FR, 444 pp. Orléans, France,BRGM.

5.14.126) Bommer, J.J., Douglas, J., Scherbaum, F., Cotton, F., Bungum, H., & Fäh, D. (2010a), **On the Selection of Ground-Motion Prediction Equations for Seismic Hazard Analysis**. Seismological Research Letters 81(5), 783-793.

5.14.127) Hong, H.P. & Goda, K. (2007), **Orientation-Dependent Ground-Motion Measure for Seismic Hazard Assessment**. Bulletin of the Seismological Society of America 97(5), 1525-1538.

5.14.128) Bommer, J.J., Douglas, J., & Strasser, F.O (2003), **Style-of-Faulting in Ground-Motion Prediction Equations**. Bulletin of Earthquake Engineering 1(2), 171-203.

5.14.129) Abrahamson, N.A. & Silva, W.J. (2008), **Summary of the Abrahamson & Silva NGA Ground-Motion Relations**. Earthquake Spectra 24(1), 67-97.

5.14.130) Boore, D.M. & Atkinson, G.M. (2008), **Ground-Motion Prediction Equations for the Average Horizontal Component of PGA, PGV, and 5%-Damped PSA at Spectral Periods Between 0.01s and 10.0 s**. Earthquake Spectra 24(1), 99-138.

5.14.131) Campbell, K.W. & Bozorgnia, Y. (2008), **NGA Ground Motion Model for the Geometric Mean Horizontal Component of PGA, PGV, PGD and 5% Damped Linear Elastic Response Spectra for Periods Ranging From 0.01 to 10s**. Earthquake Spectra 24(1), 139-171.

5.14.132) Chiou, B.S.J. & Youngs, R.R. (2008), **An NGA Model For the Average Horizontal Component of Peak Ground Motion and Response Spectra**. Earthquake Spectra 24(1), 173-215.

5.14.133) Power, M., B. Chiou, B., Abrahamson, N., Bozorgnia, Y., Shantz, T., & Roblee, C. (2008), **An overview of the NGA Project. Earthquake Spectra** 24(1), 3-21.

5.14.134) Akkar, S. & Çagnan, Z. (2010), **A Local Ground-Motion Predictive Model for Turkey and its Comparison with Other Regional and Global Ground-Motion Models**. Bulletin of the Seismological Society of America 100(6), 2978-2995.

5.14.135) Atkinson, G.M. & Boore, D.M. (2011), **Modifications to Existing Ground-Motion Prediction Equations in Light of New Data**. Bulletin of the Seismological Society of America 101(3), 1121-1135.

5.14.136) Abrahamson, N.A. & Silva, W.J. (2009), **Errata for 'Summary of the Abrahamson & Silva NGA Ground-motion Relations'**. Available from: http://peer.berkeley.edu/ngawest/nga_models.html.

5.14.137) Stafford, P.J., Strasser, F.O., & Bommer, J.J. (2008), **An Evaluation of the Applicability of the NGA Models to Ground-Motion Prediction in the Euro-Mediterranean Region**. Bulletin of Earthquake Engineering 6(2), 149-177.

© Eskom 2026/Rev 0a

5.14.138) Boore, D.M. & Joyner, W.B. (1997), **Site Amplifications for Generic Rock Sites**. Bulletin of the Seismological Society of America 87, 327–341.

5.14.139) Sandikkaya, M. A., Yilmaz, M.T., Bakir, B.S., & Yilmaz, Ö. (2010), **Site Classification of Turkish National Strong-Motion Stations**. Journal of Seismology 14, 543-563.

5.14.140) Rathje, E.M. Stokoe, II, K.H., & Rosenblad, B. (2003), **Strong Motion Station Characterization and Site Effects During the 1999 Earthquakes in Turkey**. Earthquake Spectra 19(3), 653-675.

5.14.141) Tezel, T., Erduran, M. & Alptekin, Ö. (2010), **Crustal Shear Wave Velocity Structure of Turkey by Surface Wave Dispersion Analyses**. Annals of Geophysics 50(2), 177-190.

5.14.142) Tezel, T., Shibutani, T. & Kaypak, B. (2010), **Crustal structure Variation in Western Turkey from Receiver Function Analyses**. Tectonophysics 492, 240-252.

5.14.143) Akkar, S. & Yenier, E. (2009), **Assessment of Point-Source Stochastic Simulations Using Recently Derived Ground-Motion Prediction Equations**. Bulletin of the Seismological Society of America 99(6), 3172-3191.

5.14.144) Rathje, E.M., Cichowicz, A., & Birch, D. (2012), **Seismic Site Characterization for the Thyspunt Nuclear Siting Project.** CGS Report Number 2012-1036, Rev 1.Pretoria, Council for Geoscience.

5.14.145) Park, C. (2013), **MASW for Geotechnical Site Investigation**. The Leading Edge 32(6), 936-942.

5.14.146) Abrahamson, N.A., Birkhauser, P., Koller, M., Mayer-Rosa, D., Smit, P., Sprecher, C., Tinic, S., & Graf, R. (2002), **PEGASOS – A Comprehensive Probabilistic Seismic Hazard Assessment for Nuclear Power Plants in Switzerland**. Proceedings of the Twelfth European Conference on Earthquake Engineering, London, paper no. 633.

5.14.147) Youngs, R.R., & Coppersmith, K.J. (1985), **Implications of Fault Slip Rates and Earthquake Recurrence Models to Probabilistic Hazard Estimates**, Bulletin of the Seismological Society of America 75, 939-964.

5.14.148) Wesnousky, S.G. (1986), **Earthquakes, Quaternary Faults, and Seismic Hazard in California**, Journal Geophysical Research 91, 12587-12631.

5.14.149) Kanter, L.R. (1994), **Tectonic Interpretation of Stable Continental Crust**. In: The Earthquakes of Stable Continental Regions, A.C. Johnston, K.J. Coppersmith, L.R. Kanter, & C.A. Cornell (eds.), vol. 1, chap. 2, pp. 1-98. Report EPRI TR 102261. Palo Alto, California, Electric Power Research Institute.

© Eskom 2026/Rev 0a

5.14.150) Kgaswane. E.M., Nyblade, A.A., Julià, J., Dirks, P.H.G.M., Durrheim, R.J., & Pasyanos, M.E. (2009), **Shear Wave Velocity Structure of the Lower Crust in Southern Africa: Evidence for Compositional Heterogeneity Within Archean and Proterozoic Terrains**. Journal of Geophysical Research 114, B12304, doi: 10.1029/2008JB006217.

5.14.151) Schulte, S.M. & Mooney, W.D. (2005), **An Updated Global Earthquake Catalogue for Stable Continental Regions: Reassessing the Correlation With Ancient Rifts**, Geophysical Journal International 161, 707-721.

5.14.152) van Lanen, X. & Mooney, W.D. (2007), **Integrated Geologic and Geophysical Studies of North American Continental Intraplate Seismicity**: in Continental Intraplate Earthquakes: Science, Hazard, and Policy Issues, S. Stein & S. Mazzotti (eds.), pp. 101-112, Geological Society of America Special Paper 425.

5.14.153) Klose, C.D. & Seeber, L. (2007), **Shallow Seismicity in Stable Continental Regions**. Seismological Research Letters 78(5), 554-562.

5.14.154) Sibson, R.H. (1982), **Fault Zone Models, Heat Flow, and the Depth Distribution of Earthquakes in the Continental Crust of the United States**, Bulletin of the Seismological Society of America 72(1), 151-163.

5.14.155) Tanaka, A. (2004), **Geothermal Gradient and Heat Flow Data In and Around Japan (II): Crustal Thermal Structure and Its Relationship to Seismogenic Layer**, Earth, Planets and Space 56, 1195-1199.

5.14.156) Tanaka, A., & Ishikawa, H. (2002), **Temperature at the Base of the Seismogenic Zone and Its Relationship to the Focal Depth of the Western Nagano Prefecture Area**, Journal of the Seismological Society of Japan 55, 1-10.

5.14.157) Scholz, C.H. (1998), **Earthquakes and Friction Laws**, Nature 391, 37-42.

5.14.158) Leonard, M. (2010), **Earthquake Fault Scaling: Self-Consistent Relating of Rupture Length, Width, Average Displacement, and Moment Release**, Bulletin of the Seismological Society of America 100(5A), 1971-1988.

5.14.159) Wells, D.L. & Coppersmith, K.J. (1994), **New Empirical Relationships Among Magnitude, Rupture Length, Rupture Width, Rupture Area, and Surface Displacement**. Bulletin of the Seismological Society of America 84(4), 974-1002.

5.14.160) Jackson, J.A. & White, N.J. (1989), **Normal Faulting in the Upper Continental Crust: Observations from Regions of Active Extension**. Journal of Structural Geology 11, 15-36.

5.14.161) Collettini, C. & Sibson, R.H. (2001), **Normal Faults: Normal Friction?** Geology 29, 927-930.

© Eskom 2026/Rev 0a

5.14.162) Weichert, D.H. (1980), **Estimation of the Earthquake Recurrence Parameters for Unequal Observation Periods for Different Magnitudes**. Bulletin of the Seismological Society of America 70(4), 1337-1346.

5.14.163) Veneziano, D. & Van Dyck, J. (1985) **Analysis of Earthquake Catalogs for Incompleteness and Recurrence Rates**. In Seismic Hazard Methodology for Nuclear Facilities in the Eastern U.S., Volume 2, Appendix A-6, EPRI/SOG Draft 85-1.

5.14.164) Working Group on California Earthquake Probabilities (2012), **The Uniform California Earthquake Rupture Forecast, Version 3 (UCERF3) Preliminary Model**, Technical Report #6, March 31, 2012. Available from: www.wgcep.org.

5.14.165) Youngs, R.R., Coppersmith, K.J., Taylor, C.L., Power, M.S., DiSilvestro, L.A., Angell, M.L., Hall, N.T., Wesling, J.R., & Mualchin, L. (1992), **A Comprehensive Seismic Hazard Model for the San Francisco Bay Region**. In: Proceedings of the Second Conference on Earthquake Hazards in the Eastern San Francisco Bay Area, G. Borchardt, S.E. Hirschfeld, J.J. Lienkaemper, P. McClellan, P.L. Williams & I.G. Wong (eds.), Special Publication 113, pp. 431-441, California Department of Conservation, Division of Mines and Geology.

5.14.166) Clark, D., McPherson, A., & Collins, D.C.N. (2011), **Australia's Seismogenic Neotectonic Record: A Case For Heterogeneous Intraplate Deformation**. Record 2011/11. Canberra, Geoscience Australia.

5.14.167) Working Group on California Earthquake Probabilities (2003), **Earthquake Probabilities in the San Francisco Bay Region: 2002-2031**. Open-File Report 03-214, U.S. Geological Survey.

5.14.168) Wheeler, R.L. (2011), **Reassessment of Stable Continental Regions of Southeast Asia**. Seismological Research Letters 82, 971-983.

5.14.169) Kijko, A. (2004), **Estimation of the Maximum Earthquake Magnitude, m_{max}**. Pure and Applied Geophysics 161, 1-27.

5.14.170) Bate, K.J. & Malan, J.A. (1992), **Tectonostratigraphic Evolution of the Algoa, Gamtoos and Pletmos Basins, Offshore South Africa**. In: Inversion Tectonics of the Cape Fold Belt, Karoo and Cretaceous Basins of Southern Africa, M.J. de Wit & I.G.D. Ransome (eds.), pp. 61-73, A.A. Balkema, Rotterdam.

5.14.171) Parsiegla, N., Stankiewicz, J., Gohl, K., Ryberg, T., & Uenzelmann-Neben, G. (2009), **Southern African Continental Margin: Dynamic Processes of a Transform Margin**. Geochemistry, Geophysics, Geosystems 10(3), 1-20.

5.14.172) Broad, D.S., Jungslager, E.H.A., McLachlan, I.R., & Roux, J. (2006). **Offshore Mesozoic Basins**. In: M.R. Johnson, C.R. Anhaeusser & R.J. Thomas (eds.) The Geology of South Africa.pp. 553-571, Geological Society of South Africa and the Council for Geoscience.

© Eskom 2026/Rev 0a

5.14.173) Watkeys, M.K. (2006), **Gondwana Break-up: A South African Perspective**. In: The Geology of South Africa, M.R. Johnson, C.R. Anhaeusser & R.J. Thomas (eds.), pp. 531-540, Geological Society of South Africa, Johannesburg / Council for Geoscience, Pretoria.

5.14.174) de Beer, C.H. (1998), **Structure of the Cape Fold Belt in the Ceres Arc**, Bulletin 123, 93 pp. Pretoria, Council for Geoscience

5.14.175) de Beer, C.H. (1990), **Simultaneous Folding in the Western and Southern Branches of the Cape Fold Belt**. South African Journal Geology 93(4), 583-591.

5.14.176) Ransome, I.G.D.,. & De Wit, M.J. (1992), **Preliminary Investigations Into a Microplate Model for the South Western Cape**. In: Inversion Tectonics of the Cape Fold Belt, Karoo and Cretaceous Basins of Southern Africa, M.J. de Wit & I.G.D. Ransome (eds.), pp. 257-266, A.A. Balkema, Rotterdam.

5.14.177) de Beer, C.H. (1992), **Structural Evolution of the Cape Fold Belt Syntaxis and Its Influence on Syntectonic Sedimentation in the SW Karoo Basin**. In: Inversion Tectonics of the Cape Fold Belt, Karoo and Cretaceous Basins of Southern Africa, M.J. de Wit & I.G.D. Ransome (eds.), pp. 197-206, A.A. Balkema, Rotterdam.

5.14.178) Goedhart, M.L. (2007), **Potential Onshore and Offshore Geological Hazards for the Thyspunt Nuclear Site, Eastern Cape, South Africa: A Review of the Latest Airborne And Marine Geophysical Data and Their Impact on the Existing Geological Model for the Site Vicinity Area**. Report 2007-0274, Rev. 0, 95 pp. Pretoria, Council for Geoscience.

5.14.179) Durrheim, R.J. (1987), **Seismic Reflection and Refraction Studies of the Deep Structure of the Agulhas Bank.** Geophysical Journal of the Royal Astronomical Society 89, 395-398.

5.14.180) Söhnge, A.P.G. (1934), **The Worcester Fault**, Transactions Geological Society South Africa 37, 253-277.

5.14.181) Goedhart, M.L. (2004), **Desk Study Report: A Geological Investigation of Neotectonic Reactivation Along the Ceres-Kango–Baviaanskloof-Coega Fault System in the Southern and Eastern Cape, South Africa**. CGS Report No. 2004-0189, Rev. 0, ESKOM NSIP-SHA-013852#P1-153, 129 pp. Pretoria, Council for Geoscience.

5.14.182) de Beer, C.H. (2005), **Investigation into Evidence for Neotectonic Deformation within Onland Neogene to Quaternary Deposits Between Alexander Bay and Port Elizabeth—South Coast Report**. CGS Report No. 2005-0180, Rev. 0, 187 pp. Pretoria, Council for Geoscience.

5.14.183) Paton, D.A. (2006), **Influence of Crustal Heterogeneity on Normal Fault Dimensions and Evolution: Southern South Africa Extensional System**. Journal of Structural Geology 28, 868-886.

© Eskom 2026/Rev 0a

5.14.184) Goedhart, M.L. (2005), **A Geological Investigation of Neotectonic Reactivation Along the Ceres-Kango–Baviaanskloof-Coega Fault System in the Southern and Eastern Cape, South Africa: Field Reconnaissance Report**. CGS Report No. 2005-0084, Rev. 0, 167 pp. Eskom NSIP-SHA-015892#P1-133. Pretoria, Council for Geoscience.

5.14.185) Goedhart, M.L. (2006), **A Geological Investigation of Neotectonic Reactivation Along the Ceres-Kango-Baviaanskloof-Coega Fault System in the Southern and Eastern Cape, South Africa: Trench Report**. CGS Report No. 2006-0085, Rev. 0, 302 pp. ESKOM NSIP-SHA-018229#P1-286. Pretoria, Council for Geoscience.

5.14.186) Hanson, K.L., Glaser, L., Coppersmith, R., Roberts, D.L, Claassen, D. , & Black, D.E. (2012), **Thyspunt Geological Investigations—Marine Terrace Studies**. CGS Report No. 2012-0034, Rev. 0, 126 pp. 126 pp. Pretoria, Council for Geoscience.

5.14.187) Malan, J.A., Martin, A.K. & Cartwright, J.A. (1990), **The Structural and Stratigraphic Development of the Gamtoos and Algoa Basins, Offshore South Africa**, Abstracts of the Geological Society of South Africa Geocongress 1990, 328-331.

5.14.188) Ben-Avraham, Z., Hartnady, C.J.H. & Malan, J.A. (1993), **Early Tectonic Extension Between the Agulhas Bank and the Falkland Plateau Due to the Rotation of the Lafonia Microplate**. Earth and Planetary Science Letters 117, 43-58.

5.14.189) Doherty, S. (1993), **The Seismic Expression of the St. Croix Fault Plane, Offshore Algoa Basin, Showing a History of Extension, Inversion, Compression, and Strike-slip**. Extended abstracts of the Third Annual Technical Meeting of the South African Geophysical Association, pp. 71-74, 14-16 April, Cape Town.

5.14.190) Thomson, K. (1999), **Role of Continental Break-Up, Mantle Plume Development and Fault Reactivation in the Evolution of the Gamtoos Basin, South Africa**. Marine and Petroleum Geology 16, 409-429.

5.14.191) Toerien, D.K. (1986), **Port Elizabeth sheet**. 1:250 000 geological map series. Pretoria, Geological Survey of South Africa.

5.14.192) Shone, R.W., Nolte, C.C., & Booth, P.W.K. (1990). **Pre-Cape Rocks of the Gamtoos area—A complex tectonostratigraphic package preserved as a horst block**. South African Journal of Geology 93 (4), 616-621.

5.14.193) Hälbich, I.W. (1983), **Disharmonic Folding, Detachment and Thrusting in the Cape Fold Belt.** In: Geodynamics of the Cape Fold Belt: A Contribution to the National Geodynamics Programme, A.P.G. Sönghe & I.W. Hälbich (eds.), Special Publication 12, ch. 10, pp. 115-123. Johannesburg, Geological Society of South Africa.

© Eskom 2026/Rev 0a

5.14.194) Lindeque, A., De Wit, J., Ryberg, T., Weber, M., & Chevallier, L. (2011), **Deep Crustal Profile Across the Southern Karoo Basin and Beattie Magnetic Anomaly, South Africa: An integrated Interpretation With Tectonic Implications**. South African Journal of Geology 114(3/4), 265-292.

5.14.195) de Beer, C.H. (2004), **Investigation into Evidence for Neotectonic Deformation Within Onland Neogene to Quaternary Deposits Between Alexander Bay and Port Elizabeth—Desk Study Report**, Report No. 2004-0226, 187 pp. Pretoria, Council for Geoscience.

5.14.196) Gresse, P.G., Theron, J.N., Fitch, F.J., & Miller, J.A. (1992), **Tectonic inversion and radiometric resetting of the basement in the Cape Fold Belt**. In: Inversion Tectonics of the Cape Fold Belt, Karoo and Cretaceous Basins of Southern Africa. M.J. de Wit & I.G.D. Ransome (eds.), pp. 217-228. A.A. Balkema, Rotterdam.

5.14.197) Brown, L.F., Benson, J.M., Brink, G.J., Doherty, S., Jollands, A., Jungslager, E.H.A., Keenan, J.H.G., Muntingh, A., & van Wyk, N.J.S. (1995), **Sequence Stratigraphy in Offshore South African Divergent Basins: An Atlas on Exploration for Cretaceous Lowstand Traps by SOEKOR (Pty) Ltd**. AAPG Studies in Geology #41, 184 pp.

5.14.198) de Beer, C.H. (1995), **Fold Interference From Simultaneous Shortening in Different Directions: The Cape Fold Belt Syntaxis**, Journal of African Earth Sciences 21(1), 157-169.

5.14.199) de Beer, C.H. (1999), **The Geology of the Ceres Arc**. 1:50 000 scale map. Pretoria, Council for Geoscience.

5.14.200) Toerien, D.K. (1979), **The Geology of the Oudtshoorn Area**. Explanation sheet of map 3322 (1:250 000 scale), 13 pp. Pretoria, Council for Geoscience.

5.14.201) Toerien, D.K. & Hill, R.S. (1991), **The Geology of the Port Elizabeth Area**. Explanation sheet of map 3324 (1:250 000 scale), 35 pp. Pretoria, Council for Geoscience.

5.14.202) Du Plessis, A. (1996), **Seismicity in South Africa and Its Relationship to the Geology of the Region**, Report No. 1996-0019, 12 pp. Pretoria, Council for Geoscience.

5.14.203) Hartnady, C.J.H. (1996), **Seismotectonic Provinces of South Africa: Critical Review and New Proposals**. Internal Report. Pretoria, Council for Geoscience.

5.14.204) Partridge, T.C. (1995), **A Review of Existing Data on Neotectonics and Palaeoseismicity to Assist in the Assessment of Seismic Hazard at Possible Nuclear Power Station Sites in South Africa**. Internal Report, 42 pp. Pretoria, Council for Geoscience.

© Eskom 2026/Rev 0a

5.14.205) Chevallier, L. & Woodford, A. (1999), **Morpho-tectonics and Mechanism of Emplacement of the Dolerite Rings and Sill of the Western Karoo, South Africa**. South African Journal of Geology 102(1), 43-54.

5.14.206) Weckmann, U., Jung, A., Branch, T. & Ritter, O. (2007), **Comparison of Electrical Conductivity Structures and 2D Magnetic Modelling Along Two Profiles Crossing the Beattie Magnetic Anomaly, South Africa**. South African Journal of Geology 110, 449-464.

5.14.207) Thomas, R., Marshal, C., du Plessis, A., Fitch, F., Miller, J., von Brunn, V. & Watkeys, M. (1992), **Geological Studies in Southern Natal and Transkei: Implications for the Cape Orogen**. In: Inversion Tectonics of the Cape Fold Belt, Karoo and Cretaceous Basins of Southern Africa, M. de Wit & I. Ransome (eds.), pp. 229-236, A.A. Balkema, Rotterdam.

5.14.208) Viola, G., Kounov, A., Andreoli, M.A.G. & Mattila, J. (2012), **Brittle tectonic evolution along the western margin of South Africa: More than 500 Myr of continued reactivation**. Tectonophysics 514-517, 93-114.

5.14.209) Marshall, C.G.A. (2006), **The Natal Group**. In: The Geology of South Africa, M.R. Johnson, C.R. Anhaeusser & R.J. Thomas (eds.), pp. 433-442, Geological Society of South Africa, Johannesburg / Council for Geoscience, Pretoria.

5.14.210) Tankard, A., Welsink, H., Aukes, P., Newton, R. & Stettler, E. (2009), **Tectonic Evolution of the Cape and Karoo Basins of South Africa**. Marine and Petroleum Geology 26, 1379-1412.

5.14.211) Jacobs, J. & Thomas, R.J. (1994), **Oblique Collision at About 1.1 Ga Along the Southern Margin of the Kaapvaal Continent, Southeast Africa**. Geologische Rundschau 83(2), 322-333.

5.14.212) Thomas, R.J., Von Veh, M.W. & McCourt, S. (1993), **The Tectonic Evolution of Southern Africa: An Overview.** Journal of African Earth Sciences 16(1/2), 5-24.

5.14.213) Johnston, S.T., McCourt, S., Bisnath, A. & Mitchell, A.A. (2003), **The Tugela Terrane, Natal Belt: Kibaran Magmatism and Tectonism Along the Southeast Margin of the Kaapvaal Craton**, South African Journal of Geology 106, 85-97.

5.14.214) Wright, C, Kwadiba, M.T.O., Simon, E.R., Kgaswane, E.M. & Nguuri, T.K. (2004), **Variations of the Crust of the Kaapvaal Craton, and Mantle Structure Below Southern Africa**. Earth, Planets and Space 56, 125-137.

5.14.215) Cornell, D.H., Thomas, R.J., Moen, H.F.G., Reid, D.L., Moore, J.M., & Gibson, R.L. (2006), **The Namaqua-Natal Province**. In: The Geology of South Africa, M.R. Johnson, C.R. & R.J. Thomas (eds.), pp. 325-379, Geological Society of South Africa, Johannesburg / Council for Geoscience, Pretoria.

5.14.216) de Wit, M.J. & Tinker, J. (2004), **Crustal Structures Across The Central Kaapvaal Craton From Deep-Seismic Reflection Data**. South African Journal of Geology 107, 185-206.

5.14.217) Reeves, C. (2000), **The Geophysical Mapping of Mesozoic Dyke Swarms in Southern Africa and Their Origin in the Disruption of Gondwana**. Journal of African Earth Sciences 30(3), 499-513.

5.14.218) Olivier, H.J. (1972), **Geohydrological Investigations of the Flooding Shaft 2 Orange-Fish Tunnel, Northeastern Cape Province**. Transactions of the Geological Society of South Africa 75, 197-224.

5.14.219) Altermann, W. & Hälbich, I.W. (1991), **Structural History of the Southwestern Corner of the Kaapvaal Craton and the Adjacent Namaqua Realm: New Observation and Reappraisal**. Precambrian Research 52, 133-166.

5.14.220) Singh, M., Kijko, A., & Durrheim, R. (2011), **First-Order Regional Seismotectonic Model for South Africa**. Natural Hazards 59, 383-400.

5.14.221) McCarthy, T. & Rubidge, B. (2005), **The Story of Earth & Life: A Southern African Perspective on a 4-Billion-Year Journey**. 333 pp. Struik Publishers, Cape Town

5.14.222) Hanson, K.L., Slack, C., & Coppersmith, R. (2012), **Thyspunt Geological Investigations—Kango Fault Study**, Report No. 2012-0035, Rev. 0, 43 pp. Pretoria, Council for Geoscience.

5.14.223) Crone, A.J., Machette, M.N., & Bowman, J.R. (1997), **Episodic Nature of Earthquake Activity in Stable Continental Regions Revealed by Palaeoseismicity Studies of Australian and North American Quaternary Faults**, Australian Journal of Earth Sciences 44, 203-214.

5.14.224) Crone, A.J., De Martini, P.M., Machette, M.N., Okumura, K. & Prescott, J.R. (2003), **Paleoseismicity of Two Historically Quiescent Faults in Australia: Implications for Fault Behavior in Stable Continental Regions**. Bulletin of the Seismological Society of America 93(5), 1913-1934.

5.14.225) Hill, R.S. (1988), **Quaternary Faulting in the South-Eastern Cape Province**. South African Journal of Geology 91(3), 399–403.

5.14.226) Parsiegla, N., Gohl, K. & Uenzelmann-Neben, G. (2007), **Deep Crustal structure of the sheared South African continental margin: First results of the Agulhas-Karoo Geoscience Transect.** South African Journal of Geology 110, 393-406.

5.14.227) Uenzelmann-Neben, G. & Huhn, K. (2009), **Sedimentary Deposits on the Southern South African Continental Margin: Slumping Versus Non-Deposition or Erosion by Oceanic Currents?** Marine Geology 266, 65-79.

© Eskom 2026/Rev 0a

5.14.228) Ben-Avraham, Z., Hartnady, C.J.H. & Kitchin, K.A. (1997), **Structure and Tectonics of the Agulhas-Falkland Fracture Zone**. Tectonophysics 282, 83-98.

5.14.229) Roux, J. (2011), **Offshore geophysical data**, PowerPoint presentation (given by A. Davids on behalf of the author) at SSHAC Workshop 1, April 16, Cape Town.

5.14.230) McMillan, I.K., Brink, G.I., Broad, D.S., & Maier, J.J. (1997), **Late Mesozoic Sedimentary Basins Off the South Coast of South Africa**. In: African Basins, R.C. Selley (ed.), vol. 3 in Sedimentary Basins of the World series, pp. 319-376, Elsevier, Amsterdam.

5.14.231) Satriano, C., Kiraly, E., Bernard, P. & Vilotte, J.-P. (2012), **The 2012 M_w 8.6 Sumatra Earthquake: Evidence of Westward Sequential Seismic Ruptures Associated to the Reactivation of a N-S ocean Fabric**. Geophysical Research Letters 39(L15302), doi:10.1029/2012GL052387.

5.14.232) Ishii, M., Kiser, E.,& Geist, E.L. (2013), **M_w 8.6 Sumatran Earthquake of 11 April 2012: Rare Seaward Expression of Oblique Subduction.** Geology, doi:10.1130/G33783.1. 5 pp.

5.14.233) Robinson, D.P. (2011), **A Rare Great Earthquake on an Oceanic Fossil Fracture Zone**. Geophysical Journal International 186(3), 1121-1134.

5.14.234) Bufe, C.G. (2005), **Stress Distribution Along the Fairweather-Queen Charlotte Transform Fault System**. Bulletin of the Seismological Society of America 85(5), 2001-2008.

5.14.235) Lamontagne, M., Halchuk, S., Cassidy, J.F. & Rogers, G.C. (2008), **Significant Canadian Earthquakes of the Period 1600-2006**. Seismological Research Letters 79(2), 211-223.

5.14.236) Okal, E.A. & Stein, S. (1987), **The 1942 Southwest Indian Ocean Ridge earthquake: Largest Ever Recorded on an Oceanic Transform**. Geophysical Research Letters 14(2), 147-150.

5.14.237) Yue, H., Lay, T., & Koper, K.D. (2012), **En Echelon and Orthogonal Fault Ruptures of the 11 April 2012 Great Intraplate Earthquakes**. Nature 490, 245-249.

5.14.238) Duputel, Z., Kanamori, H., Tsai, V.C., Rivera, L., Meng, L., Ampuero, J.-P., & Stock, J.M. (2012), **The 2012 Sumatra Great Earthquake Sequence**. Earth and Planetary Science Letters 351-352, 247-257.

5.14.239) Boettcher, M.S. & McGuire, J.J. (2009), **Scaling Relations for Seismic Cycles on Mid-Ocean Ridge Transform Faults.** Geophysical Research Letters 36(L21301),

© Eskom 2026/Rev 0a

5.14.240) Bird, P., Kagan, Y.Y., & Jackson, D.D. (2002), **Plate Tectonics and Earthquake Potential of Spreading Ridges and Oceanic Transform Faults**. In: Plate Boundary Zones, S. Stein & J.T. Freymueller (eds.), Vol. 30 of Geodynamics series, pp. 203-218, American Geophysical Union, Washington, D.C.

5.14.241) Bierman, P.R. (2012), **Report #1, Cosmogenic Geochronology, Southern Africa Fault Corridor Investigation**. Appendix B.3 in Hanson, K., Slack, C., & Coppersmith, R., Thyspunt Geological Investigations - Kango Fault Study. CGS Report No. 2012-0035 (Rev. 0), Council for Geoscience, Pretoria.

5.14.242) Scharf, T., Codilean, A.T., de Wit, M.J., Jansen, J.D., & Kubik, P.W. (2013), **Strong Rocks Sustain Ancient Postorogenic Topography in Southern Africa**. Geology 41, 21 pp., including supplementary material, doi:10.1130/G33806.1.

5.14.243) Erlanger, E.D. (2010), **Rock Uplift, Erosion, and Tectonic Uplift of South Africa Determined with Cosmogenic 26Al and 10Be**, MSc Thesis, Purdue University, 196 pp.

5.14.244) Hanson, K.L., Lettis, W.R., McLaren, M.K., Savage, W.U., & Hall, N.T. (2004), **Style and Rate of Quaternary Deformation of the Hosgri Fault Zone, Offshore South-Central California**. In: Evolution of Sedimentary Basins / Offshore Oil and Gas Investigations—Santa Maria Province, M.A. Keller (ed.), U.S. Geological Survey Bulletin 1995, chap. BB, 33 pp.

5.14.245) Stamps, D.S., Flesch, L.M., & Calais, E. (2010), **Lithospheric Buoyancy Forces in Africa From a Thin Sheet Approach**, International Journal of Earth Sciences 99(7), 1525-1533.

5.14.246) DeMets, C., Gordon, R.G., & Argus, D.F. (2010), **Geologically Current Plate Motions**. Geophysical Journal International 181, 1-80.

5.14.247) Argus, D.F., Gordon, R.G. & DeMets, C. (2011), **Geologically Current Motion of 56 plates Relative to the No-Net-Rotation Reference Frame**. Geochemistry, Geophysics, Geosystems 12, Q11001, doi:10.1029/2011GC003751. 13 pp.

5.14.248) Lemaux II, J., Gordon, R.G., & Royer, J.-Y. (2002), **Location of the Nubia-Somalia Boundary Along the Southwest Indian Ridge**. Geology 30, 339-342.

5.14.249) Hartnady, C.J.H. (2002), **Earthquake Hazard in Africa: Perspectives on the Nubia-Somalia Boundary**. South African Journal of Science 98, 425-428.

5.14.250) Du Toit, S.R. (1976), **Mesozoic Geology of the Agulhas Bank, South Africa**. MSc Thesis, University of Cape Town, 182 pp.

5.14.251) Nolte, C.C. (1990), **Structure and Tectonostratigraphy of the Gamtoos Belt Between Tweewaters and Classen Point, Eastern Cape Province, R.S.A**. MSc Thesis, University of Port Elizabeth, 267 pp.

© Eskom 2026/Rev 0a

5.14.252) Stankiewicz, J., Ryberg, T., Schulze, A., Lindeque, A., Weber, M.H., & de Wit, M.J. (2007), **Initial Results From Wide-Angle Seismic Refraction Lines in the Southern Cape**. South African Journal of Geology 110, 407-418.

5.14.253) Paton, D.A., MacDonald, D.I.M. & Underhill, J.R. (2006), **Applicability of Thin or Thick Skinned Structural Models in a Region of Multiple Inversion Episodes: Southern South Africa**. Journal of Structural Geology 28(11), 1933-1947.

5.14.254) de Wet, W.M. (2012), **Bathymetry of the South African Continental Shelf.** MSc. Thesis, University of Cape Town.

5.14.255) Theron, J.N. (compiler) (1992), **Ladismith Quadrant Geological Map**. 1:250 000 scale, compiled from mapping by Wickens, H. de V., Whittingham, J.K., Theron, J.N., Hiller, N., Dunlevy, J.N., Siegfried, H.P., Le Roux, P.M., Grey, P.R, Gresse, P.G., & Toerien, D.K. carried out from 1974 to 198. Map 3320, Pretoria, Council for Geoscience.

5.14.256) Malan, J.A. (compiler) (1987), **Riversdale Quadrant Geological Map**. 1:250 000 scale, compiled from mapping by Siegfried, H.P., Viljoen, J.H.A., Wickens, H. de V., Toerien, D.K. & Malan, J.A. Map 3420, Pretoria, Council for Geoscience.

5.14.257) Hagedorn, J. (1988), **Silcretes in the Western Little Karoo and their Relation to Geomorphology and Palaeoecology**. Palaeoecology of Africa 19, 371-375.

5.14.258) Mitha, V.R., Hanson, K.L., & Roberts, D.L. (2013), **Subsurface Neotectonic Investigation of the Eastern Part of the Coega Fault Corridor, Eastern Cape, South Africa**. Report 2012-0029, Rev. 0, 90 pp. Pretoria, Council for Geoscience.

5.14.259) Prasad, K. & Claassen, D. (2012), **Report on the Baviaanskloof Fault Segment of the Ceres-Kango-Baviaanskloof-Coega Fault System. Neotectonic Studies for Evidence for Possible Post-Tertiary Grahamstown Formation (Tg) Reactivation of the Fault**. Report 2012-0177, Rev. 0, 36 pp. Pretoria, Council for Geoscience.

5.14.260) Reddering, J.S.V., Claassen, D. & Coppersmith, R. (2012), **An Investigation into the Western Coega Fault for Seismic Source Characterization of the Proposed Thyspunt Nuclear Site, Eastern Cape, South Africa** Report 2012-0030, Rev. 0, 52 pp. Pretoria, Council for Geoscience.

5.14.261) McCalpin, J.P. (compiler) (2009), **Field Reconnaissance and Seismic Source Characterisation of the Kouga, "Paul Sauer", Kango, and Baviaanskloof Fault Zones, Cape Fold Belt, Republic of South Africa**. Report No. 2009-0235, Rev. 0. Pretoria, Council for Geoscience.

© Eskom 2026/Rev 0a

5.14.262) Goedhart, M.L. & Hattingh, J. (1997) **The Geology of the Coega River Mouth and Proposed Adjacent Industrial Development Zone, Eastern Cape**. Report 1997-0008, 16pp. Pretoria, Council for Geoscience.

5.14.263) Bierman, P.R. (2012), **Report #2, Cosmogenic Geochronology, Southern Africa Southern Coast Marine Terraces.** Appendix E.1 in Hanson, K.L., Glaser, L., Coppersmith, R., Roberts, D.L, Claassen, D., & Black, D.E. (2012a), Thyspunt Geological Investigations - Marine Terrace Studies. Report No. 2012-0034, Rev. 0. Pretoria, Council for Geoscience.

5.14.264) Compton, J.S. (2011), **Pleistocene Sea-Level Fluctuations and Human Evolution on the Southern Coastal Plain of South Africa**. Quaternary Science Reviews 30, 506-527.

5.14.265) Davidson, A. & Smith, S. (2007), **Geophysical survey report for Thyspunt Eskom Site Surveys South Africa**. Fugro Survey Africa (PTY) Ltd. Report Number MZ581za-01-RPT-03-01 (Client Reference: NSIP-NSI-019130#P1-215), prepared for Eskom Holdings Limited, South Africa, 85 pp. plus appendices.

5.14.266) Goedhart, M.L. (2008), **Potential Onshore and Offshore Geological Hazards for the Thyspunt Nuclear Site, Eastern Cape, South Africa: A Review of the Latest Airborne and Marine Geophysical Data and Their Impact on the Existing Geological Model for the Site Vicinity Area.** Report 2007-0274, Rev. 1, 85 pp. Pretoria, Council for Geoscience.

5.14.267) Horwood, S. (2009), **Thyspunt 8 km Radius Marine Survey: Structural Geology Report**. Report 2009-0027, Rev. 0, 11pp. Pretoria, Council for Geoscience.

5.14.268) Bazzurro, P. & Cornell, C.A. (2004), **Nonlinear Soil-Site Effects in Probabilistic Seismic Hazard Analysis**. Bulletin of the Seismological Society of America 94(6), 2110-2123.

5.14.269) Bommer, J.J. & Abrahamson, N.A. (2006), **Why Do Modern Probabilistic Seismic Hazard Analyses Lead to Increased Hazard Estimates?** Bulletin of Seismological Society of America 96(6), 1967-1977.

5.14.270) Midzi V., Saunders, I., Brandt, M.B.C,. & Molea, T. (2011**), 1-D Velocity Model For Use By the SANSN in Earthquake Location**. Seismological Research Letters 81(3), 460-466.

5.14.271) Vanmarcke, E.H. (1976), **Structural Response to Earthquakes**. In: Seismic Risk and Engineering Decisions, C. Lomnitz and E. Rosenblueth (eds), Amsterdam: Elsevier.

5.14.272) Campbell, K.W. (2010), **Proposed Site κ_0 for a Reference Hard-Rock Site in Eastern North America**. NGA-East White Paper submitted to NGA-East Geotechnical Working Group, 11 November 2010.

© Eskom 2026/Rev 0a

5.14.273) Van Houtte, C., Drouet, S., & Cotton, F. (2011), **Analysis of the Origins of κ to Compute Hard Rock to Rock Adjustment Factors for GMPEs**. Bulletin of the Seismological Society of America 101(6), 2926-2941.

5.14.274) Knetidou, O.-J., Cotton, F., Drouet, S., Chaljub, E., & Theodulidis, N. (2012), **κ: Estimates, Origins & Correlation to Site Characterisation Parameters**. AGU Fall Meeting 2012, 3-7 December, San Francisco, Paper #S51A-2392, American Geophysical Union.

5.14.275) Joyner, W. B., R. Warrick, R.E. & Fumal, T.E. (1981), **The Effect of Quaternary Alluvium on Strong Ground Motion in the Coyote Lake, California, Earthquake of 1979**. Bulletin of the Seismological Society of America 71, 1333-1349.

5.14.276) Bommer, J.J., Papaspiliou, M., & Price, W. (2011), **Earthquake Response Spectra for Seismic Design of Nuclear Power Plants in the UK**. Nuclear Engineering & Design 241(3), 968-977.

5.14.277) Fukushima, Y. (1996), **Scaling Relations for Strong Ground Motion Prediction Models With M2 Terms**. Bulletin of the Seismological Society of America 86(2), 329-336.

5.14.278) Dangkua, D.T. & Cramer, C.H. (2011), **Felt Intensity Versus Instrumental Ground Motion: A Difference Between California and Eastern North America?** Bulletin of the Seismological Society of America 101(4), 1847-1858.

5.14.279) Scherbaum, F. Kuehn, N.M., Ohrnberger, M. & Koehler, A., (2010), **Exploring the Proximity of Ground-Motion Models Using High-Dimensional Visualization Techniques**. Earthquake Spectra 26(4), 1117-1138.

5.14.280) Toro G.R. (1995), **Probabilistic Models of Site Velocity Profiles for Generic and Site-Specific Ground-Motion Amplification Studies**. Technical Report 779574, Brookhaven National Laboratory, Upton, New York.

5.14.281) Choi, W.K. (2008), **Dynamic Properties of Ash-Flow Tuffs**. PhD Thesis, University of Texas at Austin, Austin TX, 335 pp.

5.14.282) Schnabel, P.B. (1973), **Effect of Local Geology and Distance From Source on Earthquake Ground Motions**. PhD. Dissertation, University of California at Berkeley, Berkeley, CA.

5.14.283) Darendeli, M.B. & Stokoe II, K.H. (2001), **Development of a New Family of Normalized Modulus Reduction and Material Damping Curves**. Geotechnical Engineering Report GD01-1, University of Texas, Austin, Texas.

5.14.284) Kottke, A.R. & Rathje, E.M. (2008), **Technical Manual for Strata**. PEER Report 2008/10, 84 pp. Pacific Earthquake Engineering Research Center, University of California at Berkeley.

5.14.285) Silva, W.J., Abrahamson, N., Toro, G., & Costantino, C. (1997), **Description and Validation of the Stochastic Ground Motion Model: Final Report**. Brookhaven National Laboratory, Contract No. 770573, Upton, New York.

© Eskom 2026/Rev 0a

5.14.286) Rathje, E.M. & Ozbey, M.C. (2006), **Site Specific Validation of Random Vibration Theory-Based Site Response Analysis**. ASCE Journal of Geotechnical and Geoenvironmental Engineering 132(7), 911-922.

5.14.287) Rathje, E.M., Kottke, A.R. & Ozbey, M.C. (2005), **Using Inverse Random Vibration Theory to Develop Input Fourier Amplitude Spectra for Use in Site Response**. Proceedings, 16th International Conference on Soil Mechanics and Geotechnical Engineering: TC4 Earthquake Geotechnical Engineering Satellite Conference, Osaka, Japan, 160-166.

5.14.288) Toro, G.R., Abrahamson, N.A. & Schneider, J.F. (1997), **Model of Strong Ground Motions from Earthquakes in Central and Eastern North America: Best Estimates and Uncertainties**. Seismological Research Letters 68(1), 41-57.

5.14.289) Anderson, J. G. & Brune, J.N. (1999), **Probabilistic Seismic Hazard Assessment Without the Ergodic Assumption** Seismological Research Letters, 70(1), 19-28.

5.14.290) Atkinson, G. M. (2006), **Single-Station Sigma**, Bulletin of the Seismological Society of America, 96(2), 446-455.

5.14.291) Al Atik, L., Abrahamson, N.A., Bommer, J.J., Scherbaum, F., Cotton, F. & Kuehn, N. (2010), The variability of ground-motion prediction models and its components. Seismological Research Letters 81(5), 794-801.

5.14.292) Rodriguez-Marek, A., Cotton, F., Abrahamson, N.A., Akkar, S., Al Atik, L., Edwards, B., Montalva, G.A. & Dawood, H. (2013), **A model for single-station standard deviation using data from various tectonic regions**. Bulletin of the Seismological Society of America, *in press*.

5.14.293) Strasser, F.O., Abrahamson, N.A. & Bommer, J.J. (2009), **Sigma: Issues, Insights, and Challenges**. Seismological Research Letters 80(1), 40-56.

5.14.294) BSSC (2000), **The 2000 NEHRP Recommended Provisions for New Buildings and Other Structures, Part I (Provisions) and Part II (Commentary)**. FEMA 368/369, Washington D.C, Building Seismic Safety Council

5.14.295) Zhao, J.X., Irikua, K., Zhang, J., Fukushima, Y., Somerville, P.G., Asano, A., Ohno, Y., Oouchi, T., Takahashi, T. & Ogawa, H. (2006**), An Empirical Site-Classification Method for Strong-Motion Stations in Japan Using H/V Response Spectral Ratio**. Bulletin of the Seismological Society of America 96(3), 914-925.

5.14.296) McGuire, R.K. (2012), **Precision of Seismic Hazard Evaluations in Central and Eastern North America**. Proceedings of 15th World Conference on Earthquake Engineering, Lisbon, Portugal.

5.14.297) Bommer, J.J., Strasser, F.O., Pagani, M., and Monelli, D. (2013), **Quality Assurance for Logic-Tree Implementation in Probabilistic Seismic Hazard Analysis for Nuclear Applications: A Practical Example**. Seismological Research Letters 84(6), Nov/Dec**.**

5.14.298) Bommer, J.J., Strasser, F.O., Rathje, E.M., Rodriguez-Marek, A., Stafford, P.J., & Hattingh, E. (2013). **Verification and Validation Report for Calculations Performed for the Thyspunt PSHA and Compliance with RD-0016**. Report 2013-0032. Pretoria, Council for Geoscience.

5.14.299) Van der Merwe, J.H.P, Graham, A, & Hattingh. E. (2013), **Nuclear Geo-Hazards Group Integrated Management System Manual**. Report 2010-0168, Rev. 2. Pretoria, Council for Geoscience.

5.14.300) Van der Merwe, J.H.P., Graham, A., Gouverneur, M and Hattingh, E. (2013), **Nuclear Geo-Hazards Group Core Integrated Management System Procedures, Work Instructions Forms and Checklists**. Report 2013-0010, Rev. 2. Pretoria, Council for Geoscience.

5.14.301) Pinho, R. (2012), **GEM: A Participatory Framework for Open, State-of-the-Art Models and Tools for Earthquake Risk Assessment Worldwide**. Proceedings of 15th World Conference on Earthquake Engineering, Lisbon, Portugal

5.14.302) Pagani, M., Monelli, D., Crowley, H., Danciu, L., Field, E.H., Wiemer, S., & Giardini D. (2010), **GEM1 Hazard: Description Of Input Models, Calculation Engine and Main Results**. GEM Technical Report 2010-3. Pavia, Italy, GEM Foundation.

5.14.303) Silva, V., Crowley, H., Pagani, M., Monelli, D. & Pinho, R. (2013). **Development of the OpenQuake Engine, the Global Earthquake Model's Open-Source Software for Seismic Risk Assessment.** Natural Hazards, doi 10.1007/s11069-013-0618-x.

5.14.304) Thomas, P., Wong, I. & Abrahamson, N. (2010), **Verification of Probabilistic Seismic Hazard Analysis Computer Programs**. PEER Report 2010/106, Pacific Earthquake Engineering Research Center, UC Berkeley, California.

5.14.305) Veneziano, D., Agarwal, A., & Karaca, E. (2009). **Decision Making With Epistemic Uncertainty Under Safety Constraints: An Application to Seismic Design**. Probabilistic Engineering Mechanics 24, 426-437.

5.14.306) Cornell, C.A. (1968), **Engineering Seismic Risk Analysis**. Bulletin of the Seismological Society of America 58(5), 1583-1606.

5.14.307) Reiter, L. (1990), **Earthquake Hazard Analysis: Issues and Insights**. Columbia University Press, New York. 254 pp.

5.14.308) McGuire, R.K. (2008), **Probabilistic Seismic Hazard Analysis: Early History**. Earthquake Engineering & Structural Dynamics 37, 329-338.

© Eskom 2026/Rev 0a

5.14.309) Kulkarni, R.B., Youngs, R.R. & Coppersmith, K.J. (1984), **Assessment of Confidence Intervals for Results of Seismic Hazard Analysis**. Proceedings of the Eighth World Conference on Earthquake Engineering, San Francisco, vol. 1, 263-270.

5.14.310) Coppersmith, K.J. & Youngs, R.R. (1986), **Capturing Uncertainty in Probabilistic Seismic Hazard Assessments Within Intraplate Tectonic Environments**. Proceedings of the Third US National Conference on Earthquake Engineering, vol. 1, 301-312.

5.14.311) McGuire, R.K. (2004), **Seismic Hazard and Risk Analysis**. EERI Monograph MNO-10, Earthquake Engineering Research Institute, Oakland, California.

5.14.312) EPRI (1989), **Probabilistic Seismic Hazard Evaluations at Nuclear Power Sites in the Central and Eastern United State: Resolution of the Charleston earthquake issue**. EPRI Special Report NP-6395-D, Electric Power Research Institute, Palo Alto, California.

5.14.313) Bernreuter, D.L., Savy, J.B., Mensing, R.W., & Chen, J.C. (1989), **Seismic Hazard Characterization of 69 Nuclear Power Plant Sites East of the Rocky Mountains**. NUREG/CR-5250, US Nuclear Regulatory Commission, Washington D.C.

5.14.314) ANS (2008), **Probabilistic Seismic Hazard Analysis**. ANS/ANSI-2.29-2008, American Nuclear Society and American National Standards Institute.

5.14.315) Kotra, J.P., Lee, M.P., Eisenberg, N.A. & DeWispelare (1996), **Branch Technical Position on the Use of Expert Elicitation in the High-Level Radioactive Waste Program**. NUREG-1563, US Nuclear Regulatory Commission, Washington D.C.

5.14.316) McGuire, R.K. (1995), **Probabilistic Seismic Hazard Analysis and Design Earthquakes: Closing the Loop**. Bulletin of the Seismological Society of America 85(5), 1275-1284.

5.14.317) Bazzurro, P. & Cornell, C.A. (1999), **Disaggregation of Seismic Hazard**. Bulletin of the Seismological Society of America 89(2), 501-220.

5.14.318) Harmsen, S., Perkins, D., & Frankel, A. (1999), **Deaggregation of Probabilistic Ground Motions in the Central and Eastern United States**. Bulletin of the Seismological Society of America 89(1), 1-13.

5.14.319) Eskom (2010), **Safety and Quality Classification of SSR Related Products and Processes**. NSIP01432. Rev. A. Johannesburg

5.14.320) National Nuclear Regulator (2008), **RD-0034 - Quality and Safety Management Requirements for Nuclear Installations**. Rev. 0. Centurion.

5.14.321) Bommer, J.J., Van der Merwe, J.H.P and Graham, A (2013) **Safety Justification Report (safety case) for the Thyspunt SSHAC Level 3 Probabilistic Seismic Hazard Analysis**. Report 2013-0209, Pretoria Council for Geoscience.

5.14.322) ISO (2008), **Quality Management System – Requirements. ISO 9001**, South African Bureau of Standards, South Africa.

5.14.323) Bommer, J.J. & K.J. Coppersmith (2010), **Project Execution Plan: SSHAC Level 3 Probabilistic Seismic Hazard Analysis for Vibratory Ground Motion for the Thyspunt Nuclear Siting Project, South Africa**. Report 2010-0174, Rev. 5. Pretoria, Council for Geoscience.

5.14.324) Van der Merwe, J.H.P., Graham, A., Hattingh, E., & Neveling, J. (2013), **Project Quality Plan Thyspunt Nuclear Siting Project**. Report 2010-0170, Rev. 3. Pretoria, Council for Geoscience.

5.14.325) Van der Merwe, J.H.P, Graham, A and Hattingh. E. (2013), **Nuclear Geo-Hazards Group Procedure for Project Risk Register(s)**. Report 2012-0009, Rev.1. Pretoria, Council for Geoscience.

5.14.326) Hattingh, E. & Flint, N.S. (2011), **Compliance Matrix**. Report 2010-0175, Rev. 1. Pretoria, Council for Geoscience.

5.14.327) Van der Merwe, J.H.P., Hattingh, E., Delport, F., Neveling, J., Graham, A. and Gouverneur, M. (2013), **Safety Culture Enhancement Program (SCEP).** Report 2010-0192, Rev. 2. Pretoria, Council for Geoscience.

5.14.328) IAEA (1991), **Safety Culture – a Report by the International Nuclear Safety Advisory Group**. INSAG-4, Safety Series No. 75, International Atomic Energy Agency, Vienna.

5.14.329) IAEA (2002), **Key Practical Issues in Strengthening Safety Culture – a Report by the International Nuclear Safety Advisory Group**. INSAG-15, International Atomic Energy Agency, Vienna.

5.14.330) United States Nuclear Regulatory Commission (2007), **Geologic and Seismic Siting Criteria**. USNRC Regulations Title 10, Code of Federal Regulations, Section 100.23. Washington DC.

5.14.331) NNR (2006), **Requirements for Authorization Submissions Involving Computer Software and Evaluation Models for Safety Calculations**. Requirements Document RD-0016, Rev. 0, 19pp. Centurion, National Nuclear Regulator, South Africa

© Eskom 2026/Rev 0a